STELLAR PULSATION: A STUDY OF THE INFLUENCE OF OPACITY ON NUMERICAL MODELS

Zaki A. Al-Mostafa

A Thesis Submitted for the Degree of MPhil
at the
University of St Andrews

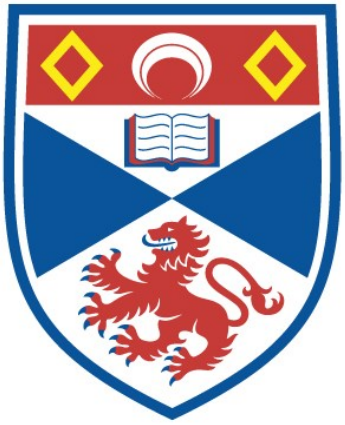

1995

STELLAR PULSATION

A STUDY OF THE INFLUENCE OF OPACITY ON NUMERICAL MODELS

BY

ZAKI A. AL-MOSTAFA

A Thesis submitted for the Degree of Master of Philosophy at the University of St. Andrews.

June, 1994.

بسم الله الرحمن الرحيم

In the name of Allah, Most Gracious, Most Merciful

ABSTRACT

A theoretical study of Population II variables has been carried out using the non-linear approach and using the more recent molecular opacities of Carson and Sharp (1991) with the atomic opacities of Iglesias and Rogers (1991). The calculations have been done using a computer code created by Dr. T. R. Carson.

More than fifty models have been constructed for different compositions for Hydrogen (X), 0.745, 0.749 and 0.750 and for Helium (Y) fixed at 0.250. These models belong to three types of stars, RR Lyrae, BL Herculis and W Virginis.

The aim of this study was to test the new opacities and compare them with the old ones (especially those of Carson).

Generally the periods of the old and new models are in very good agreement. However, the amplitudes of the new models tend to be fairly consistently smaller than those of the old models, tending towards greater agreement with observation. The new blue edges are shifted redward (toward lower temperature) with respect to the old, particularly for the larger values of the metal content Z, and less for smaller Z.

However, for the same composition all results are in excellent agreement with those of Carson, Stothers and Vemury (1981) using the opacities of Carson

The non-linear results obtained here show that the mass of RR Lyrae cannot be less than 0.6 M*sun*, while on the other hand, the BL Her variables have mass greater than 0.7 M*sun*.

TO...

My Parents,

My Wife,

My Daughters, Fatma & Sarah,

My Brothers and Sisters,

To all Moslems around the world.

Zaki

Acknowledgement

Praise be to Allah The Cherisher and Sustainer of the Worlds.

Then,

I would like to express my deep gratitude to my supervisor Dr. T. R. Carson, who has offered me great deals of his expensive time. Elaborate discussion with him and his continuous guidance throughout different phases of this project facilitate my achievement and bring this work to life.

I would like to thank my sponsor *KING ABDULAZIZ CITY FOR SCIENCE AND TECHNOLOGY*, "**KACST**", for their supports during my studies.

CERTIFICATE

I hereby certify that the candidate has fulfilled the conditions and regulations appropriate to the Degree of Master of Philosophy (*M.Phil.*) of the University of St. Andrews and that he is qualified to submit this thesis in application for that degree.

T. R. Carson
(Supervisor)

DECLARATION

I, ZAKI A. AL-MOSTAFA, hereby certify that this thesis, which is approximately 20,000 words in length, has been written by me, and that it has not been submitted in any previous application for a higher degree.

I was admitted as a research student under Ordinance No. 12 on the October 1992 and as a candidate for the degree of M.Phil. on the October 1993; the higher study for which this is a record was carried out in the University of St. Andrews between 1992 and 1994.

Zaki A. AL-Mostafa

In submitting this thesis to the University of St. Andrews I understand that I am giving permission for it to be made available for use in accordance regulations of the University Library for the time being in force, subject to any copyright vested in the work not being affected thereby. I also understand that the title and abstract will be published and that a copy of the work may be made and supplied to any bona fide library or research worker.

Zaki A. AL-Mostafa

CONTENTS

PAGE

INTRODUCTION.....1

CHAPTER **1**:

PART A

1A-1: POPULATION II CEPHEIDS.....3

PART B

1B-1: RR LYRAE STARS.....11

1B-2: BL HERCULIS STARS.....15

1B-3: W VIRGINIS STARS.....17

CHAPTER **2**:

2-1 THE NON-LINEAR THEORY.....24

2-1-1: THE PULSATION THEORY.....24

2-2 THE EQUATIONS OF STELLAR PULSATION.....26

2-2-1: THE BASIC EQUATIONS.....26

2-2-2: THE BOUNDARY CONDITIONS.....31

CHAPTER **3**:

3-1: THE METHOD OF SOLUTION.....34

3-2: THE EQUATION OF STATE 45

CHAPTER **4**:

4-1: RESULTS AND DISCUSSION.....52

PAGE

APPENDIX **A**:

A-1: LIGHT, VELOCITY & RADIUS CURVES FOR THE RR LYRAE MODELS.....67

A-2: LIGHT, VELOCITY & RADIUS CURVES FOR THE BL HERCULIS MODELS.....68

A-3: LIGHT, VELOCITY & RADIUS CURVES FOR THE W VIRGINIS MODELS.....69

APPENDIX **B**:

THE LIGHT, VELOCITY & RADIUS CURVES OF THE DECAYING MODELS.....70

APPENDIX **C**:

THE **IR** OPACITY TABLES.....71

APPENDIX **D**:

D-1: THE LINEAR THEORY.....76

D-2: THE EQUATIONS.....76

REFERENCES.....86

INTRODUCTION

During the past fifty years the pulsating variables have played an important and rather controversial role in the drama of our unfolding knowledge of the outline and dimensions of the universe of galaxies. So, the object of this study was to model Population II stars using the non-linear pulsation analysis in the hope of obtaining velocity and light curves of similar amplitudes and features to those produced by the real stars. In this study we have used the more recent molecular opacities of Carson and Sharp (1991) with the atomic opacities of Iglesias and Rogers (hereafter, IR) (1991).

This thesis is divided into four chapters and four appendices.

In Chapter One part A, a review of the Population II Cepheids. In part B we review the three types of Population II that have been used in this thesis, these are RR Lyrae, BL Herculis and W Virginis. Therein given the main properties of each type and its importance.

In Chapter Two and Three the non-linear theory and the method of solution of the equations that have been used are described.

In Chapter Four the main results are presented and discussed.

In Appendix A we present the theoretical models for RR Lyrae, BL Herculis and W Virginis. In Appendix B the decaying models are presented.

In Appendix C the IR opacities are presented and compared with the Carson.

In Appendix D the linear theory is described.

CHAPTER ONE PART *A*

1A-1. POPULATION II CEPHEIDS:-

Population II (Pop II, hereafter) cepheids generally originate from low-mass stars of low metallicity which are undergoing post core Helium (He) burning stage of their evolution (Becker 1985). Pop II are divided into three main categories which are the BL Herculis (BL Her) stars, the W Virginis (W Vir) stars and the anomalous Cepheids, see Table 1-1. Low-mass Pop II stars evolve off the suprahorizontal branch to Asymptotic Giant Branch (AGB) where the Hydrogen (H)-burning shell re-establishes itself and the double burning shell phase begins. When the Hydrogen envelope is nearly exhausted ($<5\times10^{-3}M_{sun}$) due to the last He shell flash on the AGB, one or two loop-like excursions from the AGB are possible for certain models. These excursions can intercept the instability strip, causing a star to become a W Vir variable having a period about 10-50 days (Becker 1985, Clement *et al.* 1985).

Variable stars in the H-R diagram are classified, based on their observed properties, into distinct types. The underlying mechanism for the variability is generally felt to be due to four different causes (Becker 1986):

1) geometric effects.

2) rotation.

3) eruptive processes.

4) pulsation.

In our thesis the focus will be on the fourth cause.

Type II cepheids have periods ranging upward of 1 day (Carson *et al.* 1981). The discovery of many Type II cepheids led to the introduction of distinct subclasses, such as BL Her, W Vir and RV Tau stars as well as less well defined subgroups such as the anomalous cepheids, which are more luminous at a given period than cepheids found in globular clusters. They (type II cepheids) lie on the H-R diagram between the RR Lyrae variables, at low luminosity, and the RV Tauri and long period variables at high luminosity (Becker 1985). Figure 1-1 shows that RR Lyrae and W Vir occupy roughly the same location in H-R diagram as do the classical cepheids. The long, nearly vertical, region shown on the H-R diagram lying above the main sequence, contains both the RR Lyrae and W Vir , as well as the classical cepheid and other types of pulsating stars. Because of their peculiarities, no strict definition can be given for type II cepheids. It is mostly on the theoretical basis of stellar evolution theory that all the subclasses above are regarded as Pop II (Kovacs & Buchler 1988).

The appellation " type II cepheids " usually refers to those pulsating variables belonging to the older population of the Galaxy whose luminosities are greater than those of the RR Lyrae stars and overlap the classical cepheids (Population I) (Kovacs & Buchler. 1988). We can identify these stars by their location -at least several classical cepheid scale heights above the galactic plane- or by their space velocities- which

deviate by several sigma from that which is expected for young cepheid variables - (Wallerstein & Cox 1984). Type II cepheids are variables with periods greater than a specified value in globular clusters and similar star in the field. Therefore, we can easily place a substantial number of field stars in the type II class (Wallerstein & Cox 1984).

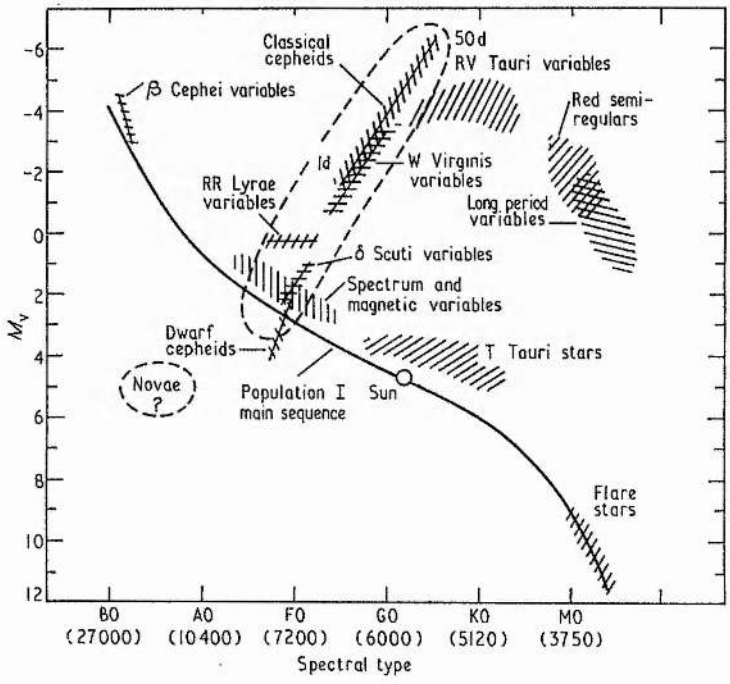

Figure 1-1. Location of various types of intrinsic variables on the H-R diagram (Cox 1974, Figure 1).

Cepheid pulsation is an envelope phenomenon. The smallness of the pulsation amplitude in the deep stellar interior depends upon the cepheid's advanced stage of evolution and is consequently highly centrally concentrated (Cox 1985).

Due to the great age of the Pop II and of the old disk stars their masses are estimated to be less than 0.8 M_{sun} (Bohm-Vitense *et al.* 1974, Wallerstein & Cox

1984, Becker 1985) - for a star to be in the instability strip its mass must be in the range 0.75 – 0.50 M_{sun} - this low mass depends on the mass of the He-core left behind by the core and shell H-to-He burning (Wallerstein & Cox 1984).

The instability region, moves toward higher effective temperature (T_{eff}, hereafter) [1] with increasing He content, (i.e. decrease in H), which leads to a decrease in the opacity (Christy 1966 , Pel 1985).

In Pop II stars there is no discrepancy between the mass that we obtain using evolution theory and using pulsation theory, as there is in classical cepheids, because masses between 0.5 M_{sun} and 0.75 M_{sun} or even larger range in mass, if extreme compositions are all considered, populate the horizontal and AGB. However, for classical cepheids there is a very strong dependence of a star's luminosity on the mass. An approximately accurate mass can be derived from a more approximate luminosity (Wallerstein & Cox 1984). The smaller M for a given L ,the lower T_{eff}, which means that Pop II will show instability at lower T_{eff} than classical cepheids (Christy 1966), see Figure 1-5.

The fact that metal-rich globular clusters do not contain Type II cepheids indicates that their metal abundance range from moderate to extreme deficiencies. Due to their low metals contents and lower opacity, allowing the main- sequence turn-off

---

[1] *which is the temperature that a black body would radiate the same amount of energy that a particular body does, its a very important quantity because some of un-directly observable parameters can be very sensitive to the accuracy of* T_{eff}. *An example is the pulsation mass which depends very strongly on* T_{eff} *because of the relationship from which it is derived:* $P \propto L^{0.83} M^{-0.66} T_{eff}^{-3.45}$.

mass to be so low, Pop II evolve faster than Pop I (Wallerstein & Cox 1984). Nevertheless, chemical peculiarities have been found in some cases, especially in the field variables. The blue edge position obtained from linear non-adiabatic models suggests He abundance between **0.25** and **0.50** (see for example, Carson *et al.* 1981, Bridger 1984, Kovacs & Buchler 1988 and Chiosi *et al.* 1992). In most of Type II cepheids spectra and during rising light there are strong absorption and emission lines of H and He I (Kovacs & Buchler 1988, Lebre & Gillet 1992).

While RR Lyrae stars have been extensively studied, the other Pop II cepheids have received less attention. The shorter period BL Her variables ($0.1 \leq P \leq 10$) have been studied by Carson and Stothers (1982), and the W Virginis variables ($10 \leq P \leq 20$) have been studied by Bridger (1984).

Many models have been constructed by Carson, Stothers & Vemury (1981) (hereafter CSV81) and Carson and Stothers (1982) (hereafter CS82). In our work we are going to use the same model parameters (i.e. the same mass, luminosity and effective temperature) as in CSV81 and CS82, but employ the more recent molecular opacities of Carson & Sharp (1991), and the atomic opacities of Iglesias and Rogers (1991).

Studying Cepheids and RR Lyrae stars, enables us to study the galactic structure, and therefore to know much about their luminosity and their intrinsic properties which can be determined from a studying of their pulsation. Also, the pulsating stars are known to be mostly in late stage of evolution, during or after core He burning, and from their pulsation characteristics we can impose some constraints on what their prior evolution may have been, Castor (1971).

Pulsation theory shows that whenever a star's evolutionary track lies within the cepheid strip, the star is unstable to surface pulsation and the star should be recognisable as a cepheid variable (Becker 1985).

Table 1-1. This table shows a short summary about the pulsation variable stars (from Becker 1986).

S Dor	High luminosity eruptive variables whose mass loss may be sue to a global pulsation instability
α Cyg	Quasi-periodic supergiants having amplitudes of 0.1 mag, possibly showing several radial and non-radial modes.
β Cep	Early B pulsating giants having periods of hours and amplitudes of around 0.1 mag, Some showing multiple modes and possibly non-radial modes.
X Cen	Possible class of B subgiant variables having periods less than an hour and amplitudes of 0.02 mag.
Be stars	Rapidly-rotating, mass-losing B stars some of which show variability which may be sue to pulsation. Example LQ And.
MAIA	Struve's hypothetical variable sequence between β Cep and δ Sct.
SRd	Semiregular yellow giants and supergiants some of which show emission lines, exhibit periods of 30 to 1100 days and amplitudes up to 4 mag, Example S Vul.
δ Cep	Radially pulsating (Pop I) variables having well-defined periods of 1 to 135 days and amplitudes generally from 0.1 to 2 mag. Some show multiple modes.
δ Sct	Dwarf to giant A-F stars having periods of hours and generally amplitudes < 0.1 mag. some show multiple modes and possibly non-radial modes.
PV Tel	Helium supergiants that appear to pulsate with periods on the order of days but with small amplitude about 0.1 mag.
R Cor Bor	Hydrogen-deficient eruptive variables which also may show quasi-periodic pulsatoinal behaviour having periods of 30 -100 days and amplitudes > 1 mag.
RV Tau	Supergiant Pop II variables exhibiting a double wave light curve with periods generally from 30 to 150 days and amplitude up to 5 mag.
W Vir	Radially pulsating stars somewhat similar to δ Cep but arising from stars of much smaller mass . More about this type of variables see section *1B-3*.
BL Her	Radial pulsators related to W Vir class but show a bump on the descending part of the light curve and periods of 1 to 8 days. See section *1B-2*.
Anomalous Cepheids	RR Lyrae like variables of higher luminosity found almost exclusively in dwarf metal-poor spherical galaxies like Draco.

RR Lyrae	Radially pulsating A-type giants of disk and Pop II composition having periods of about 1 day and amplitudes < 2 mag. Some show double mode behaviour. See section *1B-1*.
SX Phx	Subdwarf Pop II equivalent of the δ Sct class having periods of hours and amplitudes < 0.7 mag. Some show multiple modes and possibly non-radial modes.
Lc	Slowly irregularly varying supergiants of type M showing amplitudes of 1 mag. Example TZ Cas.
SRc	Semiregular pulsating supergiants having periods of 30 to several thousand days and amplitudes of about 1 mag. Example α Ori, OH - IR stars.
Lb	Slowing varying irregular giants exhibiting no indication of periodicity. Example CO Cyg.
SRa	Semiregular giants showing MIRA-like behaviour but smaller amplitudes < 2.5 mag. and periods of 35 to 1200 days. Example Z Aqr.
SRb	Semiregular giants showing periods of 20 to 2300 days that come and go. Example AF Cyg.
MIRA	Radially pulsating red giant and supergiant stars of disk and Pop II composition having amplitudes > 2.5 mag and periods of 80 to 1400 days.
GW Vir	Multiperiodic, non-radially pulsating white dwarfs of very high temperature.
DB Variables	Multiperiodic, non-radially pulsating, helium white dwarfs.
ZZ Ceti	Multiperiodic, non-radially pulsating, hydrogen white dwarfs showing periods on the order of minutes and amplitude from 0.001 to 0.3 mag.

CHAPTER ONE PART *B*

1B-1. RR LYRAE VARIABLES:-

RR Lyrae are pulsating giants variables in the period range from about one-quarter of a day to a day (Schmidt *et al.* 1990). They are of spectral type A (rarely F) and brightness amplitudes not exceeding 1 to 2 magnitudes. The period and the form of the light curves always show the same characteristics, but there are cases in which departures occur. They are Pop II stars.

It is possible to determine the photometric parallaxes and so to produce for the first time a model of the Galaxy by using the RR Lyrae in globular clusters. Because of their concentration around the galactic nucleus, our distance from them and the direction towards their positions in space are the main attributes of this model (Strohmeier 1972, Lub 1987) .

They always show the same characteristic light curves, but they differ in two or three forms of Bailey's classification, see below. According to this classification the observations of RR Lyrae were logged into stellar catalogues (see Figure 1-2):

RRa, very asymmetrical light curve (a steep ascending branch) with sharp maximum and large amplitude (up to 1.6 magnitudes), and the mean period is 0.5 days.

RRb, this group has smaller amplitude (about 0.5 magnitudes) and almost flat maxima, with a hump in light intensity on the ascending side and a corresponding shoulder on the descending branch, and the mean period is 0.7 days.

RRc, this group has almost asymmetrical light curve, often sinusoidal, and amplitude of about one-half a magnitude, and the mean period is 0.3 days.

It's clear from Figure 1-2 that group **a** and **b** are almost similar to each other, and also RR Lyrae itself manifests a type **a** light curve. However later in its 41-day cycle, it evolves type **b** characteristics, therefore, some authors join them together as one group called **RRab**, and the mean period range from 0.5 to 0.7 days. The **RRab** groups are believed to be pulsating in the fundamental mode, on the other hand, **RRc** in the first overtone mode (Hubickyj 1983).

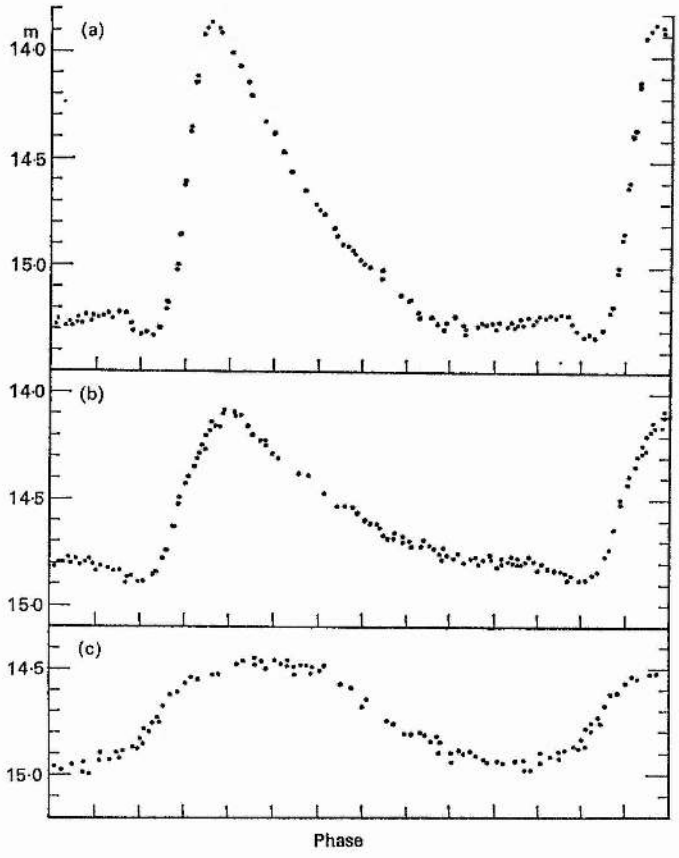

Figure 1-2. Typical light curves of RR Lyrae variables. Bailey's type **a**, **b** and **c** (Figure 38, Strohmeier 1972).

Oosterhoff divided the RR Lyrae based on the mean period into two distinctive groups, I and II. Group I variable stars have a mean period of 0.55 days for **ab** stars and 0.32 days for **c** stars, and the metallic spectral lines are weak relative to the solar abundance. Group II variable stars have mean period of 0.65 days for **ab** type and 0.37 days for **c** type, and the metallic spectral line here is weaker than the other group (Hubickyj 1983).

In Figure 1-3 we show the relation between amplitude and period for RR Lyrae stars. We can easily see that there is a smooth transition between type **a** and type **b**, while those of type **c** are clearly distinct.

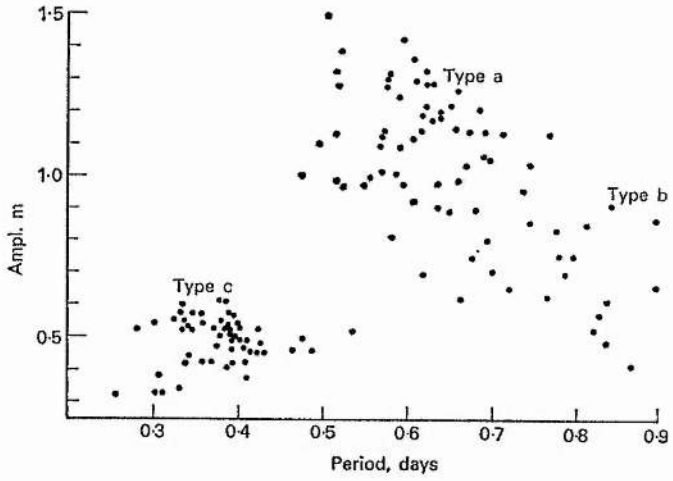

Figure 1-3. We show the relation between amplitude and period for the three types of RR Lyrae stars. The **c** types have the shortest periods and the lowest amplitudes. They are clearly distinct from the **a** and **b** types. (From Bohm-Vitense 1989 (1) Figure 16.6).

Diethelm (1983) found the following: (1) The light curves of RR Lyrae (**RRb**) in V magnitude are smooth and exhibit only a small bump just before the ascending branch, see Figure 1-4. (2) The rise to maximum light is steep and (3) The (B-V)-(U-B) two-colour diagram resulting in a characteristic " Figure-eight" loop, see Figure 5 in Diethelm (1983), which is the most important, since it's a unique feature for all RR Lyrae.

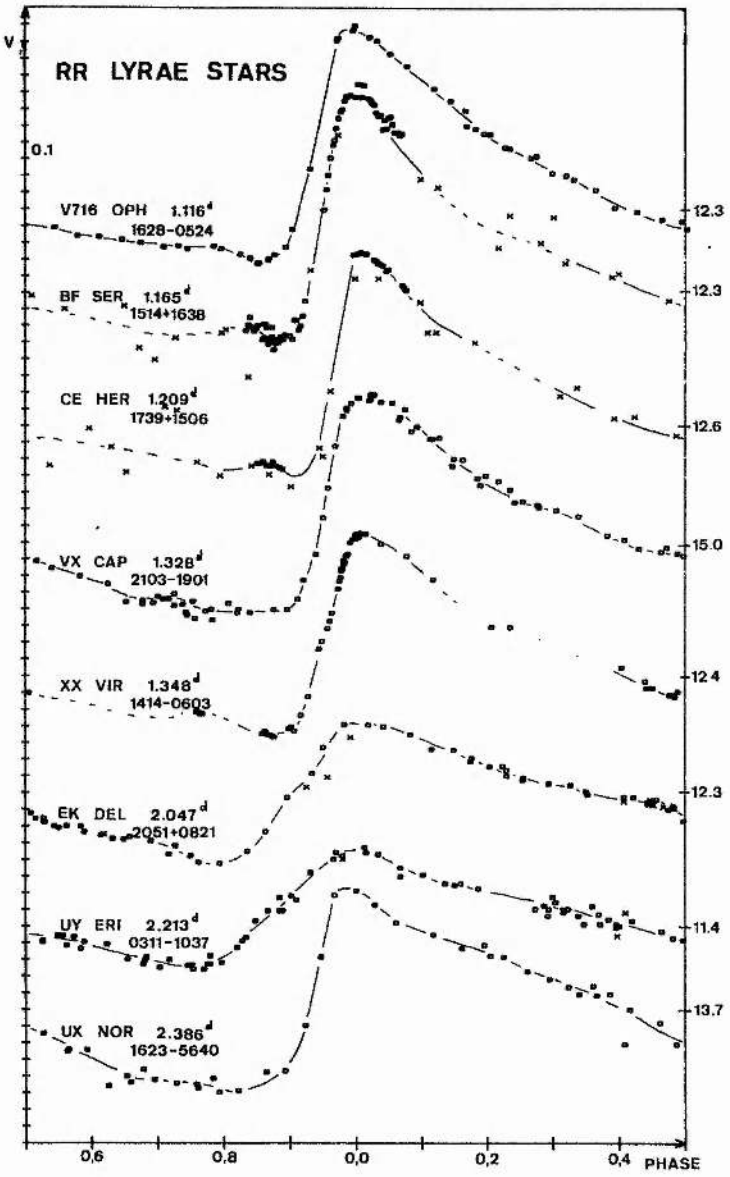

Figure 1-4. A selection of **RRd** type light curves in V magnitude (Figure 1, Diethelm 1983).

1B-2. BL HERCULIS VARIABLES:-

These variables are defined as any Cepheids of Pop II with period less than 3 days (between 1 and 3 days). The shape of the light curves show the Hertzsprung progression. Of great practical importance is the existence of a small secondary bump, which results from the pressure wave produced in either the He or H ionisation zones and reflects off the interior core reaching the surface as a secondary maximum. This first shows up on the descending branch of the light curves at a period of about 1.2 days, progresses backward in phase until it reaches light maximum for stars with periods of about 1.6 days, and then switches to the ascending branch, where for periods of about 3 days, it disappears (Carson & Stothers 1982 , Diethelm 1983 and Lawrence 1985).

Our question here is, how can a star be a BL Her? When helium is exhausted in the centre of the horizontal branch star, the star evolves upward in the H-R diagram into the suprahorizontal branch where the thick helium-burning shell phase is established. If, while on the horizontal branch, the star is located either inside or to the left of the instability strip in the H-R diagram, the post-horizontal branch evolution will cause the star's evolutionary track to intercept the instability strip. At this point the star should behave as a BL Her variable with a period between 1 - 5 days (Becker 1985).

BL Her stars originate from a very narrow mass range of about $0.6 \pm 0.05\ M_{sun}$. The total life time of this phase of variability lasts up to several million years due to the evolution proceeding on a nuclear burning time scale (Becker 1985).

In Figure 1-5 the distinction between the short period (P≤ 3 days) BL Her and the longer one (P≥6 days) W Vir maybe clearly seen. The BL Her stars form a definite

group at $2.0 \leq \log(L/L_{sun}) \leq 2.3$ whilst the W Vir stars cover a wide luminosity range above $\log(L/L_{sun}) = 2.5$. This wide spread of luminosity is explained by the fact that the phase of AGB evolution at which the star executes a blue loop is very sensitive to the mass. This means that a small range of masses suffices to provide the large observed spread in luminosity, Bridger (1983).

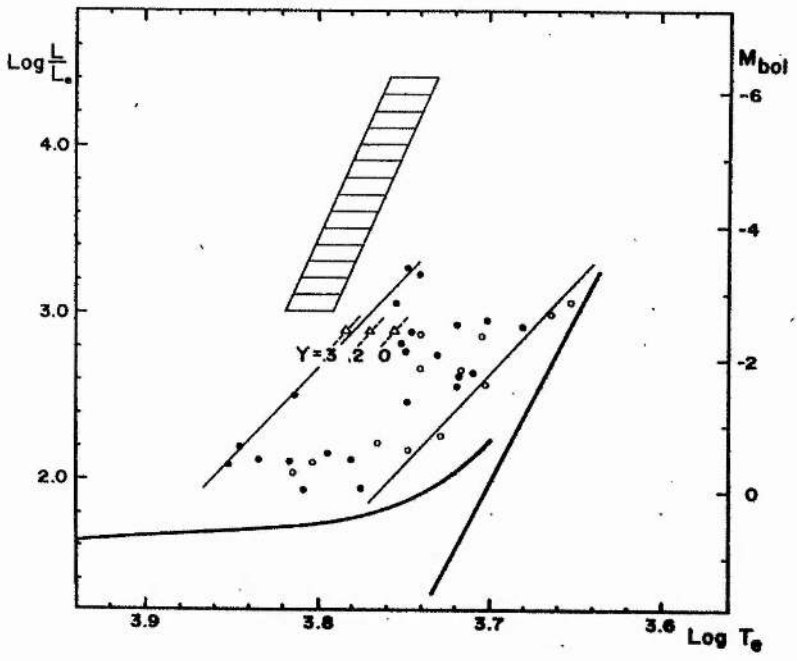

Figure 1-5. Shows theoretical HR diagram for Pop II Cepheids. The shaded region is the Pop I Cepheid instability strip. Also Shown are the theoretical models for the blue edge of the Pop II strip, with three different He abundance as indicated. Also shown the two distinction group W Vir and BL Her. Cluster variables are shown by dots and field variables by circles. (Demers and Harris 1974, Figure 2).

Most of the short period (BL Her) Pop II Cepheids show similar light curves in shape. The following characteristics can be seen in most of BL Her light curves, a steep rising branch, a pronounced maximum, a secondary hump or shoulder on the descending branch and a quite large amplitude. (see Appendix **A2** and Figure 3 in Kwee 1967 and discussion therein).

1B-3. W VIRGINIS VARIABLES:-

These variables are defined as any cepheids of Pop II with period longer than 3 days. They are the more luminous cepheids and they are identified with stars undergoing blueward loops from the second giant branch in response to He shell flashes or finally evolving to the blue as the H-burning shell near the stellar surface (Gingold 1976).

The W Vir variables - as we have seen - are considered to be the Pop II counterparts of the classical cepheids, see Figure 1-1 and table 1-1. Some of them exhibit RV Tau type behaviour (Clement *et al.* 1988).

These variables are AGB stars that undergo blue loops in response to He-shell flashes. Models with envelope mass less than $0.22\ M_{sun}$ loop enough to the blue to reach the instability strip (Clement *et al.* 1988). Depending on the envelope mass, the star may enter the instability strip several times as a result of the adjustments between the two shells - Hydrogen and Helium burning shells - (Gingold 1976). The time spent in the instability strip varies inversely with mass and independently of Y, in the range $20\times10^4 - 4\times10^4$ years (Kraft 1972, Gingold 1976).

The period range, say from 2-45 days, is roughly the same as for the classical cepheids. Most W Vir variables, however, have periods within the range of 2-20 days. They are high velocity objects and lie at great distances from the galactic plane (more than about 200-300 Parsecs, see for example Strohmeier 1972, Cox 1974) . Many of W Vir are found in globular clusters.

The light curves of the W Vir do not conform to the Hertzsprung relation, but they seem to be characterised by the presence of a shoulder on the descending branch, see Figure 1-6. The total magnitude range is about 1 magnitude, roughly the same as that of classical cepheids.

The radial velocity curves vary, in the same qualitative way as the RR Lyrae. A number of other qualitative similarities within velocity curves and spectral features of the latter kinds of stars suggest that qualitatively similar physical mechanisms are operative in the atmosphere of these two types of stars (Cox 1974).

The W Vir obey a period-luminosity relation, approximately parallel to and about 1.4 magnitude below the classical cepheids P-L relation, see Figure 1-7 (Cox 1974).

W Vir stars originate from a narrow mass range which is about $0.6 \pm 0.1\ M_{sun}$.

Bumps in the light curves are surely the result of a near resonance between the fundamental mode and the second overtone period (Wallerstein & Cox 1984).

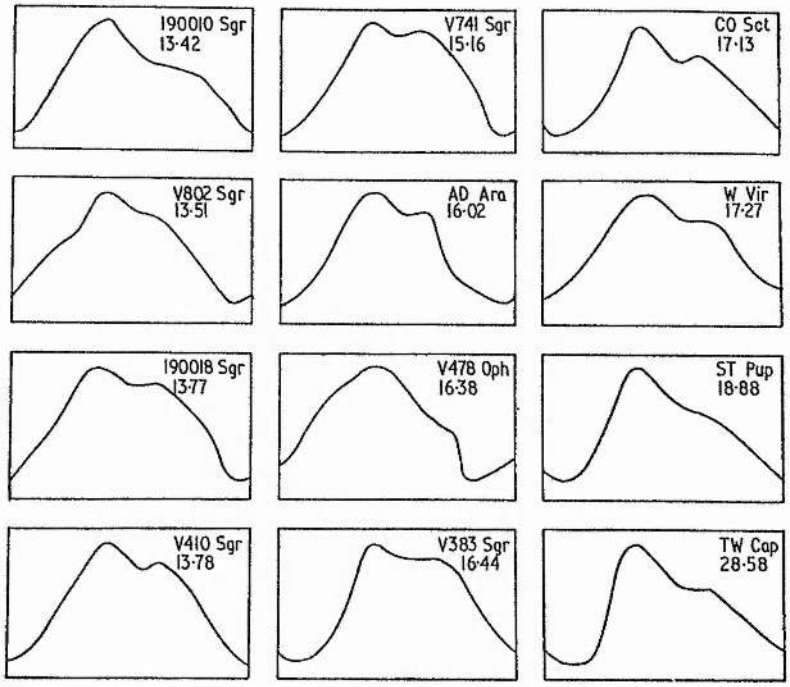

Figure 1-6. Light curves of twelve galactic W Virginis variables with star name and period (in days) indicated for each curve. Ordinates are apparent magnitude, abscissa are phase (from Cox 1974 fig. 8).

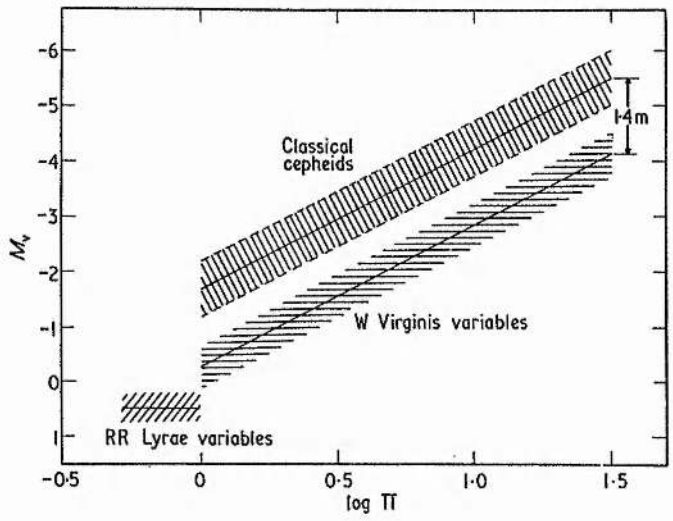

Figure 1-7. Empirical period-luminosity relation (schematic) for classical cepheids, W Virginis variables and RR Lyrae variables. Ordinate is absolute visual magnitude (from Cox 1974, fig. 9).

The relative radial excursions of W Vir are much larger than those of the classical cepheids. The radius fractional semi-amplitudes are around 0.10 - 0.30, compared to about 0.05 - 0.10 for classical cepheids, (Cox 1974).

Observations, especially of the velocity variations, of W Vir are unfortunately rather scarce. The major observation concerning velocity is that the stars with periods above 13 days have highly asymmetric velocity curves frequently accompanied by H emission lines at rise to maximum light. This is probably caused by strong outward moving shock waves (Bridger 1984).

According to the shape, the light curves of cepheids (W Vir) divide into two major classes, see Figure 1-8 :

1) Crested "C-type "; which shows a bump or standstill on descending light rather like the classical cepheids with period 5 - 10 days , Cox (1985).

2) Flat-top " F-type " sometimes has a bumps on rising light as cepheids with period 10 - 20 days, Cox (1985). The flat maximum may last for 0.3 in phase, Kwee (1967).

The C- and F- type variables occupy different positions in the H-R diagram. The crested variables are about half a magnitude brighter than the flattened one (Kwee 1968).

The mechanism for feeding stars into the Pop II instability strip at this point seem to be " blue looping " from the AGB caused by thermal instabilities in the He burning shell. As soon as the transition phase from He core-burning to He shell-burning is essentially completed and a definite narrow He shell has been found, the thermal

instability previously found to be characteristic for models with He burning shell sets in and causes the characteristic shell flashes (Schwarzschild & Harm 1970). If we make the simple assumption that metallicity varies very little, or that it has little effect on the evolution, then it is possible that a slightly higher mass star moving up the AGB executes this blue-loop at a later stage, causing the star to have a higher luminosity when passing through the instability strip producing a C-type variable (see discussions in section 1B-2). Thus we see that the C-type variables may be slightly more massive than the F-type. Assuming the two classes follow the parallel period-radius relation, which is independent of the chemical composition, then the mass ratio may be estimated as giving $Mc \sim 1.3Mf$, where Mc and Mf refer to the crested and flatted masses respectively. This fits into the range of possible masses given by Bohm-Vitense (1974) of $0.5 < M/M_{sun} < 0.75$ (Bridger 1984).

The width of the instability strip depends on a combination of mass (increasing the mass leading to shift the blue edge to the higher temperature), luminosity (increasing the luminosity leading to shift the red edge to redder colours) and chemical composition. The red edge of the strip defined as the value of T_{eff} at which the growth rate, η, is maximum, (fractional amplitude increases per period, where $\eta \propto g^{-0.5} T_{eff}^{6}$ and g is surface gravity, Cox (1980) and Chiosi *et al.* (1992)). The growth rate of W Vir instability is very rapid because of the large luminosity to mass ratio (see for example, Davis 1974, Fadeyev 1993).

The blue edge is particularly well defined by the stars in globular clusters, while the red edge is less well defined. This maybe because differential line blanketing due to the spread in metal abundance affects the colours of the cooler stars more than the hotter ones, also maybe because of neglecting the effects of convection which are

responsible for the existence of the red edge (Wallerstein & Cox 1984, Buchler & Moskalik 1992).

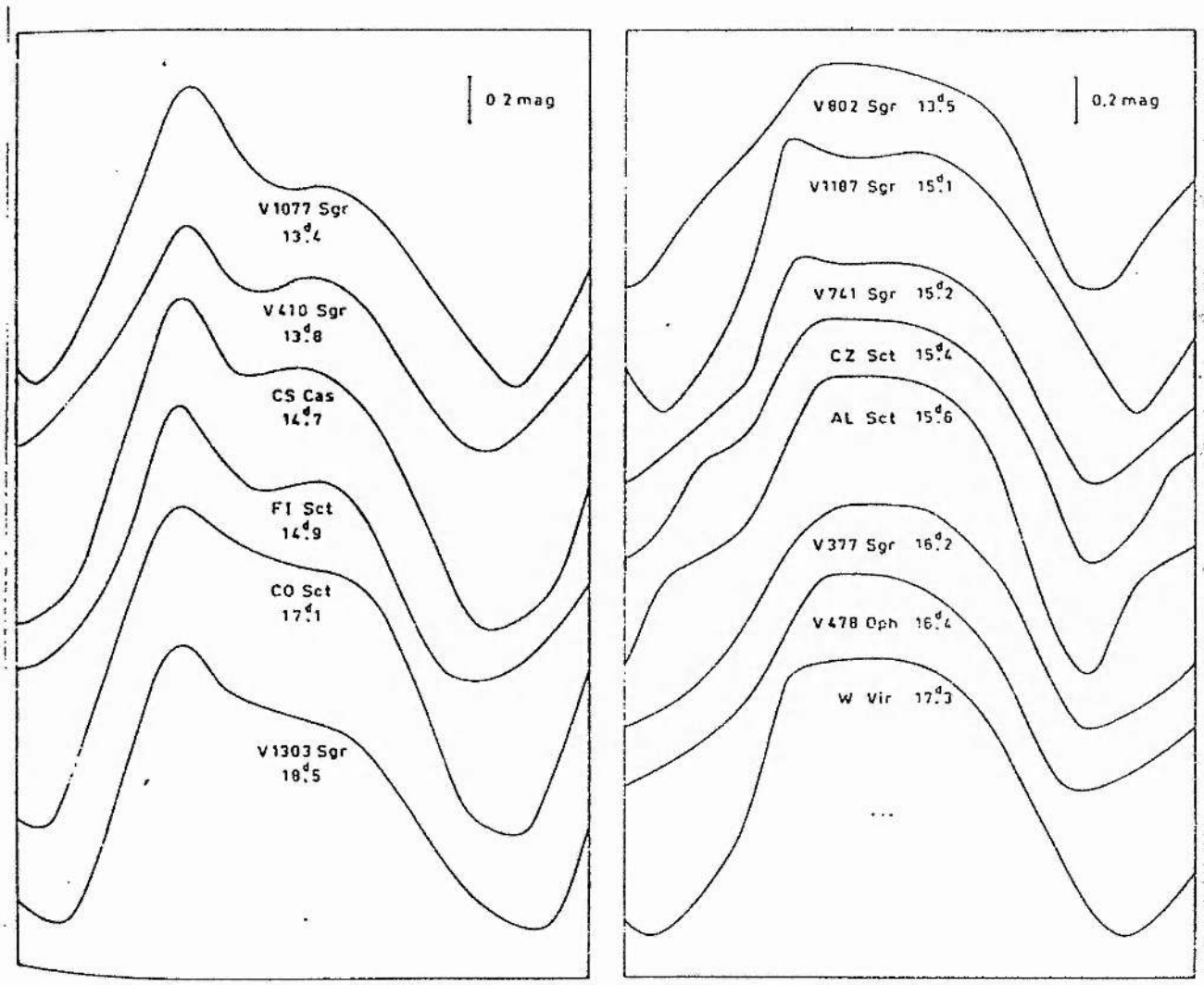

Figure 1-8. Observed Crested and Flat-toped light curves (Kwee 1967, Figures 4 and 5).

CHAPTER TWO

2-1. THE NON-LINEAR THEORY:-

Here we will mention only the non-linear approach since the linear theory is expected not to be an accurate account for the location and width of the H-R diagram, (Christy 1966, Cox 1974). The linear theory, for the sake of completeness, is briefly discussed in Appendix D.

2-1-1. THE PULSATION THEORY:-

Stars pulsate because of thermodynamic properties of their envelope material. Ionisation of H at about 10,000 K and the second ionisation of He at about 40,000 K produce destabilization by what has been called the gamma(γ) and kappa (κ) effect as these are the possible mechanisms that may cause pulsational instability in stars (Bridger 1983).

The pulsation constant Q characterise the pulsation mode of a star, and is defined as :

$$Q = P\sqrt{\bar{\rho}_* / \bar{\rho}_{sun}} \qquad (2\text{-}1)$$

where P is the period and $\bar{\rho}$ the mean density. As a function of stellar parameters, Q changes slowly for each mode, and it expresses the period-mean density relation for pulsation stars (Pijpers 1993).

The gamma effect arises from the variation in ratio of the specific heat of the gas during ionisation. If the gas in the pulsation driving layers is compressed, much of the work done on this layer is used to ionise the gas and only a small part is used to raise its temperature. During a later part of a pulsation cycle, when the gas is expanding the ionisation energy is recovered with recombination occurring the phasing of this re-emergence of energy is delayed a bit so that it actually reinforce the expansion (Keeley 1970, Wallerstein & Cox 1984).

The kappa effect, which causes a strong driving of the pulsation in the region outside the H ionisation zone, is a material property that causes destabilization of stars. In this case the energy is not hidden for part of a cycle, but it is merely blocked by the higher opacity. Energy is allowed to flow more easily during expansion, and this gives the re-expansion a push. (Keeley 1970, Wallerstein & Cox 1984).

The growth or decay rate depends on the presence of material undergoing ionisation at a sufficient mass depth to influence the flow of energy - i.e. the growth of the pulsation period correlates with both the increase of the luminosity and the decrease of the effective temperature (Fokin 1990). The blue edge of the instability strip

is set by the abundance of He. This is because, for the hotter stars, H ionisation driving is too near the stellar surface (Wallerstein & Cox 1984).

2-2. THE EQUATIONS OF STELLAR PULSATION:-

In modelling pulsating stars we have to set three assumptions which are as follows;

(1) space is Euclidean ,i.e. flat space.

(2) mass is conserved.

(3) Newtonian theory expresses the gravitation; neglect the effect of special and general relativity.

2-2-1. THE BASIC EQUATIONS:-

The derivation of the basic equations of stellar pulsation which determine the stellar structure can be found in Cox & Giuli 1968, Novotny 1973 and Kippenhahn & Weigert 1990. The equations will be listed here without the derivation. These are in Lagrangian co-ordinates (i.e. co-ordinates that move with the bulk motion of a mass element when the mass is taken as the independent variable instead of the radius). Because the physical interpretation of the equation is clearer, simpler and more straight forward in the Lagrangian than in the Eulerian description, and also removes a number of potential difficulties at the stellar surface, the Lagrangian co-ordinates has been adopted here (Deupree 1976, Cox 1980 , Kippenhahn & Weigert 1990).

The mass continuity:

$$\frac{\partial r}{\partial M_r} = \frac{1}{4\pi r^2 \rho_r} \qquad (2\text{-}2)$$

The hydrodynamic equation (equation of motion):

$$\frac{\partial^2 r}{\partial t^2} = -\frac{GM_r}{r^2} - 4\pi r^2 \frac{\partial P}{\partial M_r} \qquad (2\text{-}3)$$

Most stars are obviously in such long-lasting phases of their evolution that no changes can be observed at all. Then the stellar matter cannot be accelerated noticeably, which means that all forces acting on a given mass element of the star compensate each other. In these cases we have the hydrostatic equilibrium when, $\frac{\partial^2 r}{\partial t^2}$ is equal to zero.

The equations of mass continuity - (conservation of mass) equation 2-2 - and that of momentum - (equation of motion) equation 2-3 - determine the dynamical behaviour of the stellar envelope (Unno 1965).

The radiative energy transfer:

$$L_r = -(4\pi r^2)^2 \frac{4\sigma}{3\kappa_r} \frac{\partial (T)^4}{\partial M_r} \qquad (2\text{-}4)$$

(In some textbooks they use $a \times c$ rather than 4σ).

where:

- r : space variable (radius).
- t : time variable.
- Mr : mass enclosed within radius r.
- ρ_r : density of matter at radius r.

Lr : luminosity at radius r.

P : total pressure at radius r.

T : temperature at radius r.

κ_r : opacity at radius r.

σ : the Stefan-Boltzmann constant.

a : the radiation pressure constant $= 7.56 \times 10^{-15}\ erg\ cm^{-3}\ K^{-4}$.

The conservation of energy equation [1]:

$$\frac{\partial E}{\partial t} + P\frac{\partial V}{\partial t} = \varepsilon - \frac{\partial L}{4\pi r^2 \rho\, \partial r} = \frac{\partial Q}{\partial t} \qquad (2\text{-}5)$$

where, E : internal energy per unit mass,

V : specific volume,

ε : energy generation,

Q : heat absorbed. Not to be confused with the pulsation constant.

The alternative form of energy conservation is [2]:

---

[1] *We can write the energy equation as*

$$T\frac{\partial S}{\partial t} = \frac{\partial Q}{\partial t} = -\frac{\partial L}{\partial M_r} + \varepsilon$$

where S *and* Q *are the entropy and the specific heat respectively. First low of thermodynamics gives us* $\Delta E = Q - W$, *where* $W = PdV$ *the work done,*

$$so, \quad \frac{\partial E}{\partial t} = -\frac{\partial L}{\partial M_r} - P\frac{\partial V}{\partial t} + \varepsilon$$

[2]

$$\frac{\partial}{\partial t}\left(\frac{1}{2}\dot{r}^2-\frac{GM_r}{r}+E\right)+\frac{\partial}{\partial M_r}\left(4\pi r^2\dot{r}P+L_r\right)=0 \qquad (2\text{-}6)$$

These equations - along with formula for opacity, energy generation and equation of state and suitable boundary conditions - can be solved for the radial pulsation. Practical difficulties remains in the inclusion of convection in pulsation calculation. Convection means an exchange of energy between hotter and cooler layers in

---

$$\frac{\partial^2 r}{\partial t^2}=-\frac{GM_r}{r^2}-4\pi r^2\frac{\partial P}{\partial M_r}$$

$$\frac{\partial}{\partial t}\left(\tfrac{1}{2}\dot{r}^2-\frac{GM_r}{r}\right)=-4\pi r^2\dot{r}\frac{\partial P}{\partial M_r} \qquad ;\dot{r}=\frac{\partial}{\partial t}$$

$$-4\pi r^2\dot{r}\frac{\partial P}{\partial M_r}=-\frac{\partial}{\partial M_r}\left(4\pi r^2\dot{r}P\right)+P\frac{\partial}{\partial M_r}\left(4\pi r^2\dot{r}\right)$$

$$P\frac{\partial}{\partial M_r}\left(4\pi r^2\dot{r}\right)=P\frac{\partial}{\partial M_r}\left(\tfrac{4}{3}\pi r^3\frac{\partial}{\partial t}\right)$$

$$=P\frac{\partial}{\partial t}\frac{\partial}{\partial M_r}\left(\tfrac{4}{3}\pi r^3\right)$$

$$=P\frac{\partial}{\partial t}\,4\pi r^2\frac{\partial r}{\partial M_r}$$

$$=P\frac{\partial}{\partial t}\,\frac{1}{\rho}=P\frac{\partial V}{\partial t}$$

$\therefore$

$$-4\pi r^2\dot{r}\frac{\partial P}{\partial M_r}=-\frac{\partial}{\partial M_r}\left(4\pi r^2\dot{r}P\right)+P\frac{\partial V}{\partial t}$$

$$\frac{\partial E}{\partial t}=-P\frac{\partial V}{\partial t}-\frac{\partial L}{\partial M_r}$$

$$\therefore\quad \frac{\partial}{\partial t}\left(\tfrac{1}{2}\dot{r}^2-\frac{GM_r}{r}+E\right)=-\frac{\partial P}{\partial M_r}\left(4\pi r^2\dot{r}P+L_r\right)=0$$

a dynamically unstable region through the exchange of macroscopic mass elements, the hotter of which move upwards while the cooler ones downward. The moving mass element will finally dissolve in their new surroundings and thereby deliver their excess - or deficiency - of heat. Owing to the high density in stellar interiors, convective transport can be very efficient. However, this energy transfer can operate only if it finds a sufficient driving mechanism in the form of the buoyancy forces. Convection and pulsation tend to be mutually destructive phenomena. Rapid thermal alterations arising from pulsation may tend to prevent convection from becoming firmly established, while convection may conspires to quench pulsation by altering the thermal structure of the H ionisation region in a certain manner. This would imply that convection is relatively unimportant except when close to the red edge (i.e. convection is able to quench the pulsation at relatively low pulsation amplitudes). By ignoring the convection the light and velocity curves are relatively unchanged (Christy 1966, Clayton 1968, Deupree 1977**a**, **b**, Buchler 1990). Neglect also of rotation and magnetic fields means that the only forces acting on a mass element come from pressure and gravity. We also assume that the diffusion approximation for energy transfer by radiation holds throughout (Christy 1967, Clayton 1968, Strohmeier 1972, Stellingwerf 1975, Bridger 1983, Kippenhahn & Weigert 1990).

It is assumed that only the stellar envelope takes part of the pulsation, where there is no energy generation, and where we must include a realistic opacity law and an equation of state that includes ionisation, since these properties are basic to the existence of pulsation instability. For most problems, the central core of the star can be ignored. We believe that this region plays very little part in the pulsation.

The linear adiabatic theory showed that the amplitude of the pulsation motion decreases very rapidly toward the stellar interior due to a rapid increase in density toward the centre, therefore we ignore the nuclear energy sources near the centre. In this case the energy generation, $\mathcal{E}$, equation 2-5, can be put equal to zero - i.e. the nuclear

energy generation on the right hand side of the heat flow equation. (see for example, Christy 1967, Bridger 1983 and Milligan 1989). Thus:

$$\frac{\partial E}{\partial t}+P\frac{\partial V}{\partial t}=-\frac{\partial L}{4\pi r^2\rho\,\partial r}=-\frac{\partial L}{\partial M} \qquad (2\text{-}7)$$

2-2-2. THE BOUNDARY CONDITIONS:-

The inner boundary is chosen such that the radius of the innermost zone in the pulsation calculation is fixed at its equilibrium value which is

$$R_{(inner)}=\textbf{constant}. \qquad (2\text{-}8)$$

Thus, only the stellar envelope participates in the pulsation, this means that the luminosity and composition are constant in the initial model (Christy 1967, Bridger 1983), since the core is assumed to be non-pulsating while radiating a constant luminosity. Thus, at the inner radius

$$\frac{\partial r}{\partial t}=0 \qquad (2\text{-}9)$$

and

$$L_{(R_{inner})}=L_0 \qquad (2\text{-}10)$$

At the inner boundary the velocity is zero at all times and the luminosity is a constant (i.e. the core luminosity).

At the surface of the star we can see two boundary conditions, either:

$$P_{(tot-surface)}=P_{(rad-surface)} \qquad (2\text{-}11)$$

or

$$P_{(tot-surface)} = 0 \qquad \textbf{(2-12)}$$

Dr. Carson used the second one in his program, where

$P_{(tot)}$ is the total pressure.

$P_{(rad)}$ is the radiation pressure which should be described by the time-dependent radiative transport equation. This is not possible, because it requires knowledge of the state of gridpoints several mean free path lengths away. Therefore, the radiative boundary condition is chosen to approximate the results of diffusion theory. The radiation pressure is important only at high temperatures (Clayton 1968, Milligan 1989). By using the Eddington approximation[3], this can be expressed as

$$\left[\frac{d\ (T)^4}{d\ \tau}\right]_{surface} = \frac{3}{4}\ T_{eff}^4 = \frac{3}{2}\ T_s^4 \qquad \textbf{(2-13)}$$

where :

T_{eff} ; effective temperature.

T_s ; surface temperature.

τ ; optical depth.

---

[3]*The Eddington or simply the T-τ approximation is defined as follows*

$$T_s^4 = \frac{3}{4}\ T_{eff}^4 (\tau + 2/3)$$

CHAPTER THREE

3-1. THE METHOD OF SOLUTION:-

Equations 2-2, 2-3, 2-4 and 2-7 are treated as an initial value problem, to be integrated from initial conditions. In order to follow the non-linear behaviour of the model, it is necessary to put these equations in difference form, in a stellar envelope of about 50 mass zones. This procedure is described in Christy (1967). In our work, we will follow the same procedure as Milligan did in her Ph.D. thesis (1989). We will use a program written by Dr T. R. Carson. Some of the main features of this program are given here for the sake of completeness.

The first step is to integrate a static model and divide it up to 50 zones. The program allows two methods of division. One is simply zoning by mass, since we see the mass in each successively deeper zone is greater than the last by a constant, or equal sound travel time. Both of them gives us good results but the second one is faster which is the one that has been adopted. In both cases the mass remains in each zone constant with the time as the non-linear proceeds.

The boundary between each zone is labelled i, where $i = 1$ is the innermost zone, and $i = N$ the outermost. The centre of each zone is labelled $i - ½$. The radius is taken at the boundary. Therefore, R_i^n would be the radius of boundary i at time t^n, where n specifies the time-step. The mass of the zone, $\Delta M_{i-½}$,and the mass at the boundary, ΔM_i , are both useful quantities and are defined as follows:

$$\Delta M_{i-½} = M_i - M_{i-1} \quad \text{; mass of the zone} \qquad \textbf{(3-1)}$$

$$\Delta M_i = \frac{1}{2}\left(\Delta M_{i-½} + \Delta M_{i+½}\right) \quad \text{; mass of the boundary} \qquad \textbf{(3-2)}$$

and the specific volume V of the zone :

$$V_{i-½}^n = \frac{4\pi}{3}\,\frac{(R_i^n)^3 - (R_{i-1}^n)^3}{\Delta M_{i-½}} \qquad \textbf{(3-3)}$$

The re-zoned model extends inwards to about 0.1 R - outside nuclear energy producing region, where luminosity is constant and has a small amplitude of pulsation. We have now relaxed this envelope onto the same difference equations as used in the pulsation analysis, otherwise problems would arise in the pulsation calculations. The relaxation is achieved by an iterative scheme, which calculates $P_{N-½}$ and R_{N-1} from the outer boundary condition, then, for all $N - 1$ zones, it calculates $P_{i-½}$ from R_i and $P_{i+½}$. Using the equation of hydrostatic equilibrium in its difference form, it would work out temperature and density, obtains a value for R_{i-1}, and compares that value with the stored one. If the corrections to the values of R are more than a certain limit, the iteration is repeated. When the corrections are sufficiently small, the non-linear analysis can proceed (Milligan 1989).

Velocity U is taken at time $n + ½$ for best centring in time. Thus, the radius at the new time $n + 1$ is given by:

$$R_i^{n+1} = R_i^n + \Delta t^{n+½}\, U_i^{n+½} \tag{3-4}$$

where:

$$R_i^{n+½} = \Delta t^{n+½}\, U_i^{n+½} \tag{3-5}$$

$$\Delta t^{n+½} = t^{n+1} - t^n \tag{3-6}$$

$$\Delta t^n = t^{n+½} - t^{n-½} \tag{3-7}$$

where $\Delta t^{n+½}$ is not necessarily the same as Δt^n. The program changes the time-step as it process, in order to facilitate convergence. The first time step is usually the most stringent, so the time-step must be less than the time for sound to traverse any zone (Bridger 1983). Therefore,

$$\Delta t^{n+½} < \frac{\Delta R}{\sqrt{P_{i-½} V_{i-½}}} \tag{3-8}$$

where the square root is of the order of the mean velocity of sound on the stellar interior.

During the pulsation a shock wave develops, which can cause a rapid compression (but not an expansion), of some zones particularly in the H ionisation region. Therefore, we have to add an artificial viscosity pressure, which acts as an extra pressure which enabling the shock front to be spread over several zones, thus, improving the stability. A large C_Q makes a thicker shock front but greater stability (Christy 1967). This is:

$$Q_{i-\frac{1}{2}}^{n-\frac{1}{2}} = C_Q \; P_{i-\frac{1}{2}}^{n-\frac{1}{2}} \left[Min \left(\frac{U_i^{n-\frac{1}{2}} - U_{i-1}^{n-\frac{1}{2}}}{\sqrt{P_{i-\frac{1}{2}}^{n-\frac{1}{2}} \; V_{i-\frac{1}{2}}^{n-\frac{1}{2}}}} + \psi \;, 0 \right) \right]^2 \qquad \textbf{(3-9)}$$

where superscripts refer to time and subscripts to zone, and ψ is of the order of **0.1**. Stellingwerf (1975) found that when $\psi = 0$ we get a damping in the lower region of the envelope. As ψ gets larger the time steps gets bigger and the amplitudes are up to 50% higher than those indicated by the observation (Kovacs 1990).

We can now write the equation of pulsation in difference form, and consider the boundary condition on them. The equation of hydrodynamic equilibrium, 2-3 , can be written as:

$$U_i^{n+\frac{1}{2}} = U_i^{n-\frac{1}{2}} - \Delta t^n \left\{ \frac{GM_i}{(R_i^n)^2} + \frac{4\pi \; (R_i^n)^2}{\Delta M_i} \left[P_{i+\frac{1}{2}}^n - P_{i-\frac{1}{2}}^n + Q_{i+\frac{1}{2}}^{n-\frac{1}{2}} - Q_{i-\frac{1}{2}}^{n-\frac{1}{2}} \right] \right\} \qquad \textbf{(3-10)}$$

The boundary value of this is as follow:

Inner:

$$U_1^{n+\frac{1}{2}} = 0 \qquad \textbf{(3-11)}$$

since there is no motion considered in the interior of a star.

Outer:

$$U_N^{n+½} = U_N^{n-½} - \Delta t^n \left\{ \frac{GM_N}{(R_N^n)^2} + \frac{4\pi (R_N^n)^2}{\Delta M_N} \left[-2\left(P_{N-½}^n - \frac{aW_{N-½}^n}{3}\right) - Q_{N-½}^{n-½} \right] \right\}$$

(3-12)

where W is T^4. The expression for the outer boundary condition is obtained by defining some fictitious pressure, $P_{N-½}^n$, beyond the outer surface of the star.

For a zero surface gas pressure we have:

$$P_{rad_N}^n = \frac{1}{2}\left(P_{N+½}^n + P_{N-½}^n \right) \quad \textbf{(3-13)}$$

$$P_{N+½}^n = 2P_{rad_N}^n - P_{N-½}^n \quad \textbf{(3-14)}$$

$$P_{N+½}^n - P_{N-½}^n = \frac{2}{3} aW_{N-½}^n - 2P_{N-½} \quad \textbf{(3-15)}$$

since the atmosphere is almost isothermal. Then we can write with a good approximation (about 1% Bridger 1983)

$$P_{rad_N}^n = \frac{1}{3} aW_{N-½}^n \quad \textbf{(3-16)}$$

where $P_{(rad)}$ is the radiation pressure at the surface.

Bridger also adopted mass zones increasing inwards by a constant factor α (the Carson non-linear code which has been adopted -as mentioned earlier- incorporating mass zones of equal sound travel). Hence for consistency he used

$$\Delta M_N = \frac{1+\alpha}{2\alpha} \Delta M_{N-½} \quad \textbf{(3-17)}$$

where,

$$\alpha = \frac{\Delta M_{N-1/2}}{\Delta M_{N+1/2}} \qquad (3\text{-}18)$$

$$\Delta M_N = \frac{1}{2}\left(\Delta M_{N+1/2} + \Delta M_{N-1/2}\right) \qquad (3\text{-}19)$$

The radiative energy transfer equation, 2-4 , becomes:

$$L_i^n = \left[4\pi \left(R_i^n\right)^2\right]^2 \left[W_{i-1/2}^n - W_{i+1/2}^n\right] 2F_i^n \qquad (3\text{-}20)$$

where $2F_i^n$ is a suitable difference form of $4\sigma/3\kappa\Delta M$.

Then:

$$F_i^n = \frac{4\sigma}{3} \frac{1}{\kappa_{i+1/2}^n \Delta M_{i+1/2} + \kappa_{i-1/2}^n \Delta M_{i-1/2}} \qquad (3\text{-}21)$$

Christy (1967) found that using this relation in the iteration of the heat equation failed to converge when the front was advancing outward with large amplitude. This is because this relation can not handle the large change in opacity across a zone that occurs in such cases. It gives too little weight to the larger opacity, that means , to minimise the error produced by the use of very coarse zoning in the region of H ionisation (Castor 1971, Bridger 1983). Therefore Christy developed a new difference expression for ***F***. Thus:

$$F_i^n = \frac{4\sigma}{3}\left[\frac{W_{i+1/2}^n}{\kappa_{i+1/2}^n} + \frac{W_{i-1/2}^n}{\kappa_{i-1/2}^n}\right] \Big/ \left\{\left[\Delta M_{i+1/2}^N + \Delta M_{i-1/2}^N\right]\left[W_{i+1/2}^N + W_{i-1/2}^N\right]\right\} \qquad (3\text{-}22)$$

$\kappa_{i+1/2}$ is the opacity in cm^2/gm at $i + 1/2$.

We can now write the energy equation, 2-5 , in difference form

$$\{E^{n+1}_{i+½} - E^{n}_{i+½} + [\frac{1}{2}\ (\ P^{n}_{i+½} + P^{n+1}_{i+½}) + Q^{n+½}_{i+½}\ ][V^{n+1}_{i+½} - V^{n}_{i+½}]\}\ \Delta M_{1+½}$$

$$= \frac{\Delta t^{n+½}}{2}\ [L^{n+1}_{i} + L^{n}_{i} - L^{n+1}_{i+1} - L^{n}_{i+1}]$$

(3-23)

This is solved at each time step, by a process of iteration, which is subject to the inner and outer boundary conditions. Since no energy generation takes place in the pulsation envelope (i.e. the energy generation equal to zero). The inner boundary conditions imply that the luminosity of the innermost zone is equal to the total luminosity of the model. Thus at $i = 1$ we can determine $W^{n+1}_{½}$,thus [1]:

$$L^{n+1}_{1} = [4\pi\ (R^{n+1}_{1})^{2}]^{2}[W^{n+1}_{½} - W^{n+1}_{3/2}]2F^{n+1}_{1} = L_{0} \qquad \textbf{(3-24)}$$

where L_0 is the mean luminosity.

The outer boundary condition makes use of the Eddington approximation. The surface luminosity is given by:

---

[1]

$flux = \frac{L}{4\pi r^2}$

$L = -4\pi r^2 \frac{3}{4}\frac{\sigma}{\rho\kappa}\frac{d(T)^4}{dr} = -(4\pi r^2)^2 \frac{3}{4}\frac{\sigma}{\kappa}\frac{d(T)^4}{dM}$

$\frac{dM}{dr} = 4\pi r^2 \rho$

$L = -(4\pi r^2)^2[\frac{4}{3}\frac{\sigma}{\kappa}\frac{\Delta W}{\Delta M}] = -(4\pi r^2)^2[\Delta W]2F$

$so,\ 2F = \frac{4}{3}\frac{\sigma}{\kappa}\frac{1}{\Delta M}$

$let,\ H = 2F\Delta W = \frac{4}{3}\frac{\sigma}{\kappa}\frac{\Delta W}{\Delta M}$

$so,\ L = (4\pi r^2)^2 H = (4\pi r^2)^2 \Delta W 2F$

$\therefore flux = \frac{L}{4\pi r^2} = (4\pi r^2)H$

$$L_s = 4\pi (R_{phot.})^2 \, 2\sigma T_s^4 \tag{3-25}$$

Therefore we have to determine $R_{phot.}$, which is the radius at which the temperature is equal to the effective temperature, T_{eff} . Bridger (1983) found that R_N and R_{N-1} might be unreliable in some model. Now we can write down the outer boundary condition:

$$\{E^{n+1}_{N-½} - E^{n}_{N-½} + [\frac{1}{2}(P^{n}_{N-½} + P^{n+1}_{N-½}) + Q^{n+1}_{N-½}][V^{n+1}_{N-½} - V^{n}_{N-½}]\} \Delta M_{N-½}$$

$$= \frac{\Delta t^{n+½}}{2} \{L^{n+1}_{N-1} + L^{n}_{N-1} - 2\sigma \; 4\pi [(R^{n}_{phot.})^2 W^{n}_{N-½} + (R^{n+1}_{phot.})^2 W^{n+1}_{N-½}]\}$$

(3-26)

Equation 3-23 can now be solved for new temperature $W^{n+1}_{i-½}$ by using a Newton-Raphson iteration method. Thus we can do by making a linear expansion of the various terms in the difference equations and solve each step of the iteration procedure. Let a superscript prefix denote the number of the iteration, and let $\Delta W^{n+1}_{i+½}$ be the correction to the temperature at each iteration **i**:

$${}^{i}\Delta W^{n+1}_{i+½} = {}^{i+1}W^{n+1}_{i+½} - {}^{i}W^{n+1}_{i+½} \tag{3-27}$$

then we have:

$${}^{i+1}P^{n+1}_{i+½} = {}^{i}P^{n+1}_{i+½} + \frac{{}^{i}\partial P^{n+1}}{\partial W_{i+½}} \, {}^{i}\Delta W^{n+1}_{i+½} \tag{3-28}$$

$${}^{i+1}E^{n+1}_{i+½} = {}^{i}E^{n+1}_{i+½} + \frac{{}^{i}\partial E^{n+1}}{\partial W_{i+½}} \, {}^{i}\Delta W^{n+1}_{i+½} \tag{3-29}$$

$$ {}^{i+1}F_i^{n+1} = {}^{i}F_i^{n+1} + \frac{{}^{i}\partial F_i^{n+1}}{\partial W_{i+½}} {}^{i}\Delta W_{i+½}^{n+1} + \frac{{}^{i}\partial F_i^{n+1}}{\partial W_{i-½}} {}^{i}\Delta W_{i-½}^{n+1} \quad \textbf{(3-30)} $$

$$ {}^{i+1}L_i^{n+1} = \left[4\pi \left(R_i^{n+1}\right)^2\right]^2 \left[W_{i-½}^{n+1} - W_{i+½}^{n+1}\right] 2 F_i^{n+1} \quad \textbf{(3-31)} $$

When equations 3-27 to 3-31 are substituted into the difference form of the energy equation, 3-23 , we get:

$$ -\alpha_{i+½} {}^{i}\Delta W_{i+½}^{n+1} + \beta_{i+½} {}^{i}\Delta W_{i+½}^{n+1} - \gamma_{i+½} {}^{i}\Delta W_{i-½}^{n+1} = \delta_{i+½} \quad \textbf{(3-32)} $$

where:

$$ \alpha_{i+½} = \Delta t^{n+½} \left[A_{i+1}^{n+1}\right]^2 \left\{ {}^{i}F_{i+1}^{n+1} - \frac{{}^{i}\partial F_{i+1}^{n+1}}{\partial W_{i+½}} \left[{}^{i}W_{i+½}^{n+1} - {}^{i}W_{i+½}^{n+1} \right] \right\} \quad \textbf{(3-33)} $$

$$ \beta_{i+½} = \left\{ \frac{{}^{i}\partial E^{n+1}}{\partial W_{i+½}} + \frac{1}{2} \frac{{}^{i}\partial P^{n+1}}{\partial W_{i+½}} \left[V_{i+½}^{n+1} - V_{i+½}^{n}\right] \right\} \Delta M_{i+½} + \alpha_{i-½} + \gamma_{i+3/2} \quad \textbf{(3-34)} $$

$$ \gamma_{i+½} = \Delta t^{n+½} \left[A_i^{n+1}\right]^2 \left\{ {}^{i}F_i^{n+1} + \frac{\partial F_i^{n+1}}{\partial W_{i-½}} \left[{}^{i}W_{i-½}^{n+1} - {}^{i}W_{i+½}^{n+1} \right] \right\} \quad \textbf{(3-35)} $$

$$ \delta_{i+½} = \frac{\Delta t^{n+½}}{2} \left[{}^{i}L_i^{n+1} + L_i^{n} - {}^{i}L_{i+1}^{n+1} - L_i^{n} \right] - \Delta M_{i+½} \left\{ {}^{i}E_{i+½}^{n+1} - E_{i+½}^{n} + \left[\frac{1}{2} \left(P_{i+½}^{n} + {}^{i}P_{i+½}^{n+1} \right) + Q_{i+½}^{n+½} \right] \left[V_{i+½}^{n+1} - V_{i+½}^{n} \right] \right\} \quad \textbf{(3-36)} $$

$$A_i^{n+1} = 4\pi \left(R_i^{n+1}\right)^2 \qquad \textbf{(3-37)}$$

Equation 3-32 is a matrix equation of the form $\underline{M}\ \underline{X} = \underline{D}$, where $\underline{M}$ is a tridiagonal matrix with elements α, β and γ, $\underline{X}$ is the solution matrix containing new values of ${}^{i+1}\Delta W_{i+\frac{1}{2}}^{n+1}$ and $\underline{D}$ is a column matrix with elements δ. The equation can be solved using a standard technique.

Equations 3-33 to 3-37 provide most of the elements of matrix $\underline{M}$. The boundary conditions give the following values for the remaining elements:

$$\alpha_{\frac{1}{2}} = 2\left(A_1^{n+1}\right)^2 \left\{ {}^{i}F_1^{n+1} - \frac{{}^{i}\partial F_1^{n+1}}{\partial W_{\frac{3}{2}}} \left[{}^{i}W_{\frac{1}{2}}^{n+1} - {}^{i}W_{\frac{3}{2}}^{n+1} \right] \right\} \qquad \textbf{(3-38)}$$

$$\beta_{\frac{1}{2}} = 2\left(A_1^{n+1}\right)^2 \left\{ {}^{i}F_1^{n+1} + \frac{{}^{i}\partial F_1^{n+1}}{\partial W_{\frac{1}{2}}} \left[{}^{i}W_{\frac{1}{2}}^{n+1} - {}^{i}W_{\frac{3}{2}}^{n+1} \right] \right\} \qquad \textbf{(3-39)}$$

$$\gamma_{\frac{1}{2}} = 0 \qquad \textbf{(3-40)}$$

$$\delta_{\frac{1}{2}} = 2\left(A_1^{n+1}\right)^2 \left\{ {}^{i}F_1^{n+1} \left[{}^{i}W_{\frac{1}{2}}^{n+1} - {}^{i}W_{\frac{3}{2}}^{n+1} \right] \right\} + L_0 \qquad \textbf{(3-41)}$$

$$\alpha_{N-\frac{1}{2}} = 0 \qquad \textbf{(3-42)}$$

$$\beta_{N-\frac{1}{2}} = \Delta t^{n+\frac{1}{2}} \left\{ \left(A_{N-1}^{n+1}\right)^2 \left[{}^{i}F_{N-1}^{n+1} - \frac{{}^{i}\partial F_{N-1}^{n+1}}{\partial W_{N-\frac{1}{2}}} \left({}^{i}W_{N-\frac{1}{2}}^{n+1} - {}^{i}W_{N-\frac{1}{2}}^{n+1} \right) \right] \right\} + \sigma A_{phot.}^{n+1} \qquad \textbf{(3-43)}$$

$$\gamma_{N-\frac{1}{2}} = \Delta t^{n+\frac{1}{2}} \left\{ (A_{N-1}^{n+1})^2 \left[{}^{i}F_{N-1}^{n+1} + \frac{{}^{i}\partial F_{N-1}^{n+1}}{\partial W_{N-\frac{3}{2}}} ({}^{i}W_{N-\frac{3}{2}}^{n+1} - {}^{i}W_{N-\frac{1}{2}}^{n+1}) \right] \right\}$$

(3-44)

$$\delta_{N-\frac{1}{2}} = \frac{\Delta t^{n+\frac{1}{2}}}{2} \left[L_{N-1}^{n} + {}^{i}L_{N-1}^{n+1} - 2\sigma \left(A_{phot.}^{n} W_{N-\frac{1}{2}}^{n} + {}^{i}A_{phot.}^{n+1} W_{N-\frac{1}{2}}^{n+1} \right) \right] - \Delta M_{N-\frac{1}{2}}$$

$$\left\{ {}^{i}E_{N-\frac{1}{2}}^{n+1} - E_{N-\frac{1}{2}}^{n} + \left[\frac{1}{2} (P_{N-\frac{1}{2}}^{n} + {}^{i}P_{N-\frac{1}{2}}^{n+1}) + Q_{N-\frac{1}{2}}^{n+\frac{1}{2}} \right] \left[V_{N-\frac{1}{2}}^{n+1} - V_{N-\frac{1}{2}}^{n} \right] \right\}$$

(3-45)

To solve the matrix, we look for two sets of equations $X_{i+\frac{1}{2}}$ and $Y_{i+\frac{1}{2}}$ such that

$$\Delta W_{i+\frac{1}{2}}^{n+1} = X_{i+\frac{1}{2}} \Delta W_{i+\frac{3}{2}}^{n+1} + Y_{i+\frac{1}{2}} \qquad \textbf{(3-46)}$$

then

$$\Delta W_{i-\frac{1}{2}}^{n+1} = X_{i-\frac{1}{2}} \Delta W_{i+\frac{1}{2}}^{n+1} + Y_{i-\frac{1}{2}} \qquad \textbf{(3-47)}$$

Substituting 3-47 into 3-32 and dropping time superscripts, we get:

$${}^{i}\Delta W_{i-\frac{1}{2}}^{n+1} = \frac{\alpha_{i+\frac{1}{2}}}{\beta_{i+\frac{1}{2}} - \gamma_{i+\frac{1}{2}} X_{i-\frac{1}{2}}} {}^{i}\Delta W_{i+\frac{3}{2}} + \frac{\delta_{i+\frac{1}{2}} + \gamma_{i+\frac{1}{2}} Y_{i-\frac{1}{2}}}{\beta_{i+\frac{1}{2}} - \gamma_{i+\frac{1}{2}} X_{i-\frac{1}{2}}} \qquad \textbf{(3-48)}$$

So we obtain:

$$X_{i+\frac{1}{2}} = \frac{\alpha_{i+\frac{1}{2}}}{\beta_{i+\frac{1}{2}} - \gamma_{i+\frac{1}{2}} X_{i-\frac{1}{2}}} \qquad \textbf{(3-49)}$$

and

$$Y_{i+½} = \frac{\delta_{i+½} + \gamma_{i+½} Y_{i-½}}{\beta_{i+½} - \gamma_{i+½} X_{i-½}} \qquad (3\text{-}50)$$

So starting at $i = 1$, all of $X_{i+½}$ and $Y_{i+½}$ can be calculated from 3-49 and 3-50. At the surface $\alpha_{N-½} = 0$, i.e. $X_{N-½}$ is zero, therefor,

$$^{i}\Delta W_{N-½} = Y_{N-½} \qquad (3\text{-}51)$$

so all the $^{i}\Delta W_{N+½}$ can be found from 3-48. Iteration proceeds until the temperature correction terms are as small as is desired.

3-2. THE EQUATION OF STATE:-

In order to solve the stellar structure equations it is necessary to have an equation expressing the relation between P, T and ρ , and to have available values of entropy per unit mass, S, and internal energy, E, for the stellar material. Here the stellar envelope is assumed to be homogeneous and the radiation pressure is constant.

Let A_i be the atomic mass of element i, β_i be the abundance by mass of element i, α_i be the abundance by number of element i, and μ be the mean molecular weight, thus:

$$\alpha_i = \frac{\beta_i / A_i}{\sum_{i=1}^{all} \beta_i / A_i} = \mu \beta_i / A_i \qquad (3\text{-}52)$$

$$\mu = \frac{1}{\sum_{i=1}^{all} \beta_i / A_i} \qquad (3\text{-}53)$$

The quantity N may not be known, depending on whether the pressure or density is known. If P is known then $N = P_g / KT$, where $N_n = N - N_e$, $P_g = P_{ion} + P_e$. If the density is known then $N_n = N_o \rho / \mu$ .Where the number density of element i is given by:

$$N_i = \frac{N_0 \rho \alpha_i}{\mu} \qquad (3\text{-}54)$$

where:

N_o is Avogadro's number, and K is Boltzmann constant.

If we let N_{ij} be the number density of element i in ionisation stage j, and N_e be the electron density. Then, the electron number density is given by:

$$N_e = \sum_{i=1}^{all} \sum_{j=1}^{all} j \; N_{ij}(N_e, T) \qquad (3\text{-}55)$$

This expression is non-linear in N_e which can be solved by iteration.

If the formation of molecules is ignored, we can write the following expression:

$$P = P_{ion} + P_e + P_r \tag{3-56}$$

where :

the radiation pressure is

$$P_r = \frac{1}{3} a T^4 , \tag{3-57}$$

the electron pressure is

$$P_e = N_e K T , \tag{3-58}$$

the ion pressure is

$$P_{ion} = N_n K T \tag{3-59}$$

N_e ;the electron number density

N_n ;the nuclei number density

N ;the total number density of all particles

$$N = N_e + N_n \tag{3-60}$$

The prefix '***ion***' denotes the contribution from free ions which remains to be calculated.

To find the number density N_{ij} of element ***i*** in ionisation state ***j***, we can use Saha's equation:

$$\frac{N_{ij}}{N_i} = \frac{\prod_{j=\omega_i}^{J_i-1} N_e \Phi_{ij}(T)}{\sum_{i=1}^{all} \left[\prod_{j=\omega_i}^{J_i-1} N_e \Phi_{ij}(T) \right]} \qquad \textbf{(3-61)}$$

in which we have:

$$\Phi_{ij}(T) = \frac{N_{ij}}{N_{ij+1} N_e} = \frac{1}{2} \frac{\beta_{ij}}{\beta_{ij+1}} \left[\frac{h^2}{2\pi m_e KT} \right]^{3/2} \exp\left(\chi_{ij} / KT \right) \qquad \textbf{(3-62)}$$

$$\beta_{ij} = \frac{g_i!}{(g_i - p_i)! p_i!} \qquad \textbf{(3-63)}$$

where,

J_i ; the highest ionisation state of element ***i*** .

β_{ij} ; the partition function for the ionic species(***ij***).

g_{ij} ; the statistical weight of the outer shell.

p_{ij} ; the number of electrons in the outermost shell.

χ_{ij} ; the ionisation energy.

h ; the Planck constant.

m_e ;the electron mass.

The total number density of free ions is given by:

$$N_{ion} = \sum_{i=1}^{all} \sum_{j}^{J_i - 1} N_{ij} \tag{3-64}$$

the partial entropy per unit mass is:

$$S_{ion} = \frac{E_{ion}}{T} + \frac{1}{\rho T} \left[P_{ion} - \sum_{i=1}^{all} N_{ion_i} \, \eta_{ion_i} KT \right] \tag{3-65}$$

and the partial internal energy per unit mass is:

$$E_{ion} = \frac{1}{\rho} \left[\sum_{i=1}^{all} \sum_{j=\omega_i}^{J_i - 1} N_{ij} \, \chi_{ij} + \frac{3}{2} N_{ion} KT \right] \tag{3-66}$$

the total energy per unit volume is given by

$$E = E_{ion} + c_v T + aT^4 \; ; \tag{3-67}$$

$$c_v = \frac{3}{2} N_e \, K \tag{3-68}$$

then;

$$E = E_{ion} + \frac{3}{2} N_e \, KT + aT^4 \tag{3-69}$$

$$TS = P + U + \eta KT \tag{3-70}$$

in which the degeneracy factor η_{ion_i} is defined by:

$$e^{\eta_{ion\ i}} = N \Big/ \left[2\pi A_i KT \Big/ h^2\right]^2. \qquad \textbf{(3-71)}$$

The equation of state also allow for the formation of the molecules H_2, N_2 and CO, being the most abundant of the diatomic molecules. For these the abundances are readily obtained by the solution of quadratic equations since the equilibria are not coupled. The expression for the pressure and stellar thermodynamic properties are then suitably modified.

Some references that were useful here are; Christy 1967, Clayton 1968, Cox & Giuli 1968, Copeland *et al.* 1970, Bowers & Deeming 1984 , Bridger 1983 and Milligan 1989.

CHAPTER FOUR

4-1. RESULTS & DISCUSSION :-

In this work, as mentioned earlier, we have used a program code written by Dr. T. R. Carson. The input data were as follows: the star's mass, luminosity, effective temperature or radius, the hydrogen content X, helium content Y and metal content Z and number of the zones required. The results are shown in table 4-1. We have used the Iglesias and Rogers opacity tables which have been modified by Dr. Carson to include molecular opacity of lowest temperature. This work has been done using the SUN computer system at the University of St. Andrews.

In our work we have used the same parameters that were used by CS82 & CSV81 (models 1 - 20), three models from Bridger 1983 (models 31, 32 and 34), five models from Hubickyj 1983 (models 35 - 39), and the other models have been adopted by the author. Figure 4-1 shows our models in HR diagram, the observed stars - using table 1 in Bohm-Vitense *et al.* 1974 and tables 2-1a and b in Bridger 1983 -. Also shown the observed blue and red edges, equations 4-1 and 4-2 respecivly, which have been adopted from Demers & Harris 1974 (these edges only for BL Her and W Vir stars).

$$\log(L / L_{sun}) = -10.75 \log T_{eff} + 43.5 \qquad \textbf{(4-1)}$$

$$\log(L / L_{sun}) = -10.75 \log T_{eff} + 42.4 \qquad \textbf{(4-2)}$$

However, the individual stars from Demers & Harris have not been located in Figure 4-1 since the temperatures were not given numerically.

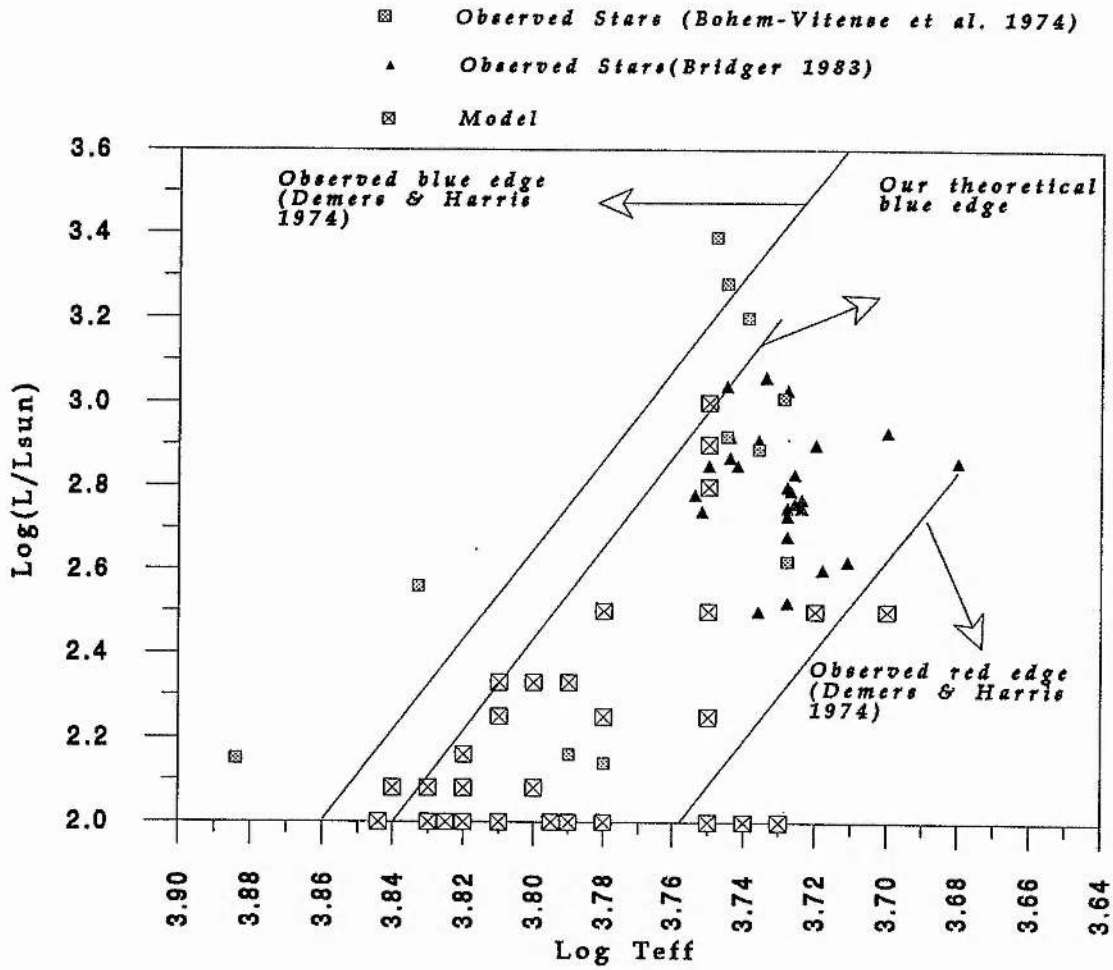

Figure 4-1. Shows the observed stars, blue edge and red edge, and theoretical blue edge and models.

The main results are summarised in table 4-1 which contains the following;

KE ; peak kinetic energy.

Δ ; full amplitude.

Asymmetry ; time spent on the descending branch of the surface velocity curve (or surface luminosity curve) divided by time spent on the ascending branch.

ϕ_v ; phase after zero velocity on the ascending branch of the surface velocity curve of the second (not necessarily the secondary) bump on this curve plus unity.

ϕ_l ; phase after mean bolometric magnitude on the ascending branch of the surface luminosity curve of the second (not necessarily the secondary) bump on this curve plus unity.

Table 4-1. Shows a summary of our models' results.

Parameter					Model		
	1	2	3	4	5	6	7
M/M*sun*	0.6	0.6	0.6	0.6	0.6	0.6	0.6
log(L/L*sun*)	2.00	2.00	2.00	2.25	2.25	2.50	2.50
log T*eff*	3.81	3.78	3.75	3.78	3.75	3.78	3.75
R/Rsun	8.06	9.26	10.63	12.35	14.18	16.46	18.90
P(days)	1.14	1.53	1.91	2.39	3.25	3.99	5.41
KE (10^{40} ergs)	1.0	1.9	3.0	1.8	4.9	1.25	5.4
Δ R/R	0.17	0.20	0.25	0.20	0.28	0.15	0.27
Δ V(km/s) *17/24	46	50	48	43	47	26	43
Δ M*bol*	1.4	1.5	1.3	1.2	1.4	0.7	1.3
Asymmetry (vel.)	1.70	1.7	3.9	3.1	2.8	2.9	1.8
Asymmetry (lum.)	6.7	3.7	4.8	2.9	4.0	1.4	2.6
ϕ_{υ}	1.44:	1.49	0.87	0.95	0.82	1.85	1.40
ϕ_{l}	1.55	1.48	0.89	1.02	0.87	1.88	1.38
X	0.745	0.745	0.745	0.745	0.745	0.745	0.745
Z	0.005	0.005	0.005	0.005	0.005	0.005	0.005

Parameter				Model			
	8	9	10	11	12	13	14
M/M*sun*	0.6	0.8	0.6	0.6	0.6	0.6	0.6
log(L/L*sun*)	2.50	2.00	2.00	2.00	2.08	2.00	2.16
log T*eff*	3.72	3.81	3.83	3.82	3.83	3.79	3.82
R/R*sun*	21.70	8.06	7.35	7.70	8.06	8.84	9.26
P(days)	7.20	0.94	0.96	1.04	1.19	1.35	1.48
KE (10^{40} ergs)	7.3	0.9	0.01	0.4	0.001	1.7	0.013
Δ R/R	0.26	0.10	0.05	0.10	0.005	0.23	0.018
Δ V(km/s) *17/24	31	30	13	28	1	56	4
Δ M*bol*	1.2	0.9	0.4	0.9	0.04	1.6	0.1
Asymmetry (vel.)	2.8	3.3	1.5	1.3	1.0	1.5	1.1
Asymmetry (lum.)	2.0	2.2	1.2	2.1	1.1	4.3	1.1
ϕ_{υ}	***	1.42	***	***	***	***	1.62
ϕ_{l}	0.83	1.48	1.55	1.60	***	1.53	1.41
X	0.745	0.745	0.745	0.745	0.745	0.745	0.745
Z	0.005	0.005	0.005	0.005	0.005	0.005	0.005

Parameter			Model				
	15	16	17	18	19	20	21
M/M*sun*	0.6	0.6	0.6	0.55	0.55	0.55	0.6
log(L/L*sun*)	2.08	2.25	2.33	2.00	2.00	2.00	2.33
log T*eff*	3.80	3.81	3.80	3.79	3.795	3.825	3.79
R/Rsun	9.26	10.75	12.35	8.84	8.64	7.53	12.93
P(days)	1.52	1.92	2.42	1.50	1.55	1.17	2.75
KE (10^{40} ergs)	1.5	0.08	0.38	1.6	1.3	0.02	2.9
Δ R/R	0.17	0.04	0.09	0.21	0.21	0.03	0.26
Δ V(km/s) *17/24	37	9	17	50	49	6	48
Δ M*bol*	1.2	0.3	0.6	1.6	1.6	0.2	1.9
Asymmetry (vel.)	3.2	1.0	1.1	1.7	1.4	1.3	2.1
Asymmetry (lum.)	3.2	1.5	3.1	5.9	6.4	1.1	9.0
ϕ_{υ}	1.33	***	0.89	1.23	***	1.53	***
ϕ_{l}	1.33	0.75	0.88	1.17	1.15	1.47	***
X	0.745	0.745	0.745	0.745	0.745	0.745	0.745
Z	0.005	0.005	0.005	0.005	0.005	0.005	0.005

Parameter				Model			
	22	23	24	25	26	27	31
M/M*sun*	0.6	0.6	0.6	0.6	0.6	0.6	0.6
log(L/L*sun*)	2.33	2.08	2.08	2.50	2.00	2.00	2.80
log T*eff*	3.81	3.82	3.84	3.70	3.73	3.74	3.75
R/Rsun	11.79	8.44	7.70	23.80	11.66	11.13	26.70
P(days)	2.28	1.27	1.08	9.29	2.37	2.17	9.67
KE (10^{40} ergs)	0.02	0.2	0.004	12.2	4.6	4.2	8.0
Δ R/R	0.02	0.07	0.009	0.40	0.28	0.28	0.33
Δ V(km/s) *17/24	4	17	2	51	50	53	39
Δ M*bol*	0.2	0.5	0.08	1.5	1.4	1.4	1.4
Asymmetry (vel.)	2.2	2.0	1.1	1.0	1.8	1.9	1.1
Asymmetry (lum.)	0.9	1.7	1.0	1.6	3.3	3.3	3.1
ϕ_{υ}	***	1.45	***	***	0.83	0.81	1.52
ϕ_{l}	***	1.49	***	***	0.82	0.86	1.48
X	0.745	0.745	0.745	0.745	0.745	0.745	0.745
Z	0.005	0.005	0.005	0.005	0.005	0.005	0.005

Parameter				Model			
	32	34	35	36	37	38	39
M/M*sun*	0.6	0.6	0.6	0.6	0.6	0.6	0.6
log(L/L*sun*)	3.00	2.90	1.40	1.60	1.70	1.80	2.00
log T*eff*	3.75	3.75	3.88	3.869	3.863	3.856	3.844
R/Rsun	33.62	29.96	2.93	3.88	7.47	5.18	6.89
P(days)	12.99	11.60	0.21	0.34	0.43	0.55	0.88
KE (10^{40} ergs)	***	7.8	0.13	0.13	0.04	0.03	0.001
Δ R/R	***	0.31	0.03	0.05	0.03	0.03	0.005
Δ V(km/s) *17/24	***	31	21	21	10	7	14
Δ M*bol*	***	1.1	0.6:	0.5:	0.4:	0.3:	0.05
Asymmetry (vel.)	***	1.0	2.33	1.0	0.89	0.82	1.04
Asymmetry (lum.)	***	2.6	3.17	1.0	1.04	0.96	1.08
ϕ_{υ}	***	1.47	***	***	***	***	***
ϕ_{l}	***	1.51	***	***	***	***	***
X	0.745	0.745	0.750	0.750	0.750	0.750	0.750
Z	0.005	0.005	0.000	0.000	0.000	0.000	0.000

Parameter				Model			
	40	41	42	43	44	45	46
M/M*sun*	0.6	0.6	0.6	0.6	0.6	0.5	0.5
log(L/L*sun*)	1.40	1.60	1.70	1.80	2.00	2.00	2.00
log T*eff*	3.88	3.869	3.863	3.856	3.844	3.844	3.83
R/Rsun	2.93	3.88	4.47	5.18	6.89	6.89	7.35
P(days)	0.22	0.34	0.43	0.56	0.89	0.99	1.12
KE (10^{40} ergs)	0.22	0.14	0.096	0.08	0.03	0.002	0.03
Δ R/R	0.06	0.04	0.03	0.04	0.03	0.008	0.03
Δ V(km/s)*17/24	25	21	14	11	8	2	8
Δ M*bol*	0.98:	0.67:	0.45:	0.47:	0.26	0.064	0.22
Asymmetry (vel.)	1.94	***	***	***	***	***	1.22
Asymmetry (lum.)	2.33	***	***	***	***	***	1.00
ϕ_{υ}	***	***	***	***	***	***	***
ϕ_{l}	***	***	***	***	***	***	***
X	0.749	0.749	0.749	0.749	0.749	0.750	0.745
Z	0.001	0.001	0.001	0.001	0.001	0.000	0.005

Parameter					Model		
	47	48	49	50	51	52	53
M/M*sun*	0.5	0.6	0.7	0.7	0.7	0.6	0.5
log(L/L*sun*)	2.00	2.00	2.00	2.00	2.00	2.00	2.00
log T*eff*	3.83	3.83	3.83	3.83	3.81	3.81	3.81
R/Rsun	7.35	7.35	7.35	7.35	8.06	8.06	8.06
P(days)	1.11	0.99	0.90	0.92	1.06	1.17	1.33
KE (10^{40} ergs)	0.1	0.3	0.5	***	1.9	1.3	0.8
ΔR/R	0.06	0.08	0.07	0.5:	0.14	0.15	0.17
ΔV(km/s)*17/24	16	22	19	22:	43	42	42.5
ΔM*bol*	0.52	0.74	0.67	0.52:	1.20	1.11	1.45
Asymmetry (vel.)	1.94	1.99	1.5	***	2.64	3.17	1.41
Asymmetry (lum.)	1.5	3.17	2.45	1.27	3.26	2.33	2.92
ϕ_{υ}	1.44	***	11.35	***	1.62	1.54	1.60
ϕ_{l}	1.47	1.18	1.33	1.35	1.60	1.54	1.59
X	0.750	0.750	0.750	0.745	0.749	0.749	0.749
Z	0.000	0.000	0.000	0.005	0.001	0.001	0.001

In table 4-2 we are going to make a comparison of the present calculated period in column seven with others that have been calculated by CSV81, CS82, Bridger 1983 (B83) in column two, Kovacs, Buchler and Marom 1991 (KBM91) in column three, Hubickyj 1983 in column four, Van Albada and Baker 1971 (VB71) in column five and Iben 1971 in column six.

Table 4-2.

Model No.	Period CSV81/ CS82/ B83	Period KBM91	Period Hubickyj 1983	Period VB71	Period Iben 1971	Period Author
1	1.23	1.158	1.265	1.172	1.152	1.14
2	1.63	1.460	1.603	1.491	1.541	1.53
3	2.07	1.839	2.032	1.896	1.827	1.91
4	2.70	2.328	2.620	2.418	2.332	2.39
5	3.52	2.934	3.320	3.075	2.938	3.25
6	4.54	3.714	4.281	3.922	3.758	3.99

7	5.95	4.680	5.425	4.987	4.724	5.41
8	8.44	5.897	6.876	6.342	5.949	7.20
9	1.02	0.970	1.046	0.964	0.961	0.94
10	1.04	0.993	1.080	0.999	0.988	0.96
11	1.13	1.073	1.169	1.082	1.067	1.04
12	1.22	1.153	1.264	1.166	1.150	1.19
13	1.47	1.351	1.482	1.376	1.343	1.35
14	1.56	1.446	1.601	1.475	1.445	1.48
15	1.59	1.453	1.602	1.483	1.448	1.52
16	2.07	1.848	2.067	1.901	1.852	1.92
17	2.67/2.47§	2.318	2.618	2.405	2.328	2.42
18	1.58	1.426	1.569	1.460	1.419	1.50
19	1.64	1.455	1.606	1.497	1.450	1.55
20	1.24	1.155	1.267	1.177	1.151	1.17
21	*****	2.503	2.833	2.605	2.514	2.75
22	*****	2.146	2.419	2.220	2.156	2.28
23	*****	1.245	1.368	1.263	1.242	1.27
24	*****	1.068	1.168	1.076	1.065	1.08
25	*****	6.879	8.052	7.445	6.938	9.29
26	*****	2.146	2.380	2.226	2.131	2.37
27	*****	1.987	2.199	2.054	1.973	2.17
31	12.60	8.196	9.780	8.910	8.351	9.64
32	17.30	11.908	14.485	13.118	12.211	12.99
34	14.60	9.879	11.902	10.811	10.099	11.60
35	*****	0.206	0.224	0.210	0.215	0.21
36	*****	0.329	0.362	0.337	0.342	0.34
37	*****	0.417	0.462	0.429	0.433	0.43
38	*****	0.533	0.594	0.551	0.553	0.55
39	*****	0.859	0.967	0.983	0.887	0.88
40	*****	0.212	0.224	0.210	0.215	0.22
41	*****	0.337	0.362	0.337	0.342	0.34
42	*****	0.426	0.462	0.429	0.433	0.43
43	*****	0.544	0.594	0.551	0.553	0.56
44	*****	0.873	0.967	0.893	0.887	0.89
45	*****	0.968	1.091	1.011	0.995	0.99
46	*****	1.111	1.218	1.131	1.108	1.12
47	*****	1.081	1.218	1.131	1.108	1.11
48	*****	0.960	1.080	0.999	0.988	0.99
49	*****	0.868	0.976	0.899	0.896	0.90
50	*****	0.903	0.967	0.899	0.896	0.92
51	*****	1.033	1.143	1.056	1.045	1.06
52	*****	1.140	1.265	1.172	1.152	1.17
53	*****	1.281	1.427	1.327	1.292	1.33

§ Lawrence 1985 found that there is a printing mistake in CS82 model no. 8 the period is 2.47 not 2.67.

* No calculations have been done for these models neither in CSV81, CS82 nor B83.

From the above table we can see that there are, more-or-less, an agreement between the present periods and the previous periods. Also, clearly seen that there are a disagreement between the periods that have been calculated by Bridger (1983) and that calculated by the other author (models 31, 32 and 34).

In our work we have used the Iglesias & Rogers (1991) (IR, hereafter) opacity tables which differ from the Los ALmos (LA, hereafter) and Carson opacity tables by including more metal lines (a strong increase due to Fe line splitting). The LA opacites considerably underestimate the contribution of the heavy elements such as Fe in two temperature domains (Stothers & Chin 1991, Moskalik *et al.* 1992). These (IR) tables solved most of the major problems (Cox 1991, Kovacs *et al.* 1991). Tables 1C, 2C and 3C, in Appendix C, represent the IR opacity for different composition. Each table gives $\log(\kappa)$ for 34 values of $\log(T)$ with 9 values of $\log(\rho)$ for each temperature. The opacities for these tables are plotted in Figures 1C and 2C in Appendix C. For the sake of comparison we plotted the Carson opacities using table 5 in CSV81.

Comparing IR with Carson opacity when (X, Y, Z) = (0.745, 0.250, 0.005) we can see that - more-or-less-, for $-5 \geq \log(\rho) \geq -11$, there is an agreement between the two opacities, while in the other hand this agreement failed for $\log(\rho) > -5$ with $\log(T) \leq 5.5$. This disagreement may due to the heavier elements not the Hydrogen and Helium (Carson 1994, Private Communication)

Generally speaking we can say that using IR opacities the amplitudes and the period are less than that calculated with different opacities, this conclusion is the same to that found by Moskalik *et al.* (1992).

The blue edge with the new opacity tables, for RR Lyrae with Z = 0.001 and less, agree with the old one (for example Hubickyj 1983Who used the Carson opacities).

However, on the other hand, the blue edge for log (L/L*sun*) ≥ 2.00 with Z = 0.005 shifted redward about 300 K, which agrees with that found for Pop I in Moskalik *et al.* (1992), see Figure 4-2. Once the model has been calculated to be a decaying one, and the light curve to be a sinusoidal (not always), the blue edge can be determined. Kovacs *et al.* (1991) found that the main effect of the IR opacities is to shift the non-linear fundamental blue edge toward lower T_{eff} (redward).

Comparing our results, we can say that for RR Lyrae the mass can not be less than 0.6, if the star at 0.55 M*sun* this star do not enter the RR Lyrae variable region (Cox *et al.* 1983), while for BL Her there can be variability with masses greater than 0.7 M*sun* if evolution theory includes them, but it does not.

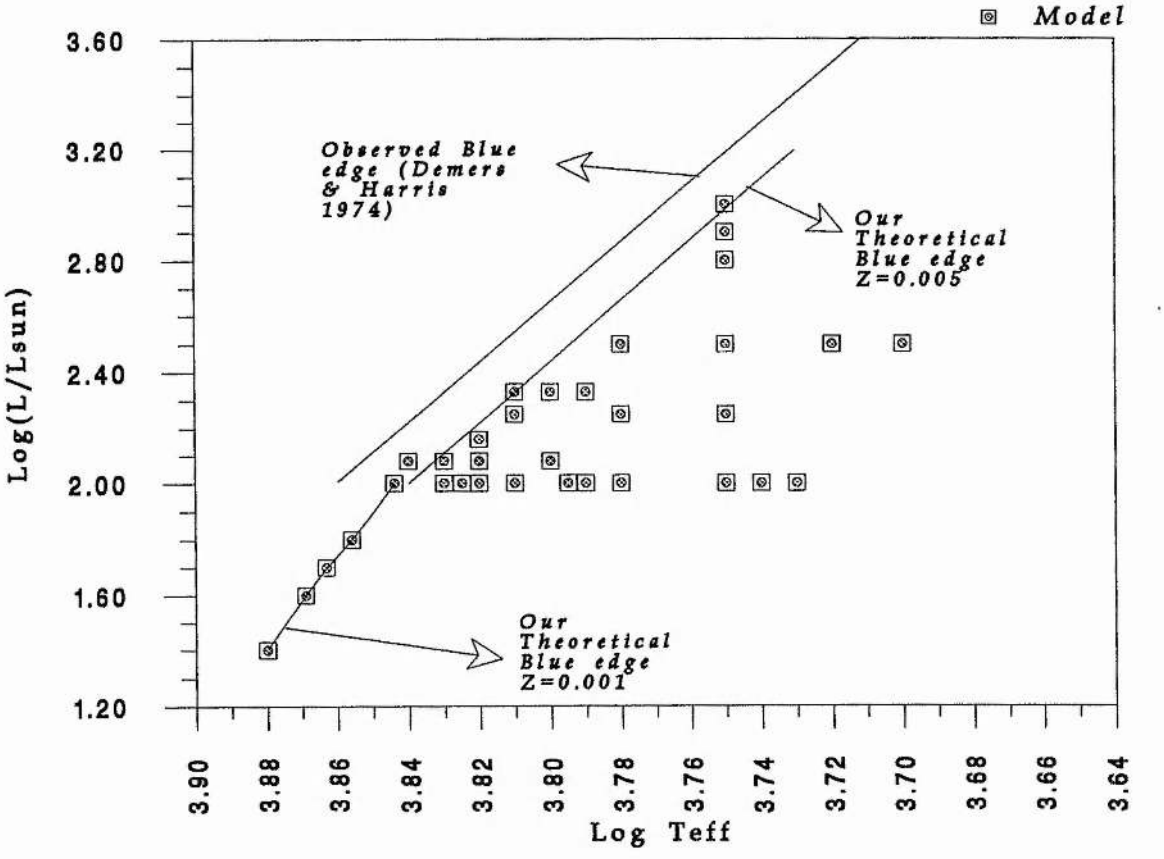

Figure 4-2. Shows the observed and theoretical blue edges.

The bump progression in our models can be seen easily for the BL Her stars (see Appendix A). The centre of the progression lies between 1.5 - 1.55 days, whereas this centre in Carson & Stothers 1982 seems to occur at 1.6 days.

LIGHT CURVE SHAPES:-

Here we are going to represent a comparison between the observed stars and the models that we have constructed. The comparison is based on the shape of the light curves, the luminosity amplitudes and on the shape of the velocity curves if available, see Table 4-3.

BL Her, the prototype of its class, with a period of 1.31 days, can be compared with model **1** (P=1.14). For comparison we show in Figure 4-3 the luminosity and velocity curves, observed and the theoretical one constructed by CSV81 which can be compared with our theoretical model No.**1** (see Appendix A-2).

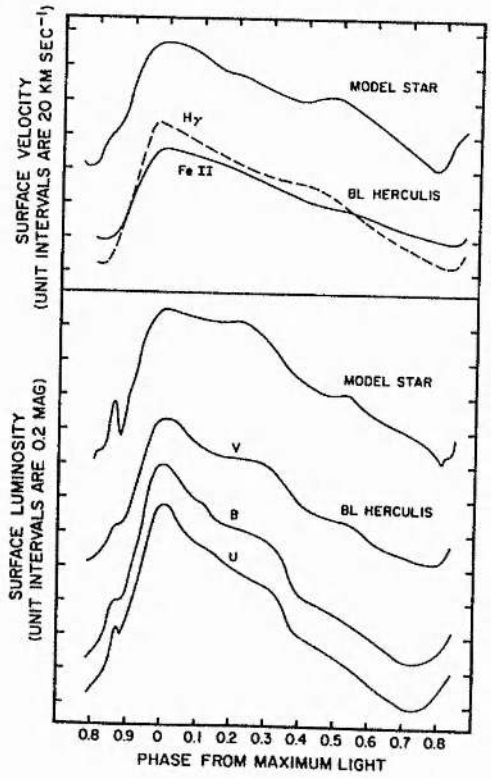

Figure 4-3. Surface velocity and surface luminosity curves for BL Her and for the theoretical model with 1.23 day (model no. 1) of CSV81. The velocity of BL Her have been transformed to the astrocentric co-ordinate system (CSV81 Figure 5).

BX Del (P=1.09) is a medium amplitude variable with a rather rounded feature light curve that is mimicked quite well by our theoretical light curves of either model **11** (P=1.04) or model **9** (P=0.94). Similar in light curve and period to **BX Del** is **XZ Cet** (P=0.8231).

BF Ser (P=1.165) with an amplitude about 1.5 mag. can be compared with model **1**. Similar in period to **BF Ser** are **V716 Oph** (P=1.1159) and model **51** (P=1.06).

KZ Cen (P=1.519) is a distant halo star (CS82). Its rounded light peak and its prominent post maximum shoulder are represented in model **15** (P=1.52). Similar in period and light curve is **HQ Cra** (P=1.415).

RX Aur (P=11.63). Its rounded light peak and its prominent post maximum shoulder are well represented in model **34** (P=11.60).

XX Vir (P=1.348). Its sharp ascending branch and smooth descending branch are well represented in model **13** (P=1.35). Models similar in light curves and period are **18** (P=1.50) and **19** (P=1.55).

GL Cyg (P=3.370). We can compare it with model **5** (P=3.25). The model's light curve seems not to be the same as the star's, but after smoothing the model's we get a good comparison. Similar in period to **GL Cyg** is **BE Cra** (P=3.334).

V553 Cen (P=2.06). Its flat light curve peak and a shock in the ascending branch are well represented in model **16** (P=1.92). This star seems to be near to the blue edge. The velocity curve of this star has been compared with the model's and gives a good comparison. Similar in light curve to **V553** is **RT Tra** (P=1.95).

VX Cap (P=1.3276). Its sharp ascending branch and slightly descending branch are well represented in model **53** (P=1.33).

UX Nor (P=2.858). If we ignore its peak, the light curve is well represented in model **4** (P=2.39). Both have sharp ascending branch and slow descending branch.

V7 M19 (P=0.244) is a medium amplitude variable, its light curve represented in model **40** (P=0.22).

V971 Aql (P1.624). Its sharp ascending branch and the shock on the descending branch are well represented in model **2** (P=1.53).

Model **3** (P=1.91). Its sharp ascending and the shock at phase 0.2 are well represented by either **V439 Oph** (P=1.839), **VZ Aql** (P=1.668) or **V839 Sgr** (P=1.835).

VY Cyg (P=7.857). Its light curve can be represented by model **8** (P=7.20). Similar in light curve to **VY Cyg** is **BB Her**(P=7.507).

V802 Sgr (P=13.5135). Its flat top light curve is well represented in model **25** (P=9.29). Similar in light curve to **V802 Sgr** are **W Vir** (P=17.2768), **V377 Sgr** (P=16.19326) and **V741 Sgr** (P=15.156).

Table 4-3. Observed stars that used for comparison with the models.

Star	Period (days)	Δ M	ϕ_1	References
BL Her	1.307	0.8	1.59	1, 2, 5, 6
BX Del	1.09 1.04	0.8		1, 2 3
XZ Cet	0.8231	0.5		11
BF Ser	1.165 1.13	1.5		2 3
V716 Oph	1.12	1.4		1, 3
KZ Cen	1.519	1.35	1.50	1, 5
HQ Cra	1.415	1.05	1.07	2, 4
RX Aur	11.62	0.7		13
XX Vir	1.348	1.2	1.56	1, 2, 5
GL Cyg	3.37	1.35		5
BE Cra	3.334	1.2		5
V553 Cen	2.06	0.5	0.88	1, 7, 11
RT Tra	1.946	0.75		2, 4, 11
VX Cap	1.3276	1.4		3
UX Nor	2.3858	1.2		2, 3
V7 M19	0.244	0.2		12
V971 Aql	1.624	0.9		2, 4
V439 Oph	1.839	0.75	0.93	1, 2
VZ Aql	1.668	0.9	0.82	2, 4
V839 Sgr	1.835	1.2	0.92	1, 2, 4
VY Cyg	7.857	0.9		14
BB Her	7.507	0.6		14
V802 Sgr	13.5135	0.9		14
W Vir	17.2768	1.2	0.30	14, 15
V377 Sgr	16.19326	1		14
V741 Sgr	13.156	1	0.31	14, 15

References:- **(1)** CS82. **(2)** Diethelm 1983. **(3)** Lawrence 1985. **(4)** Kwee & Diethelm 1984. **(5)** Payne-Gaposchkin 1956. **(6)** Smith *et al.* 1978. **(7)** Lloyd, Wisse & Wisse 1972. **(8)** Michalowska-Smak & Smak 1965. **(9)** Zessevich 1966. **(10)** Lee 1974. **(11)** Dean *et al.* 1977. **(12)** Clement & Sawyer Hogg 1978. **(13)** Mitchell, Steinmetz & Johnson 1964. **(14)** Kwee & Braun 1967. **(15)** Bridger 1983.

In this work we have been adopted the 50 mass zones as mentioned earlier. But for the sake of comparison a new model -model(56)- has been created which has the same parameters as model (1) but using 100 mass zones. Comparing the two models gives us the following :

With 50 mass zones the period and kinetic energy (P=1.14 day, KE (10^{40} ergs) = 1.0) were less than with the 100 mass zones (1.19,1.3 respectively). These two quantities with the 100 are, more-or-less, agreeable with CSV81. The amplitudes are less in the 100 ($\Delta R/R$=0.144, ΔV=43 Km/sec and ΔM_{bol} =1.2 mag.) than in the 50 (0.17, 46 and 1.4 respectively).

The features of the light and velocity curves in the 100 are more clearly than in the 50, see Figure 4-4. Unfortunately the 100 mass zone models required a very long time to converge compared with the 50 zone models (the 100 mass zone models required about 440 time steps for each period while in the 50 zone models it was about 250). This is to be expected since the maximum time step is controlled by the sound travel time across the zones.

CONCLUSION:-

Generally speaking we can say that using the IR opacities we get results which agree well with previous work using different opacities.

Generally the periods of the old and new models are in very good agreement. However, the amplitudes of the new models tend to be fairly consistently smaller than those of the old models, tending towards greater agreement with observation. The new blue edges are shifted redward (toward lower temperature) with respect to the old, particularly for the larger values of the metal content Z, and less for the smaller Z.

Our non-linear results obtained here shows that the mass of RR Lyrae cannot be less than 0.6 M*sun*, while on the other hand the BL Her variables have mass greater than 0.7 M*sun*.

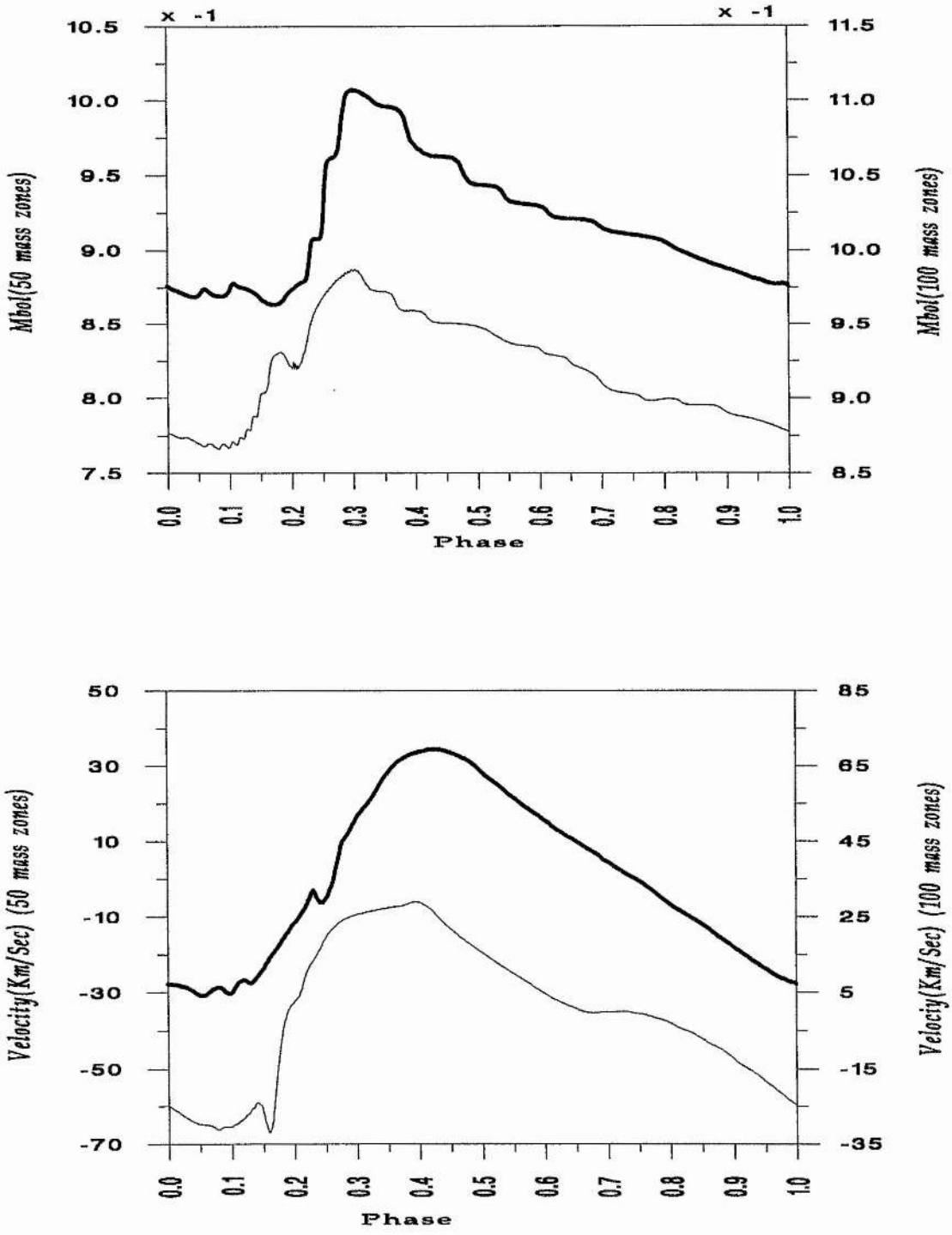

Figure 4-4. Comparison between the light curves (top) and velocity curves (bottom), using a 50 mass zones (upper) and a 100 mass zones (lower).

APPENDIX *A*

A-1. LIGHT, VELOCITY & RADIUS CURVES FOR THE RR LYRAE MODELS:-

In this Appendix, we present the light, velocity and radius curves of the RR Lyrae models. These light curves have been produced using a programme code created by Dr. T. R. Carson. For each model the mass, the luminosity, the temperature, the amount of hydrogen and metals and the period in days, are mentioned.

Model(35)

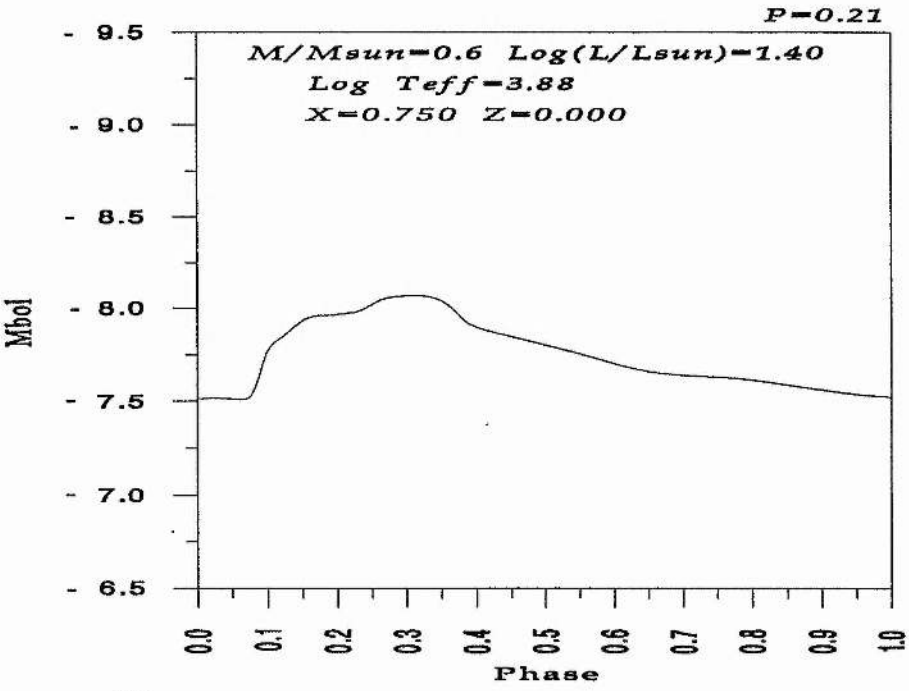
P=0.21
M/Msun=0.6 Log(L/Lsun)=1.40
Log Teff=3.88
X=0.750 Z=0.000
Mbol
- 9.5
- 9.0
- 8.5
- 8.0
- 7.5
- 7.0
- 6.5
0.0 0.1 0.2 0.3 0.4 0.5 0.6 0.7 0.8 0.9 1.0
Phase

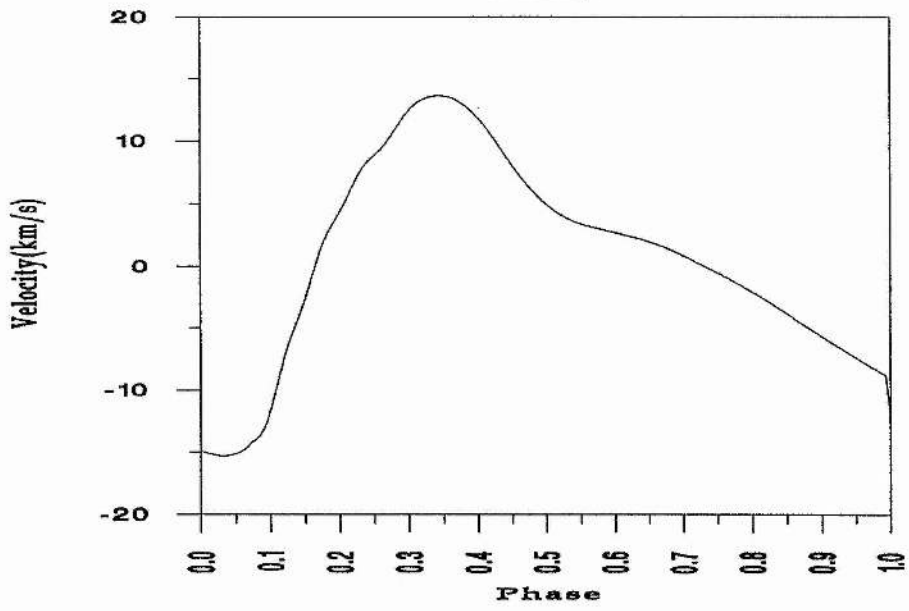
Velocity(km/s)
20
10
0
-10
-20
0.0 0.1 0.2 0.3 0.4 0.5 0.6 0.7 0.8 0.9 1.0
Phase

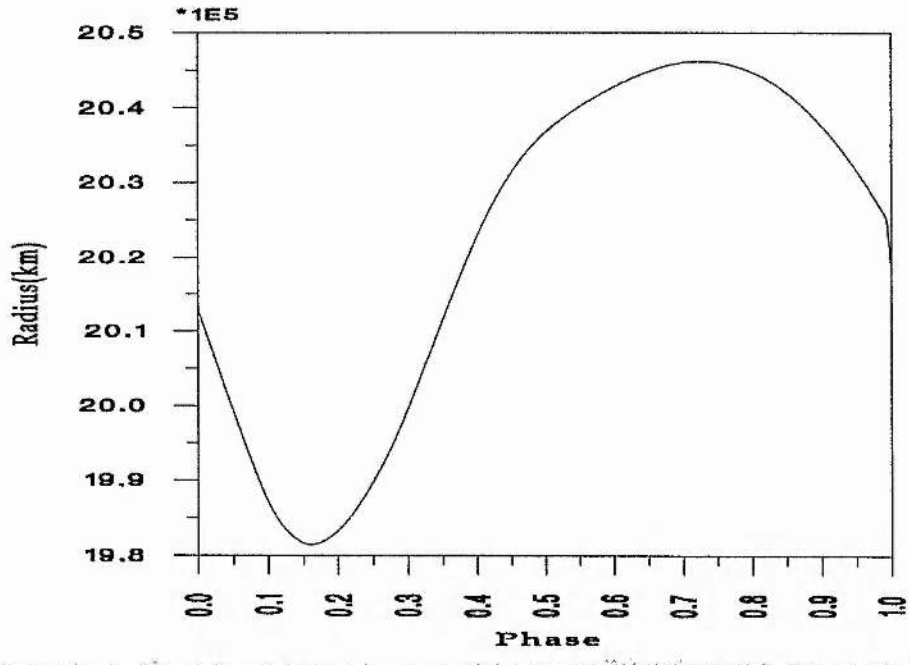
*1E5
Radius(km)
20.5
20.4
20.3
20.2
20.1
20.0
19.9
19.8
0.0 0.1 0.2 0.3 0.4 0.5 0.6 0.7 0.8 0.9 1.0
Phase

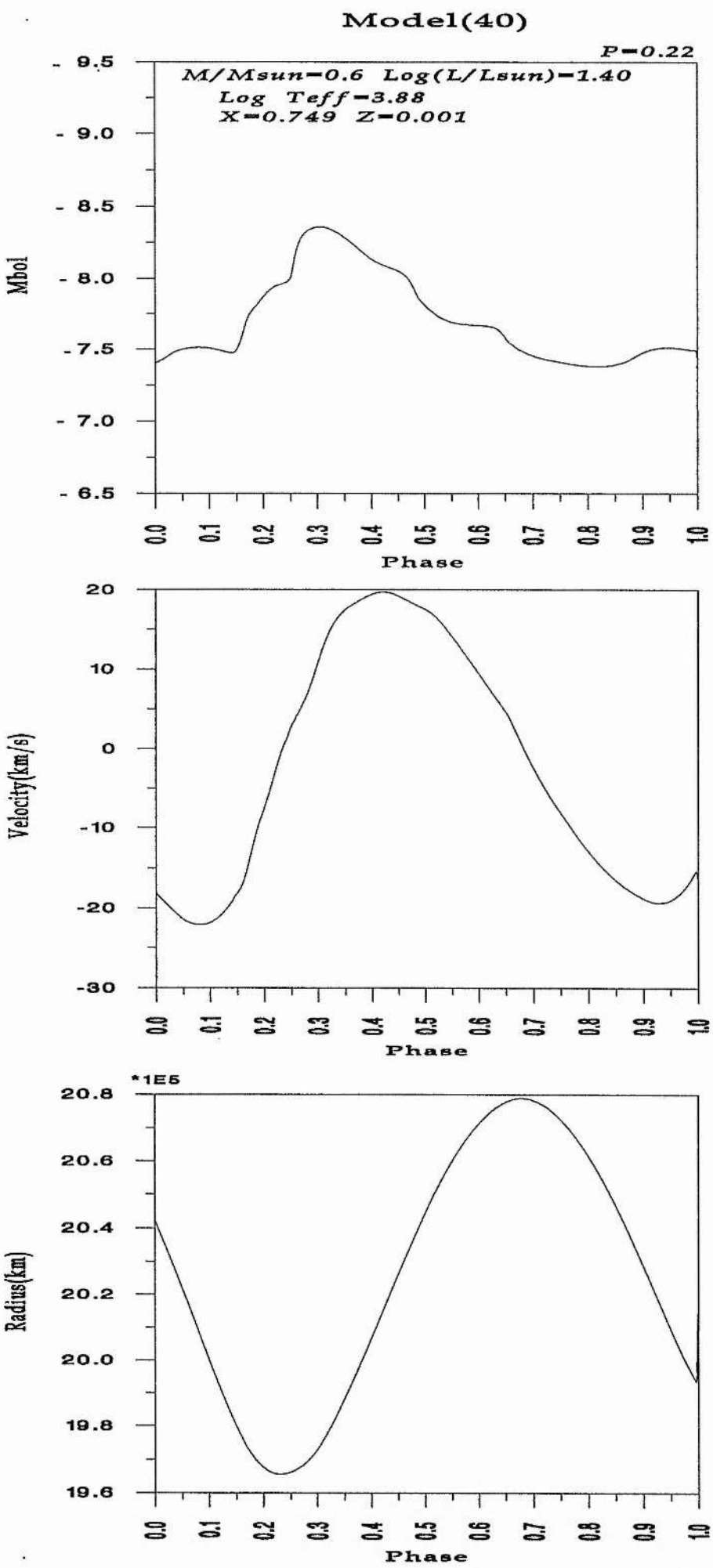
Model(40)
P=0.22
M/Msun=0.6 Log(L/Lsun)=1.40
Log Teff=3.88
X=0.749 Z=0.001
Mbol
Phase
Velocity(km/s)
Phase
*1E5
Radius(km)
Phase

A-2. LIGHT, VELOCITY & RADIUS CURVES FOR THE BL HER MODELS:-

In this section, we present the light, velocity and radius curves of the BL Her models. These curves have been produced using a programme code created by Dr. T. R. Carson. For each model the mass, the luminosity, the temperature, the amount of hydrogen and metals and the period in days, are mentioned.

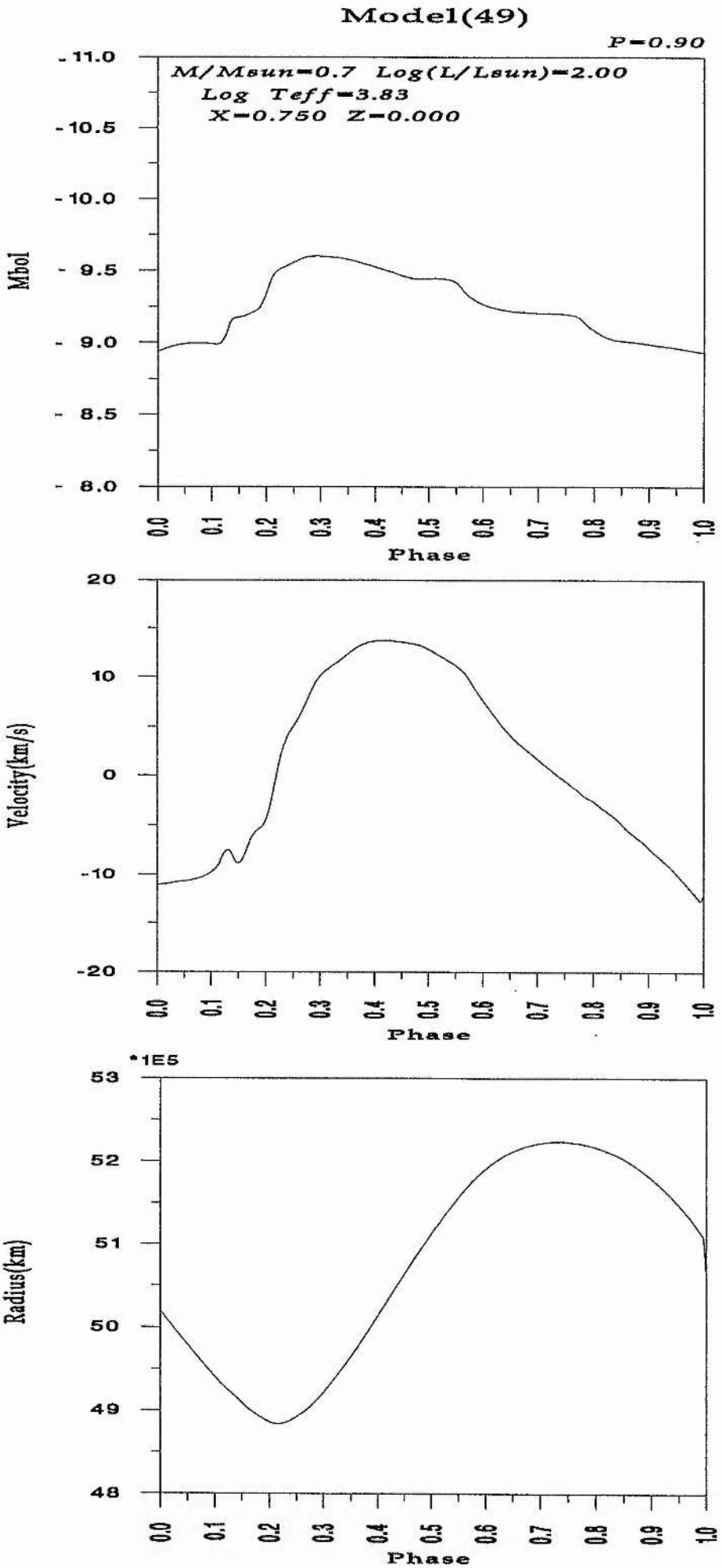
Model(49)
P=0.90
M/Msun=0.7 Log(L/Lsun)=2.00
Log Teff=3.83
X=0.750 Z=0.000
Mbol
-11.0
-10.5
-10.0
-9.5
-9.0
-8.5
-8.0
0.0
0.1
0.2
0.3
0.4
0.5
0.6
0.7
0.8
0.9
1.0
Phase
Velocity(km/s)
20
10
0
-10
-20
Phase
*1E5
Radius(km)
53
52
51
50
49
48
Phase

Model(9)

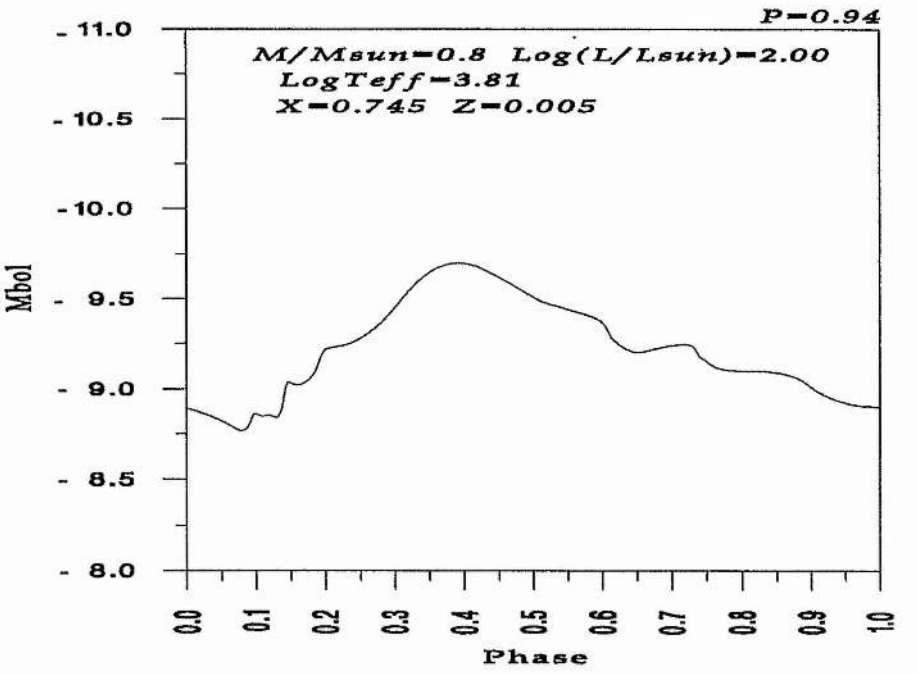
P=0.94
M/Msun=0.8 Log(L/Lsun)=2.00
LogTeff=3.81
X=0.745 Z=0.005
Mbol
- 11.0
- 10.5
- 10.0
- 9.5
- 9.0
- 8.5
- 8.0
0.0 0.1 0.2 0.3 0.4 0.5 0.6 0.7 0.8 0.9 1.0
Phase

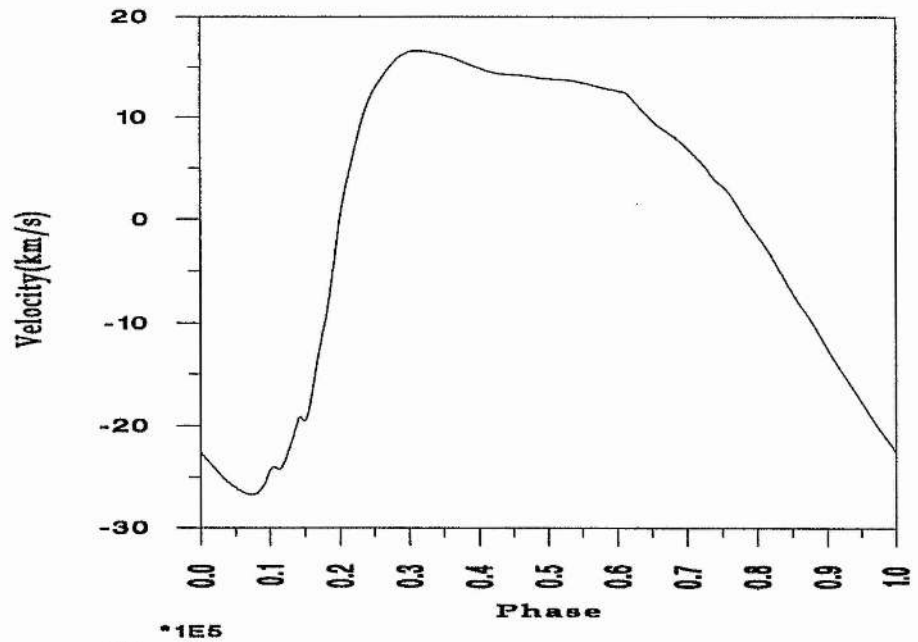
Velocity(km/s)
20
10
0
-10
-20
-30
0.0 0.1 0.2 0.3 0.4 0.5 0.6 0.7 0.8 0.9 1.0
Phase

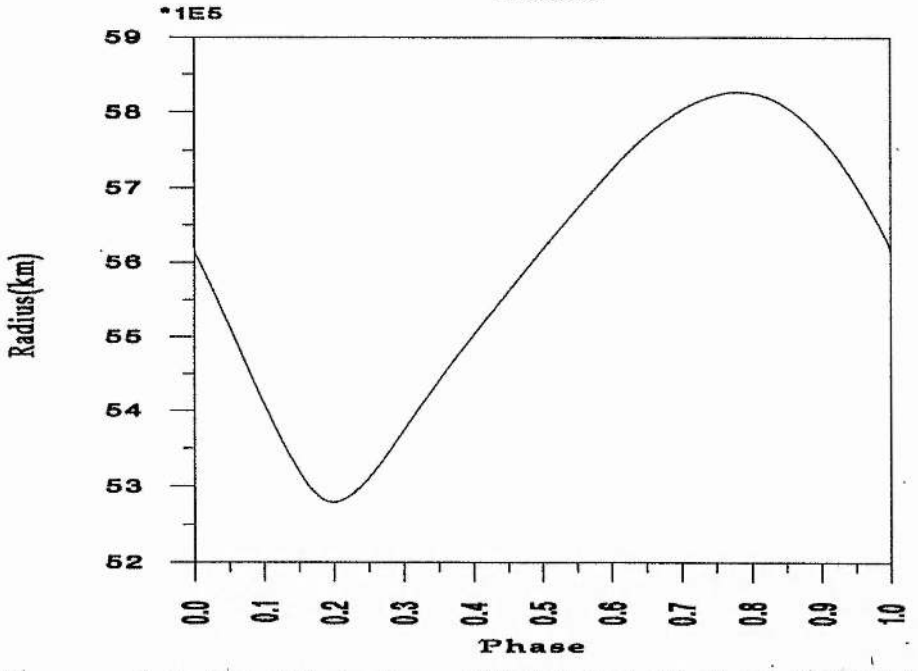
*1E5
Radius(km)
59
58
57
56
55
54
53
52
0.0 0.1 0.2 0.3 0.4 0.5 0.6 0.7 0.8 0.9 1.0
Phase

Model(48)

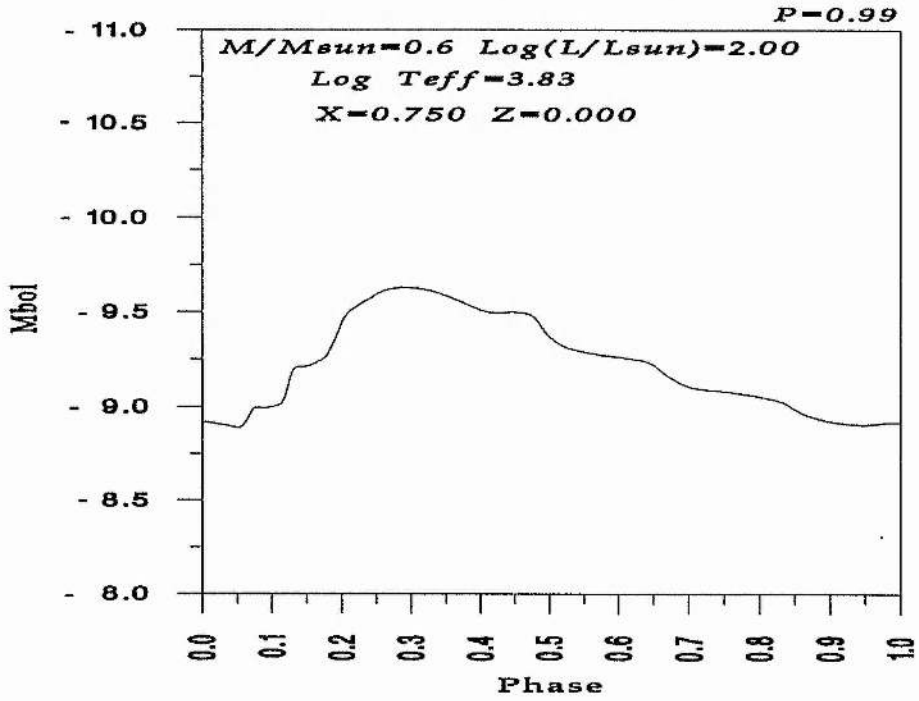
P=0.99
M/Msun=0.6 Log(L/Lsun)=2.00
Log Teff=3.83
X=0.750 Z=0.000
Mbol
- 11.0
- 10.5
- 10.0
- 9.5
- 9.0
- 8.5
- 8.0
0.0 0.1 0.2 0.3 0.4 0.5 0.6 0.7 0.8 0.9 1.0
Phase

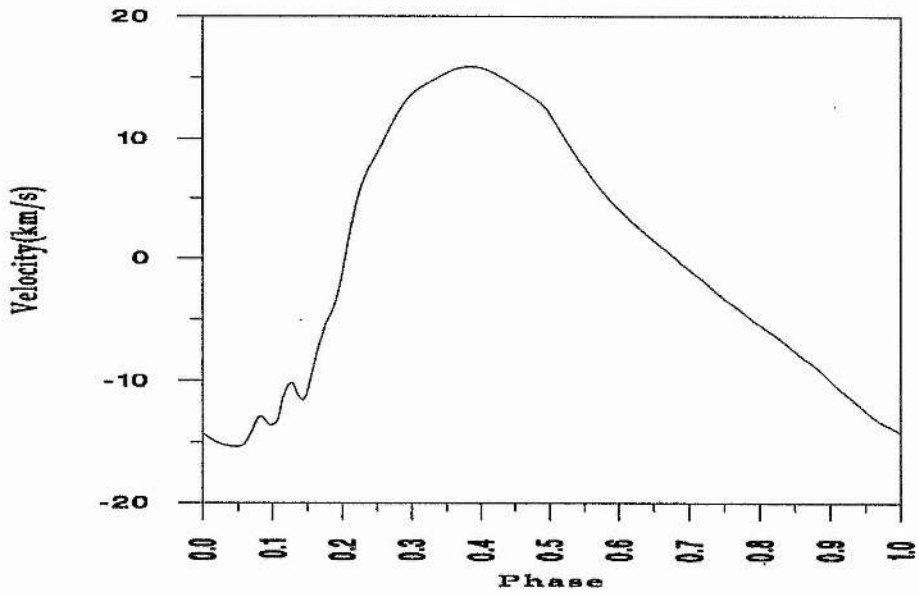
Velocity(km/s)
20
10
0
-10
-20
0.0 0.1 0.2 0.3 0.4 0.5 0.6 0.7 0.8 0.9 1.0
Phase

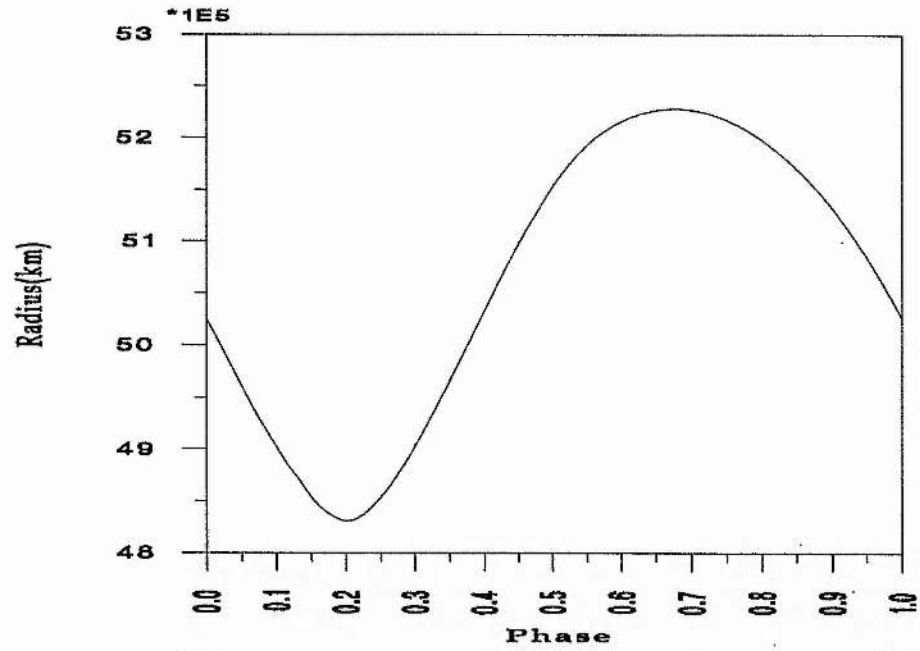
*1E5
Radius(km)
53
52
51
50
49
48
0.0 0.1 0.2 0.3 0.4 0.5 0.6 0.7 0.8 0.9 1.0
Phase

Model(11)

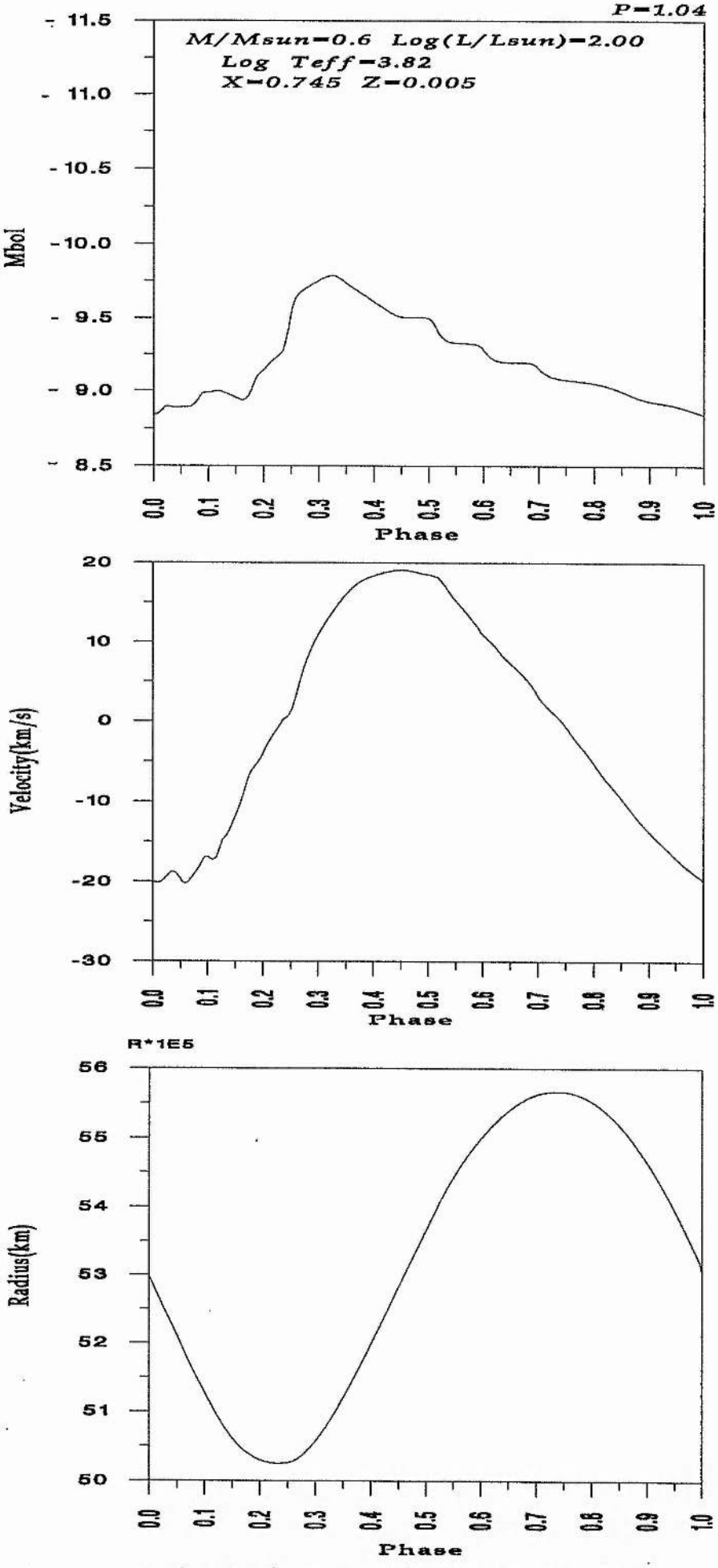
P=1.04
M/Msun=0.6 Log(L/Lsun)=2.00
Log Teff=3.82
X=0.745 Z=0.005
Mbol
-11.5
-11.0
-10.5
-10.0
-9.5
-9.0
-8.5
0.0
0.1
0.2
0.3
0.4
0.5
0.6
0.7
0.8
0.9
1.0
Phase
Velocity(km/s)
20
10
0
-10
-20
-30
Phase
R*1E5
Radius(km)
56
55
54
53
52
51
50
Phase

Model(51)

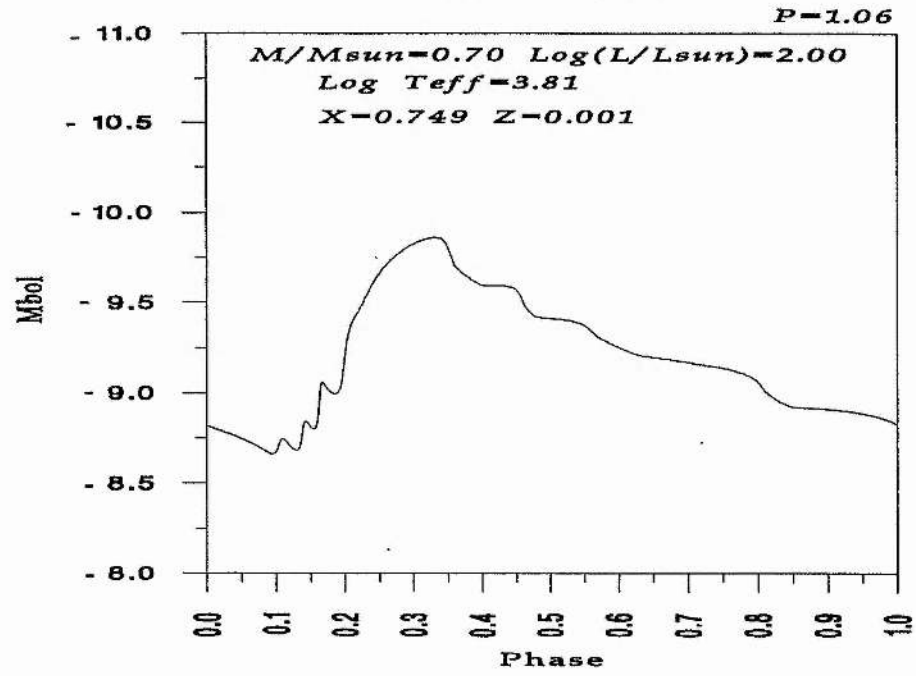
P=1.06
M/Msun=0.70 Log(L/Lsun)=2.00
Log Teff=3.81
X=0.749 Z=0.001
Mbol
- 11.0
- 10.5
- 10.0
- 9.5
- 9.0
- 8.5
- 8.0
0.0 0.1 0.2 0.3 0.4 0.5 0.6 0.7 0.8 0.9 1.0
Phase

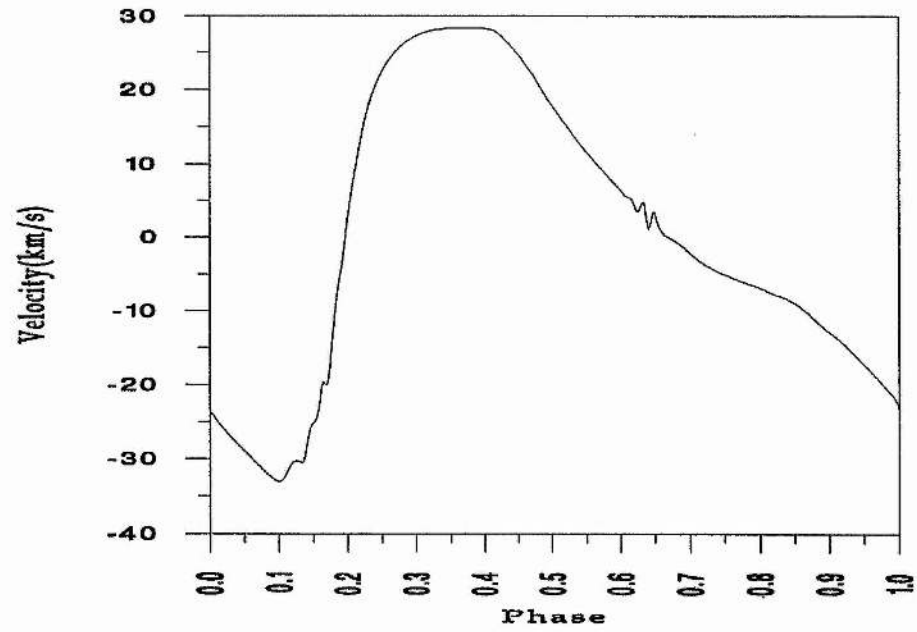
Velocity(km/s)
30
20
10
0
-10
-20
-30
-40
0.0 0.1 0.2 0.3 0.4 0.5 0.6 0.7 0.8 0.9 1.0
Phase

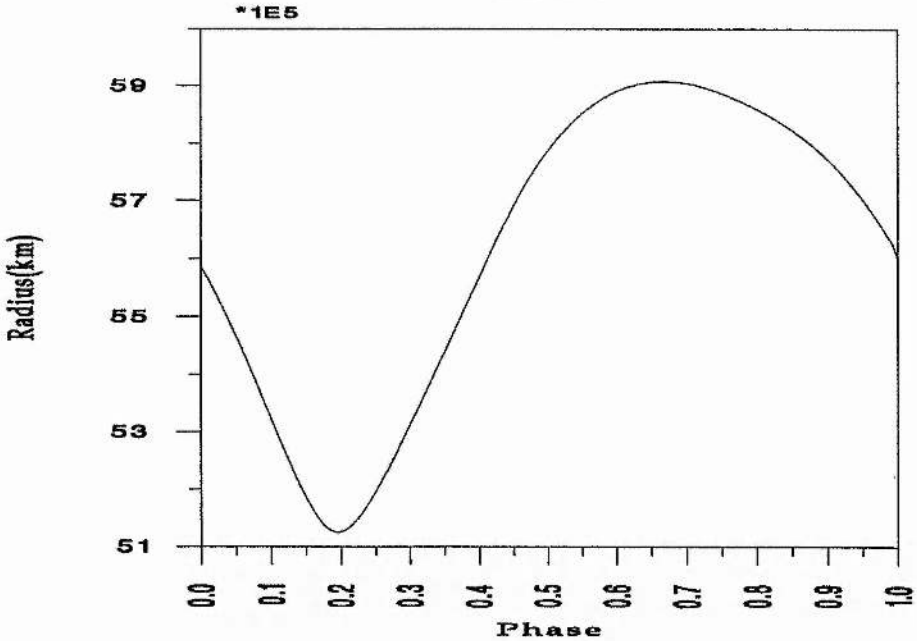
*1E5
Radius(km)
59
57
55
53
51
0.0 0.1 0.2 0.3 0.4 0.5 0.6 0.7 0.8 0.9 1.0
Phase

Model(1)

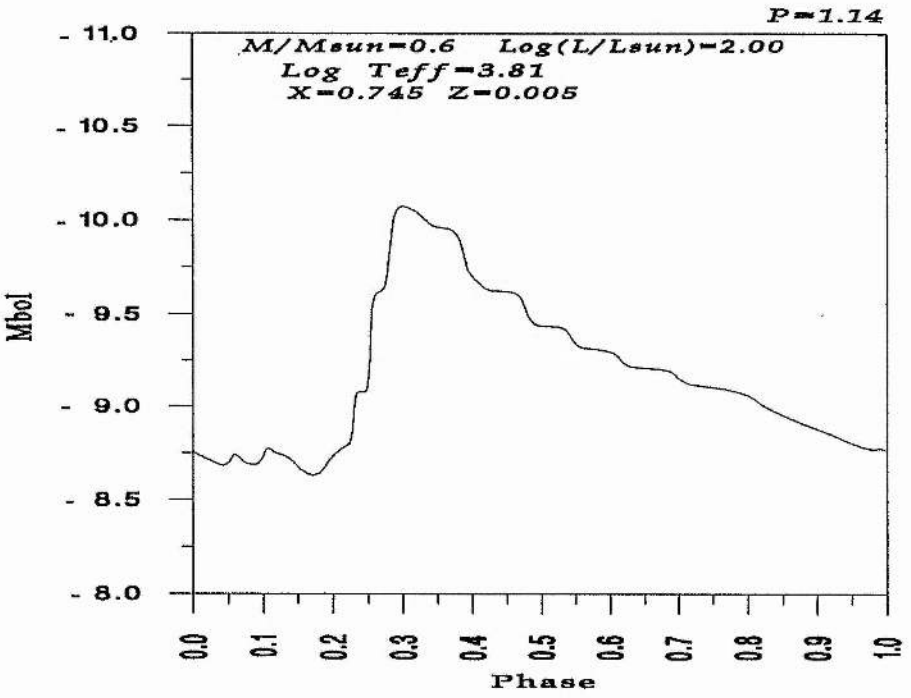
P=1.14
M/Msun=0.6 Log(L/Lsun)=2.00
Log Teff=3.81
X=0.745 Z=0.005
Mbol
- 11.0
- 10.5
- 10.0
- 9.5
- 9.0
- 8.5
- 8.0
0.0 0.1 0.2 0.3 0.4 0.5 0.6 0.7 0.8 0.9 1.0
Phase

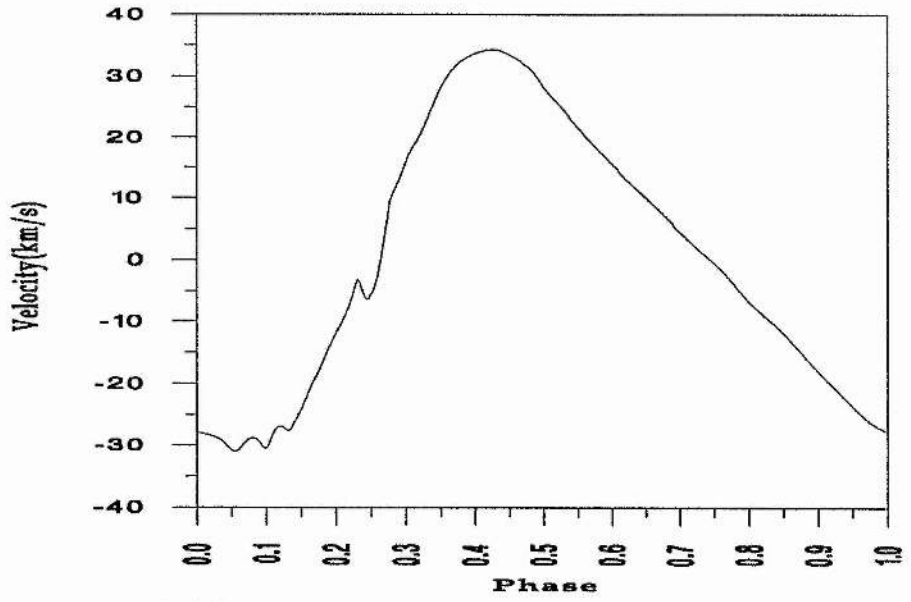
Velocity(km/s)
40
30
20
10
0
-10
-20
-30
-40
0.0 0.1 0.2 0.3 0.4 0.5 0.6 0.7 0.8 0.9 1.0
Phase

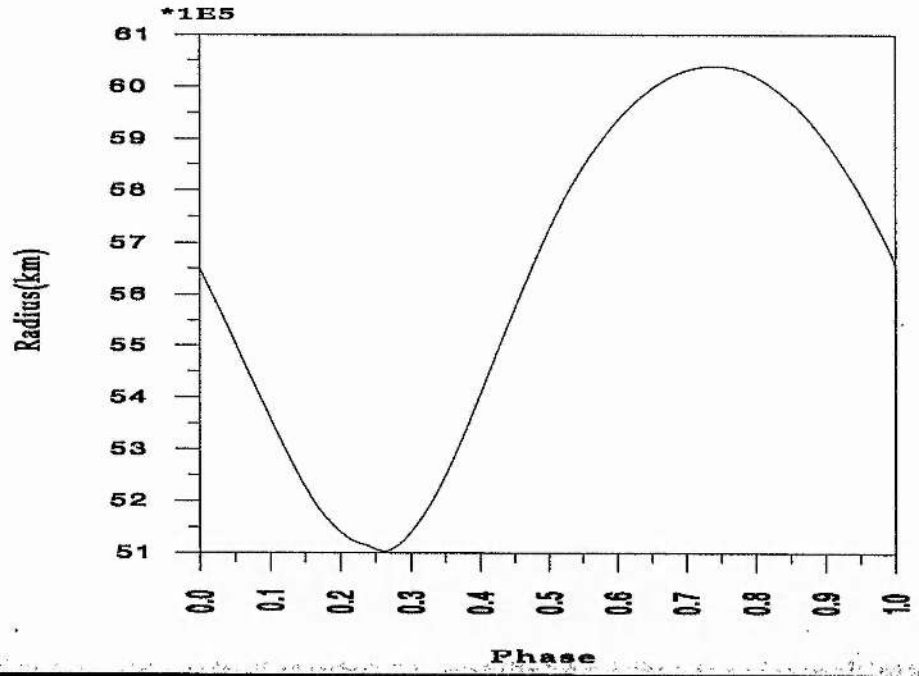
*1E5
Radius(km)
61
60
59
58
57
56
55
54
53
52
51
0.0 0.1 0.2 0.3 0.4 0.5 0.6 0.7 0.8 0.9 1.0
Phase

Model(52)

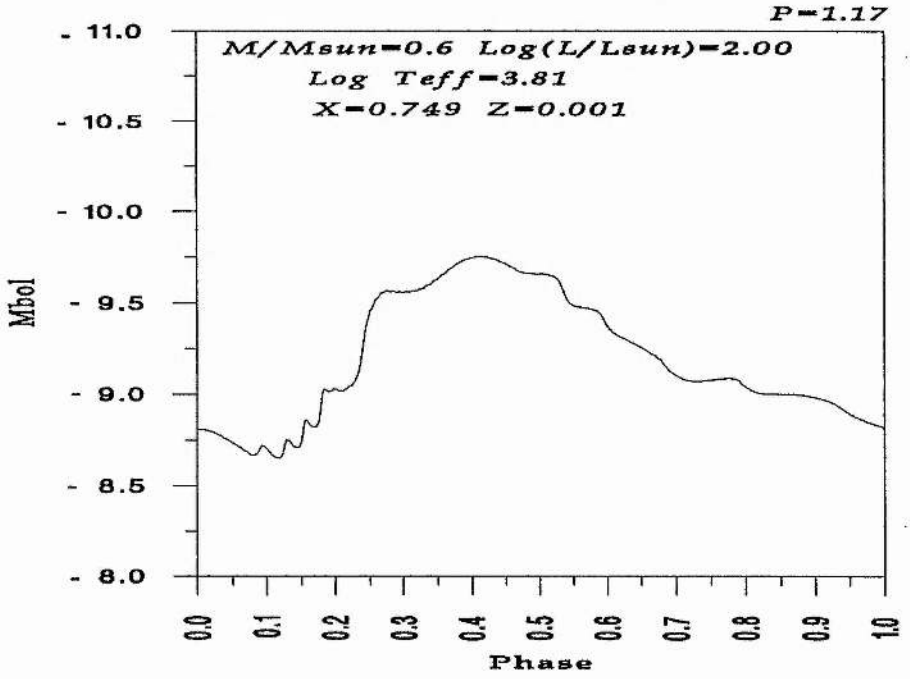
P=1.17
M/Msun=0.6 Log(L/Lsun)=2.00
Log Teff=3.81
X=0.749 Z=0.001
Mbol
- 11.0
- 10.5
- 10.0
- 9.5
- 9.0
- 8.5
- 8.0
0.0 0.1 0.2 0.3 0.4 0.5 0.6 0.7 0.8 0.9 1.0
Phase

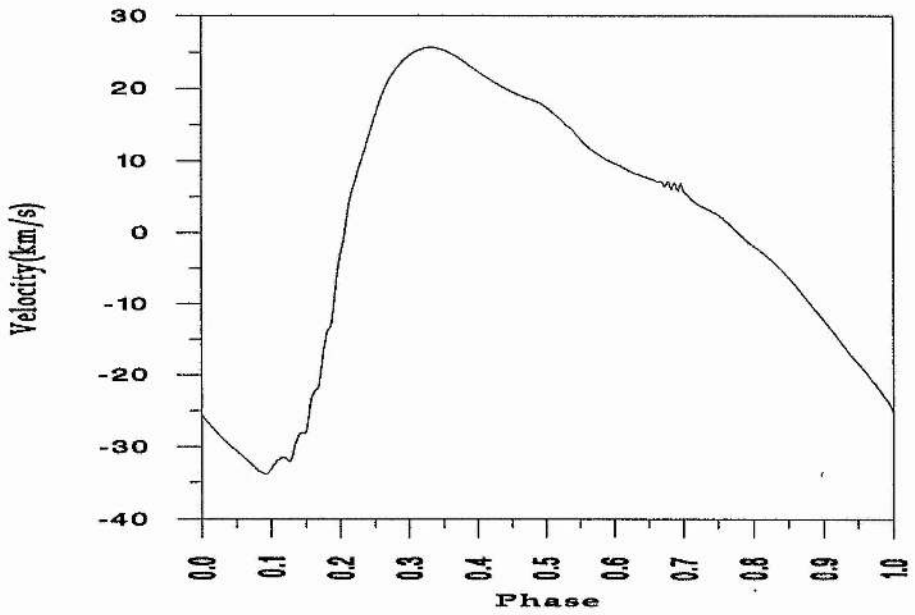
Velocity(km/s)
30
20
10
0
-10
-20
-30
-40
0.0 0.1 0.2 0.3 0.4 0.5 0.6 0.7 0.8 0.9 1.0
Phase

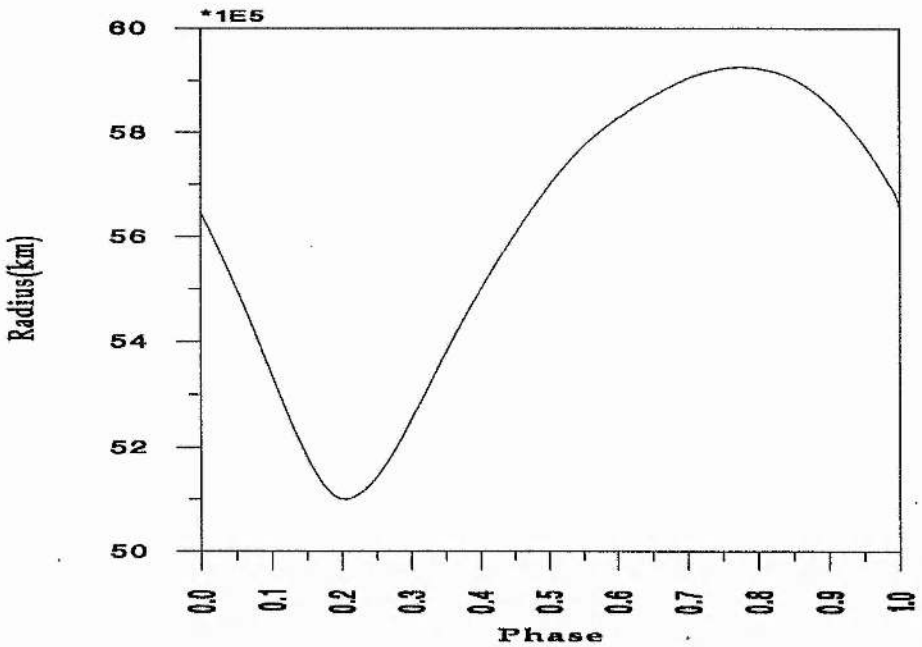
*1E5
Radius(km)
60
58
56
54
52
50
0.0 0.1 0.2 0.3 0.4 0.5 0.6 0.7 0.8 0.9 1.0
Phase

Model(53)

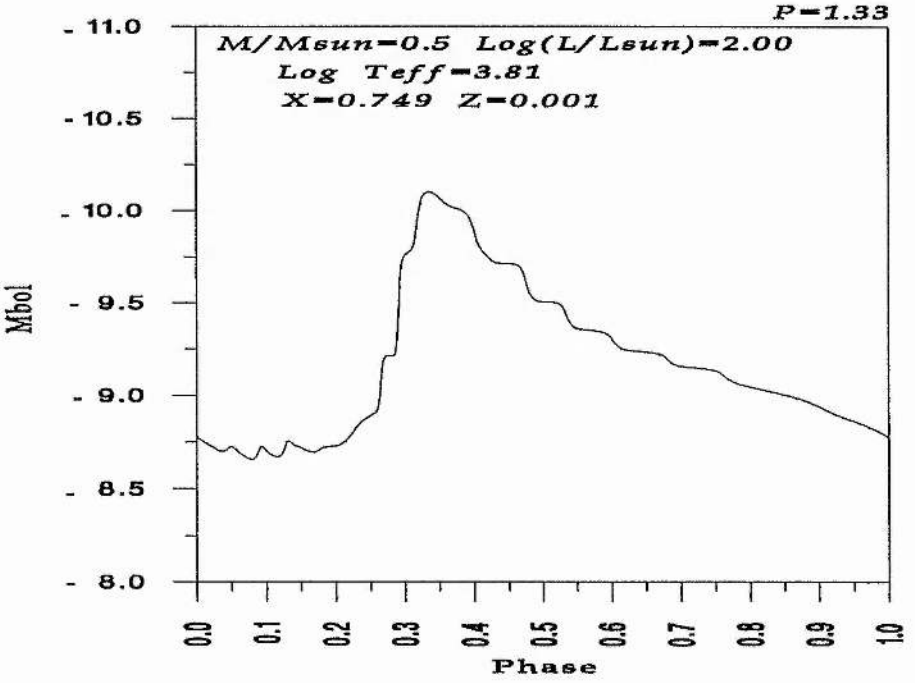
P=1.33
M/Msun=0.5 Log(L/Lsun)=2.00
Log Teff=3.81
X=0.749 Z=0.001
Mbol
- 11.0
- 10.5
- 10.0
- 9.5
- 9.0
- 8.5
- 8.0
0.0 0.1 0.2 0.3 0.4 0.5 0.6 0.7 0.8 0.9 1.0
Phase

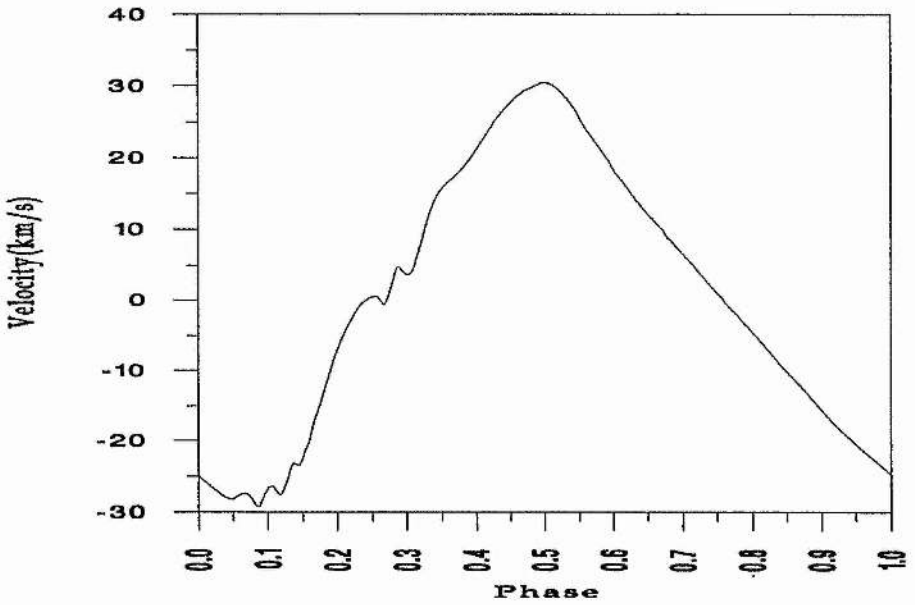
Velocity(km/s)
40
30
20
10
0
-10
-20
-30
0.0 0.1 0.2 0.3 0.4 0.5 0.6 0.7 0.8 0.9 1.0
Phase

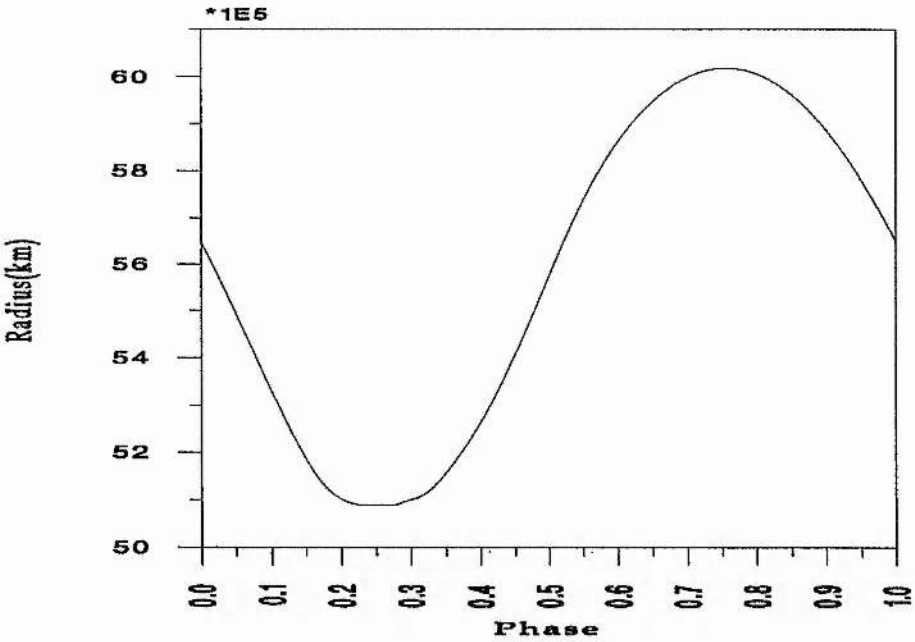
*1E5
Radius(km)
60
58
56
54
52
50
0.0 0.1 0.2 0.3 0.4 0.5 0.6 0.7 0.8 0.9 1.0
Phase

Model(13)

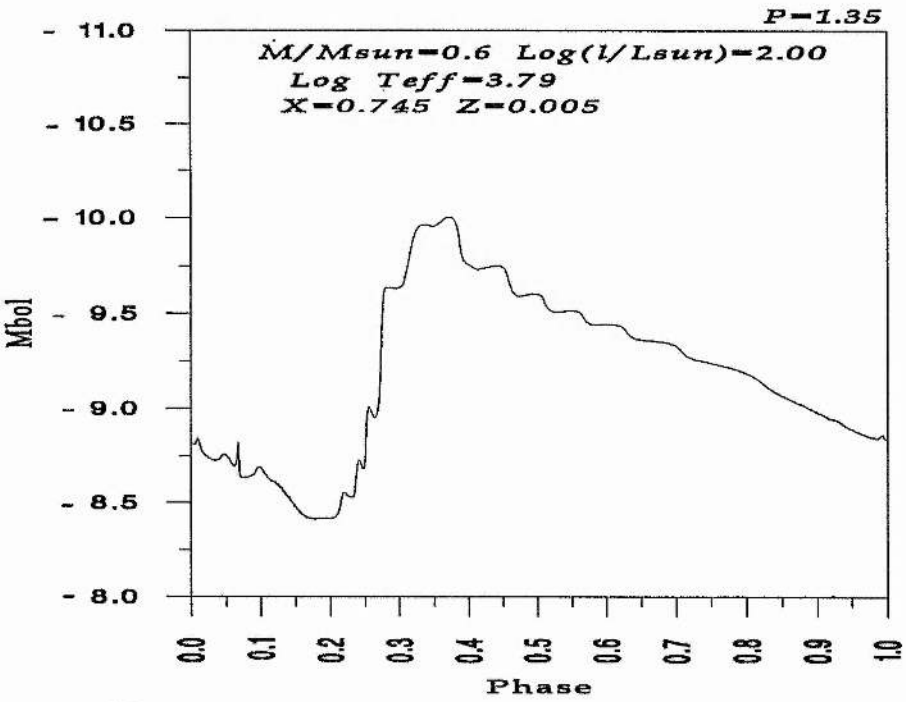
P=1.35
M/Msun=0.6 Log(l/Lsun)=2.00
Log Teff=3.79
X=0.745 Z=0.005
Mbol
11.0
10.5
10.0
9.5
9.0
8.5
8.0
0.0
0.1
0.2
0.3
0.4
0.5
0.6
0.7
0.8
0.9
1.0
Phase

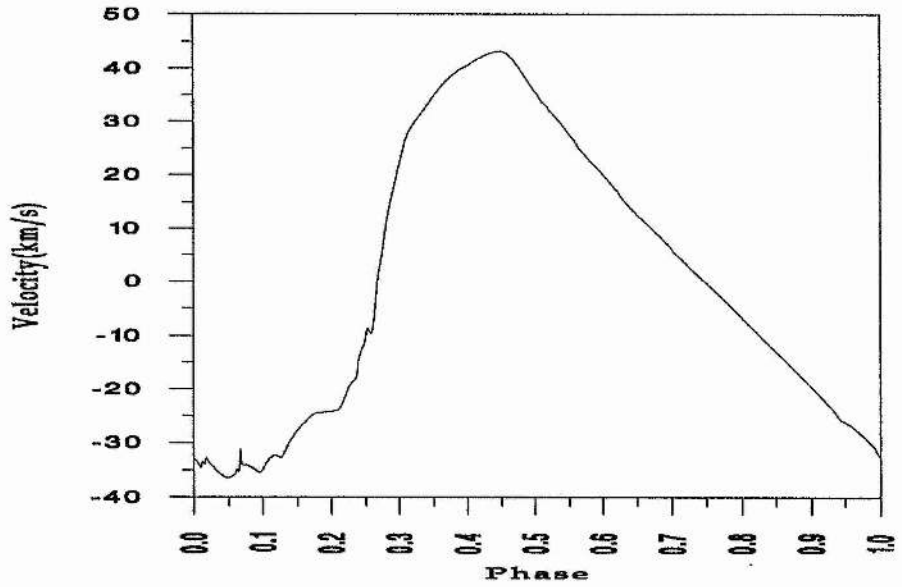
Velocity(km/s)
50
40
30
20
10
0
-10
-20
-30
-40
0.0
0.1
0.2
0.3
0.4
0.5
0.6
0.7
0.8
0.9
1.0
Phase

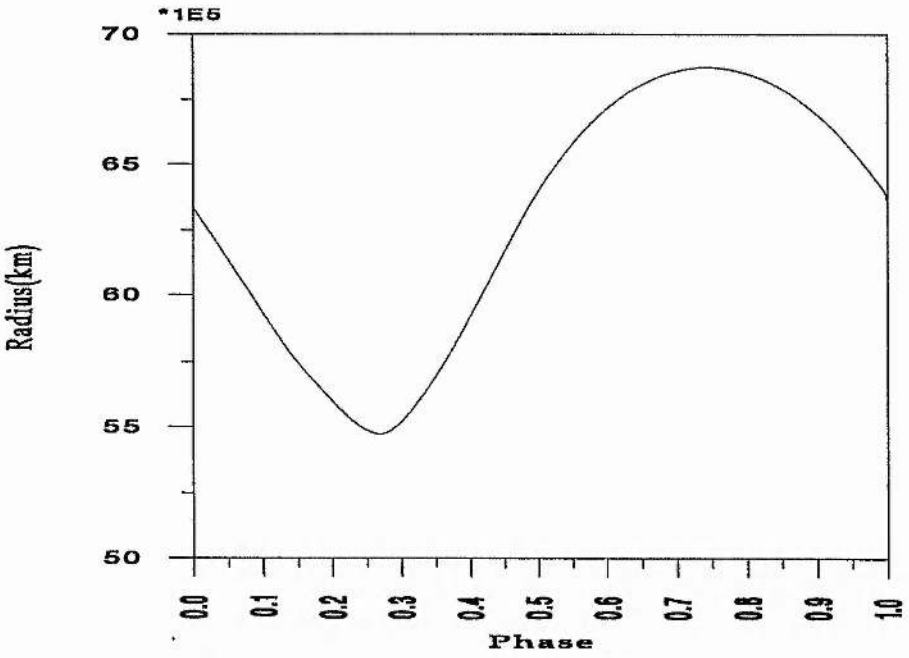
*1E5
Radius(km)
70
65
60
55
50
0.0
0.1
0.2
0.3
0.4
0.5
0.6
0.7
0.8
0.9
1.0
Phase

Model(18)

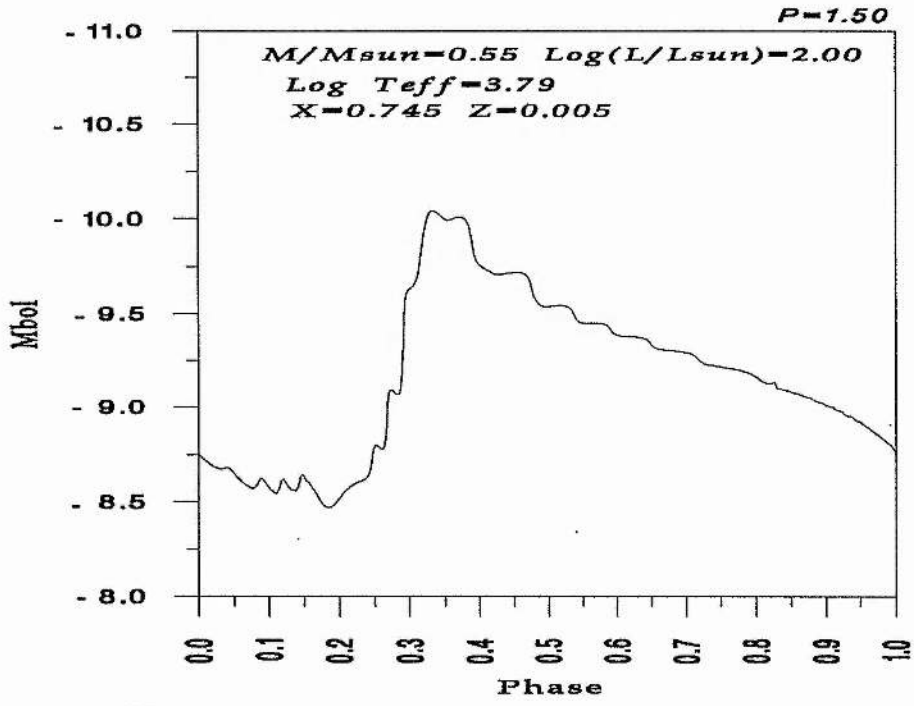
P=1.50
M/Msun=0.55 Log(L/Lsun)=2.00
Log Teff=3.79
X=0.745 Z=0.005
Mbol
- 11.0
- 10.5
- 10.0
- 9.5
- 9.0
- 8.5
- 8.0
0.0 0.1 0.2 0.3 0.4 0.5 0.6 0.7 0.8 0.9 1.0
Phase

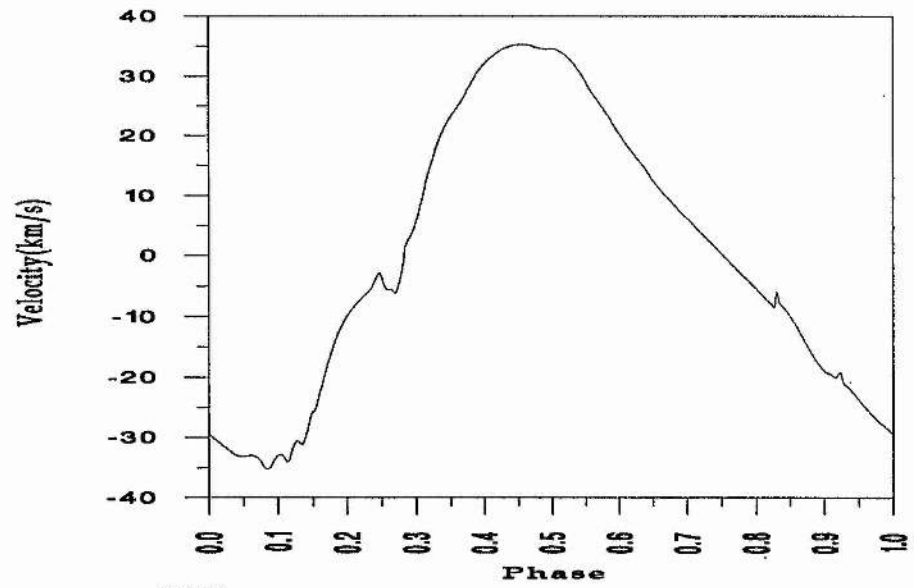
Velocity(km/s)
40
30
20
10
0
-10
-20
-30
-40
0.0 0.1 0.2 0.3 0.4 0.5 0.6 0.7 0.8 0.9 1.0
Phase

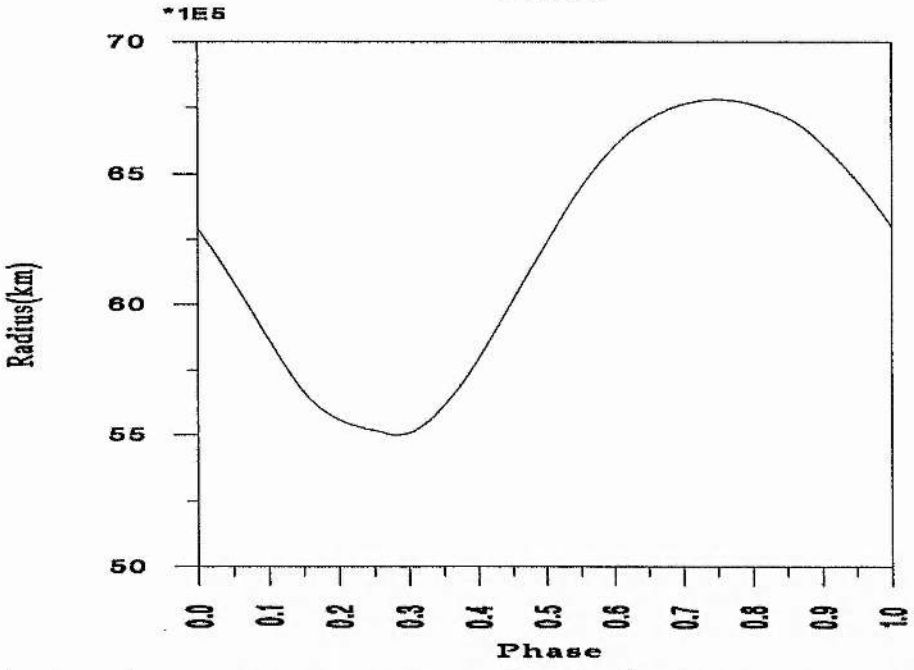
*1E5
Radius(km)
70
65
60
55
50
0.0 0.1 0.2 0.3 0.4 0.5 0.6 0.7 0.8 0.9 1.0
Phase

Model(2)

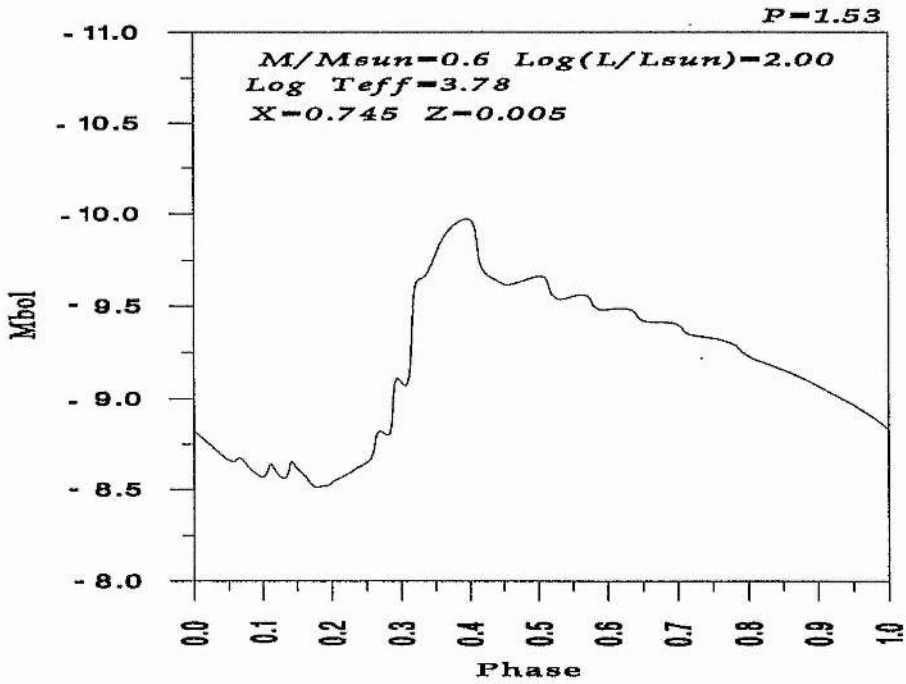
P=1.53
M/Msun=0.6 Log(L/Lsun)=2.00
Log Teff=3.78
X=0.745 Z=0.005
Mbol
- 11.0
- 10.5
- 10.0
- 9.5
- 9.0
- 8.5
- 8.0
0.0 0.1 0.2 0.3 0.4 0.5 0.6 0.7 0.8 0.9 1.0
Phase

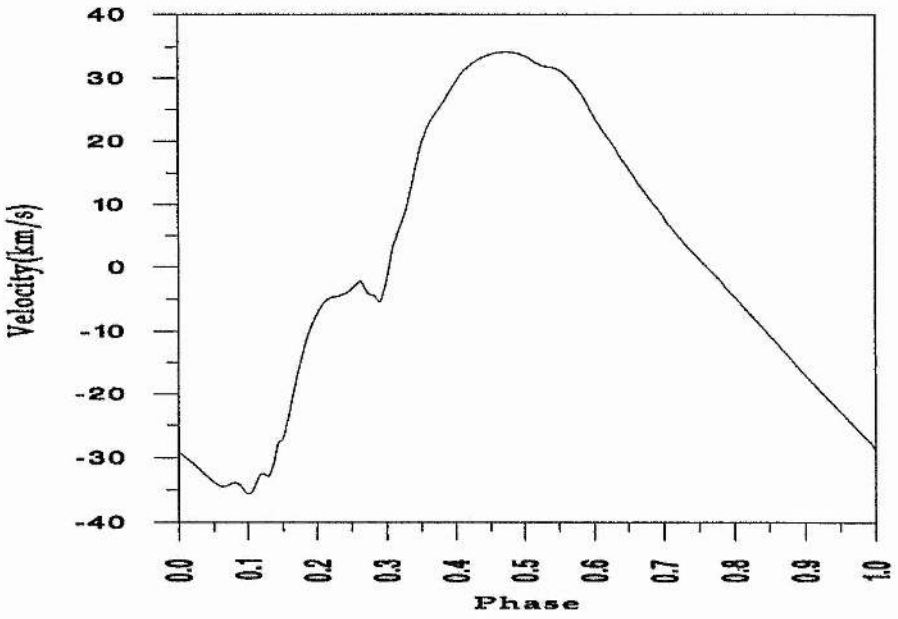
Velocity(km/s)
40
30
20
10
0
-10
-20
-30
-40
0.0 0.1 0.2 0.3 0.4 0.5 0.6 0.7 0.8 0.9 1.0
Phase

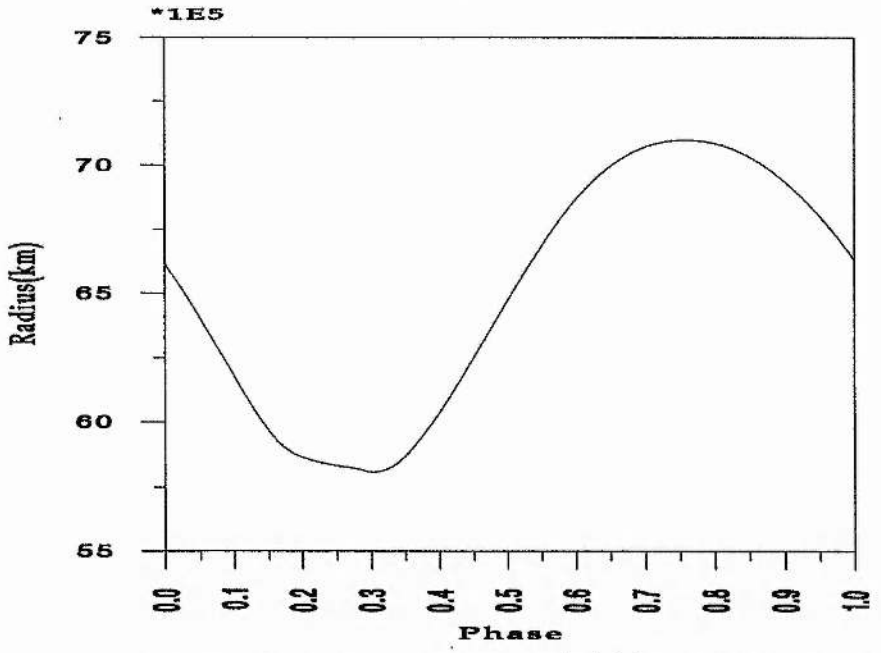
*1E5
Radius(km)
75
70
65
60
55
0.0 0.1 0.2 0.3 0.4 0.5 0.6 0.7 0.8 0.9 1.0
Phase

Model(19)

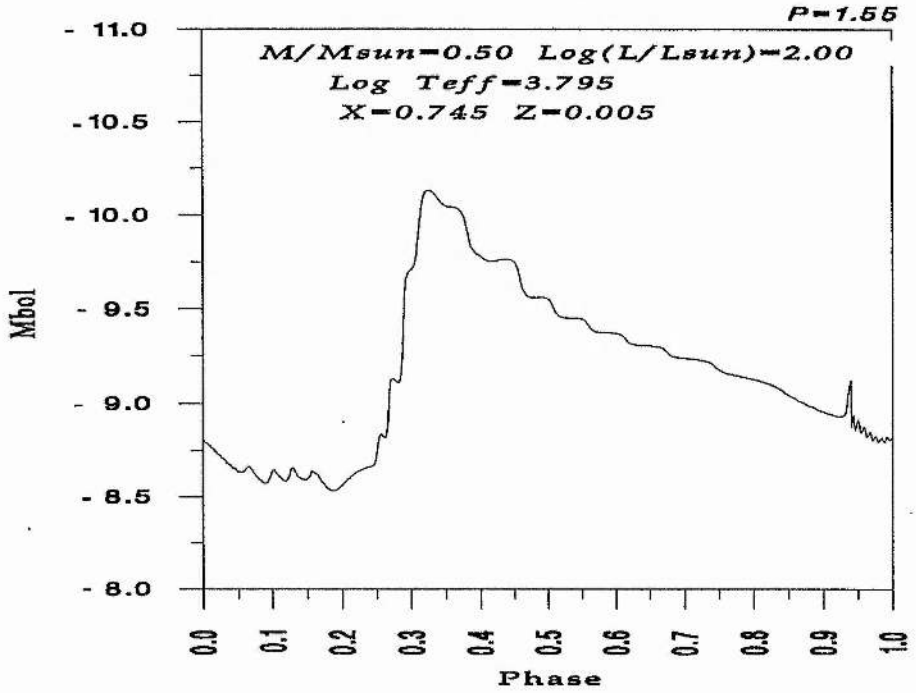
P=1.55
M/Msun=0.50 Log(L/Lsun)=2.00
Log Teff=3.795
X=0.745 Z=0.005
Mbol
- 11.0
-10.5
- 10.0
- 9.5
- 9.0
- 8.5
- 8.0
0.0
0.1
0.2
0.3
0.4
0.5
0.6
0.7
0.8
0.9
1.0
Phase

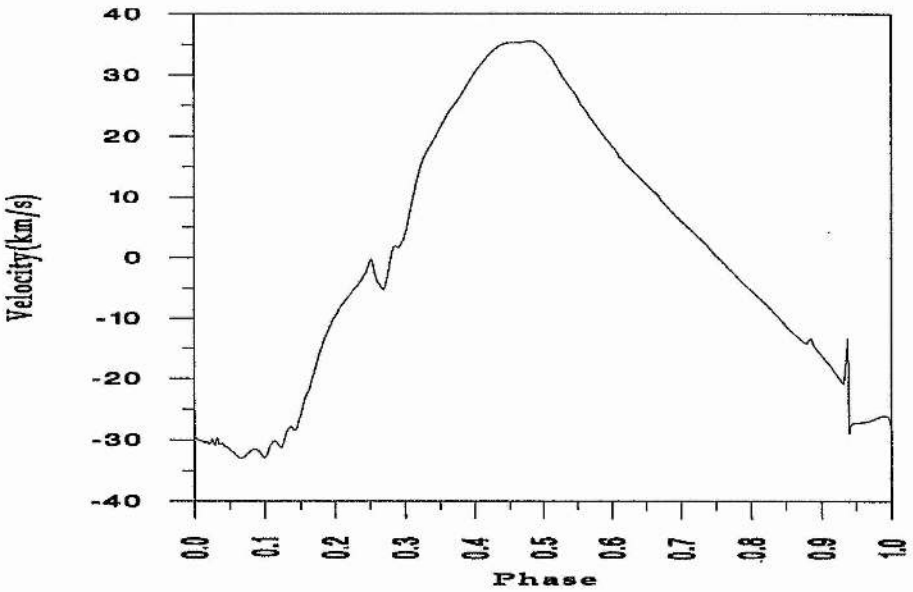
Velocity(km/s)
40
30
20
10
0
-10
-20
-30
-40
0.0
0.1
0.2
0.3
0.4
0.5
0.6
0.7
0.8
0.9
1.0
Phase

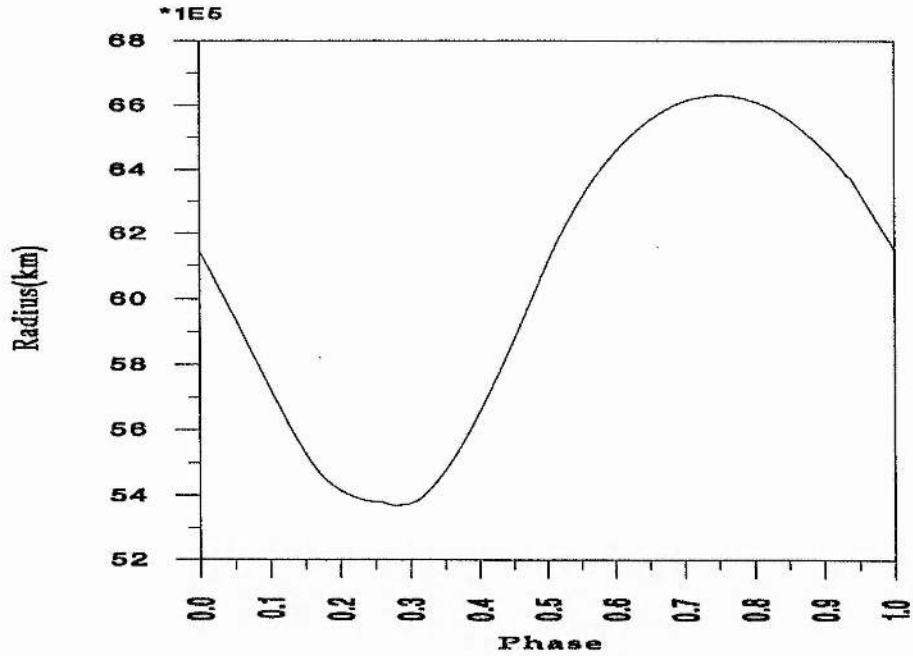
*1E5
Radius(km)
68
66
64
62
60
58
56
54
52
0.0
0.1
0.2
0.3
0.4
0.5
0.6
0.7
0.8
0.9
1.0
Phase

Model(3)

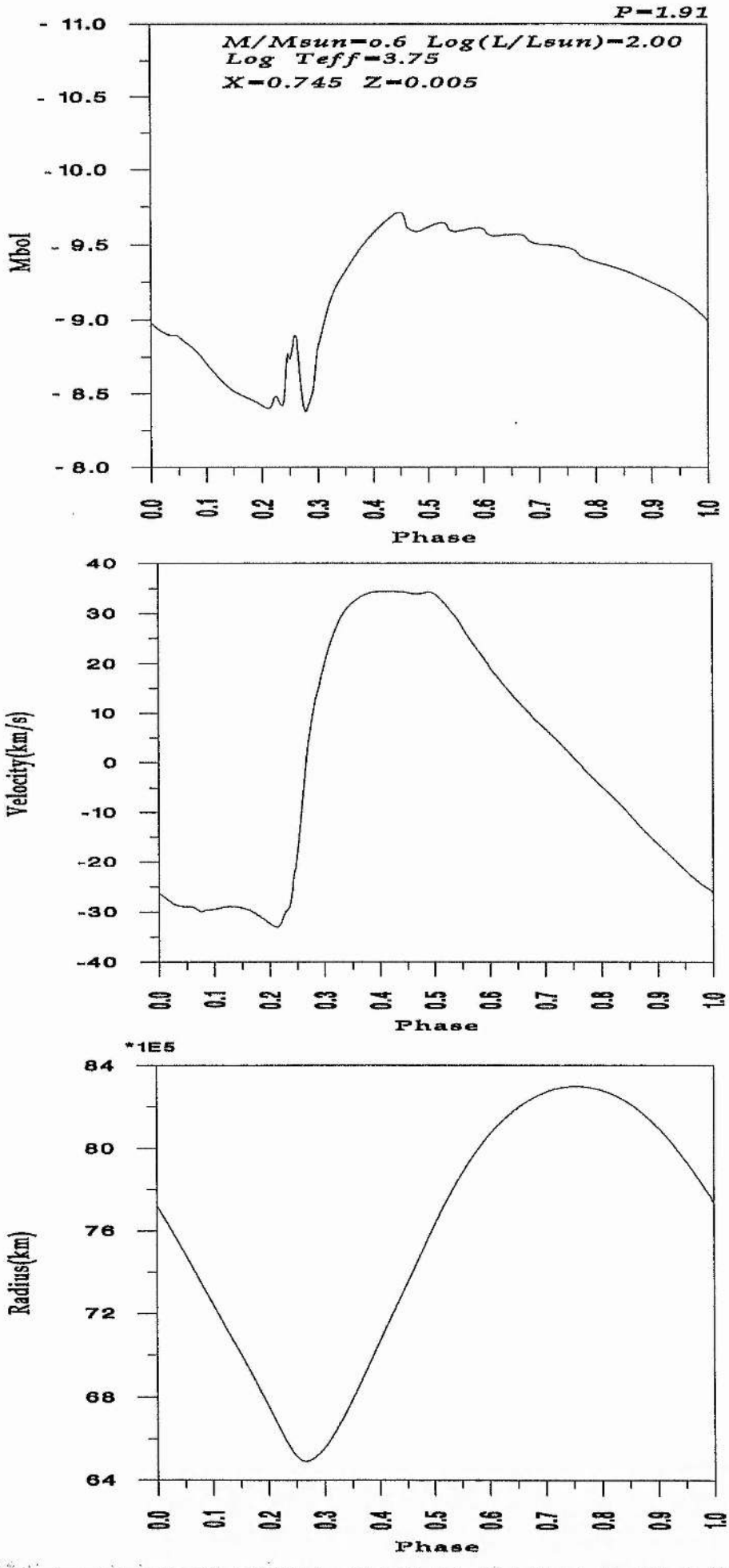
P=1.91
M/Msun=0.6 Log(L/Lsun)=2.00
Log Teff=3.75
X=0.745 Z=0.005
Mbol
- 11.0
- 10.5
- 10.0
- 9.5
- 9.0
- 8.5
- 8.0
0.0 0.1 0.2 0.3 0.4 0.5 0.6 0.7 0.8 0.9 1.0
Phase
Velocity(km/s)
40
30
20
10
0
-10
-20
-30
-40
0.0 0.1 0.2 0.3 0.4 0.5 0.6 0.7 0.8 0.9 1.0
Phase
*1E5
Radius(km)
84
80
76
72
68
64
0.0 0.1 0.2 0.3 0.4 0.5 0.6 0.7 0.8 0.9 1.0
Phase

Model(27)

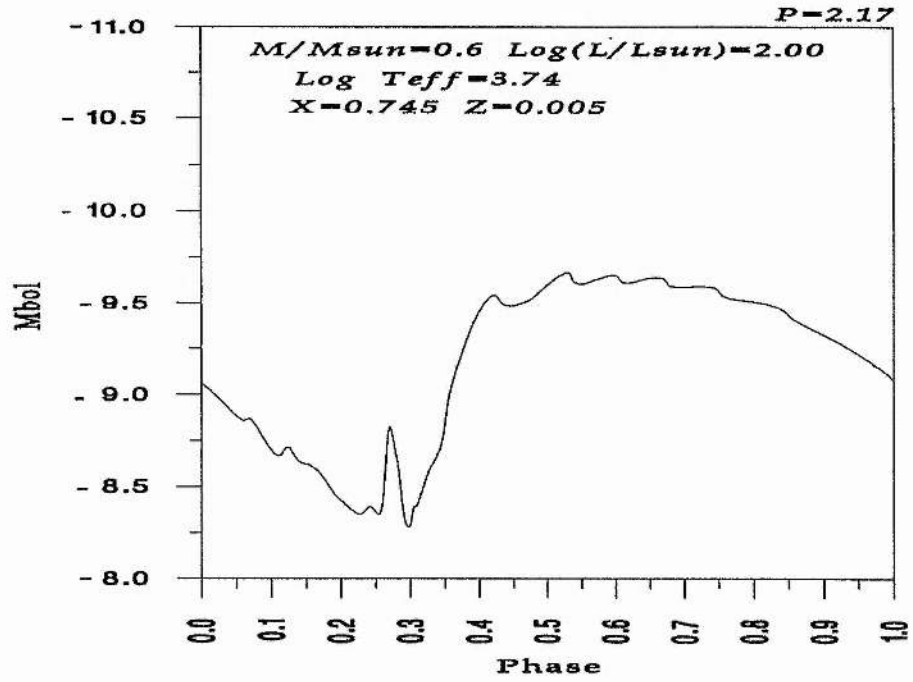
P=2.17
M/Msun=0.6 Log(L/Lsun)=2.00
Log Teff=3.74
X=0.745 Z=0.005
Mbol
-11.0
-10.5
-10.0
-9.5
-9.0
-8.5
-8.0
0.0
0.1
0.2
0.3
0.4
0.5
0.6
0.7
0.8
0.9
1.0
Phase

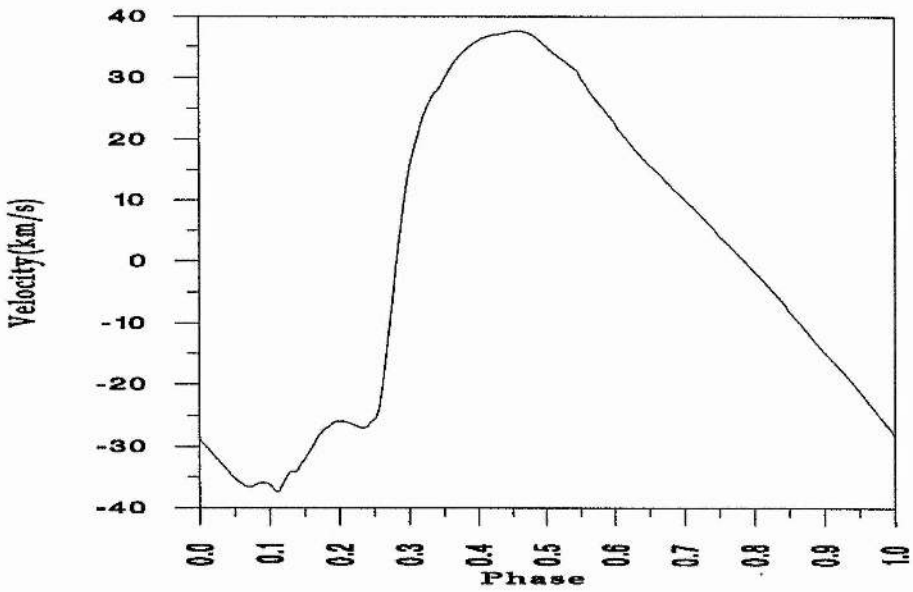
Velocity(km/s)
40
30
20
10
0
-10
-20
-30
-40
0.0
0.1
0.2
0.3
0.4
0.5
0.6
0.7
0.8
0.9
1.0
Phase

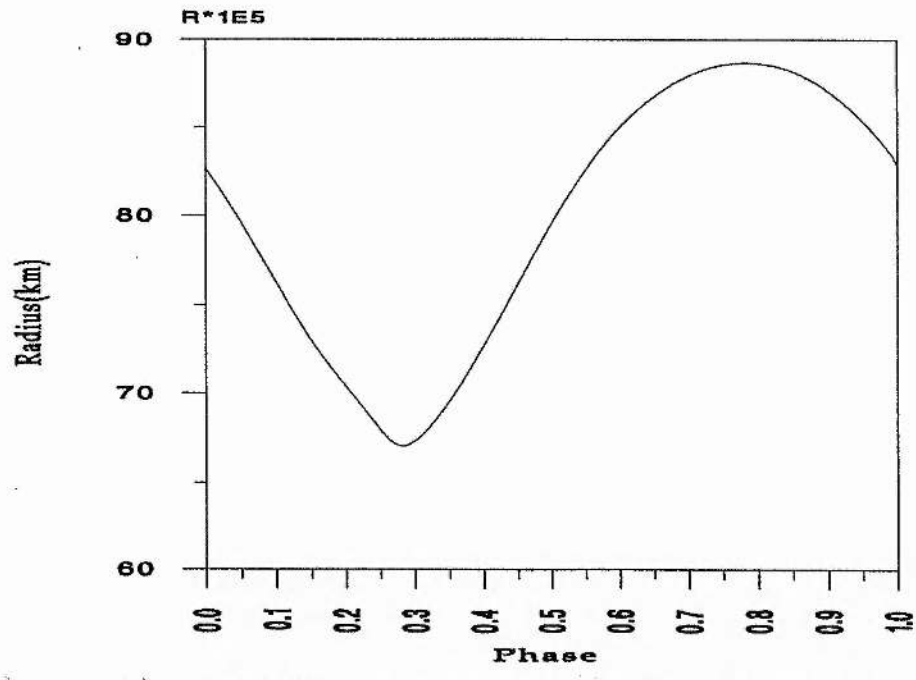
R*1E5
Radius(km)
90
80
70
60
0.0
0.1
0.2
0.3
0.4
0.5
0.6
0.7
0.8
0.9
1.0
Phase

Model(26)

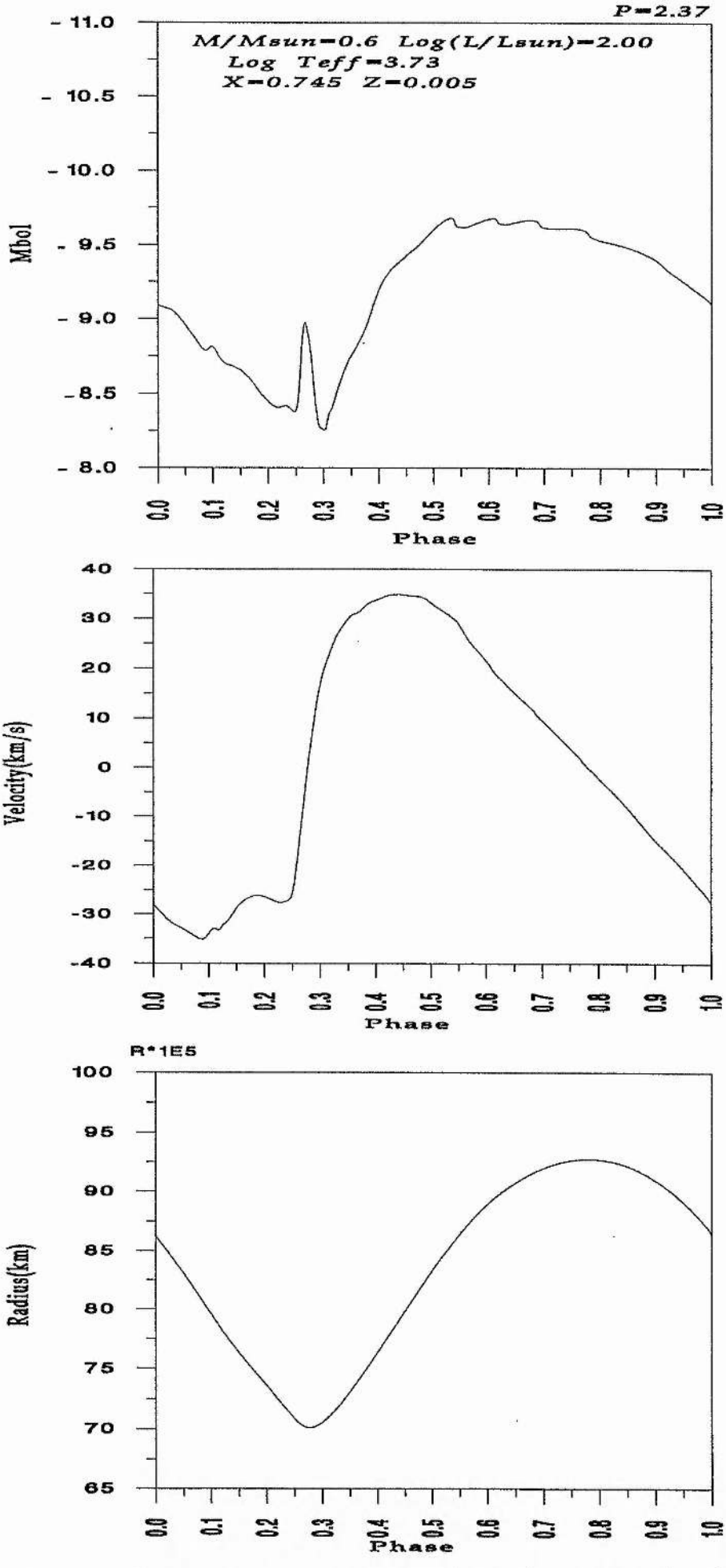
P=2.37
M/Msun=0.6 Log(L/Lsun)=2.00
Log Teff=3.73
X=0.745 Z=0.005
Mbol
-11.0
-10.5
-10.0
-9.5
-9.0
-8.5
-8.0
0.0
0.1
0.2
0.3
0.4
0.5
0.6
0.7
0.8
0.9
1.0
Phase
Velocity(km/s)
40
30
20
10
0
-10
-20
-30
-40
Phase
R*1E5
Radius(km)
100
95
90
85
80
75
70
65
Phase

Model(15)

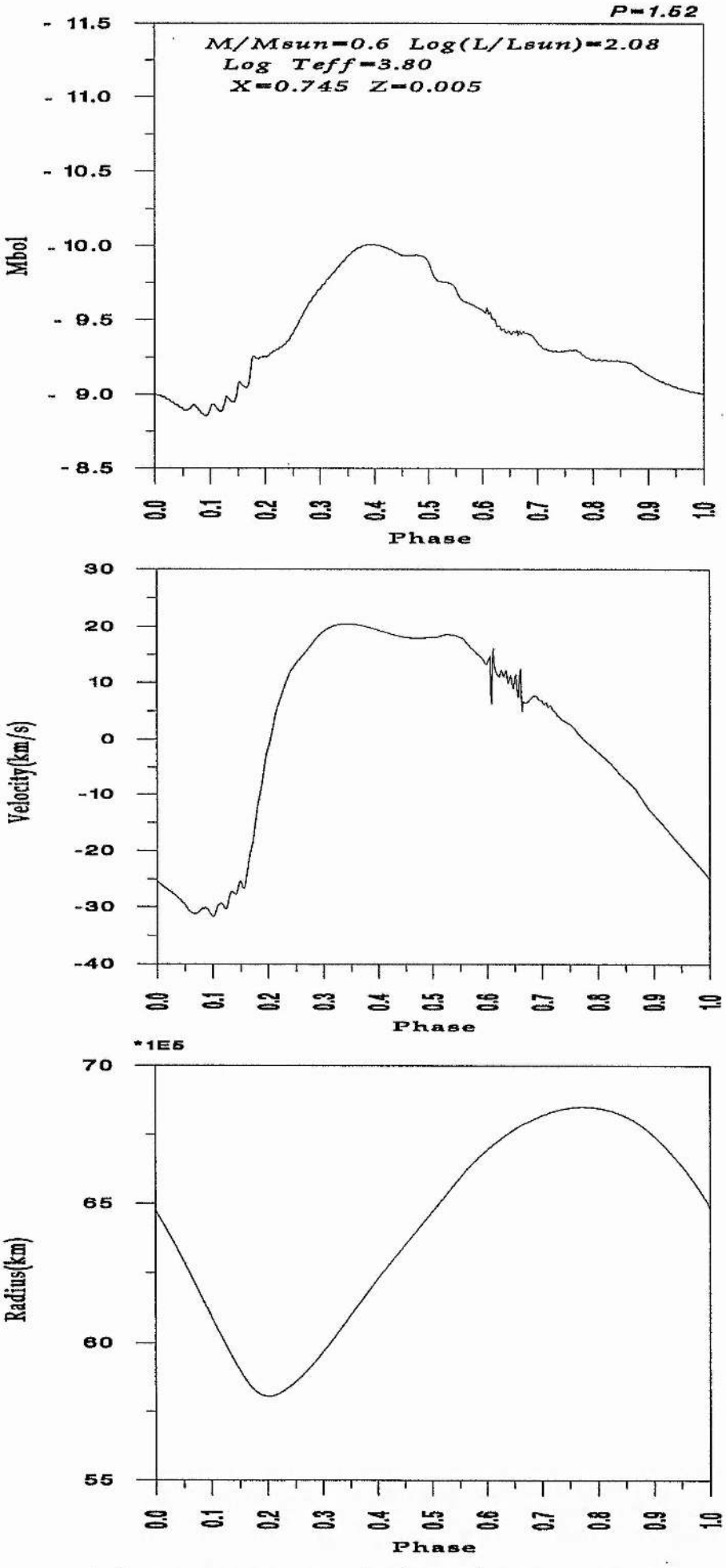
P=1.52
M/Msun=0.6 Log(L/Lsun)=2.08
Log Teff=3.80
X=0.745 Z=0.005
Mbol
- 11.5
- 11.0
- 10.5
- 10.0
- 9.5
- 9.0
- 8.5
0.0 0.1 0.2 0.3 0.4 0.5 0.6 0.7 0.8 0.9 1.0
Phase
Velocity(km/s)
30
20
10
0
-10
-20
-30
-40
0.0 0.1 0.2 0.3 0.4 0.5 0.6 0.7 0.8 0.9 1.0
Phase
*1E5
Radius(km)
70
65
60
55
0.0 0.1 0.2 0.3 0.4 0.5 0.6 0.7 0.8 0.9 1.0
Phase

Model(4)

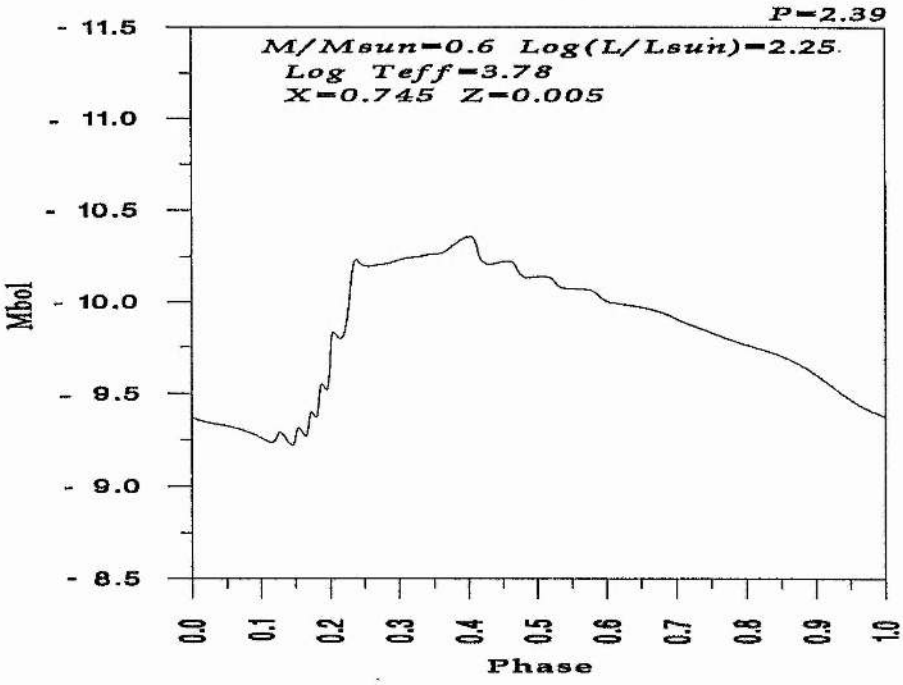
P=2.39
M/Msun=0.6 Log(L/Lsun)=2.25
Log Teff=3.78
X=0.745 Z=0.005
Mbol
- 11.5
- 11.0
- 10.5
- 10.0
- 9.5
- 9.0
- 8.5
0.0 0.1 0.2 0.3 0.4 0.5 0.6 0.7 0.8 0.9 1.0
Phase

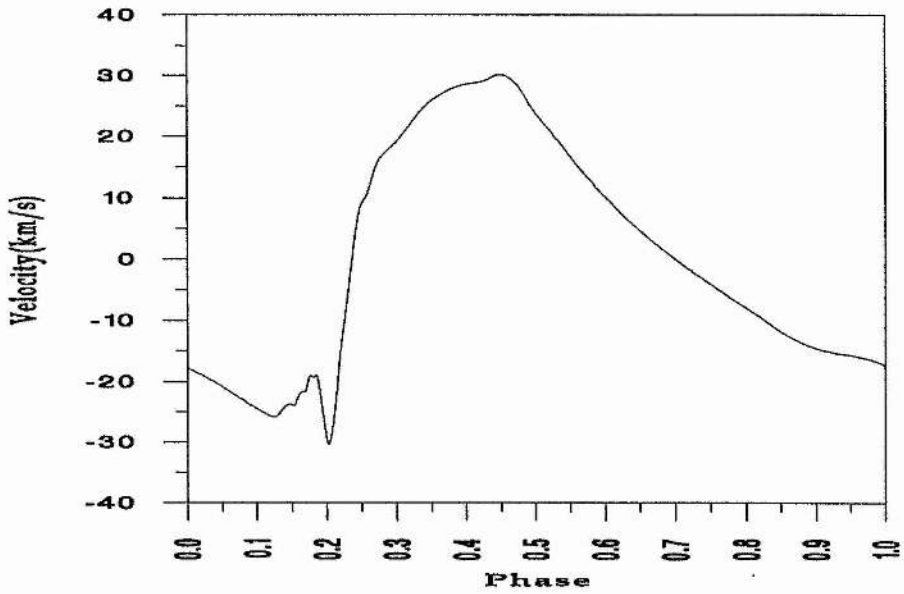
Velocity(km/s)
40
30
20
10
0
-10
-20
-30
-40
0.0 0.1 0.2 0.3 0.4 0.5 0.6 0.7 0.8 0.9 1.0
Phase

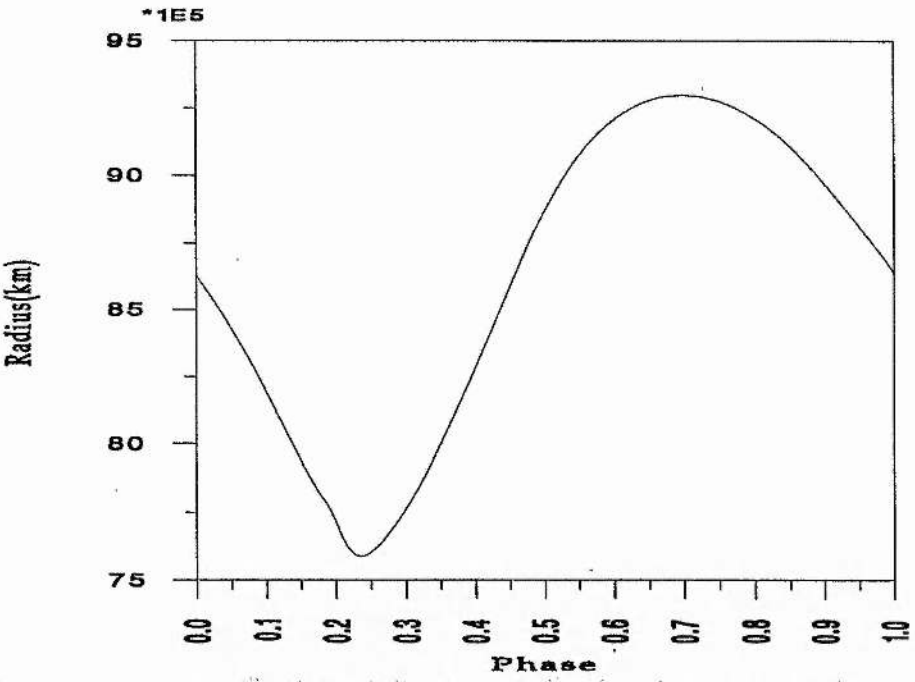
*1E5
Radius(km)
95
90
85
80
75
0.0 0.1 0.2 0.3 0.4 0.5 0.6 0.7 0.8 0.9 1.0
Phase

Model(5)

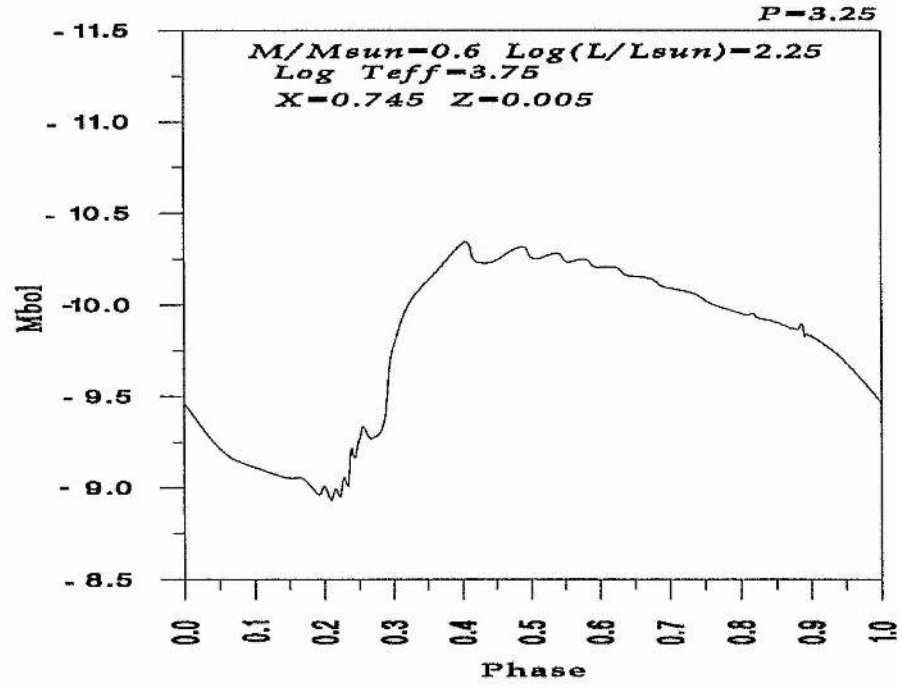
P=3.25
M/Msun=0.6 Log(L/Lsun)=2.25
Log Teff=3.75
X=0.745 Z=0.005
Mbol
-11.5
-11.0
-10.5
-10.0
-9.5
-9.0
-8.5
0.0
0.1
0.2
0.3
0.4
0.5
0.6
0.7
0.8
0.9
1.0
Phase

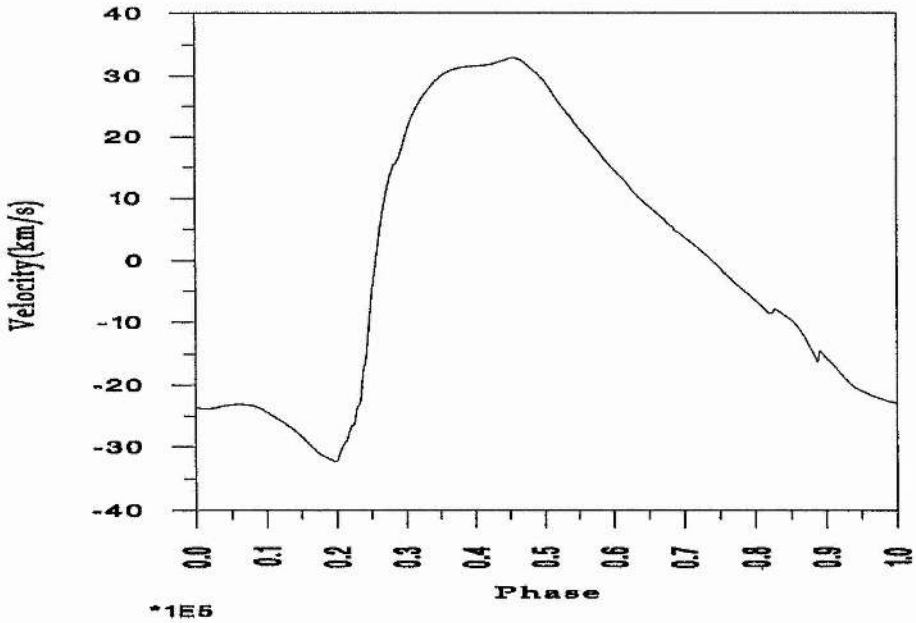
Velocity(km/s)
40
30
20
10
0
-10
-20
-30
-40
0.0
0.1
0.2
0.3
0.4
0.5
0.6
0.7
0.8
0.9
1.0
Phase

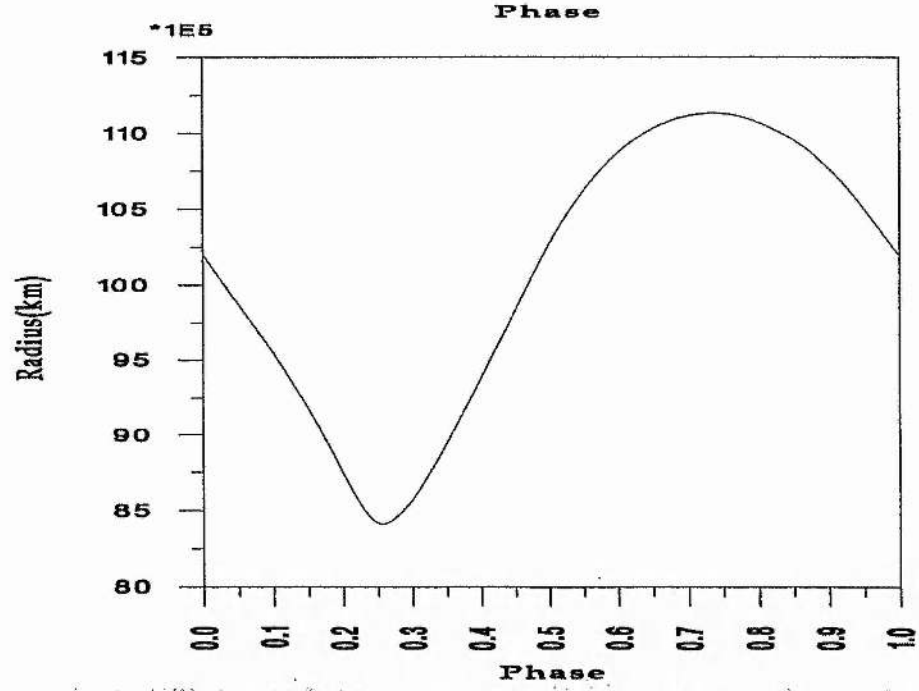
*1E5
Radius(km)
115
110
105
100
95
90
85
80
0.0
0.1
0.2
0.3
0.4
0.5
0.6
0.7
0.8
0.9
1.0
Phase

Model(21)

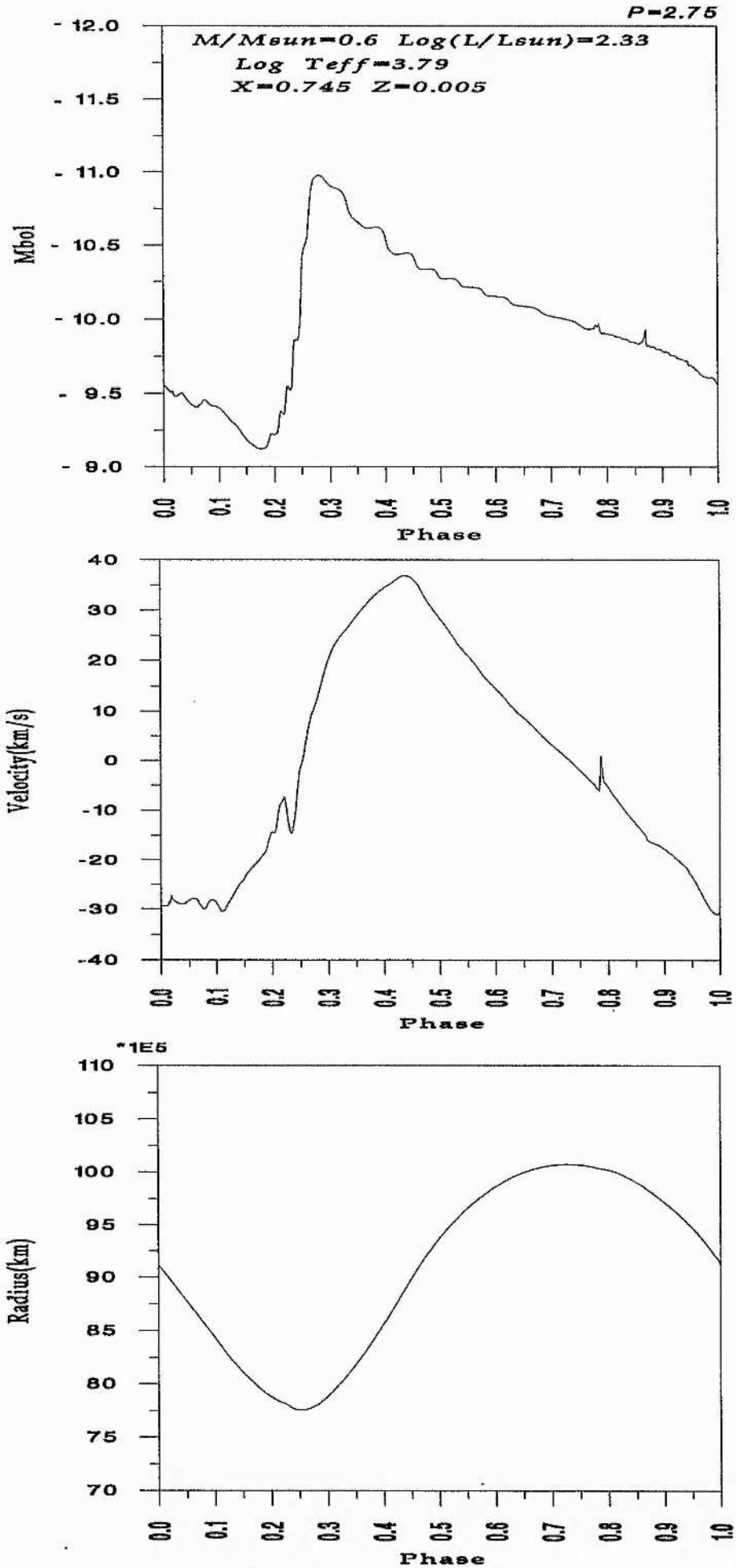
P=2.75
M/Msun=0.6 Log(L/Lsun)=2.33
Log Teff=3.79
X=0.745 Z=0.005
Mbol
- 12.0
- 11.5
- 11.0
- 10.5
- 10.0
- 9.5
- 9.0
0.0 0.1 0.2 0.3 0.4 0.5 0.6 0.7 0.8 0.9 1.0
Phase
Velocity(km/s)
40
30
20
10
0
-10
-20
-30
-40
0.0 0.1 0.2 0.3 0.4 0.5 0.6 0.7 0.8 0.9 1.0
Phase
*1E5
Radius(km)
110
105
100
95
90
85
80
75
70
0.0 0.1 0.2 0.3 0.4 0.5 0.6 0.7 0.8 0.9 1.0
Phase

A-3. LIGHT, VELOCITY & RADIUS CURVES FOR THE W VIR MODELS:-

In this section, we present the light, velocity and radius curves of the W Vir models. These curves have been produced using a programme code created by Dr. T. R. Carson. For each model the mass, the luminosity, the temperature, the amount of hydrogen and metals and the period in days, are mentioned.

Model(6)

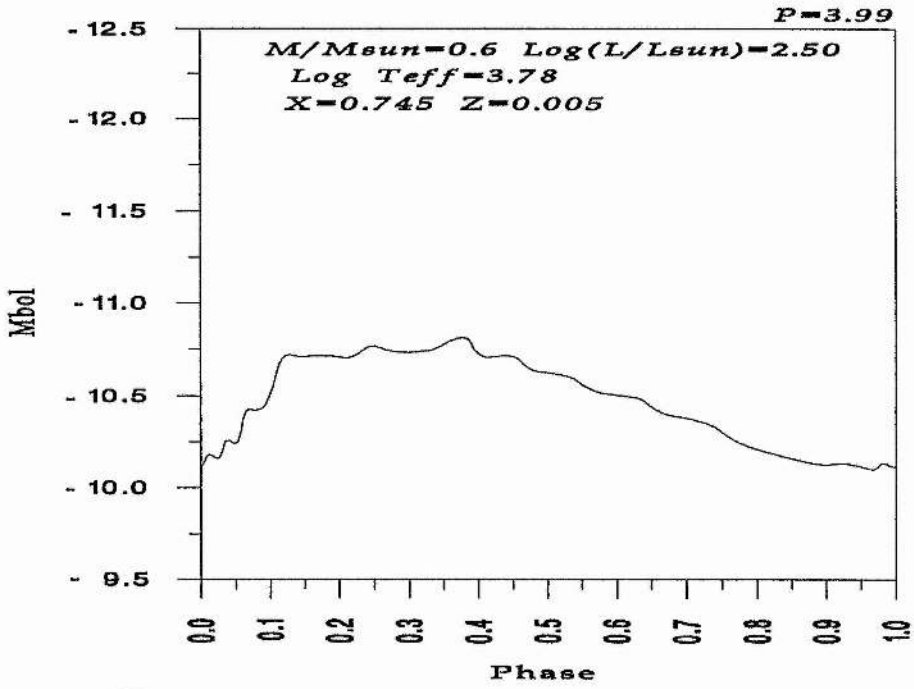
P=3.99
M/Msun=0.6 Log(L/Lsun)=2.50
Log Teff=3.78
X=0.745 Z=0.005
Mbol
-12.5
-12.0
-11.5
-11.0
-10.5
-10.0
-9.5
0.0
0.1
0.2
0.3
0.4
0.5
0.6
0.7
0.8
0.9
1.0
Phase

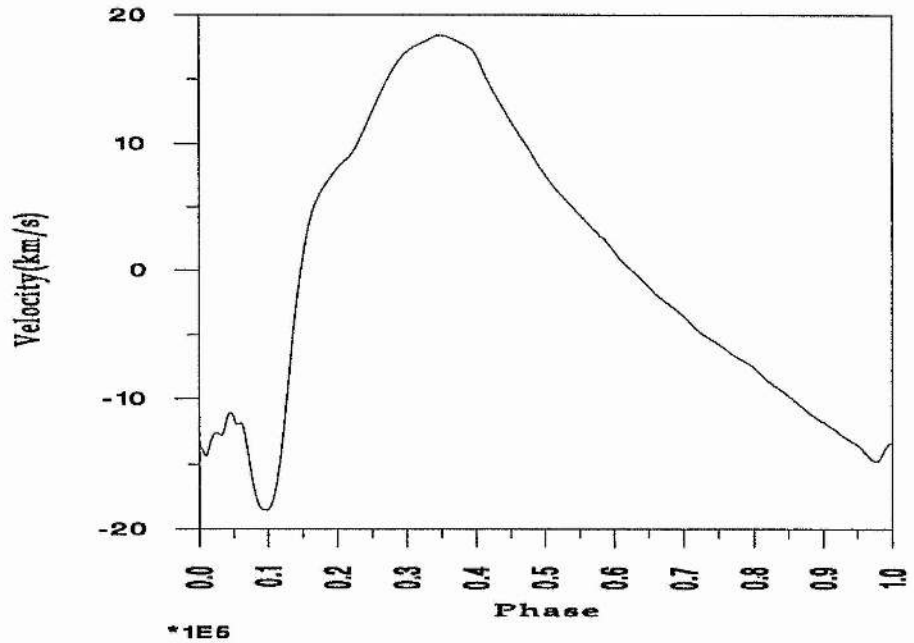
Velocity(km/s)
20
10
0
-10
-20
0.0
0.1
0.2
0.3
0.4
0.5
0.6
0.7
0.8
0.9
1.0
Phase

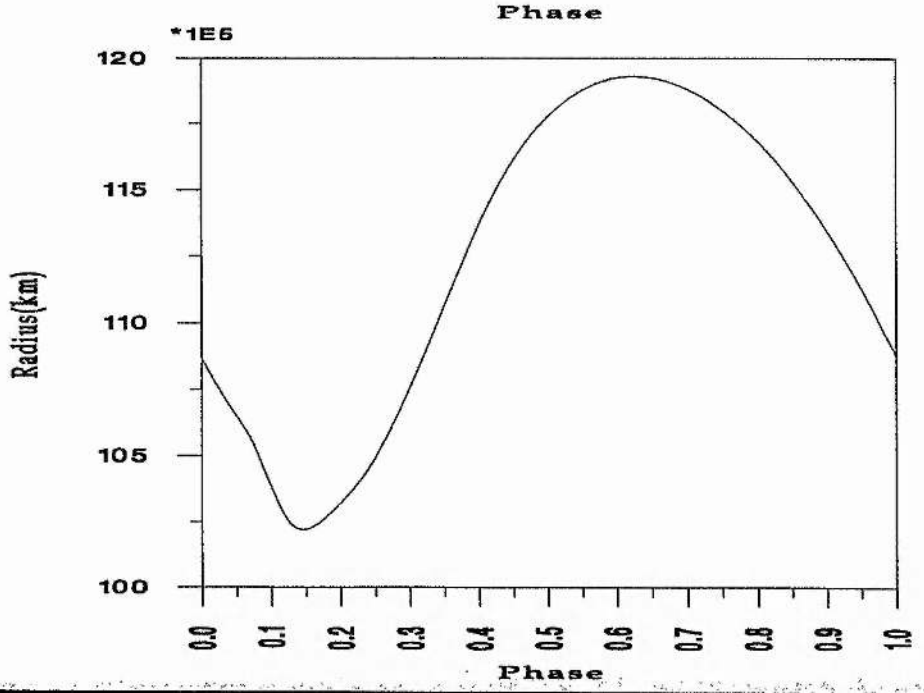
*1E6
Radius(km)
120
115
110
105
100
0.0
0.1
0.2
0.3
0.4
0.5
0.6
0.7
0.8
0.9
1.0
Phase

Model(7)

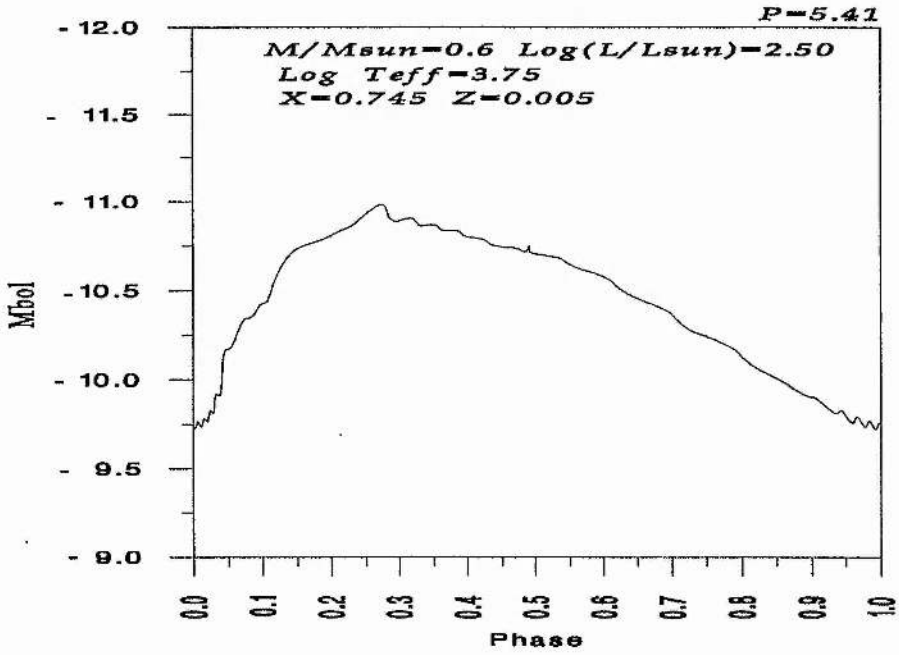
P=5.41
M/Msun=0.6 Log(L/Lsun)=2.50
Log Teff=3.75
X=0.745 Z=0.005
Mbol
-12.0
-11.5
-11.0
-10.5
-10.0
-9.5
-9.0
0.0
0.1
0.2
0.3
0.4
0.5
0.6
0.7
0.8
0.9
1.0
Phase

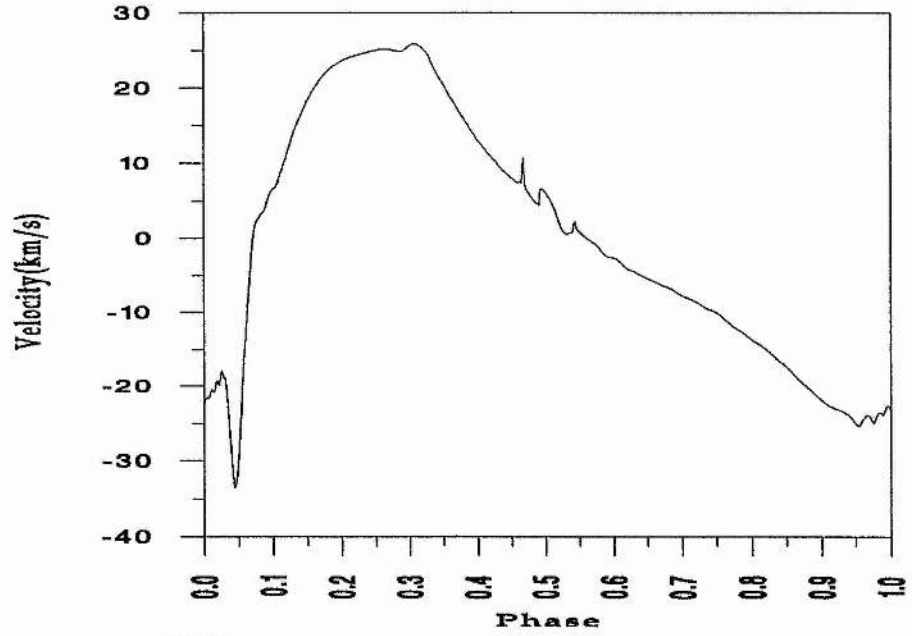
Velocity(km/s)
30
20
10
0
-10
-20
-30
-40
0.0
0.1
0.2
0.3
0.4
0.5
0.6
0.7
0.8
0.9
1.0
Phase

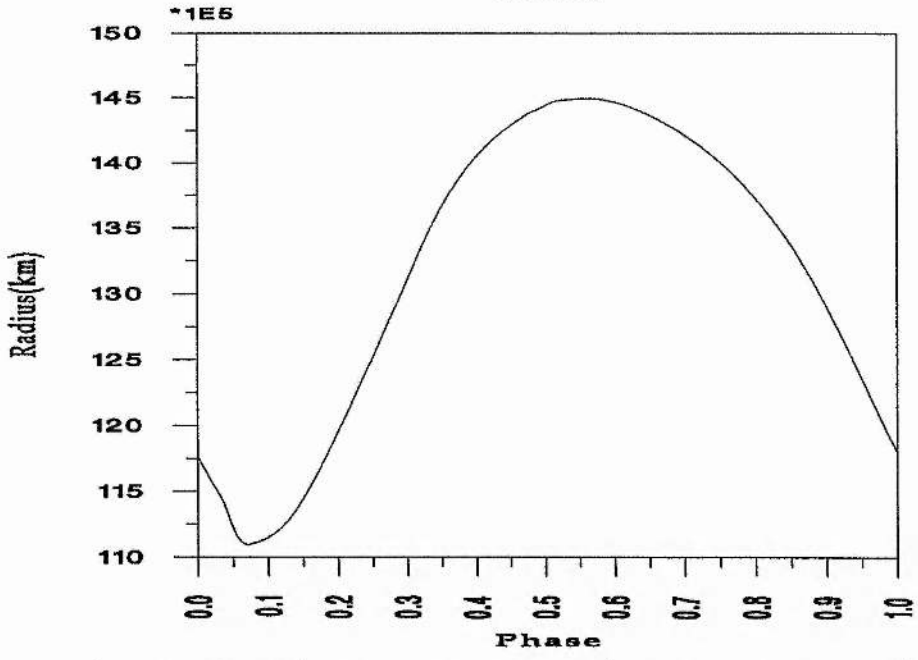
*1E5
Radius(km)
150
145
140
135
130
125
120
115
110
0.0
0.1
0.2
0.3
0.4
0.5
0.6
0.7
0.8
0.9
1.0
Phase

Model(8)

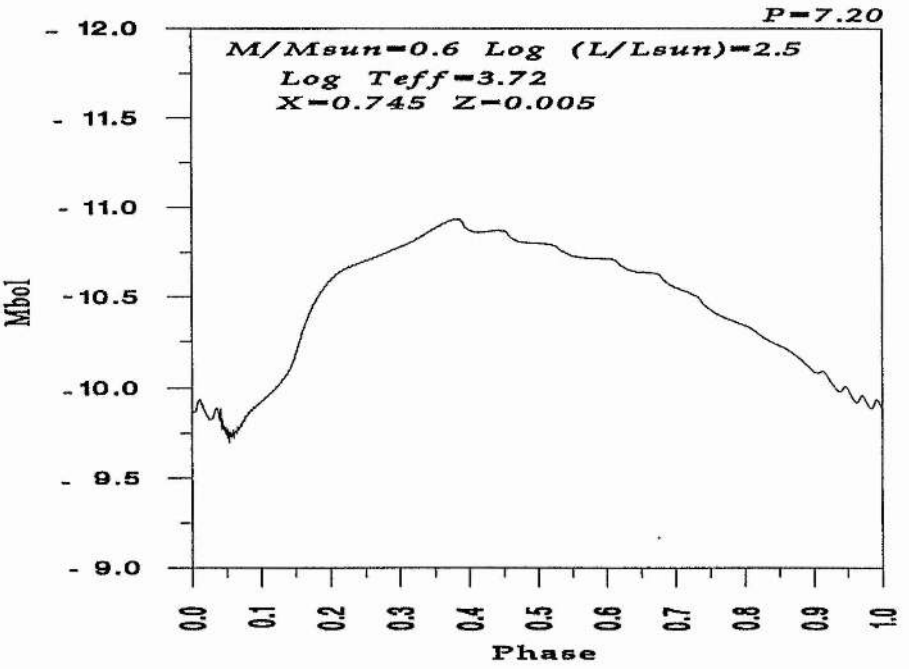
P=7.20
M/Msun=0.6 Log (L/Lsun)=2.5
Log Teff=3.72
X=0.745 Z=0.005
Mbol
- 12.0
- 11.5
- 11.0
-10.5
-10.0
- 9.5
- 9.0
0.0 0.1 0.2 0.3 0.4 0.5 0.6 0.7 0.8 0.9 1.0
Phase

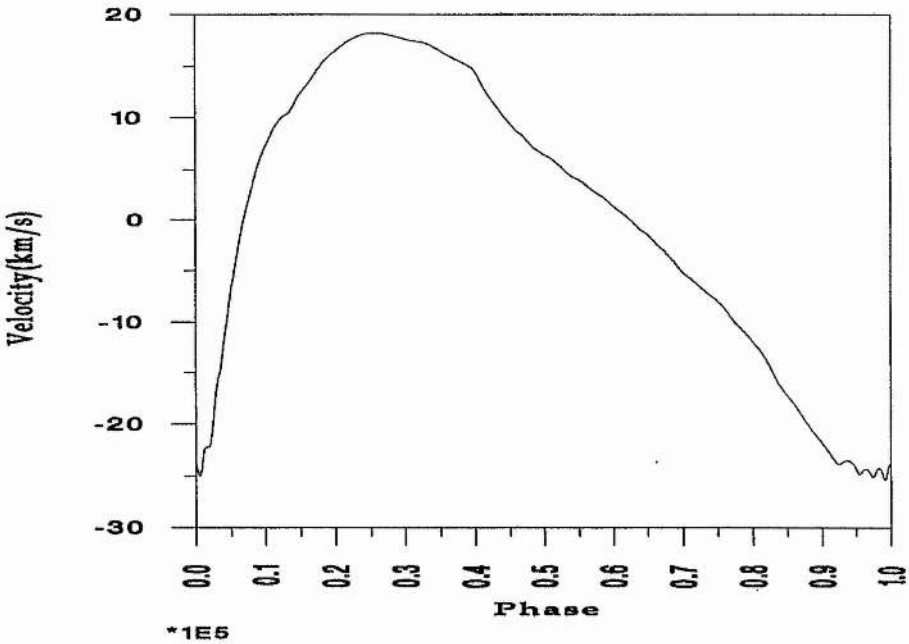
Velocity(km/s)
20
10
0
-10
-20
-30
0.0 0.1 0.2 0.3 0.4 0.5 0.6 0.7 0.8 0.9 1.0
Phase

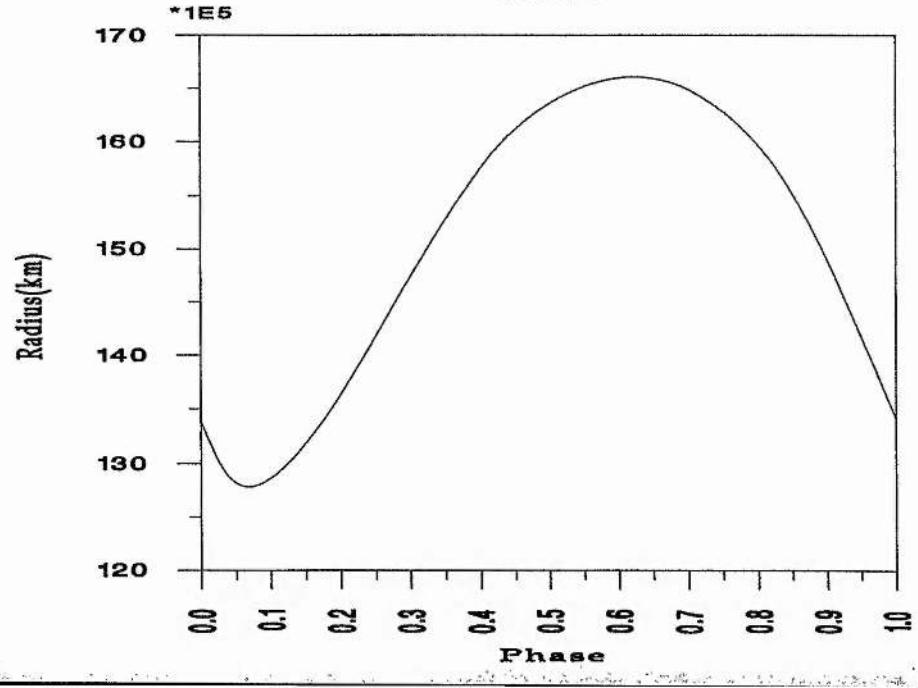
*1E5
Radius(km)
170
160
150
140
130
120
0.0 0.1 0.2 0.3 0.4 0.5 0.6 0.7 0.8 0.9 1.0
Phase

Model(25)

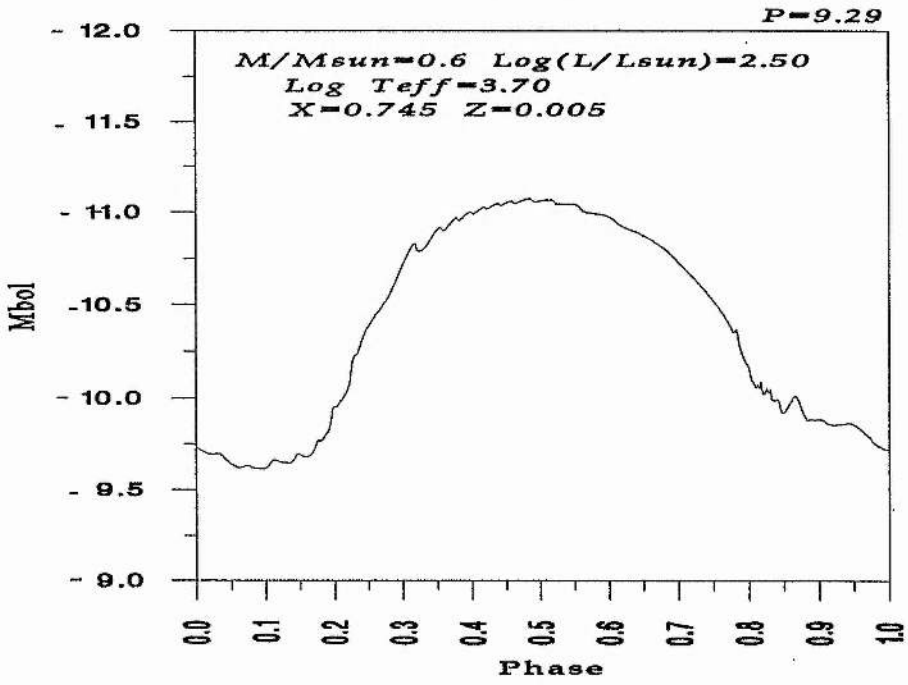
P=9.29
M/Msun=0.6 Log(L/Lsun)=2.50
Log Teff=3.70
X=0.745 Z=0.005
Mbol
12.0
11.5
11.0
10.5
10.0
9.5
9.0
0.0
0.1
0.2
0.3
0.4
0.5
0.6
0.7
0.8
0.9
1.0
Phase

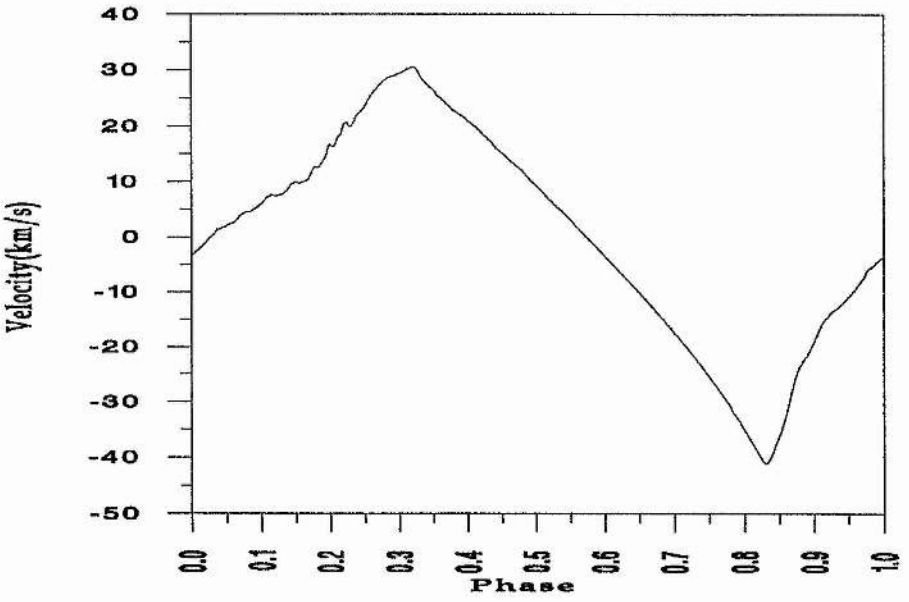
Velocity(km/s)
40
30
20
10
0
-10
-20
-30
-40
-50
0.0
0.1
0.2
0.3
0.4
0.5
0.6
0.7
0.8
0.9
1.0
Phase

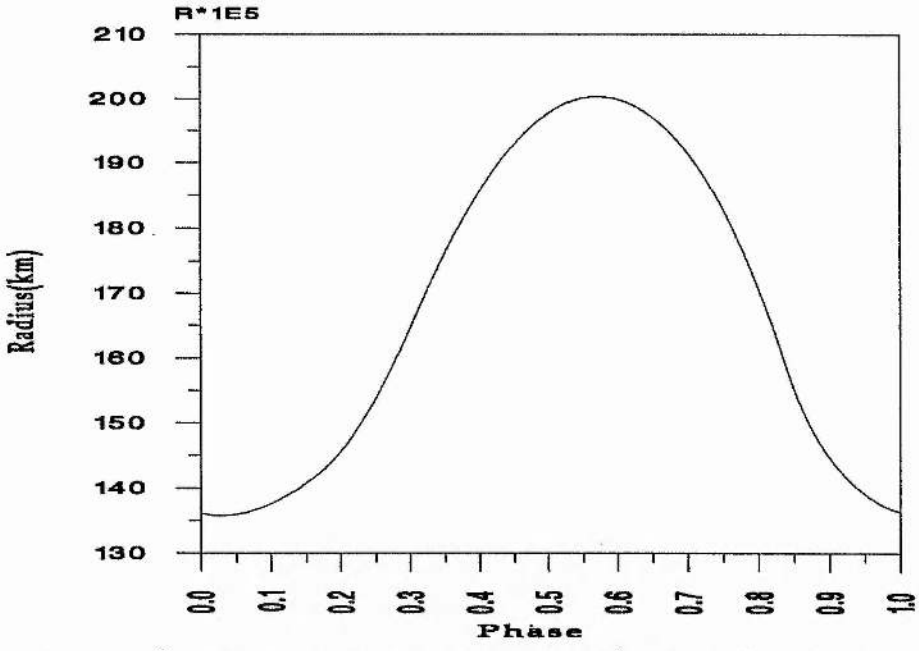
R*1E5
Radius(km)
210
200
190
180
170
160
150
140
130
0.0
0.1
0.2
0.3
0.4
0.5
0.6
0.7
0.8
0.9
1.0
Phase

Model(31)

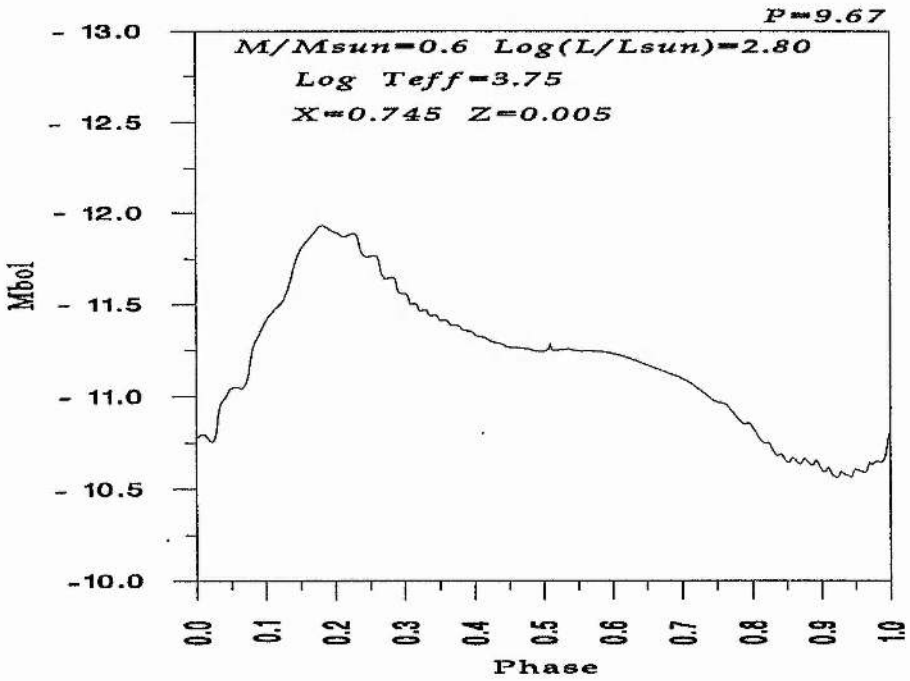
P=9.67
M/Msun=0.6 Log(L/Lsun)=2.80
Log Teff=3.75
X=0.745 Z=0.005
Mbol
- 13.0
- 12.5
- 12.0
- 11.5
- 11.0
- 10.5
-10.0
0.0 0.1 0.2 0.3 0.4 0.5 0.6 0.7 0.8 0.9 1.0
Phase

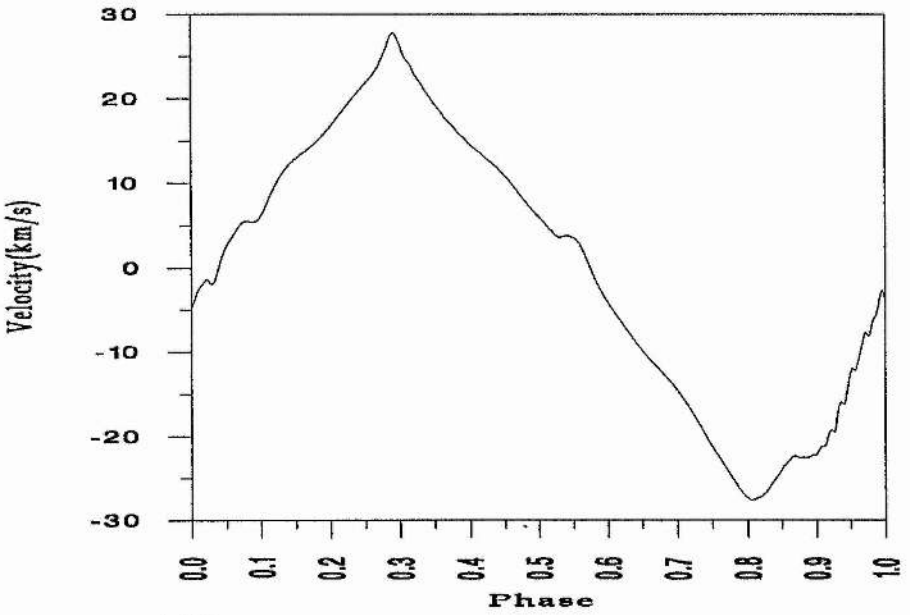
Velocity(km/s)
30
20
10
0
-10
-20
-30
0.0 0.1 0.2 0.3 0.4 0.5 0.6 0.7 0.8 0.9 1.0
Phase

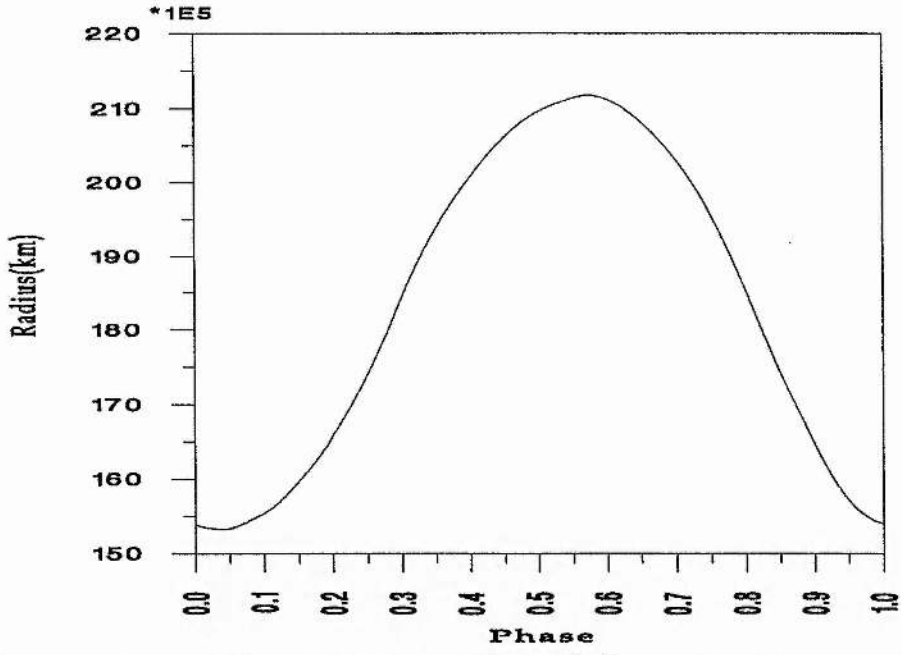
*1E5
Radius(km)
220
210
200
190
180
170
160
150
0.0 0.1 0.2 0.3 0.4 0.5 0.6 0.7 0.8 0.9 1.0
Phase

Model(34)

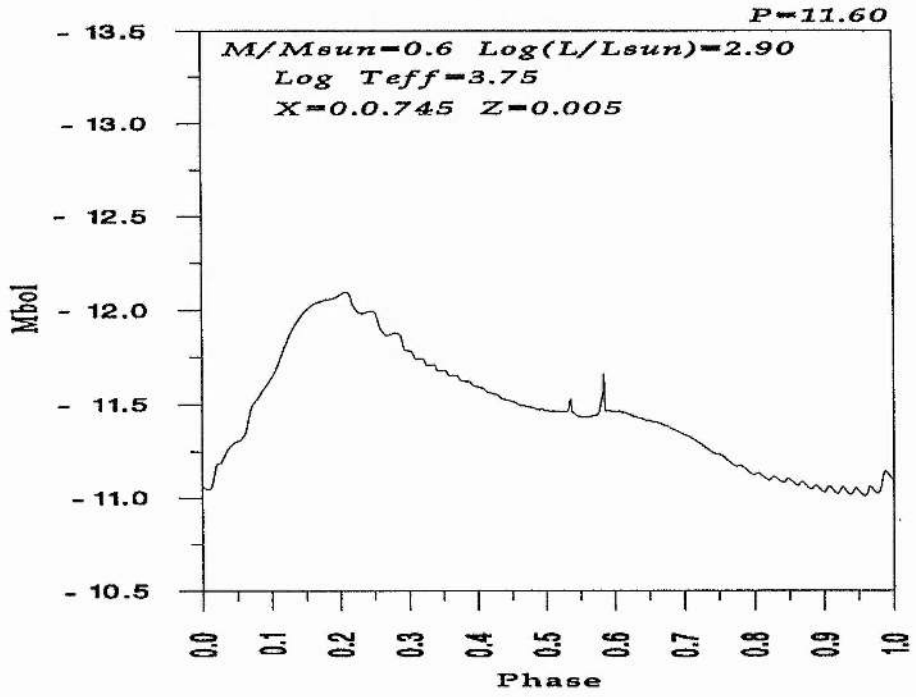
P=11.60
M/Msun=0.6 Log(L/Lsun)=2.90
Log Teff=3.75
X=0.0.745 Z=0.005
Mbol
- 13.5
- 13.0
- 12.5
- 12.0
- 11.5
- 11.0
- 10.5
0.0 0.1 0.2 0.3 0.4 0.5 0.6 0.7 0.8 0.9 1.0
Phase

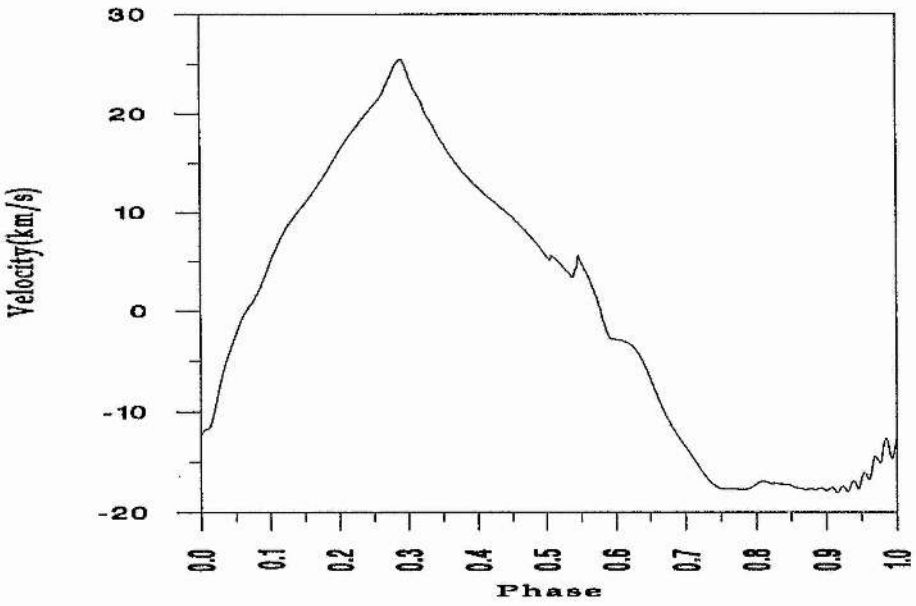
Velocity(km/s)
30
20
10
0
-10
-20
0.0 0.1 0.2 0.3 0.4 0.5 0.6 0.7 0.8 0.9 1.0
Phase

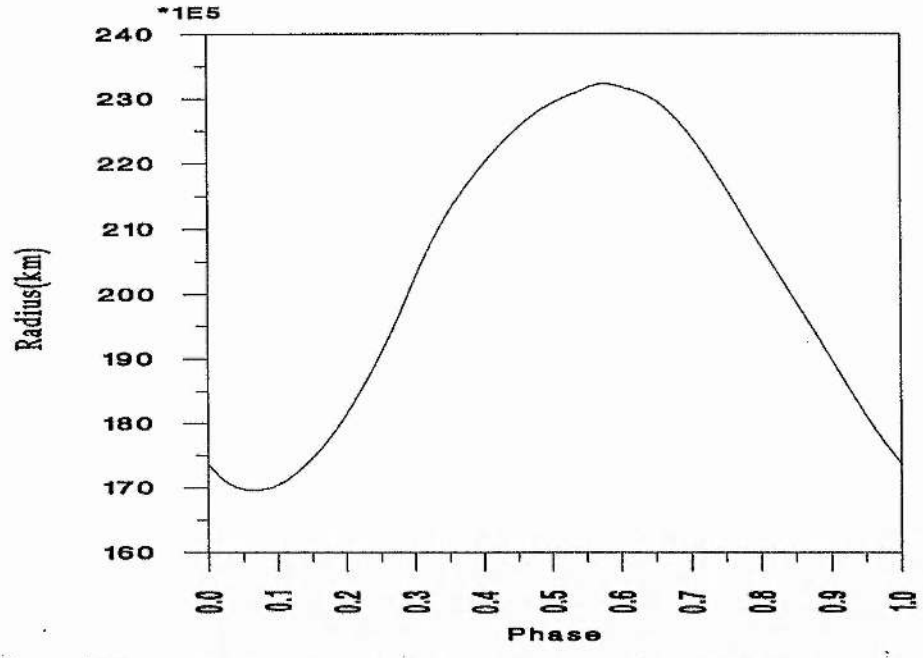
*1E5
Radius(km)
240
230
220
210
200
190
180
170
160
0.0 0.1 0.2 0.3 0.4 0.5 0.6 0.7 0.8 0.9 1.0
Phase

APPENDIX *B*

In this Appendix, we present the light, velocity and radius curves of the decaying models. These curves have been produced using a programme code created by Dr. T. R. Carson. For each model the mass, the luminosity, the temperature, the amount of hydrogen and metals and the period in days, are mentioned. The amplitudes of these models are small with a sinusoidal shape (not always).

Model(36)

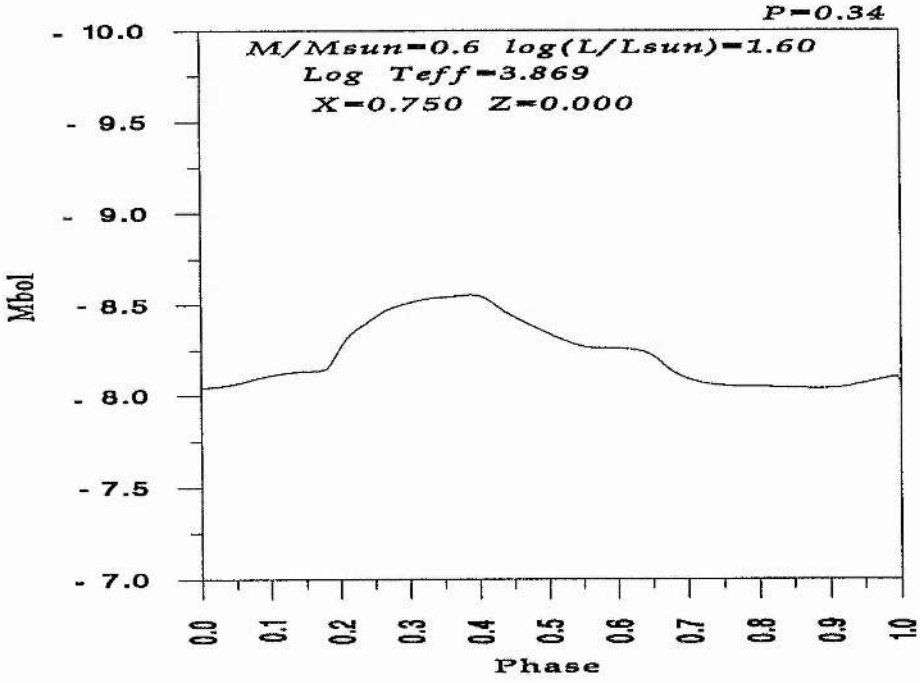
P=0.34
M/Msun=0.6 log(L/Lsun)=1.60
Log Teff=3.869
X=0.750 Z=0.000
Mbol
- 10.0
- 9.5
- 9.0
- 8.5
- 8.0
- 7.5
- 7.0
0.0 0.1 0.2 0.3 0.4 0.5 0.6 0.7 0.8 0.9 1.0
Phase

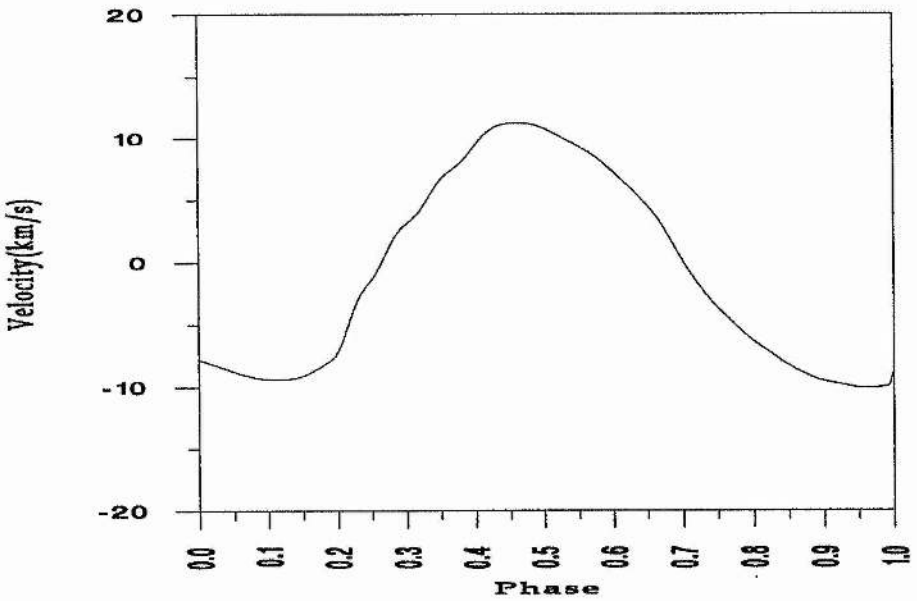
Velocity(km/s)
20
10
0
-10
-20
0.0 0.1 0.2 0.3 0.4 0.5 0.6 0.7 0.8 0.9 1.0
Phase

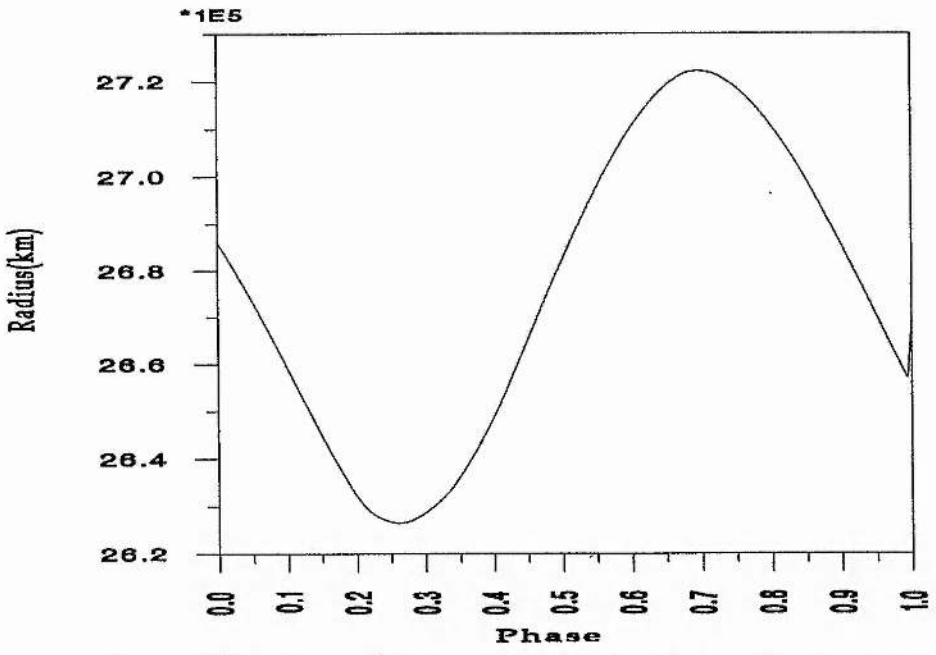
*1E5
Radius(km)
27.2
27.0
26.8
26.6
26.4
26.2
0.0 0.1 0.2 0.3 0.4 0.5 0.6 0.7 0.8 0.9 1.0
Phase

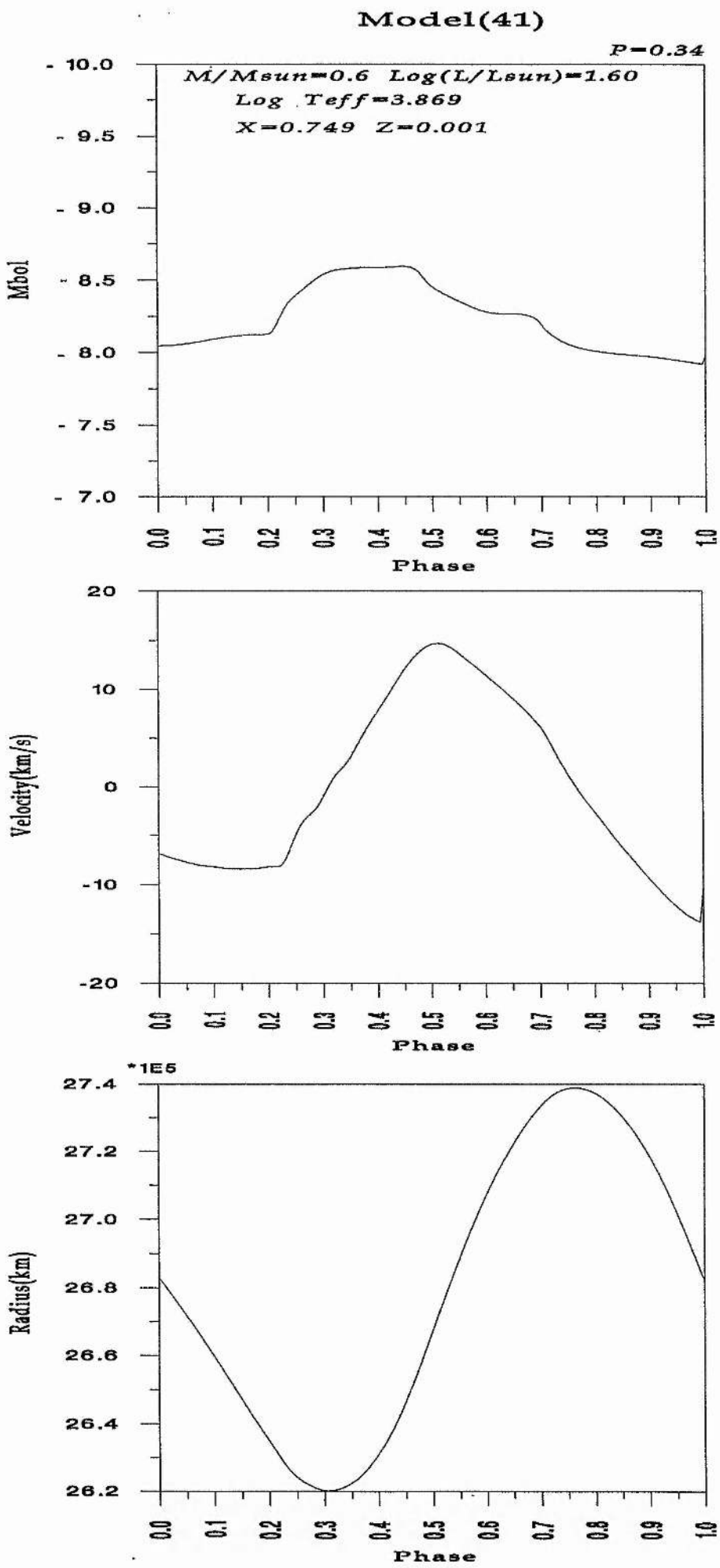
Model(41)
P=0.34
M/Msun=0.6 Log(L/Lsun)=1.60
Log Teff=3.869
X=0.749 Z=0.001
Mbol
- 10.0
- 9.5
- 9.0
- 8.5
- 8.0
- 7.5
- 7.0
0.0 0.1 0.2 0.3 0.4 0.5 0.6 0.7 0.8 0.9 1.0
Phase
Velocity(km/s)
20
10
0
-10
-20
0.0 0.1 0.2 0.3 0.4 0.5 0.6 0.7 0.8 0.9 1.0
Phase
*1E5
Radius(km)
27.4
27.2
27.0
26.8
26.6
26.4
26.2
0.0 0.1 0.2 0.3 0.4 0.5 0.6 0.7 0.8 0.9 1.0
Phase

Model(42)

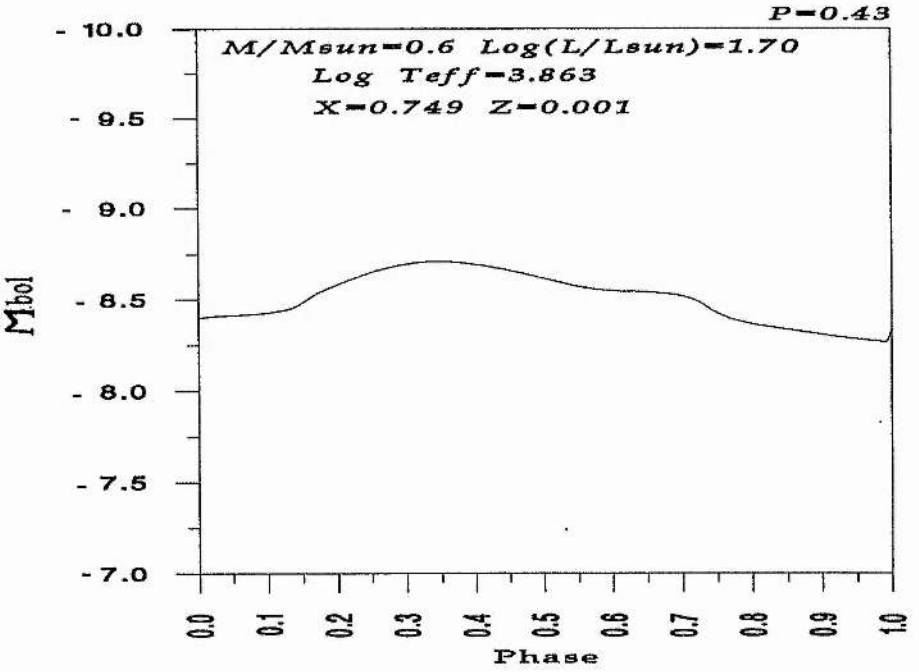
P=0.43
M/Msun=0.6 Log(L/Lsun)=1.70
Log Teff=3.863
X=0.749 Z=0.001
Mbol
- 10.0
- 9.5
- 9.0
- 8.5
- 8.0
- 7.5
- 7.0
0.0 0.1 0.2 0.3 0.4 0.5 0.6 0.7 0.8 0.9 1.0
Phase

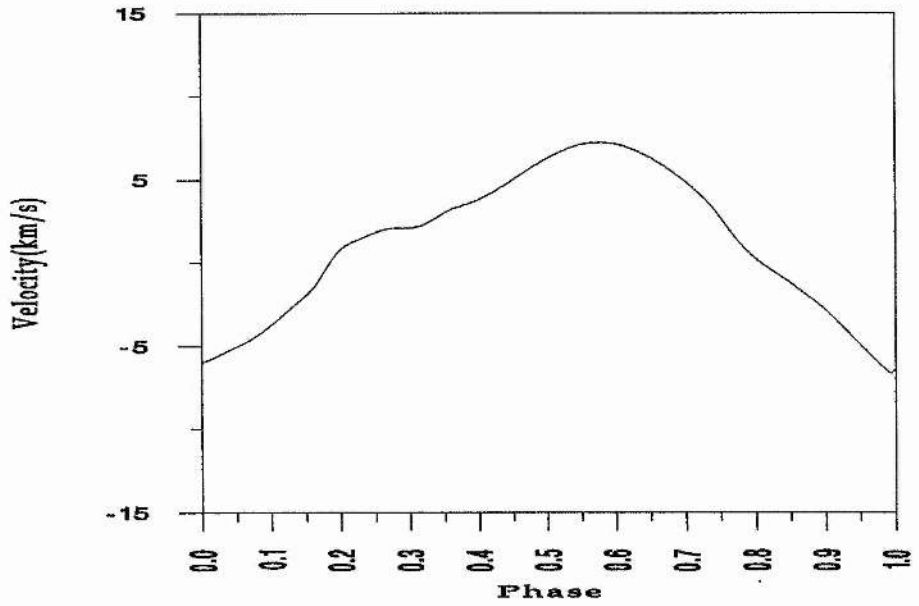
Velocity(km/s)
15
5
-5
-15
0.0 0.1 0.2 0.3 0.4 0.5 0.6 0.7 0.8 0.9 1.0
Phase

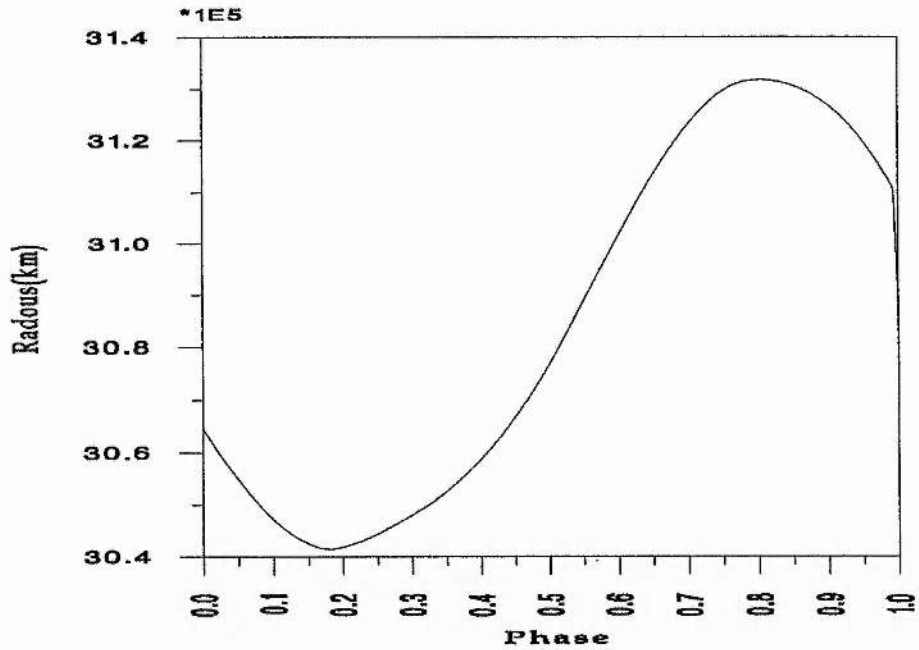
*1E5
Radous(km)
31.4
31.2
31.0
30.8
30.6
30.4
0.0 0.1 0.2 0.3 0.4 0.5 0.6 0.7 0.8 0.9 1.0
Phase

Model(37)

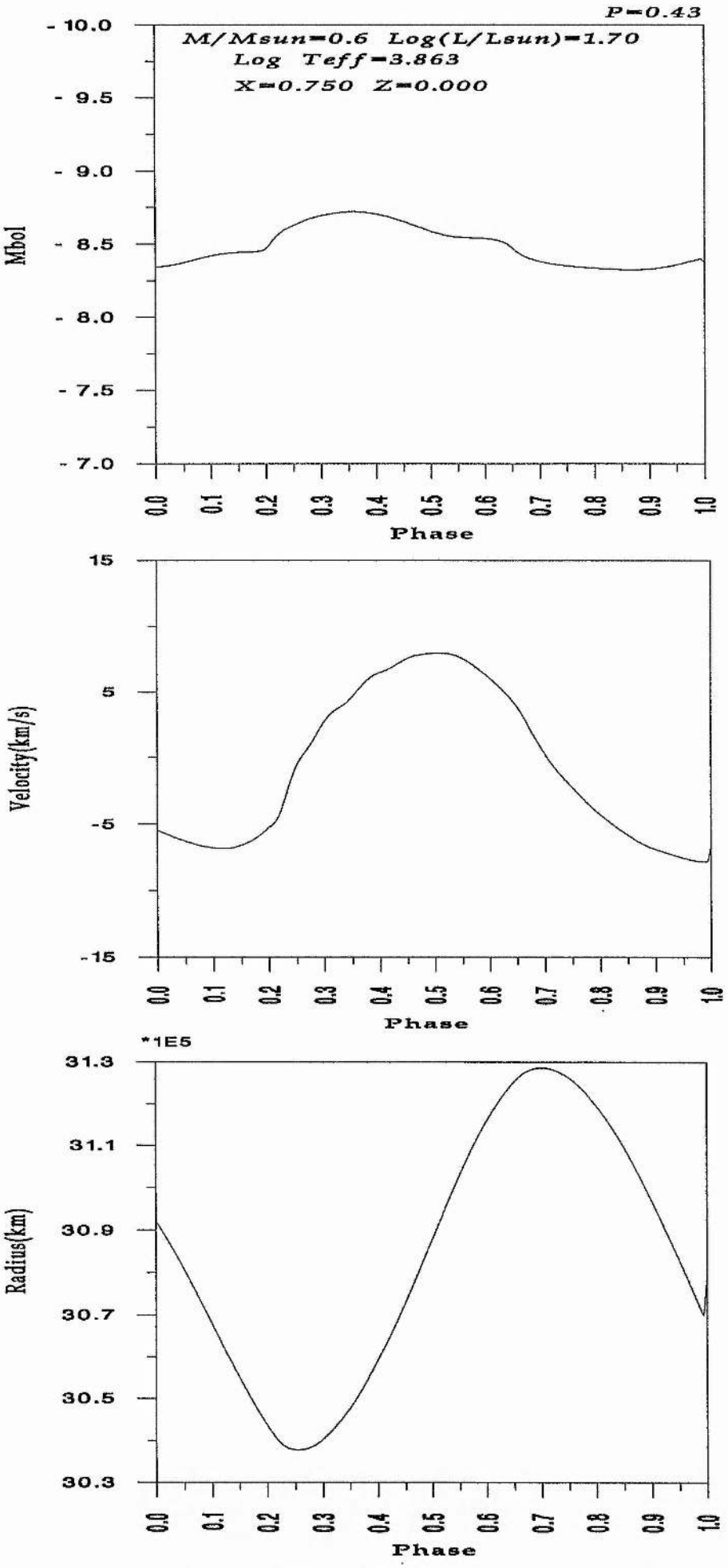
P=0.43
M/Msun=0.6 Log(L/Lsun)=1.70
Log Teff=3.863
X=0.750 Z=0.000
Mbol
-10.0
-9.5
-9.0
-8.5
-8.0
-7.5
-7.0
0.0
0.1
0.2
0.3
0.4
0.5
0.6
0.7
0.8
0.9
1.0
Phase
Velocity(km/s)
15
5
-5
-15
Phase
*1E5
Radius(km)
31.3
31.1
30.9
30.7
30.5
30.3
Phase

Model(38)

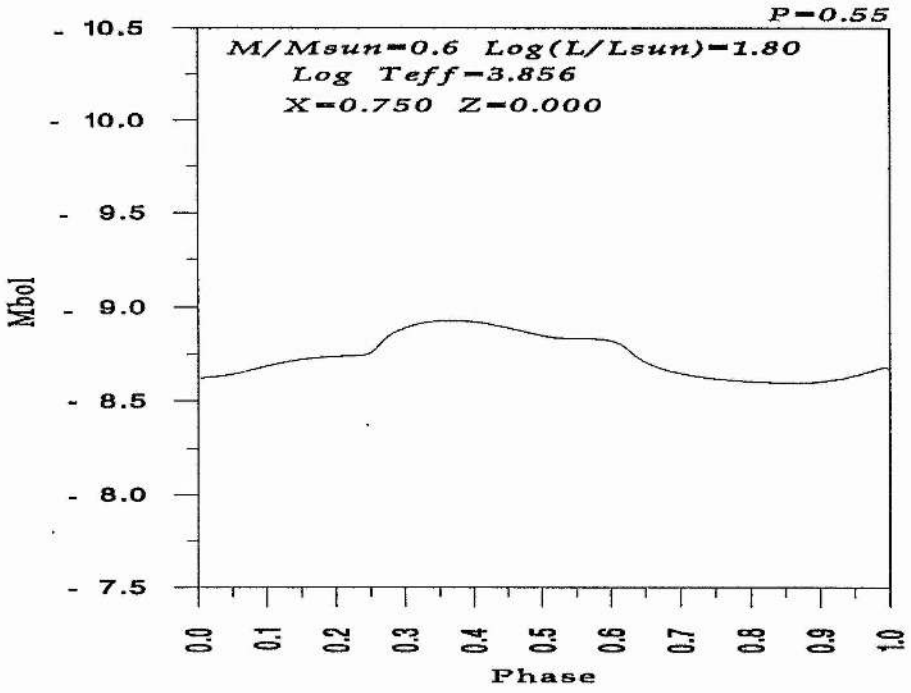
P=0.55
M/Msun=0.6 Log(L/Lsun)=1.80
Log Teff=3.856
X=0.750 Z=0.000
Mbol
- 10.5
- 10.0
- 9.5
- 9.0
- 8.5
- 8.0
- 7.5
0.0 0.1 0.2 0.3 0.4 0.5 0.6 0.7 0.8 0.9 1.0
Phase

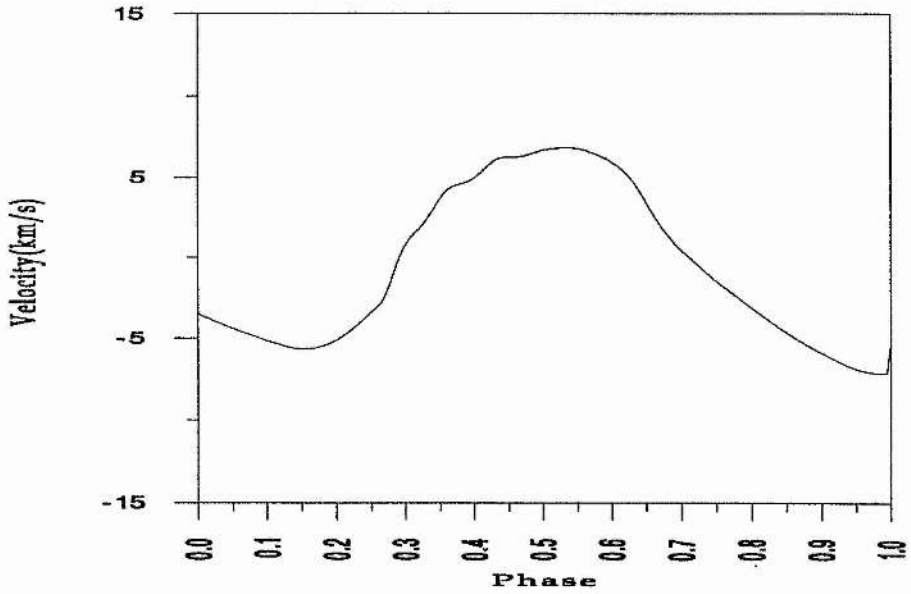
Velocity(km/s)
15
5
-5
-15
0.0 0.1 0.2 0.3 0.4 0.5 0.6 0.7 0.8 0.9 1.0
Phase

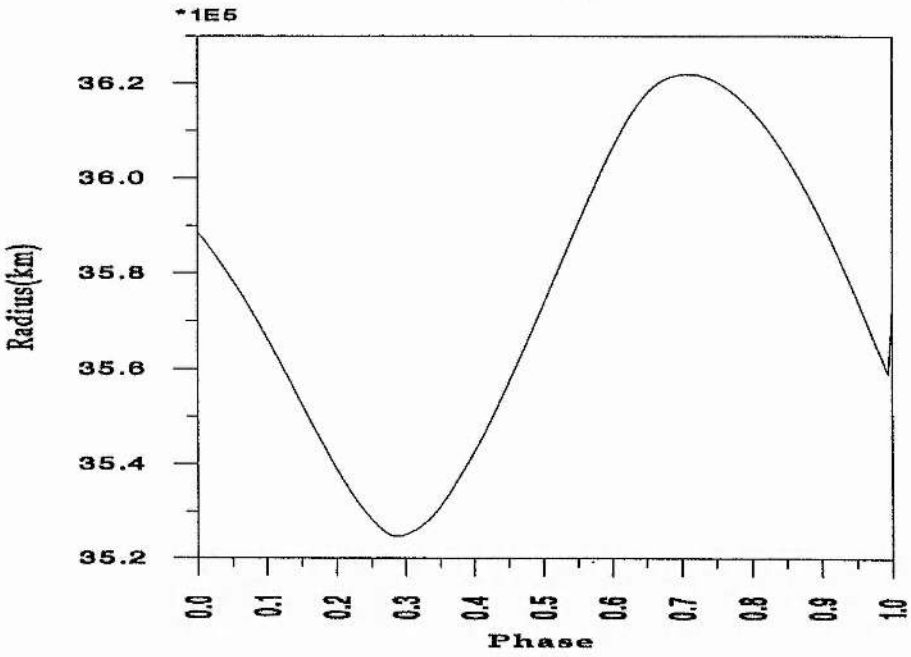
*1E5
Radius(km)
36.2
36.0
35.8
35.6
35.4
35.2
0.0 0.1 0.2 0.3 0.4 0.5 0.6 0.7 0.8 0.9 1.0
Phase

Model(43)

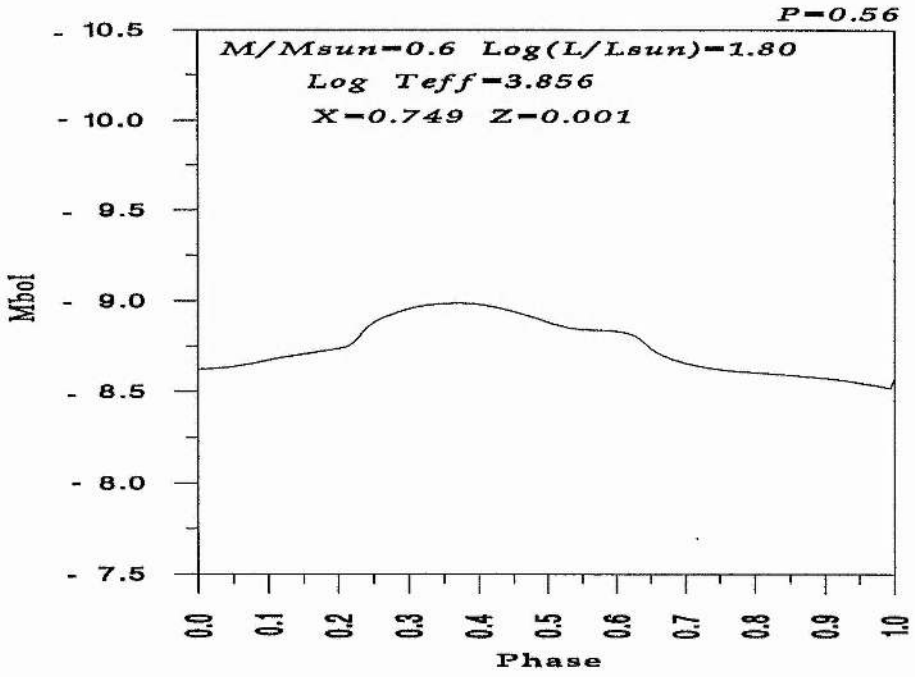
P=0.56
M/Msun=0.6 Log(L/Lsun)=1.80
Log Teff=3.856
X=0.749 Z=0.001
Mbol
- 10.5
- 10.0
- 9.5
- 9.0
- 8.5
- 8.0
- 7.5
0.0 0.1 0.2 0.3 0.4 0.5 0.6 0.7 0.8 0.9 1.0
Phase

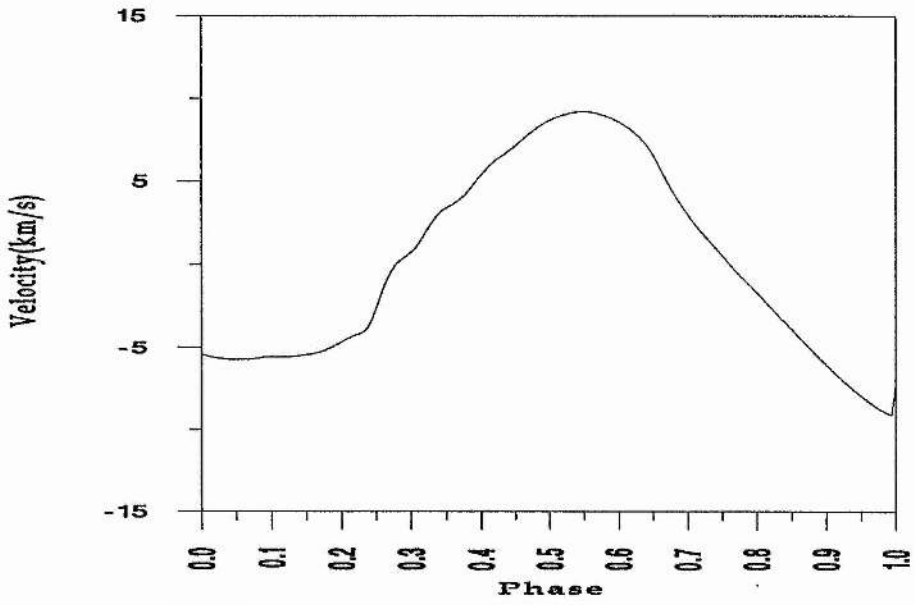
Velocity(km/s)
15
5
-5
-15
0.0 0.1 0.2 0.3 0.4 0.5 0.6 0.7 0.8 0.9 1.0
Phase

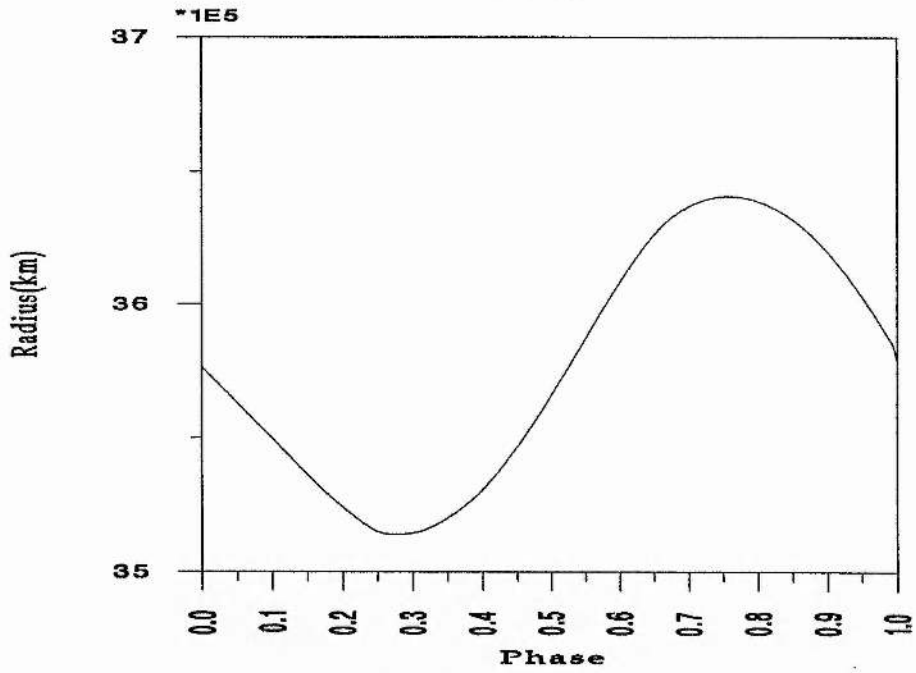
*1E5
Radius(km)
37
36
35
0.0 0.1 0.2 0.3 0.4 0.5 0.6 0.7 0.8 0.9 1.0
Phase

Model(39)

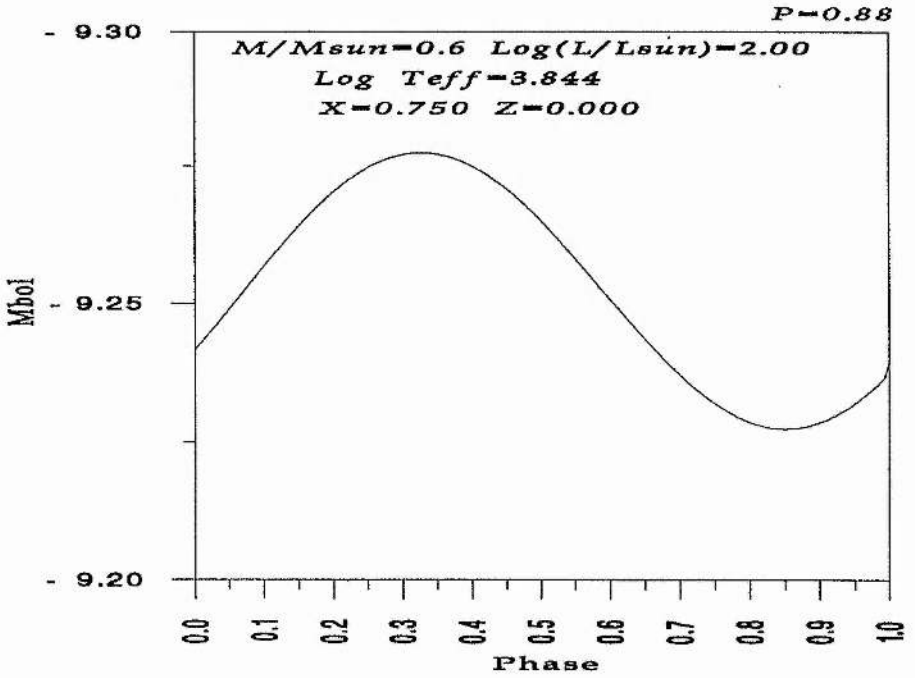
P=0.88
M/Msun=0.6 Log(L/Lsun)=2.00
Log Teff=3.844
X=0.750 Z=0.000
Mbol
- 9.30
- 9.25
- 9.20
0.0
0.1
0.2
0.3
0.4
0.5
0.6
0.7
0.8
0.9
1.0
Phase

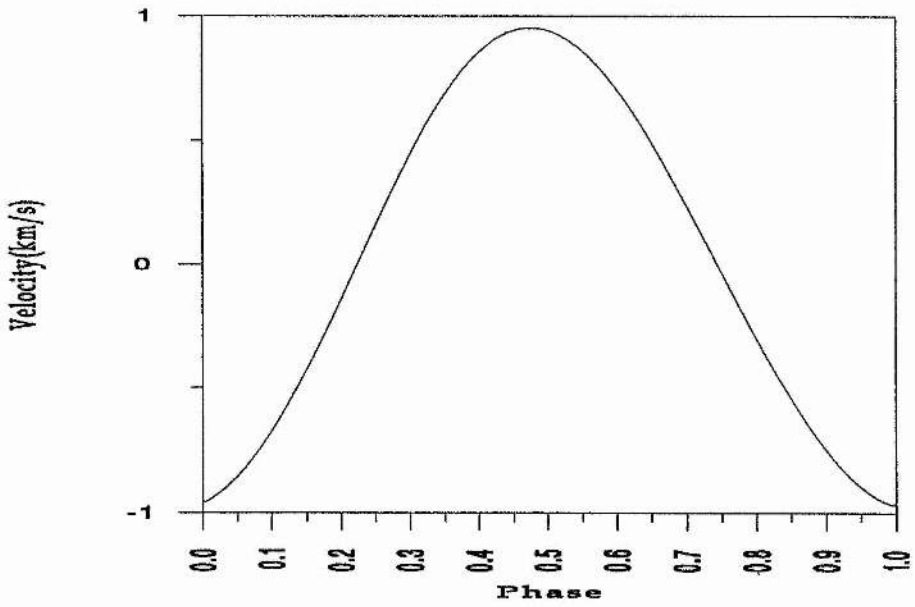
Velocity(km/s)
1
0
-1
0.0
0.1
0.2
0.3
0.4
0.5
0.6
0.7
0.8
0.9
1.0
Phase

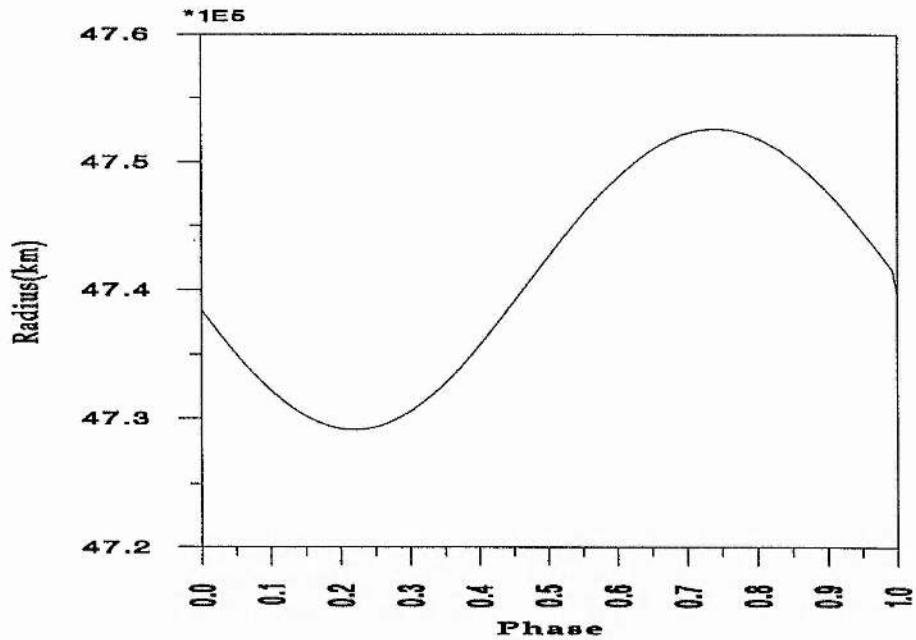
*1E5
Radius(km)
47.6
47.5
47.4
47.3
47.2
0.0
0.1
0.2
0.3
0.4
0.5
0.6
0.7
0.8
0.9
1.0
Phase

Model(44)

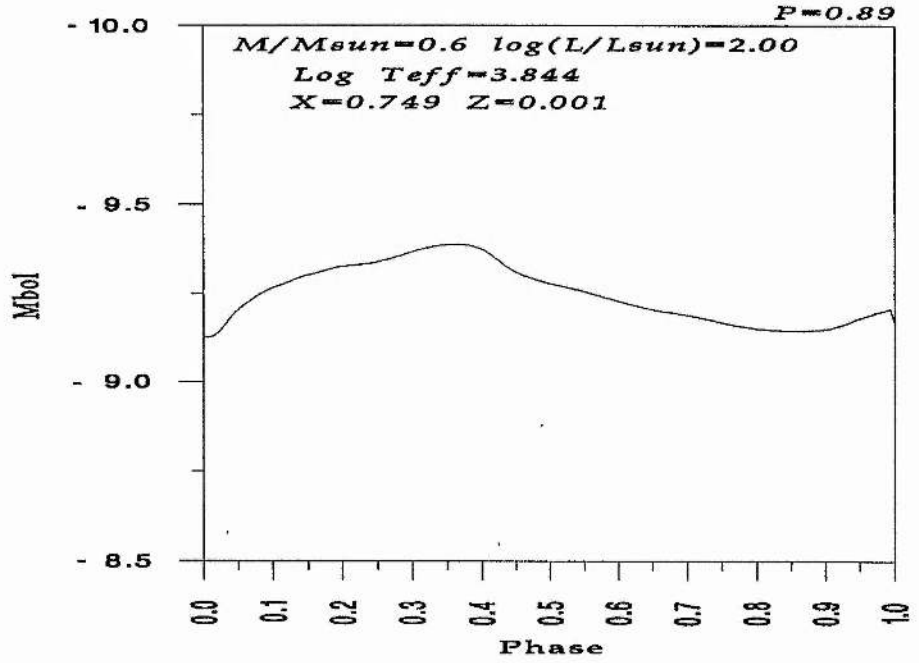
P=0.89
M/Msun=0.6 log(L/Lsun)=2.00
Log Teff=3.844
X=0.749 Z=0.001
Mbol
- 10.0
- 9.5
- 9.0
- 8.5
0.0 0.1 0.2 0.3 0.4 0.5 0.6 0.7 0.8 0.9 1.0
Phase

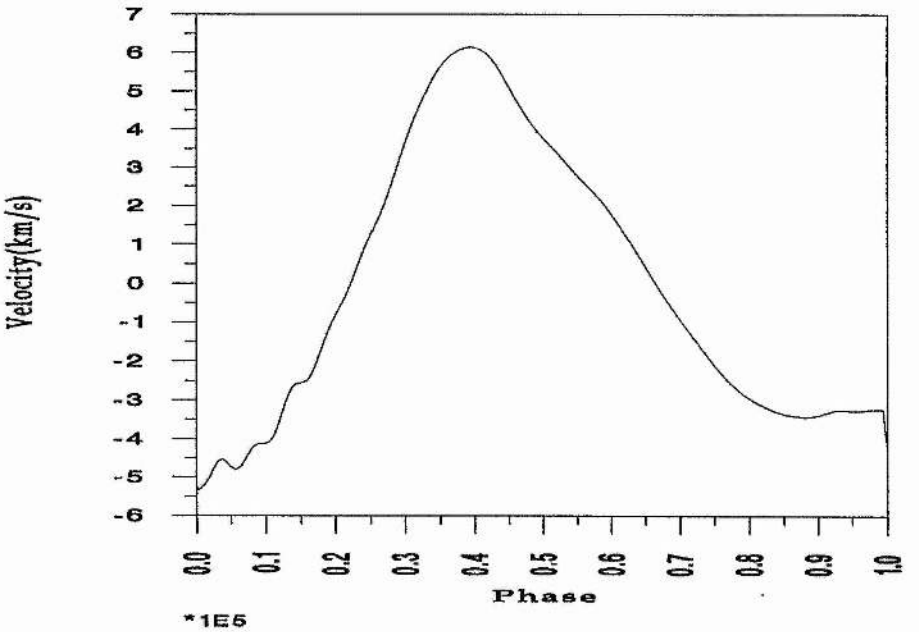
Velocity(km/s)
7 6 5 4 3 2 1 0 -1 -2 -3 -4 -5 -6
0.0 0.1 0.2 0.3 0.4 0.5 0.6 0.7 0.8 0.9 1.0
Phase

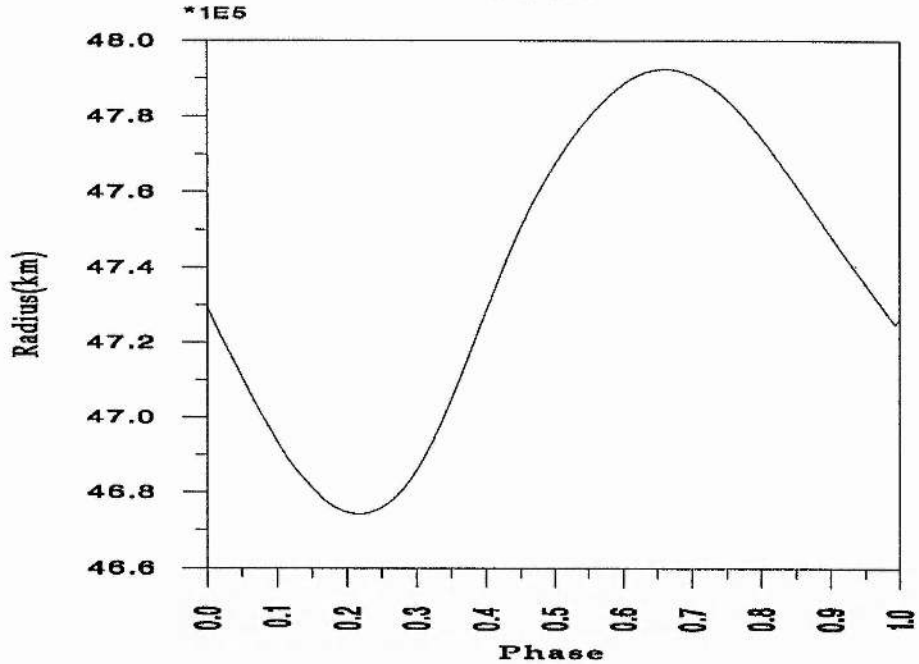
*1E5
Radius(km)
48.0
47.8
47.6
47.4
47.2
47.0
46.8
46.6
0.0 0.1 0.2 0.3 0.4 0.5 0.6 0.7 0.8 0.9 1.0
Phase

Model(50)

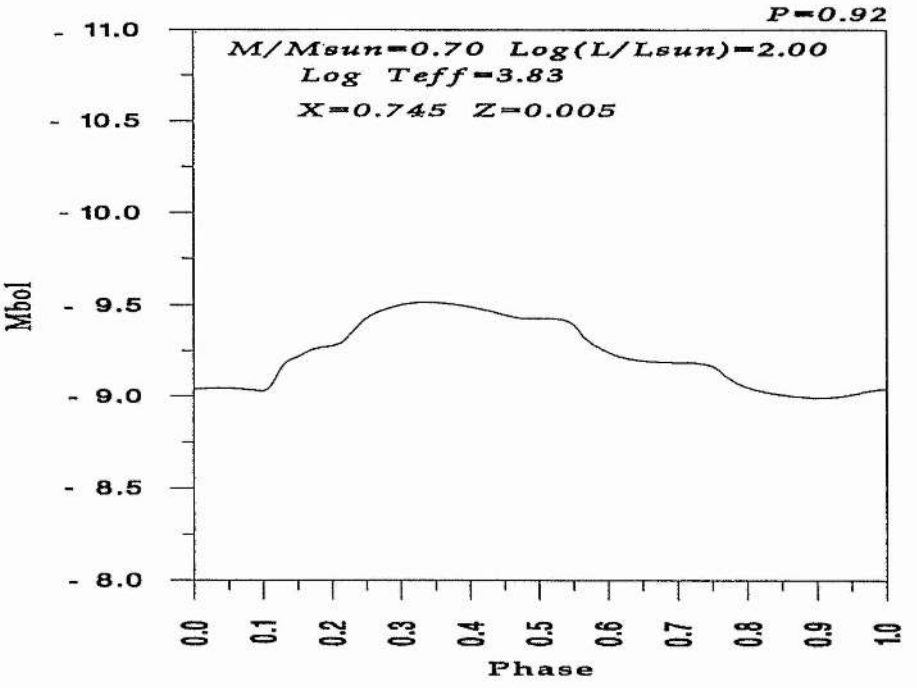
P=0.92
M/Msun=0.70 Log(L/Lsun)=2.00
Log Teff=3.83
X=0.745 Z=0.005
Mbol
11.0
10.5
10.0
9.5
9.0
8.5
8.0
0.0
0.1
0.2
0.3
0.4
0.5
0.6
0.7
0.8
0.9
1.0
Phase

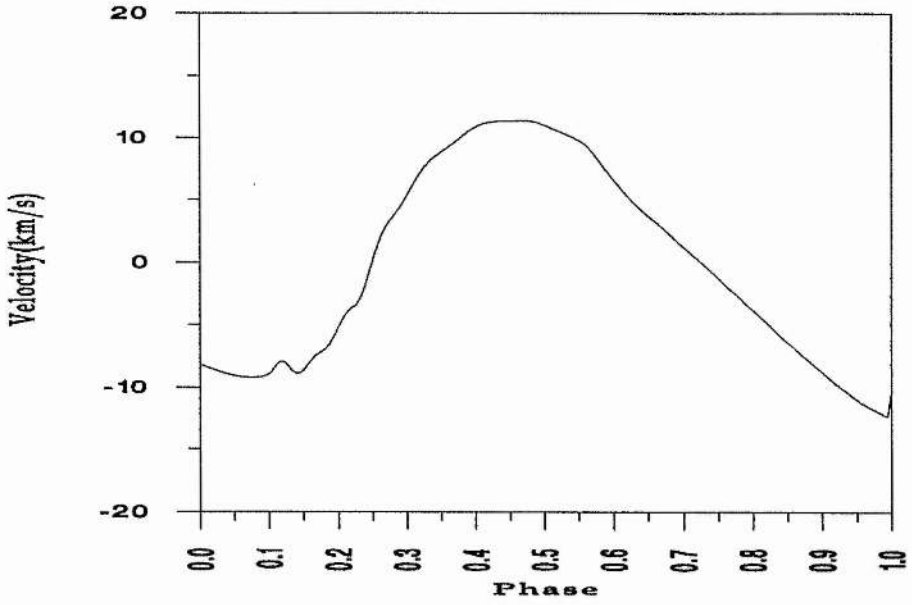
Velocity(km/s)
20
10
0
-10
-20
0.0
0.1
0.2
0.3
0.4
0.5
0.6
0.7
0.8
0.9
1.0
Phase

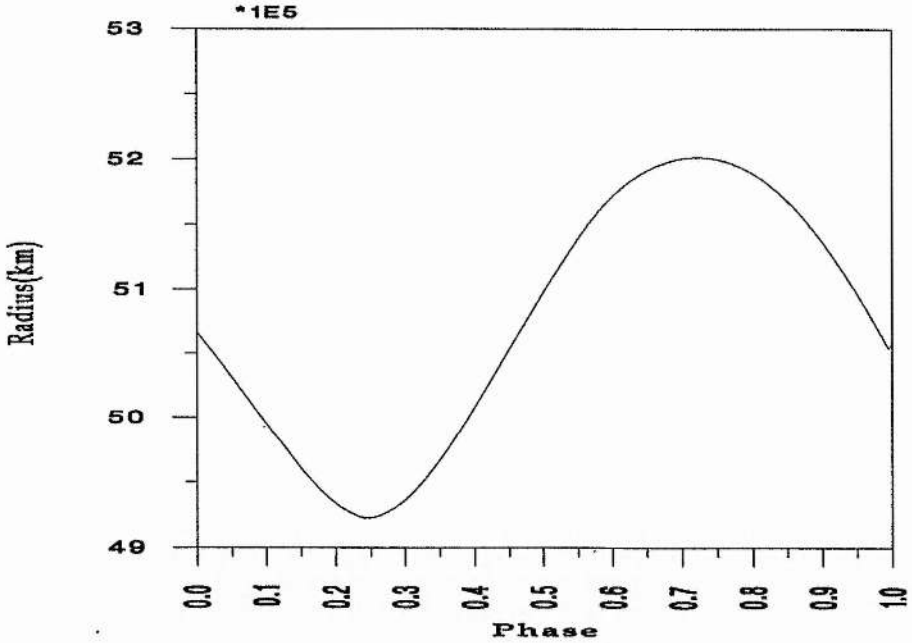
*1E5
Radius(km)
53
52
51
50
49
0.0
0.1
0.2
0.3
0.4
0.5
0.6
0.7
0.8
0.9
1.0
Phase

Model(10)

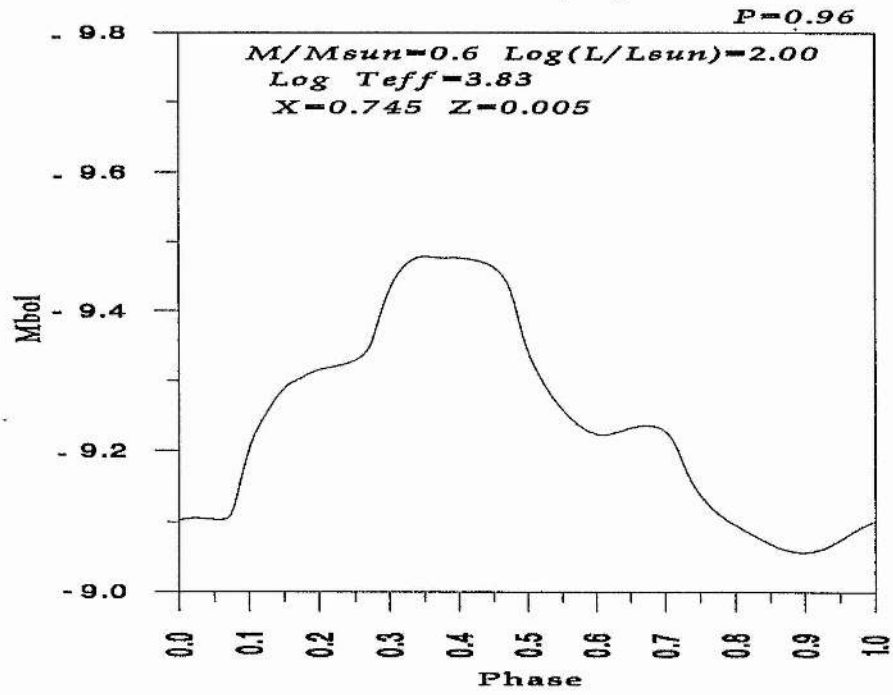
P=0.96
M/Msun=0.6 Log(L/Lsun)=2.00
Log Teff=3.83
X=0.745 Z=0.005
Mbol
- 9.8
- 9.6
- 9.4
- 9.2
- 9.0
0.0 0.1 0.2 0.3 0.4 0.5 0.6 0.7 0.8 0.9 1.0
Phase

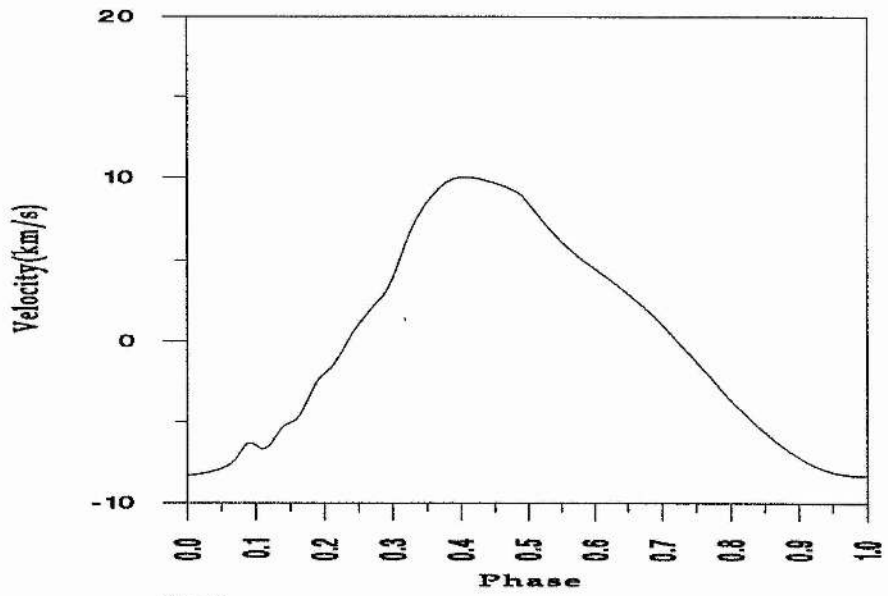
Velocity(km/s)
20
10
0
-10
0.0 0.1 0.2 0.3 0.4 0.5 0.6 0.7 0.8 0.9 1.0
Phase

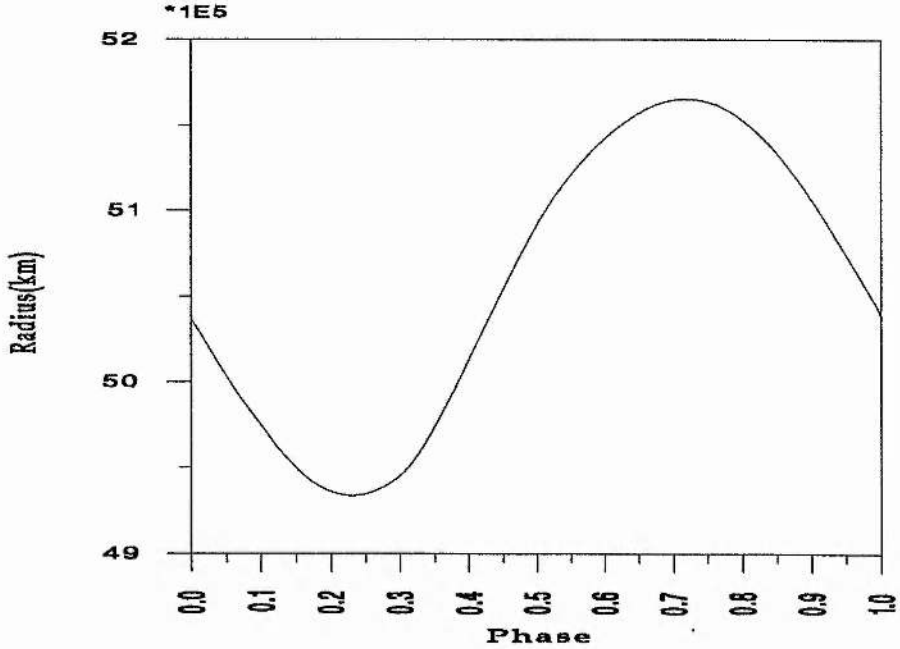
*1E5
Radius(km)
52
51
50
49
0.0 0.1 0.2 0.3 0.4 0.5 0.6 0.7 0.8 0.9 1.0
Phase

Model(45)

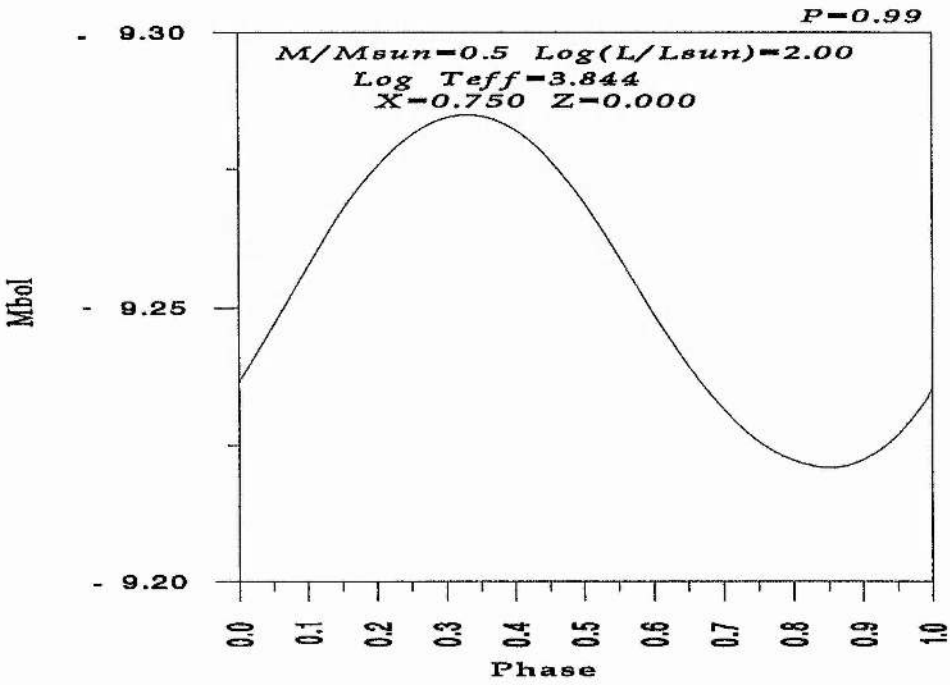
P=0.99
M/Msun=0.5 Log(L/Lsun)=2.00
Log Teff=3.844
X=0.750 Z=0.000
Mbol
9.30
9.25
9.20
0.0
0.1
0.2
0.3
0.4
0.5
0.6
0.7
0.8
0.9
1.0
Phase

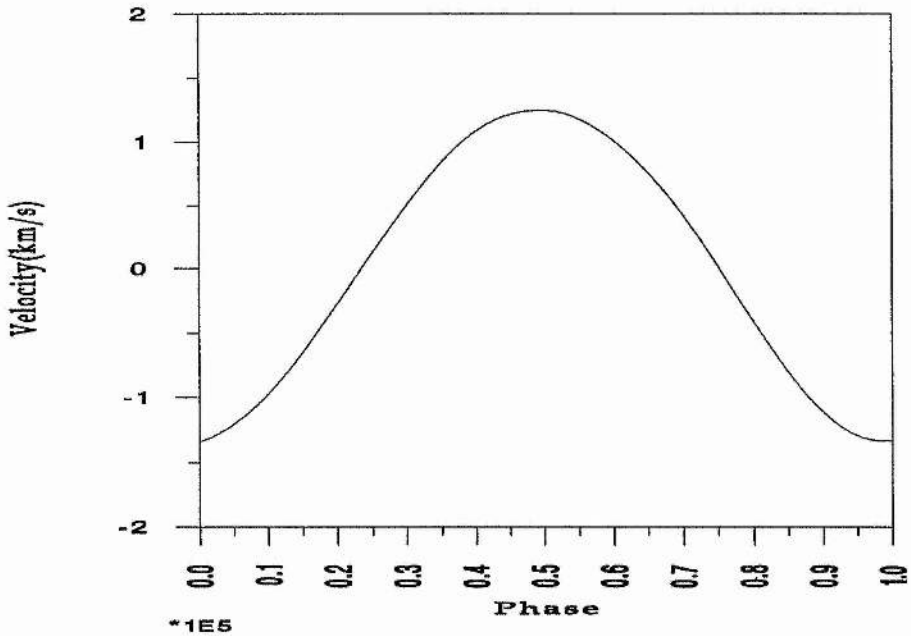
Velocity(km/s)
2
1
0
-1
-2
0.0
0.1
0.2
0.3
0.4
0.5
0.6
0.7
0.8
0.9
1.0
Phase

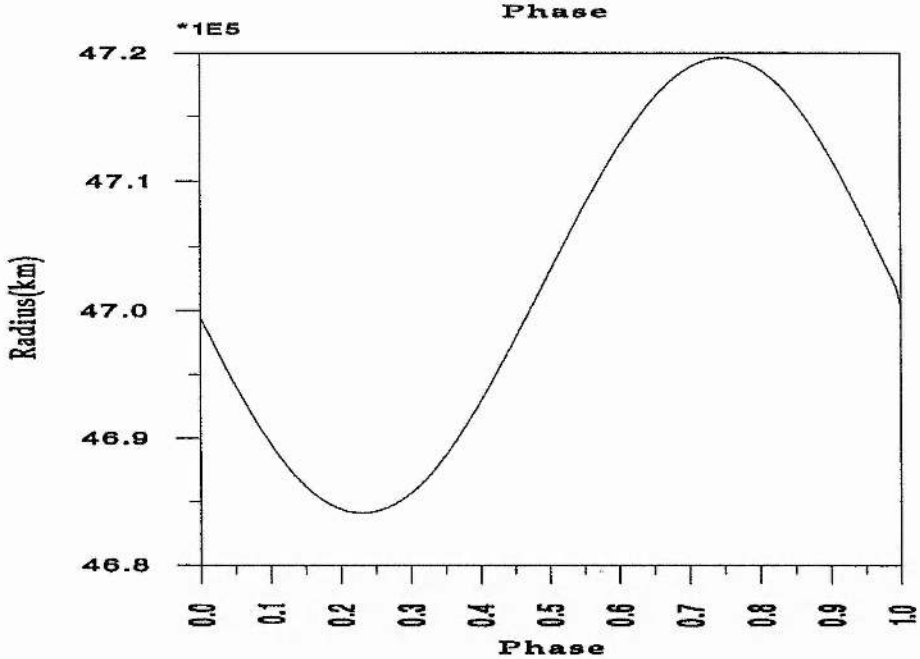
*1E5
Radius(km)
47.2
47.1
47.0
46.9
46.8
0.0
0.1
0.2
0.3
0.4
0.5
0.6
0.7
0.8
0.9
1.0
Phase

Model(47)

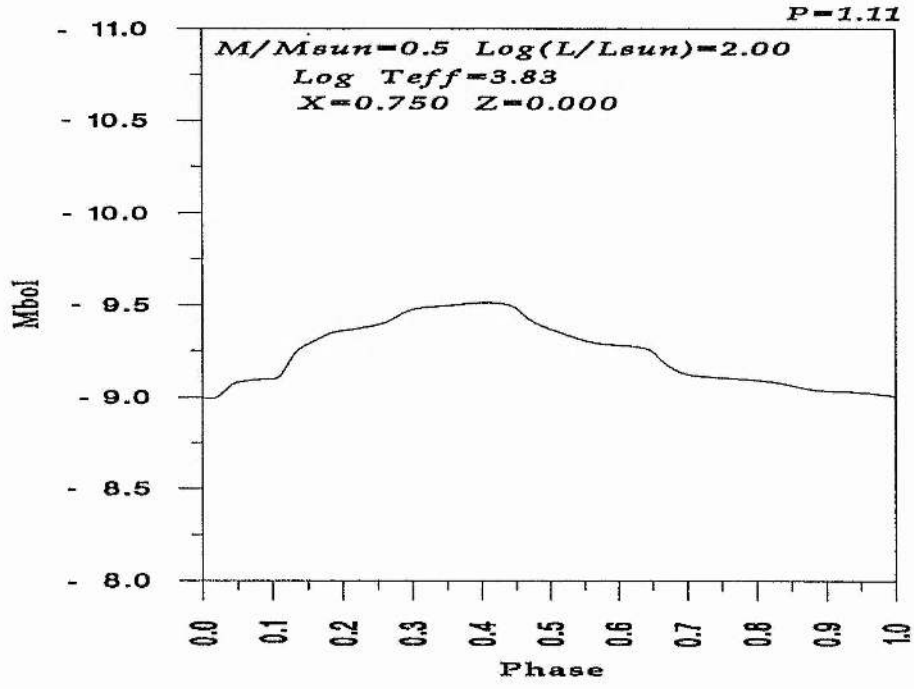
P=1.11
M/Msun=0.5 Log(L/Lsun)=2.00
Log Teff=3.83
X=0.750 Z=0.000
Mbol
- 11.0
- 10.5
- 10.0
- 9.5
- 9.0
- 8.5
- 8.0
0.0 0.1 0.2 0.3 0.4 0.5 0.6 0.7 0.8 0.9 1.0
Phase

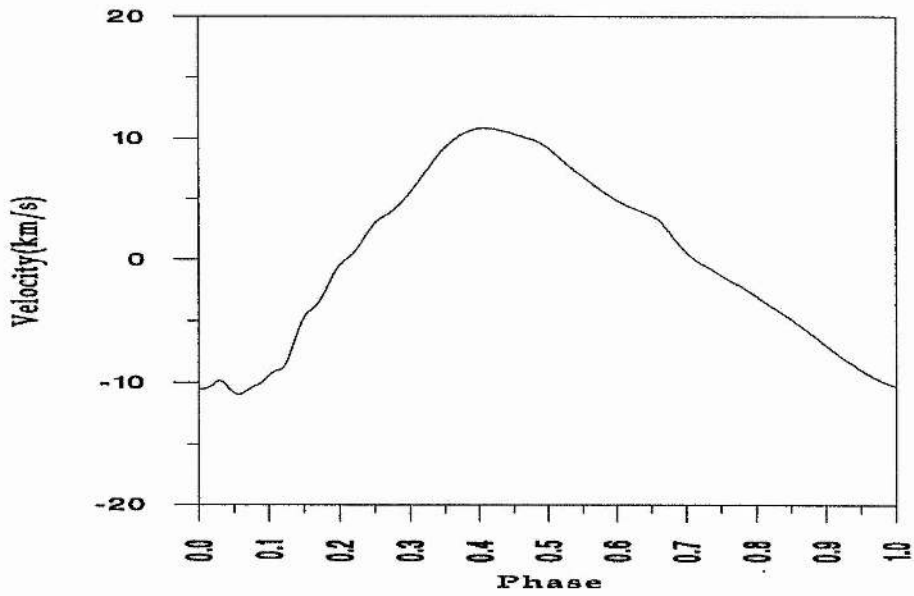
Velocity(km/s)
20
10
0
-10
-20
0.0 0.1 0.2 0.3 0.4 0.5 0.6 0.7 0.8 0.9 1.0
Phase

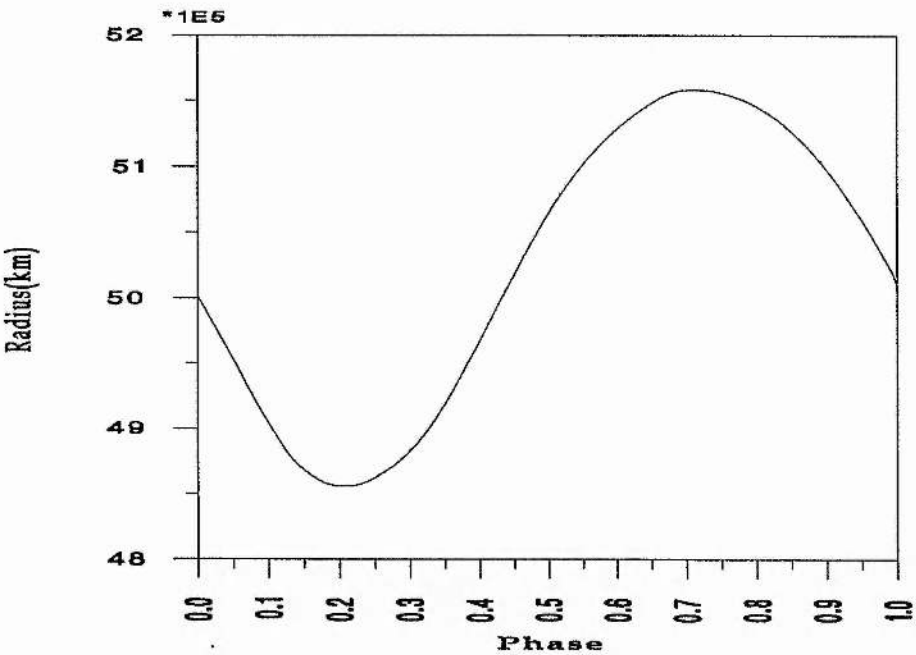
*1E5
Radius(km)
52
51
50
49
48
0.0 0.1 0.2 0.3 0.4 0.5 0.6 0.7 0.8 0.9 1.0
Phase

Model(46)

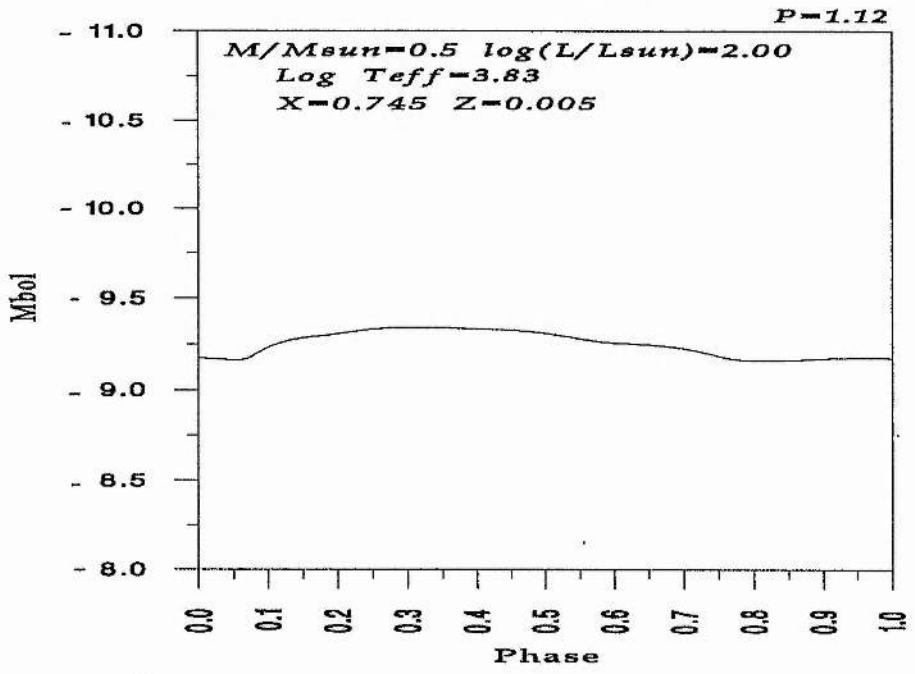
P=1.12
M/Msun=0.5 log(L/Lsun)=2.00
Log Teff=3.83
X=0.745 Z=0.005
Mbol
- 11.0
- 10.5
- 10.0
- 9.5
- 9.0
- 8.5
- 8.0
0.0 0.1 0.2 0.3 0.4 0.5 0.6 0.7 0.8 0.9 1.0
Phase

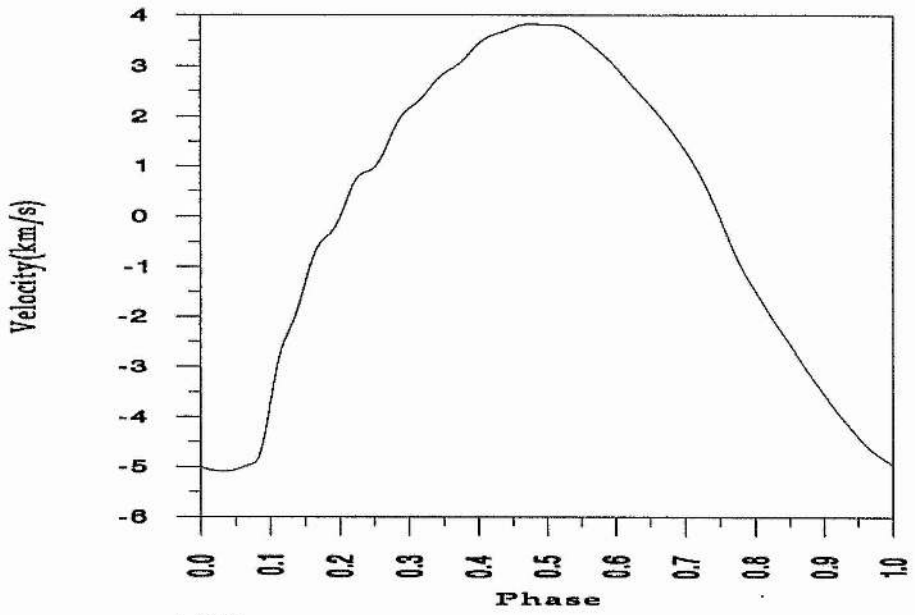
Velocity(km/s)
4
3
2
1
0
-1
-2
-3
-4
-5
-6
0.0 0.1 0.2 0.3 0.4 0.5 0.6 0.7 0.8 0.9 1.0
Phase

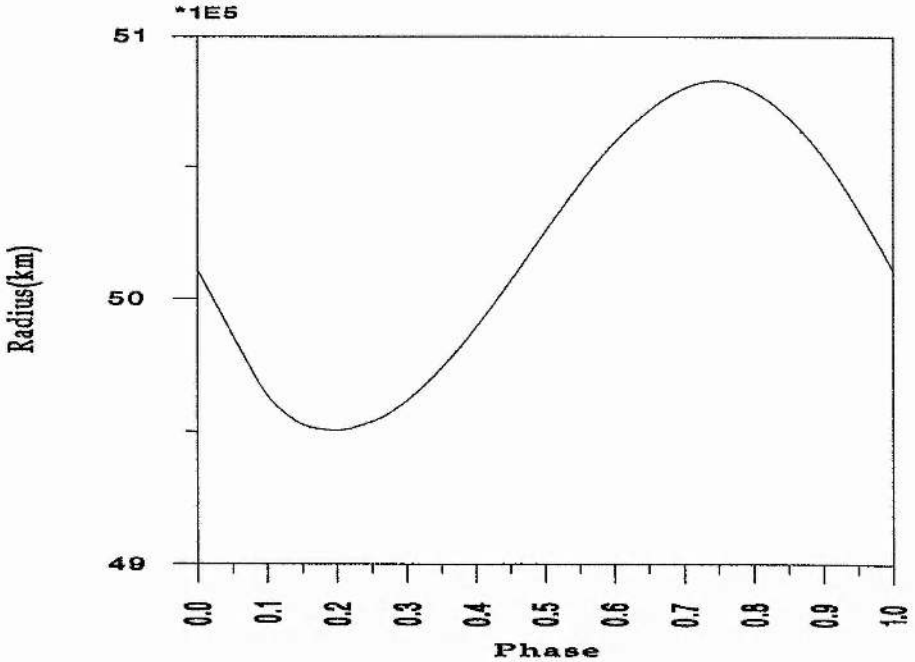
*1E5
Radius(km)
51
50
49
0.0 0.1 0.2 0.3 0.4 0.5 0.6 0.7 0.8 0.9 1.0
Phase

Model(46)

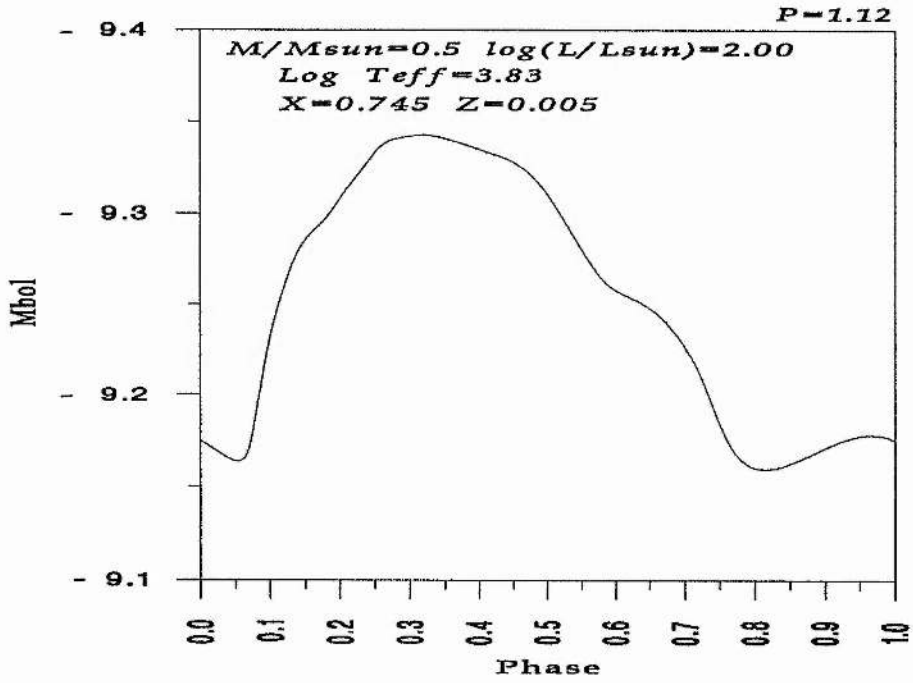
P=1.12
M/Msun=0.5 log(L/Lsun)=2.00
Log Teff=3.83
X=0.745 Z=0.005
Mbol
9.4
9.3
9.2
9.1
0.0
0.1
0.2
0.3
0.4
0.5
0.6
0.7
0.8
0.9
1.0
Phase

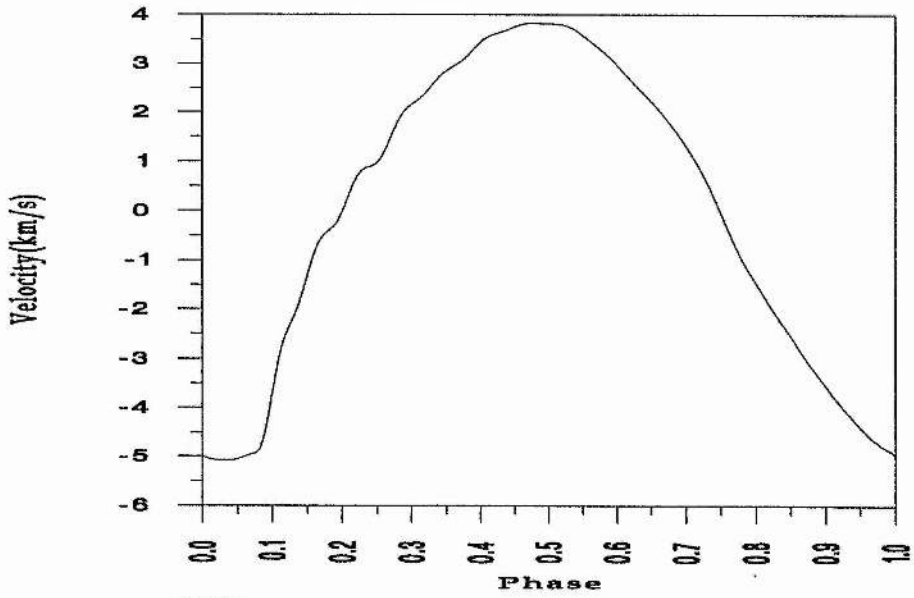
Velocity(km/s)
4
3
2
1
0
-1
-2
-3
-4
-5
-6
0.0
0.1
0.2
0.3
0.4
0.5
0.6
0.7
0.8
0.9
1.0
Phase

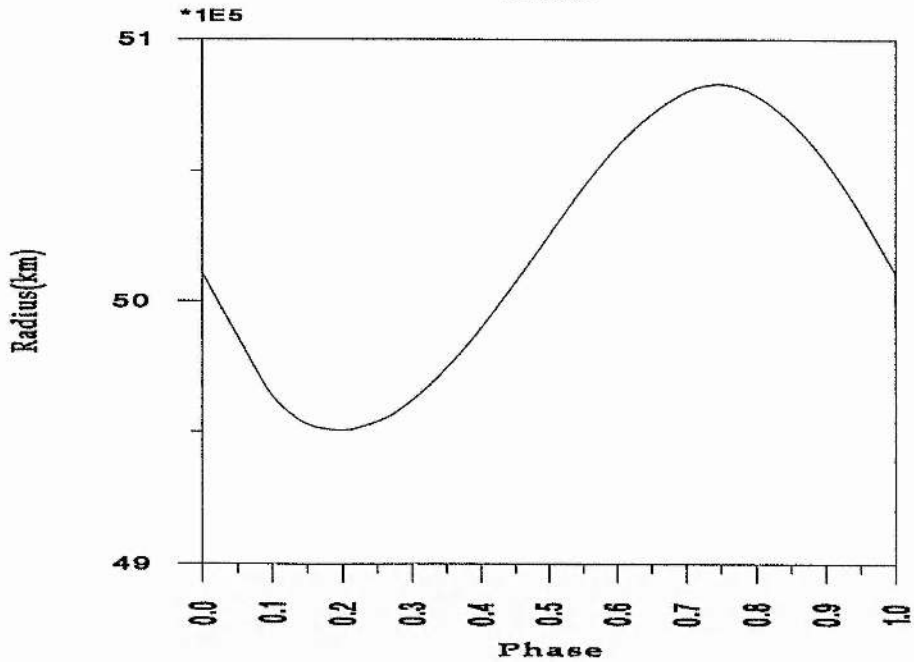
*1E5
Radius(km)
51
50
49
0.0
0.1
0.2
0.3
0.4
0.5
0.6
0.7
0.8
0.9
1.0
Phase

Model(20)

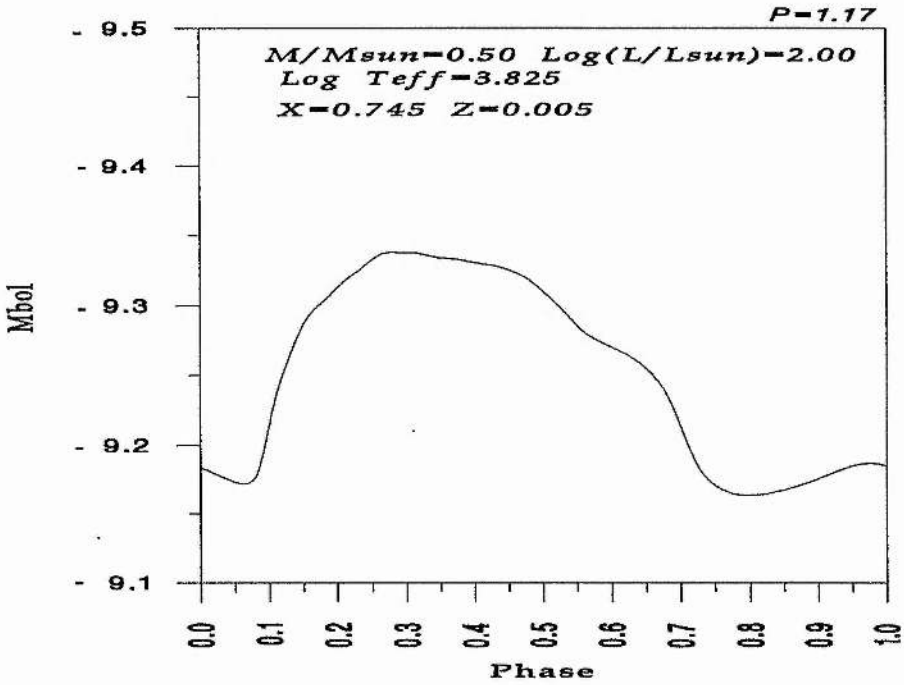
P=1.17
M/Msun=0.50 Log(L/Lsun)=2.00
Log Teff=3.825
X=0.745 Z=0.005
Mbol
- 9.5
- 9.4
- 9.3
- 9.2
- 9.1
0.0 0.1 0.2 0.3 0.4 0.5 0.6 0.7 0.8 0.9 1.0
Phase

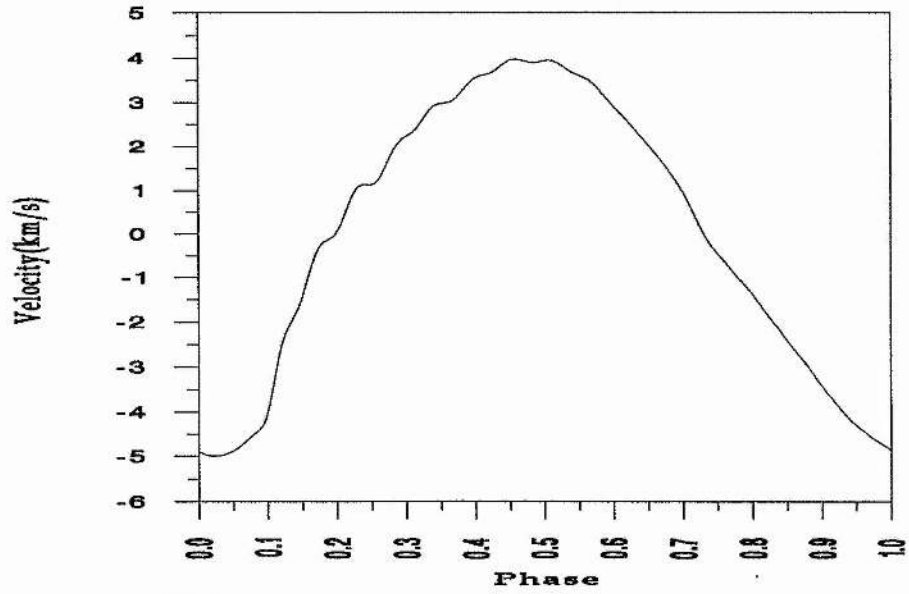
Velocity(km/s)
5 4 3 2 1 0 -1 -2 -3 -4 -5 -6
0.0 0.1 0.2 0.3 0.4 0.5 0.6 0.7 0.8 0.9 1.0
Phase

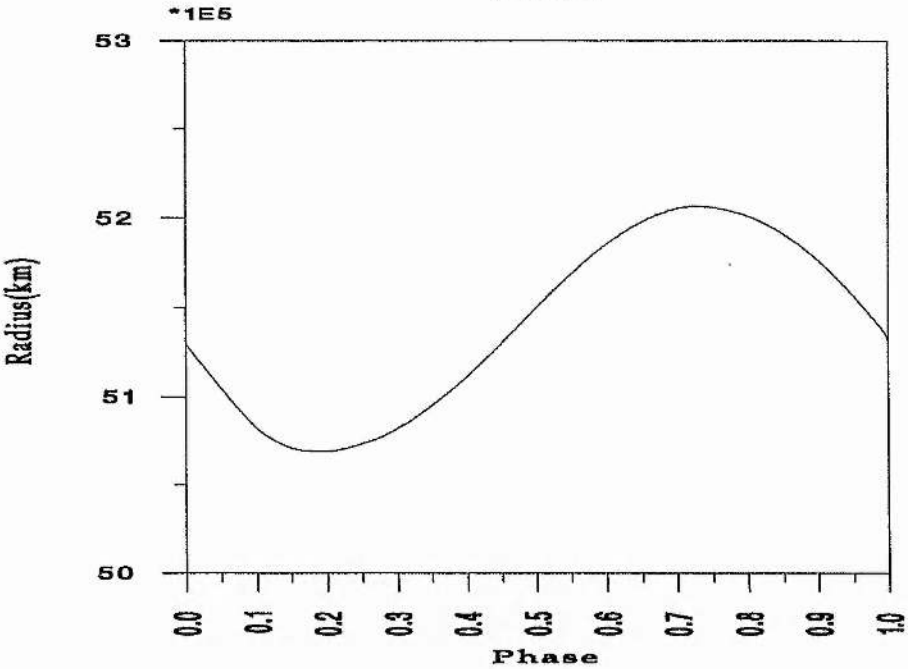
*1E5
Radius(km)
53
52
51
50
0.0 0.1 0.2 0.3 0.4 0.5 0.6 0.7 0.8 0.9 1.0
Phase

Model(24)

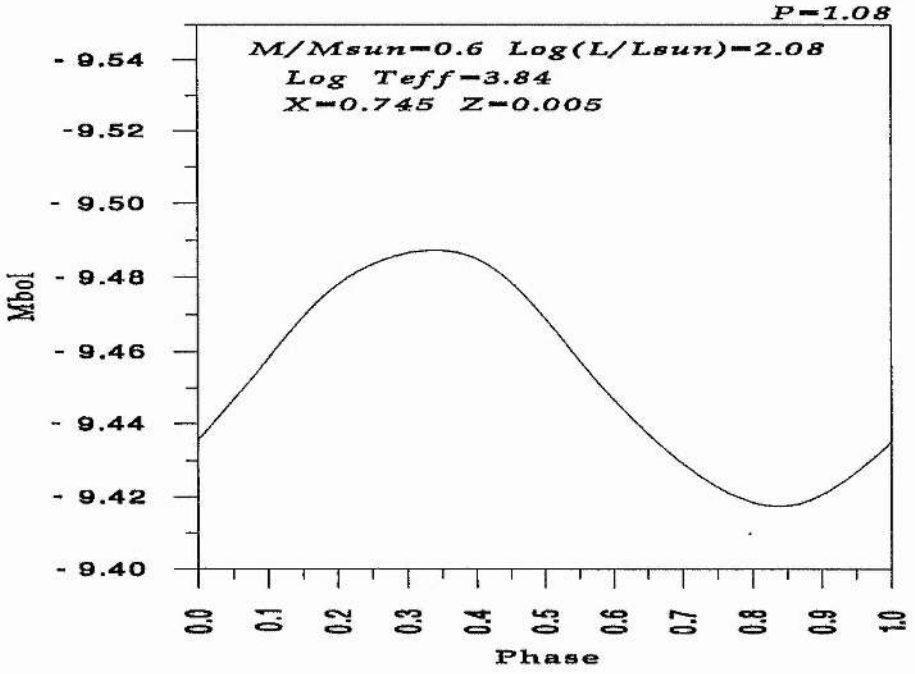
P=1.08
M/Msun=0.6 Log(L/Lsun)=2.08
Log Teff=3.84
X=0.745 Z=0.005
Mbol
- 9.54
-9.52
- 9.50
- 9.48
- 9.46
- 9.44
- 9.42
- 9.40
0.0 0.1 0.2 0.3 0.4 0.5 0.6 0.7 0.8 0.9 1.0
Phase

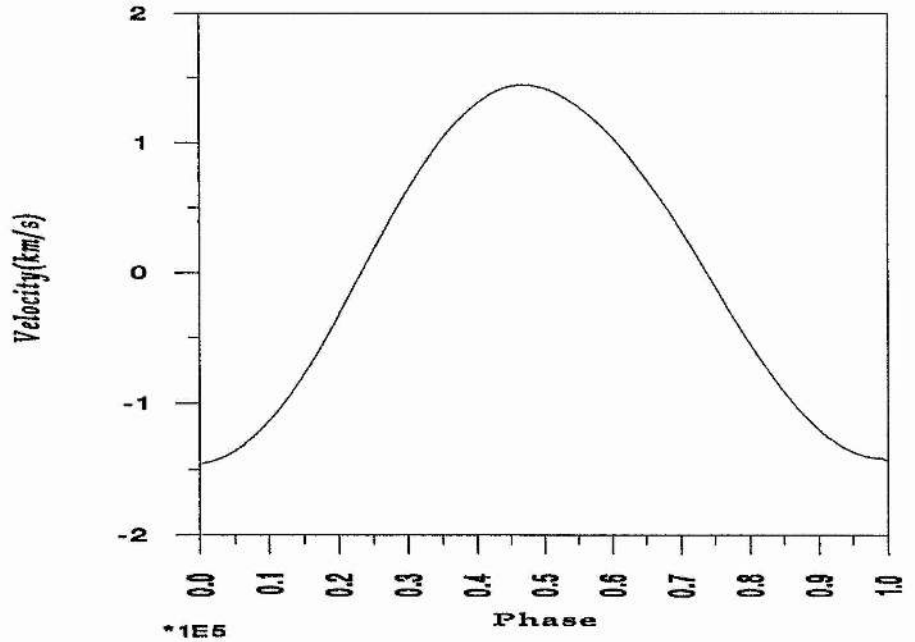
Velocity(km/s)
2
1
0
-1
-2
0.0 0.1 0.2 0.3 0.4 0.5 0.6 0.7 0.8 0.9 1.0
Phase

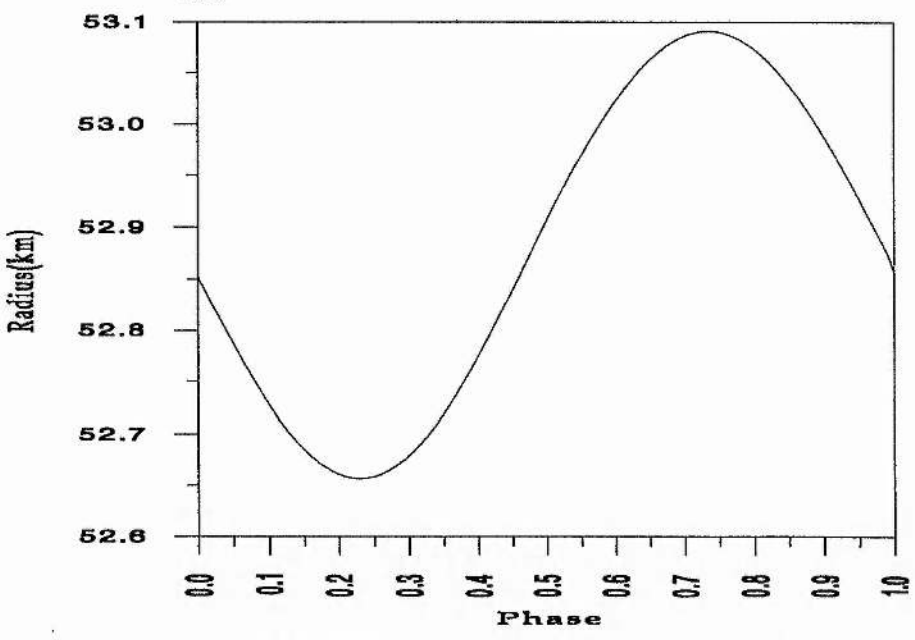
*1E5
Radius(km)
53.1
53.0
52.9
52.8
52.7
52.6
0.0 0.1 0.2 0.3 0.4 0.5 0.6 0.7 0.8 0.9 1.0
Phase

Model(12)

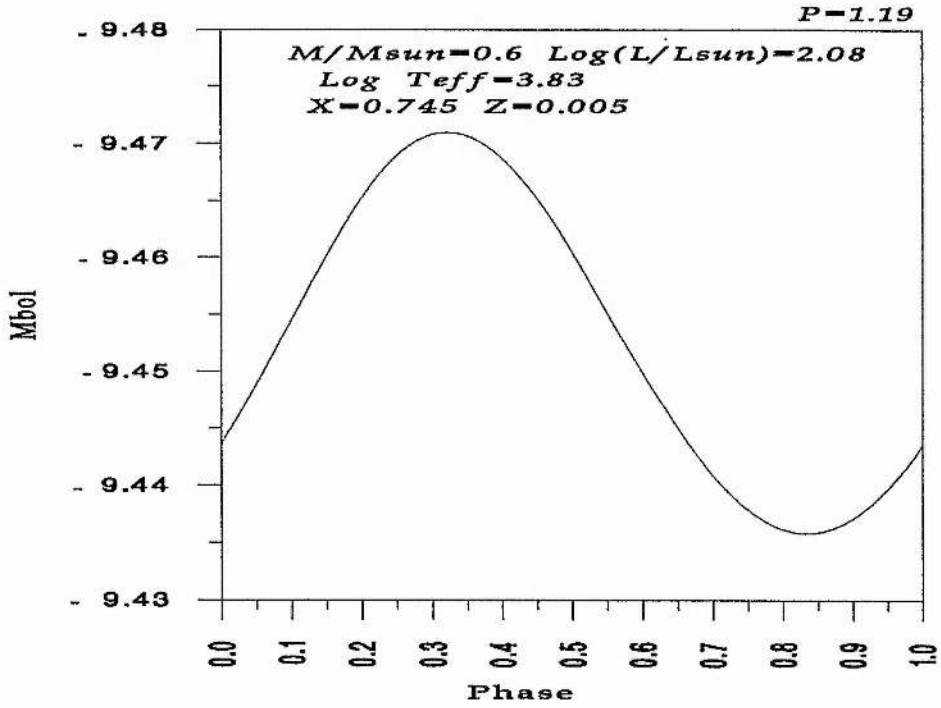
P=1.19
M/Msun=0.6 Log(L/Lsun)=2.08
Log Teff=3.83
X=0.745 Z=0.005
Mbol
- 9.48
- 9.47
- 9.46
- 9.45
- 9.44
- 9.43
0.0 0.1 0.2 0.3 0.4 0.5 0.6 0.7 0.8 0.9 1.0
Phase

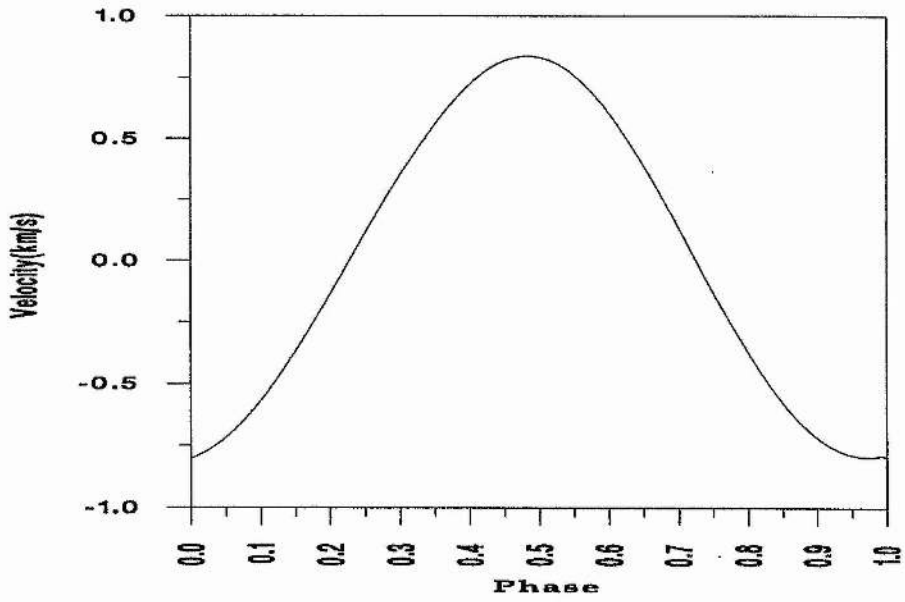
Velocity(km/s)
1.0
0.5
0.0
-0.5
-1.0
0.0 0.1 0.2 0.3 0.4 0.5 0.6 0.7 0.8 0.9 1.0
Phase

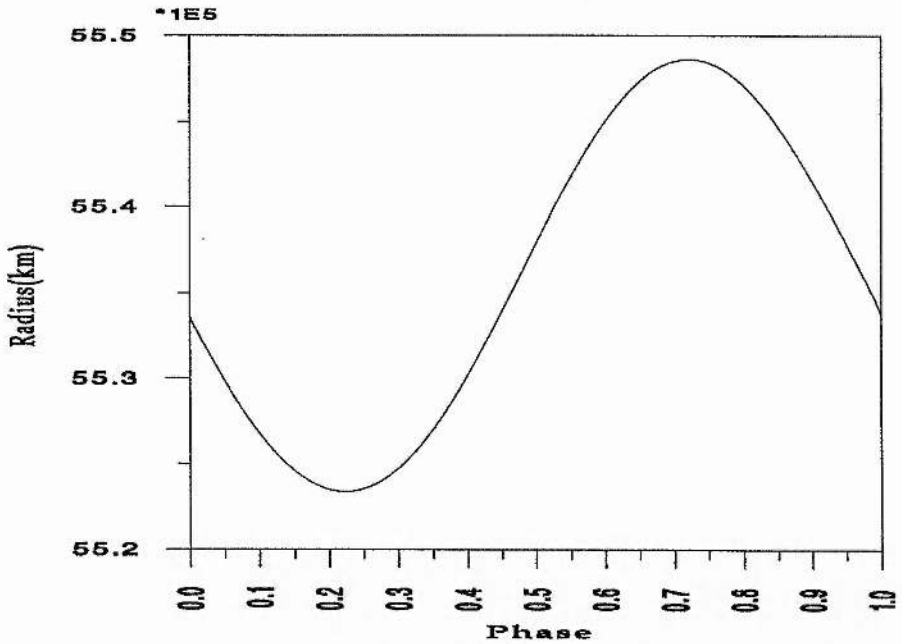
*1E5
Radius(km)
55.5
55.4
55.3
55.2
0.0 0.1 0.2 0.3 0.4 0.5 0.6 0.7 0.8 0.9 1.0
Phase

Model(23)

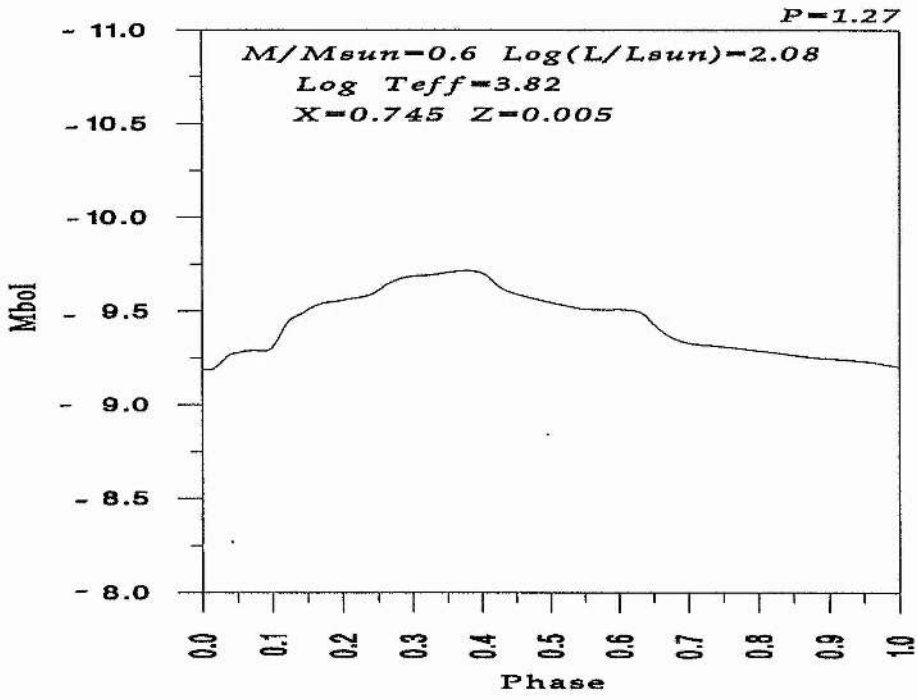
P=1.27
M/Msun=0.6 Log(L/Lsun)=2.08
Log Teff=3.82
X=0.745 Z=0.005
Mbol
- 11.0
- 10.5
- 10.0
- 9.5
- 9.0
- 8.5
- 8.0
0.0 0.1 0.2 0.3 0.4 0.5 0.6 0.7 0.8 0.9 1.0
Phase

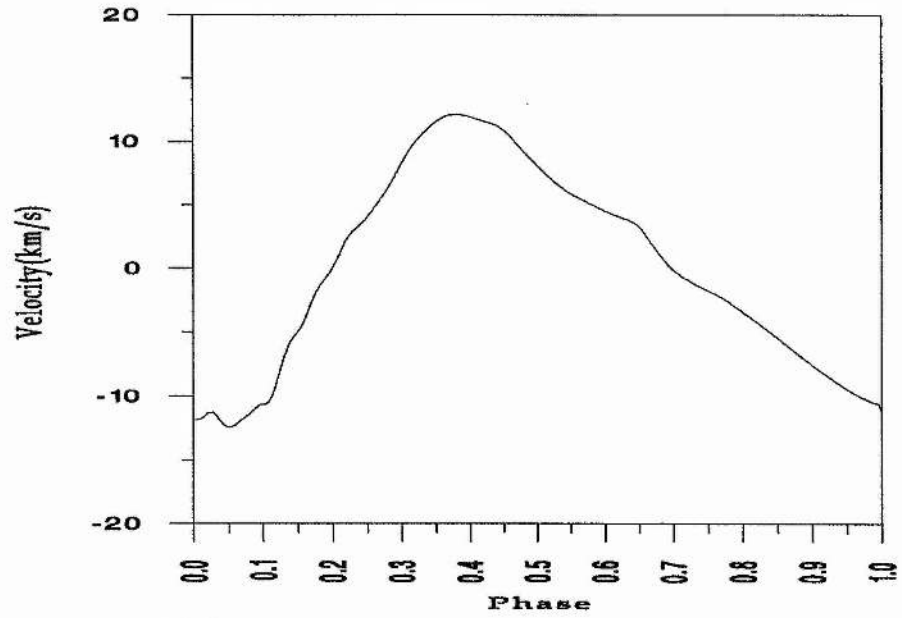
Velocity(km/s)
20
10
0
-10
-20
0.0 0.1 0.2 0.3 0.4 0.5 0.6 0.7 0.8 0.9 1.0
Phase

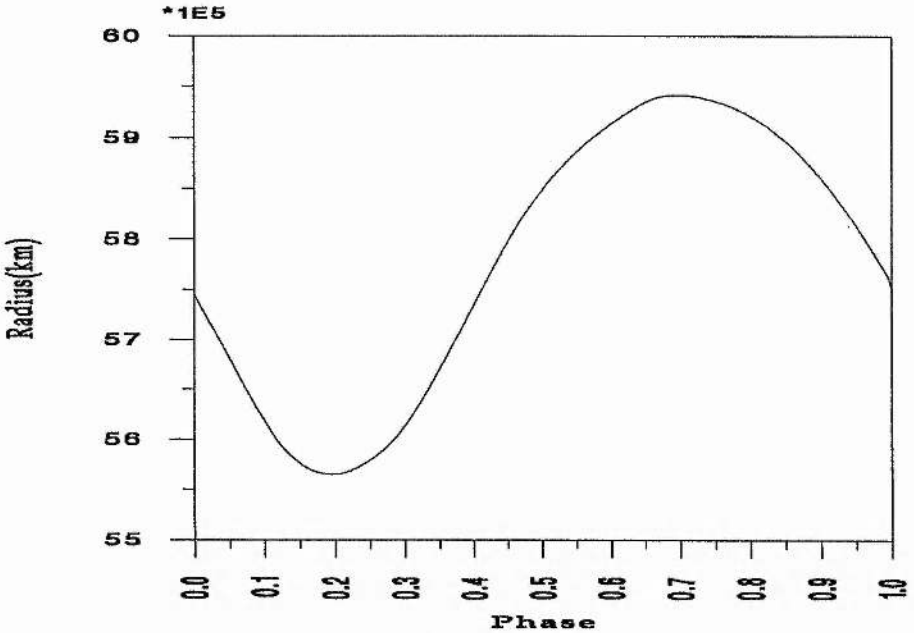
*1E5
Radius(km)
60
59
58
57
56
55
0.0 0.1 0.2 0.3 0.4 0.5 0.6 0.7 0.8 0.9 1.0
Phase

Model(14)

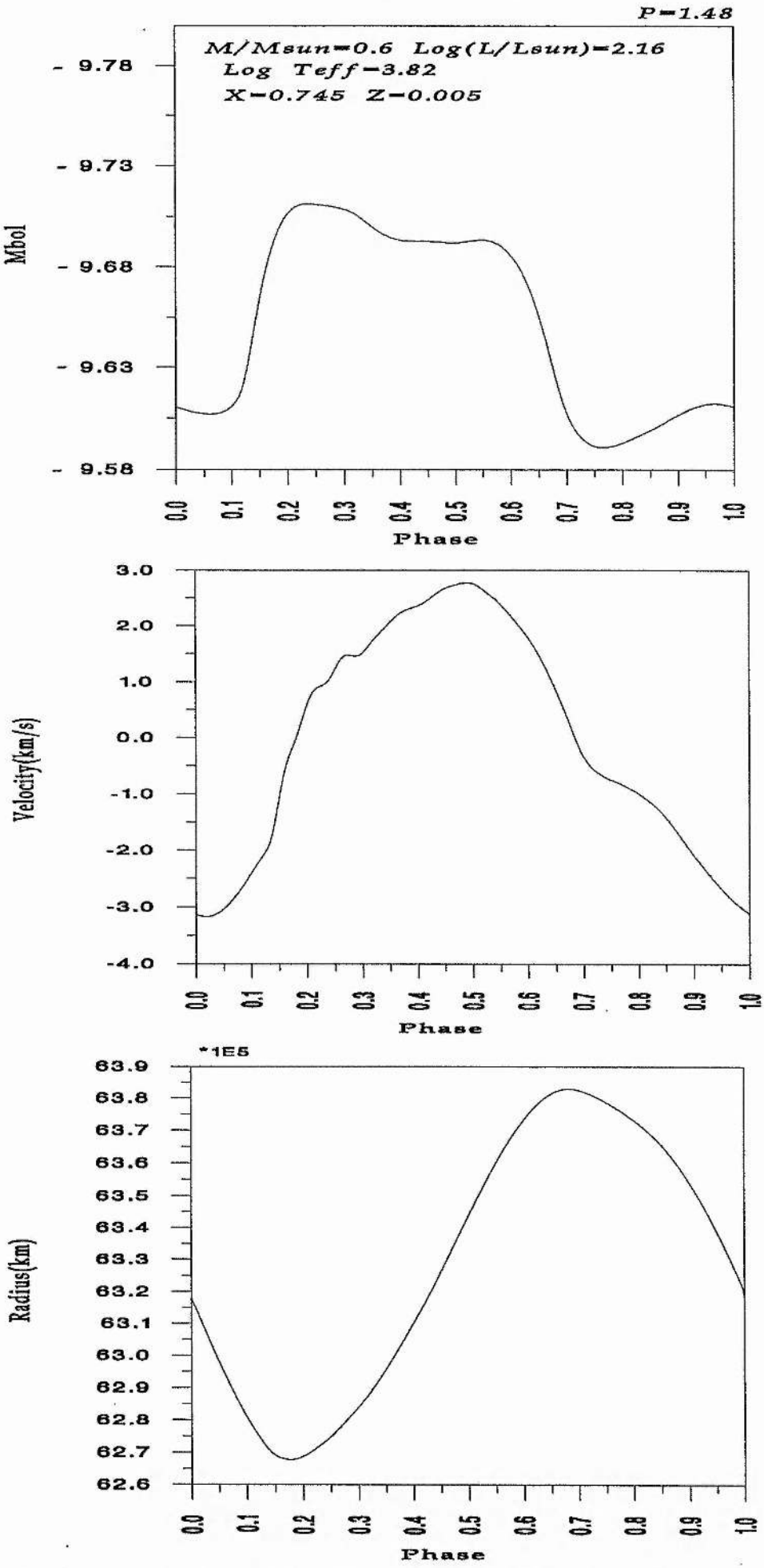
P=1.48
M/Msun=0.6 Log(L/Lsun)=2.16
Log Teff=3.82
X=0.745 Z=0.005
Mbol
- 9.78
- 9.73
- 9.68
- 9.63
- 9.58
0.0 0.1 0.2 0.3 0.4 0.5 0.6 0.7 0.8 0.9 1.0
Phase
Velocity(km/s)
3.0
2.0
1.0
0.0
-1.0
-2.0
-3.0
-4.0
0.0 0.1 0.2 0.3 0.4 0.5 0.6 0.7 0.8 0.9 1.0
Phase
*1E5
Radius(km)
63.9
63.8
63.7
63.6
63.5
63.4
63.3
63.2
63.1
63.0
62.9
62.8
62.7
62.6
0.0 0.1 0.2 0.3 0.4 0.5 0.6 0.7 0.8 0.9 1.0
Phase

Model(16)

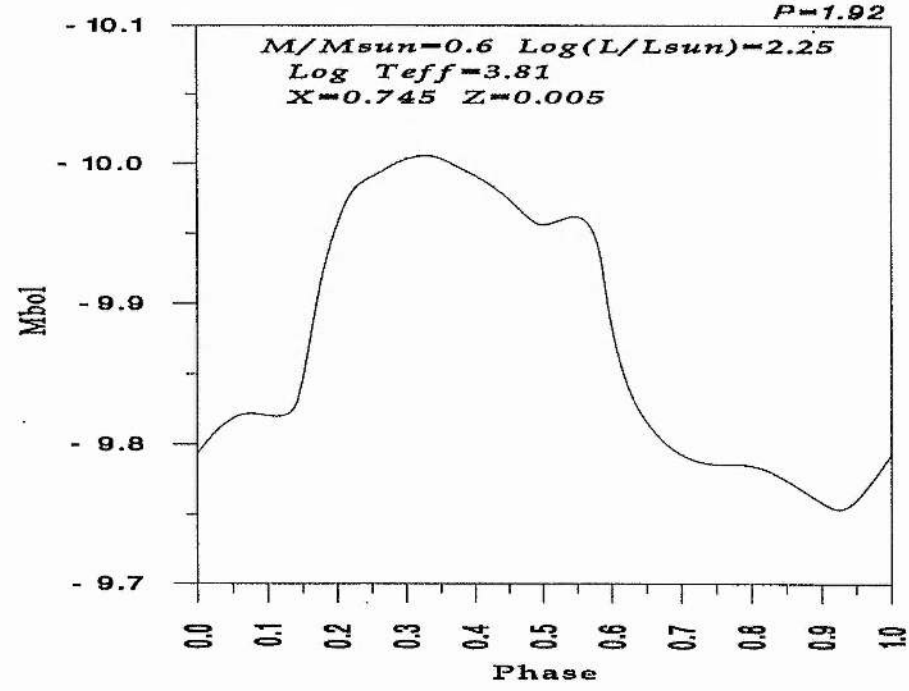
P=1.92
M/Msun=0.6 Log(L/Lsun)=2.25
Log Teff=3.81
X=0.745 Z=0.005
Mbol
- 10.1
- 10.0
- 9.9
- 9.8
- 9.7
0.0 0.1 0.2 0.3 0.4 0.5 0.6 0.7 0.8 0.9 1.0
Phase

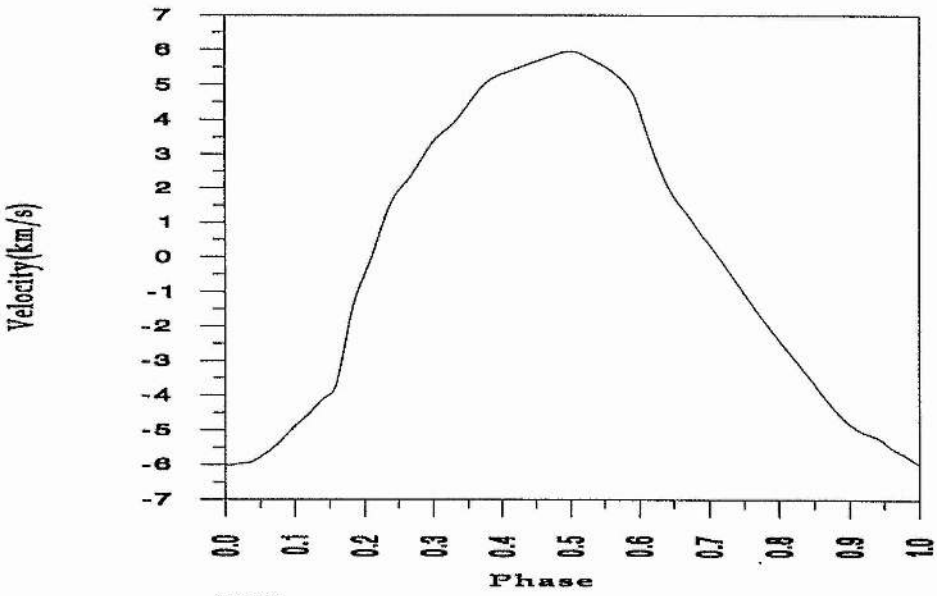
Velocity(km/s)
7 6 5 4 3 2 1 0 -1 -2 -3 -4 -5 -6 -7
0.0 0.1 0.2 0.3 0.4 0.5 0.6 0.7 0.8 0.9 1.0
Phase

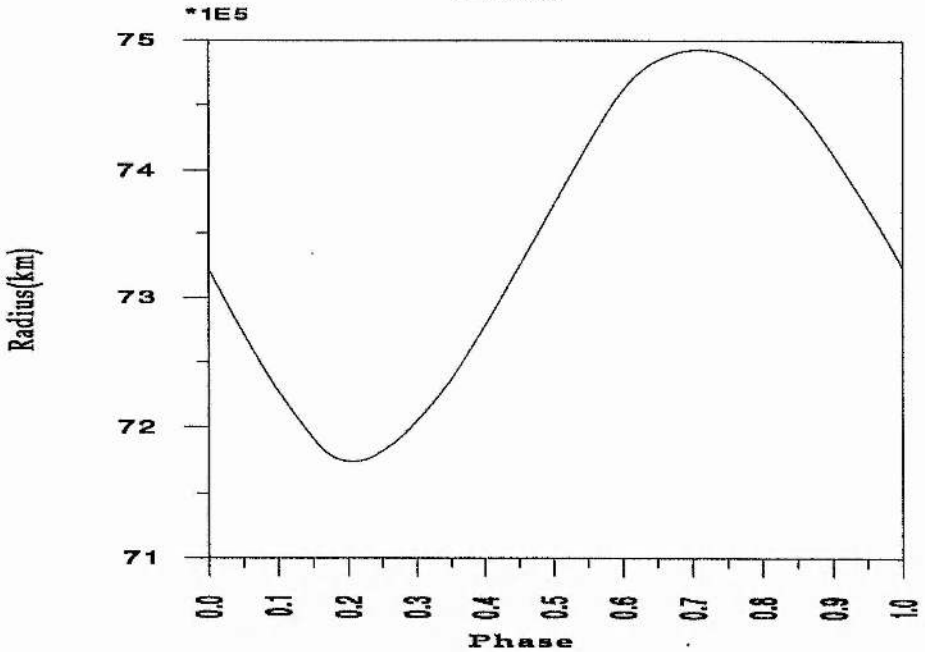
*1E5
Radius(km)
75
74
73
72
71
0.0 0.1 0.2 0.3 0.4 0.5 0.6 0.7 0.8 0.9 1.0
Phase

Model(22)

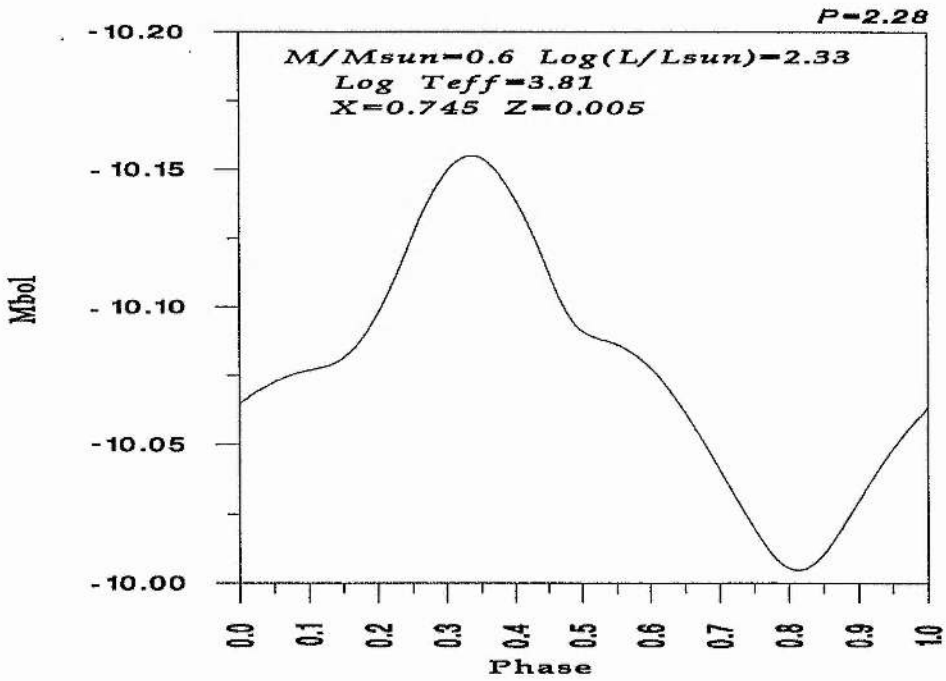
P=2.28
M/Msun=0.6 Log(L/Lsun)=2.33
Log Teff=3.81
X=0.745 Z=0.005
Mbol
-10.20
-10.15
-10.10
-10.05
-10.00
0.0
0.1
0.2
0.3
0.4
0.5
0.6
0.7
0.8
0.9
1.0
Phase

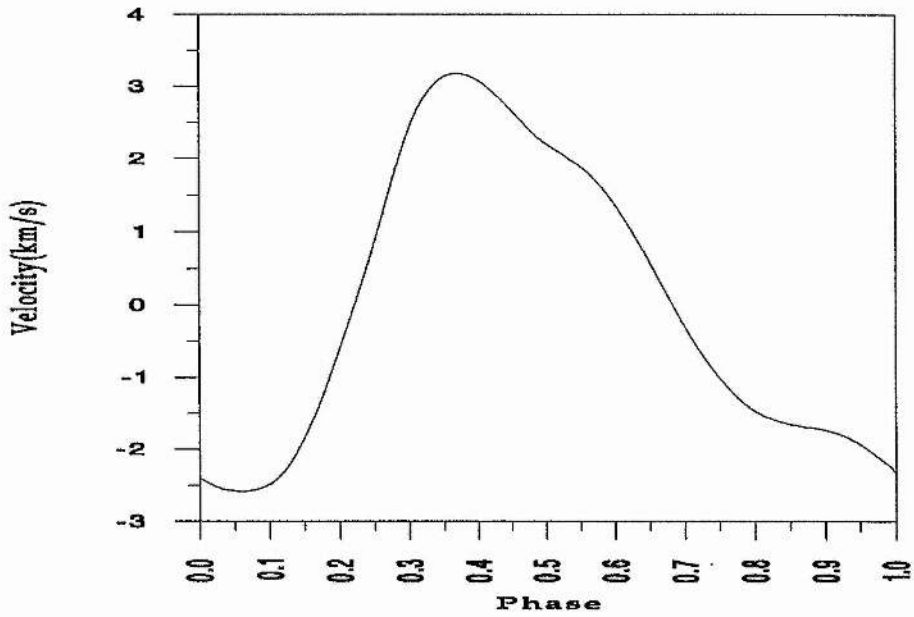
Velocity(km/s)
4
3
2
1
0
-1
-2
-3
0.0
0.1
0.2
0.3
0.4
0.5
0.6
0.7
0.8
0.9
1.0
Phase

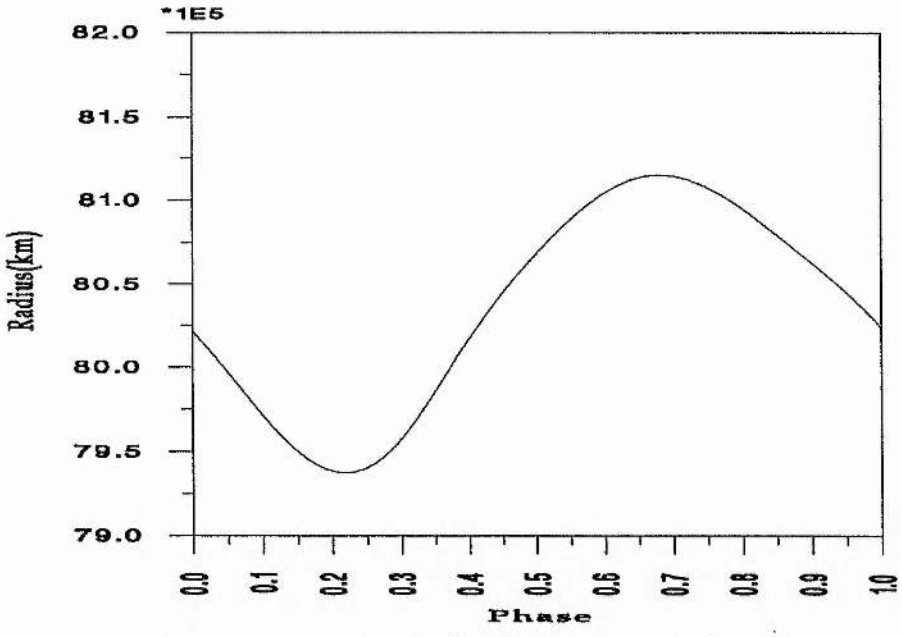
*1E5
Radius(km)
82.0
81.5
81.0
80.5
80.0
79.5
79.0
0.0
0.1
0.2
0.3
0.4
0.5
0.6
0.7
0.8
0.9
1.0
Phase

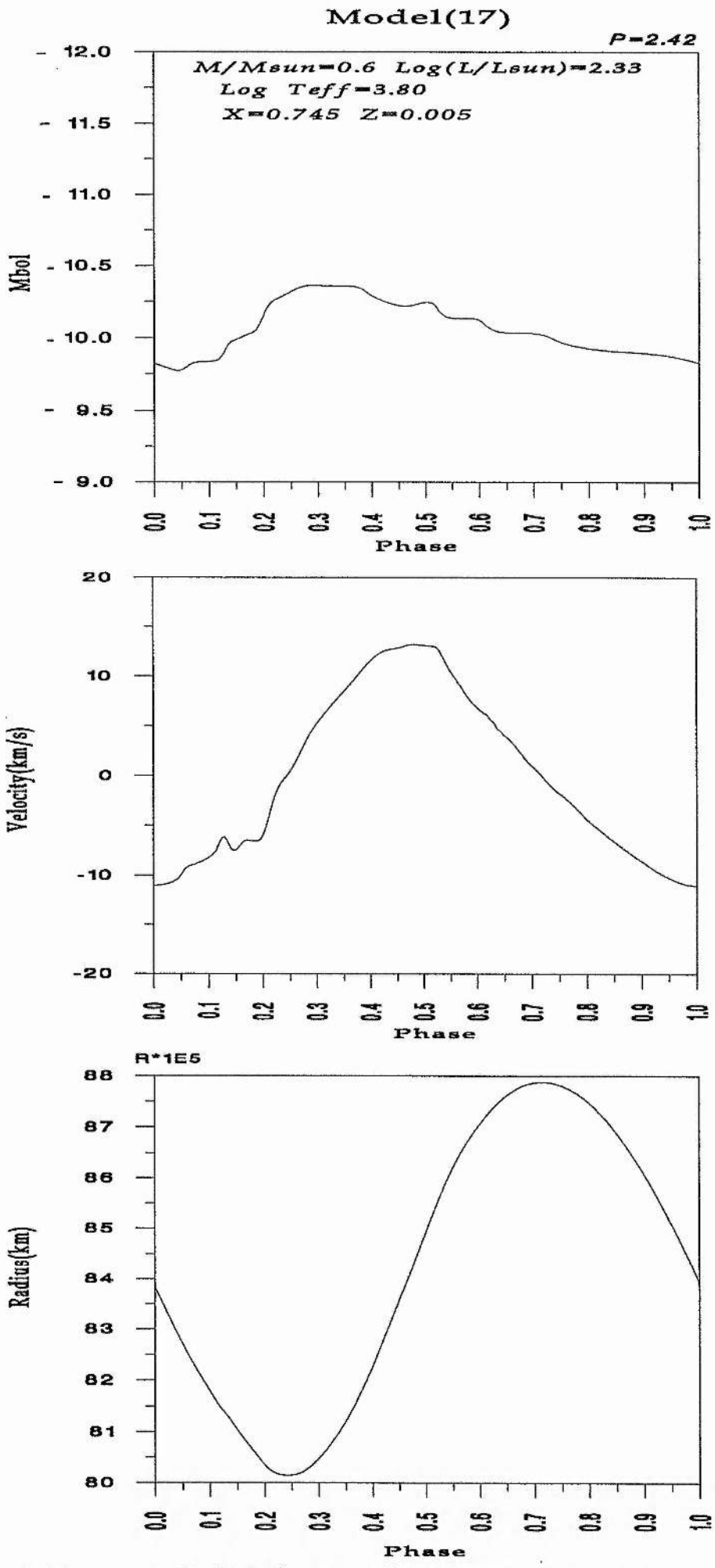
Model(17)
P=2.42
M/Msun=0.6 Log(L/Lsun)=2.33
Log Teff=3.80
X=0.745 Z=0.005
Mbol
- 12.0
- 11.5
- 11.0
- 10.5
- 10.0
- 9.5
- 9.0
0.0 0.1 0.2 0.3 0.4 0.5 0.6 0.7 0.8 0.9 1.0
Phase
Velocity(km/s)
20
10
0
-10
-20
0.0 0.1 0.2 0.3 0.4 0.5 0.6 0.7 0.8 0.9 1.0
Phase
R*1E5
Radius(km)
88
87
86
85
84
83
82
81
80
0.0 0.1 0.2 0.3 0.4 0.5 0.6 0.7 0.8 0.9 1.0
Phase

Model(32)

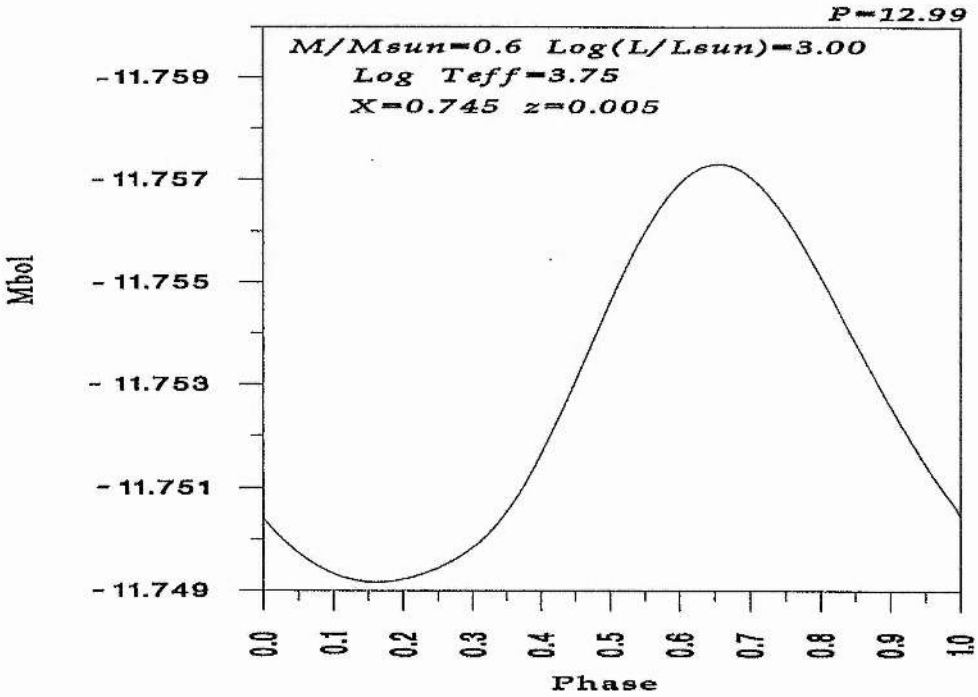
P=12.99
M/Msun=0.6 Log(L/Lsun)=3.00
Log Teff=3.75
X=0.745 z=0.005
Mbol
-11.759
-11.757
-11.755
-11.753
-11.751
-11.749
0.0
0.1
0.2
0.3
0.4
0.5
0.6
0.7
0.8
0.9
1.0
Phase

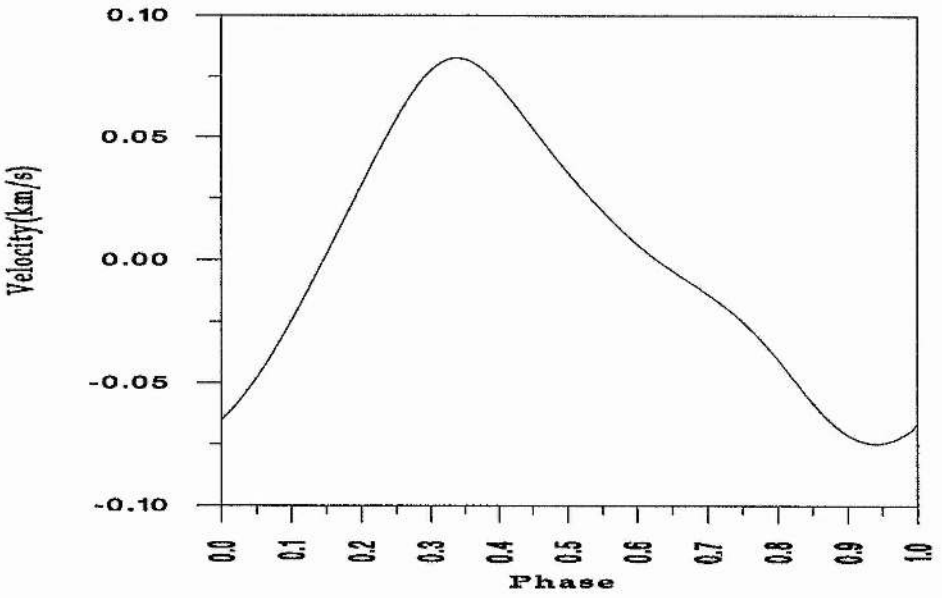
Velocity(km/s)
0.10
0.05
0.00
-0.05
-0.10
0.0
0.1
0.2
0.3
0.4
0.5
0.6
0.7
0.8
0.9
1.0
Phase

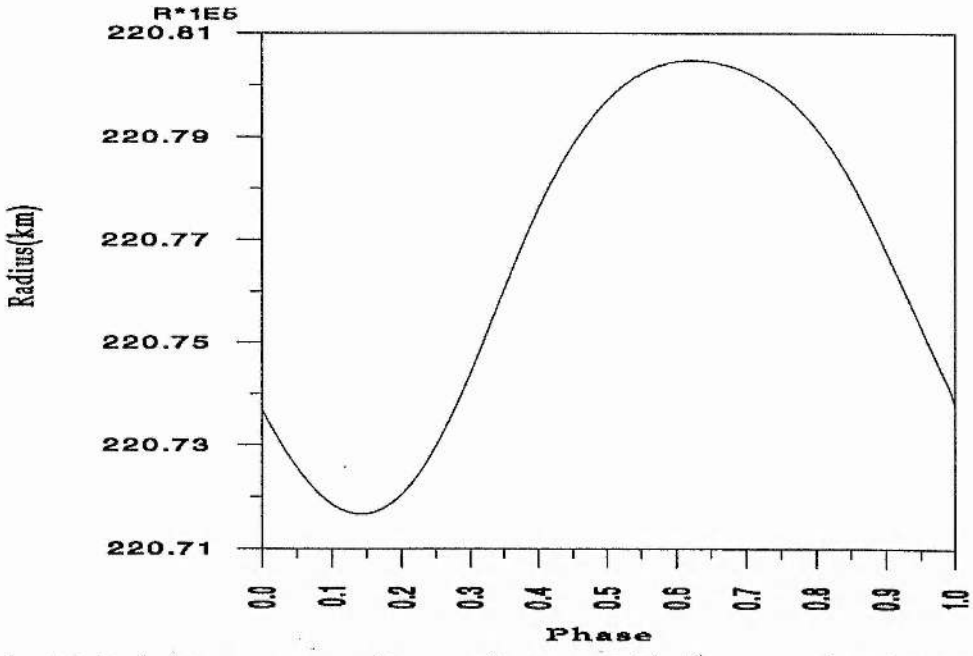
R*1E5
Radius(km)
220.81
220.79
220.77
220.75
220.73
220.71
0.0
0.1
0.2
0.3
0.4
0.5
0.6
0.7
0.8
0.9
1.0
Phase

APPENDIX *C*

Table 1C. Shows the IR opacity for composition X=0.745, Y=0.250 and Z=0.005.

log (Opacity) cm^2/G

	log(Rho)	I	I+1	I+2	I+3	I+4	I+5	I+6	I+7	I+8
log(T)	I									
3.7	-11	-2.8864	-2.8467	-2.4977	-2.0075	-1.4425	-0.8250	-0.1693	0.5643	1.1972
3.8	-11	-1.4456	-1.5229	-1.2827	-0.8958	-0.4589	0.0204	0.5538	1.1377	1.7865
3.9	-11	-0.1588	-0.0269	0.1075	0.3187	0.6139	0.9872	1.4476	2.0072	2.6850
4.0	-11	-0.0089	0.6785	1.2798	1.5993	1.7849	1.9369	2.0554	2.1403	2.1917
4.1	-10	0.3736	1.2579	2.1024	2.5848	2.8124	2.8114	2.5818	2.1236	1.4369
4.2	-10	0.0797	0.7917	1.7544	2.6992	3.3444	3.6287	3.5557	3.1251	2.3371
4.3	-10	-0.0993	0.4717	1.3603	2.3737	3.3773	4.2785	5.0795	5.7803	6.3808
4.4	-10	-0.1735	0.2583	1.0817	2.1064	3.1734	4.2494	5.3368	6.4359	7.5464
4.5	-10	-0.1767	0.1774	0.8840	1.8918	2.9866	4.1422	5.3655	6.6566	8.0155
4.6	-9	0.1393	0.8201	1.7471	2.8086	3.9261	5.0992	6.3279	7.6124	8.9526
4.7	-9	-0.0666	0.5736	1.5467	2.5760	3.6059	4.6477	5.6993	6.7606	7.8317
4.8	-9	-0.2308	0.2214	1.0479	2.0933	3.1669	4.1082	4.9010	5.5452	6.0409
4.9	-9	-0.2987	-0.0148	0.6356	1.6072	2.6764	3.7307	4.7260	5.6646	6.5466
5.0	-9	-0.3264	-0.1334	0.3831	1.2559	2.2963	3.3657	4.3866	5.3589	6.2828
5.2	-8	-0.1026	0.1569	0.7774	1.6873	2.6264	3.4733	4.2120	4.8433	5.3673
5.4	-8	-0.3254	-0.1356	0.2680	0.9540	1.7210	2.4167	3.0024	3.4819	3.8552
5.6	-7	-0.4188	-0.2715	0.2246	0.9760	1.6274	2.1832	2.6788	3.1129	3.4854
5.8	-7	-0.4501	-0.4285	-0.3149	0.1272	0.9611	1.5911	2.0853	2.4620	2.7215
6.0	-7	-0.4474	-0.4446	-0.4117	-0.2707	0.2079	1.0014	1.6242	2.0590	2.3060
6.2	-6	-0.4493	-0.4240	-0.3567	-0.1704	0.3937	1.1429	1.5911	1.7026	1.4793
6.4	-6	-0.4572	-0.4607	-0.4369	-0.3466	-0.0247	0.5419	1.0149	1.3409	1.5287
6.6	-5	-0.4614	-0.4592	-0.4439	-0.3603	-0.0411	0.3960	0.8339	1.3720	2.0057
6.8	-5	-0.4603	-0.4635	-0.4608	-0.4463	-0.3637	-0.1006	0.2765	0.8137	1.5224
7.0	-5	-0.4668	-0.4673	-0.4671	-0.4620	-0.4427	-0.3560	-0.1186	0.3067	0.9577
7.2	-4	-0.4729	-0.4731	-0.4722	-0.4643	-0.4337	-0.3278	-0.0737	0.3632	0.9847
7.4	-4	-0.4815	-0.4820	-0.4820	-0.4810	-0.4726	-0.4318	-0.3081	-0.0533	0.4226
7.6	-3	-0.4938	-0.4962	-0.4948	-0.4943	-0.4880	-0.4406	-0.3181	-0.0314	0.4780
7.8	-3	-0.5175	-0.5171	-0.5171	-0.5159	-0.5146	-0.5052	-0.4606	-0.3448	-0.0288
8.0	-3	-0.5503	-0.5503	-0.5503	-0.5503	-0.5503	-0.5485	-0.5376	-0.5169	-0.3849
8.2	-2	-0.6029	-0.6029	-0.6029	-0.5974	-0.6121	-0.6009	-0.6035	-0.6107	-0.2517
8.4	-2	-0.6863	-0.6863	-0.6863	-0.6863	-0.6832	-0.5843	-0.7943	-0.6516	-0.4343
8.6	-1	-0.8186	-0.8186	-0.8186	-0.7763	-1.0076	-0.1696	-0.7529	-0.3352	1.7566
8.8	-1	-1.0281	-1.0281	-1.0281	-1.0281	-0.6422	-0.9888	-2.1763	0.0160	2.1800
9.0	-1	-1.3603	-1.3603	-1.3603	-1.3603	-1.3603	-2.7122	6.0626	-1.2497	4.1329

Table 2C. Shows the IR opacity for composition X=0.749, Y=0.250 and Z=0.001.

log(Opacity) cm^2/G

	log(Rho)	I	I+1	I+2	I+3	I+4	I+5	I+6	I+7	I+8
log(T)	I									
3.7	-11	-2.9310	-2.9167	-2.5884	-2.1295	-1.6083	-1.0187	-0.3693	0.3434	0.9853
3.8	-11	-1.4460	-1.5316	-1.3019	-0.9233	-0.4984	-0.0380	0.4670	1.0075	1.6126
3.9	-11	-0.1591	-0.0269	0.1061	0.3148	0.6061	0.9748	1.4288	1.9784	2.6298
4.0	-11	-0.0243	0.6690	1.2726	1.5909	1.7702	1.9115	2.0151	2.0808	2.1086
4.1	-10	0.3431	1.2293	2.0853	2.5659	2.7959	2.8036	2.5890	2.1521	1.4929
4.2	-10	0.0361	0.7502	1.7260	2.6790	3.3280	3.6105	3.5299	3.0863	2.2796
4.3	-10	-0.1445	0.4234	1.3306	2.3531	3.3652	4.2736	5.0805	5.7858	6.3895
4.4	-10	-0.2111	0.2068	1.0410	2.0837	3.1592	4.2498	5.3577	6.4828	7.6252
4.5	-10	-0.2175	0.1271	0.8456	1.8674	2.9674	4.1408	5.4001	6.7454	8.1765
4.6	-9	0.0926	0.7752	1.7173	2.7925	3.9183	5.0881	6.3026	7.5618	8.8655
4.7	-9	-0.1165	0.5172	1.5027	2.5477	3.5912	4.6322	5.6680	6.6987	7.7244
4.8	-9	-0.2726	0.1611	0.9838	2.0338	3.1301	4.0981	4.9249	5.6105	6.1549
4.9	-9	-0.3357	-0.0706	0.5699	1.5434	2.6225	3.7052	4.7541	5.7710	6.7558
5.0	-9	-0.3714	-0.1870	0.3123	1.1927	2.2431	3.3306	4.3989	5.4479	6.4776
5.2	-8	-0.2587	-0.0047	0.6432	1.5744	2.5301	3.4483	4.3231	5.1548	5.9435
5.4	-8	-0.3889	-0.2648	0.0555	0.6814	1.4402	2.2141	3.0220	3.8656	4.7448
5.6	-7	-0.4343	-0.3418	-0.0001	0.6194	1.2792	1.9881	2.7766	3.6434	4.5886
5.8	-7	-0.4528	-0.4392	-0.3634	-0.0682	0.5795	1.2416	1.9018	2.5692	3.2440
6.0	-7	-0.4509	-0.4493	-0.4318	-0.3428	-0.0155	0.6376	1.2935	1.8723	2.3738
6.2	-6	-0.4532	-0.4406	-0.4007	-0.2820	0.1119	0.7408	1.2182	1.5168	1.6377
6.4	-6	-0.4577	-0.4595	-0.4478	-0.4021	-0.2192	0.1711	0.6380	1.1922	1.8405
6.6	-5	-0.4600	-0.4598	-0.4510	-0.4078	-0.2328	0.1102	0.6526	1.4913	2.6217
6.8	-5	-0.4597	-0.4622	-0.4611	-0.4521	-0.4033	-0.2298	0.1333	0.7687	1.6752
7.0	-5	-0.4661	-0.4661	-0.4661	-0.4631	-0.4491	-0.3881	-0.1905	0.2381	0.9650
7.2	-4	-0.4720	-0.4720	-0.4712	-0.4665	-0.4466	-0.3647	-0.1284	0.3412	1.0611
7.4	-4	-0.4809	-0.4809	-0.4809	-0.4796	-0.4742	-0.4454	-0.3401	-0.0772	0.4242
7.6	-3	-0.4926	-0.4951	-0.4937	-0.4934	-0.4878	-0.4477	-0.3306	-0.0416	0.4760
7.8	-3	-0.5163	-0.5160	-0.5159	-0.5148	-0.5136	-0.5054	-0.4635	-0.3516	-0.0383
8.0	-3	-0.5491	-0.5491	-0.5491	-0.5491	-0.5491	-0.5474	-0.5377	-0.5198	-0.3905
8.2	-2	-0.6018	-0.6018	-0.6018	-0.5961	-0.6118	-0.5999	-0.6036	-0.6201	-0.3023
8.4	-2	-0.6852	-0.6852	-0.6852	-0.6852	-0.6820	-0.5830	-0.8103	-0.6853	-0.4685
8.6	-1	-0.8174	-0.8174	-0.8174	-0.7743	-1.0147	-0.1430	-0.8580	-0.6083	1.2403
8.8	-1	-1.0270	-1.0270	-1.0270	-1.0270	-0.6338	-1.0367	-2.2010	-0.0688	2.0296
9.0	-1	-1.3591	-1.3591	-1.3591	-1.3591	-1.3591	-2.7352	6.2674	-2.3611	1.4377

Table 3C. Shows the IR opacity for composition X=0.750, Y=0.250 and Z=0.000.

log(Opacity) cm^2/G

	log(Rho)	I	I+1	I+2	I+3	I+4	I+5	I+6	I+7	I+8
log (T)	I									
3.7	-11	-2.9470	-2.9563	-2.6459	-2.2094	-1.7315	-1.2336	-0.7466	-0.3648	0.1048
3.8	-11	-1.4595	-1.5507	-1.3260	-0.9497	-0.5278	-0.0738	0.4181	0.9328	1.4602
3.9	-11	-0.1735	-0.0398	0.0921	0.2984	0.5861	0.9488	1.3943	1.9332	2.5713
4.0	-11	-0.0431	0.6536	1.2606	1.5806	1.7577	1.8880	1.9714	2.0080	1.9977
4.1	-10	0.3080	1.2004	2.0708	2.5515	2.7840	2.7971	2.5906	2.1647	1.5193
4.2	-10	-0.0053	0.7144	1.7051	2.6666	3.3197	3.6007	3.5132	3.0573	2.2330
4.3	-10	-0.1905	0.3768	1.3068	2.3400	3.3579	4.2769	5.0992	5.8245	6.4530
4.4	-10	-0.2462	0.1617	1.0084	2.0672	3.1496	4.2509	5.3738	6.5183	7.6843
4.5	-10	-0.2539	0.0836	0.8156	1.8514	2.9563	4.1393	5.4139	6.7801	8.2378
4.6	-9	0.0535	0.7434	1.6997	2.7823	3.9123	5.0829	6.2947	7.5476	8.8417
4.7	-9	-0.1640	0.4658	1.4711	2.5320	3.5844	4.6344	5.6802	6.7217	7.7590
4.8	-9	-0.3120	0.1023	0.9279	1.9948	3.1139	4.0843	4.8884	5.5260	5.9971
4.9	-9	-0.3664	-0.1167	0.5164	1.5001	2.5936	3.6984	4.7821	5.8458	6.8896
5.0	-9	-0.4074	-0.2267	0.2619	1.1477	2.2134	3.3169	4.4260	5.5409	6.6614
5.2	-8	-0.4019	-0.1441	0.5227	1.4776	2.4849	3.4390	4.3230	5.1379	5.8836
5.4	-8	-0.4519	-0.4012	-0.1782	0.3648	1.1934	2.1220	3.0208	3.8873	4.7212
5.6	-7	-0.4488	-0.4025	-0.2200	0.2330	0.9912	1.8885	2.8390	3.8465	4.9109
5.8	-7	-0.4567	-0.4477	-0.4013	-0.2289	0.2042	0.9324	1.8323	2.8858	4.0929
6.0	-7	-0.4567	-0.4559	-0.4464	-0.3936	-0.2074	0.2353	0.9639	1.9221	3.1101
6.2	-6	-0.4580	-0.4554	-0.4424	-0.3789	-0.1694	0.3056	1.0504	2.0386	3.2716
6.4	-6	-0.4588	-0.4590	-0.4554	-0.4368	-0.3544	-0.1029	0.4164	1.2142	2.2900
6.6	-5	-0.4611	-0.4597	-0.4552	-0.4286	-0.3197	-0.0257	0.5934	1.6364	3.0986
6.8	-5	-0.4631	-0.4632	-0.4618	-0.4550	-0.4166	-0.2770	0.0855	0.7617	1.7415
7.0	-5	-0.4609	-0.4659	-0.4669	-0.4639	-0.4530	-0.3987	-0.2150	0.2176	0.9713
7.2	-4	-0.4719	-0.4716	-0.4715	-0.4686	-0.4517	-0.3781	-0.1454	0.3362	1.0822
7.4	-4	-0.4806	-0.4806	-0.4806	-0.4795	-0.4743	-0.4503	-0.3505	-0.0827	0.4214
7.6	-3	-0.4923	-0.4948	-0.4934	-0.4931	-0.4888	-0.4498	-0.3333	-0.0443	0.4736
7.8	-3	-0.5160	-0.5157	-0.5157	-0.5145	-0.5133	-0.5062	-0.4641	-0.3533	-0.0383
8.0	-3	-0.5489	-0.5489	-0.5489	-0.5489	-0.5489	-0.5471	-0.5373	-0.5207	-0.3924
8.2	-2	-0.6015	-0.6015	-0.6015	-0.5958	-0.6115	-0.6043	-0.6055	-0.6253	-0.2944
8.4	-2	-0.6849	-0.6849	-0.6849	-0.6849	-0.6816	-0.5826	-0.8491	-0.6830	-0.4909
8.6	-1	-0.8172	-0.8172	-0.8172	-0.7738	-1.0151	-0.1803	-0.9407	-0.6446	1.3474
8.8	-1	-1.0267	-1.0267	-1.0267	-1.0267	-0.6317	-1.0360	-2.6483	-0.0388	1.6775
9.0	-1	-1.3589	-1.3589	-1.3589	-1.3589	-1.3589	-2.7410	6.2736	-3.4044	1.4271

Following we represent the IR opacity using the above tables and the Carson opacity for (0.745,0.250,0.005). There mentioned the composition and the density for each value being plotted.

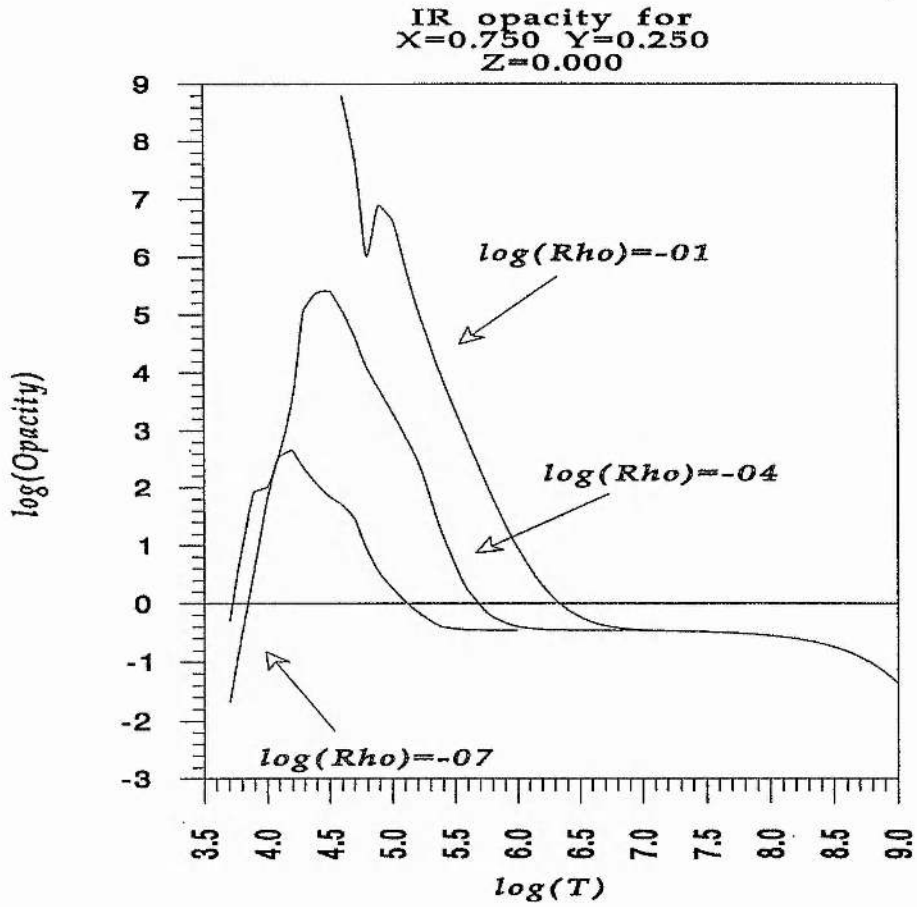
IR opacity for
X=0.750 Y=0.250
Z=0.000
log(Rho)=-01
log(Rho)=-04
log(Rho)=-07
log(Opacity)
log(T)
9
8
7
6
5
4
3
2
1
0
-1
-2
-3
3.5
4.0
4.5
5.0
5.5
6.0
6.5
7.0
7.5
8.0
8.5
9.0

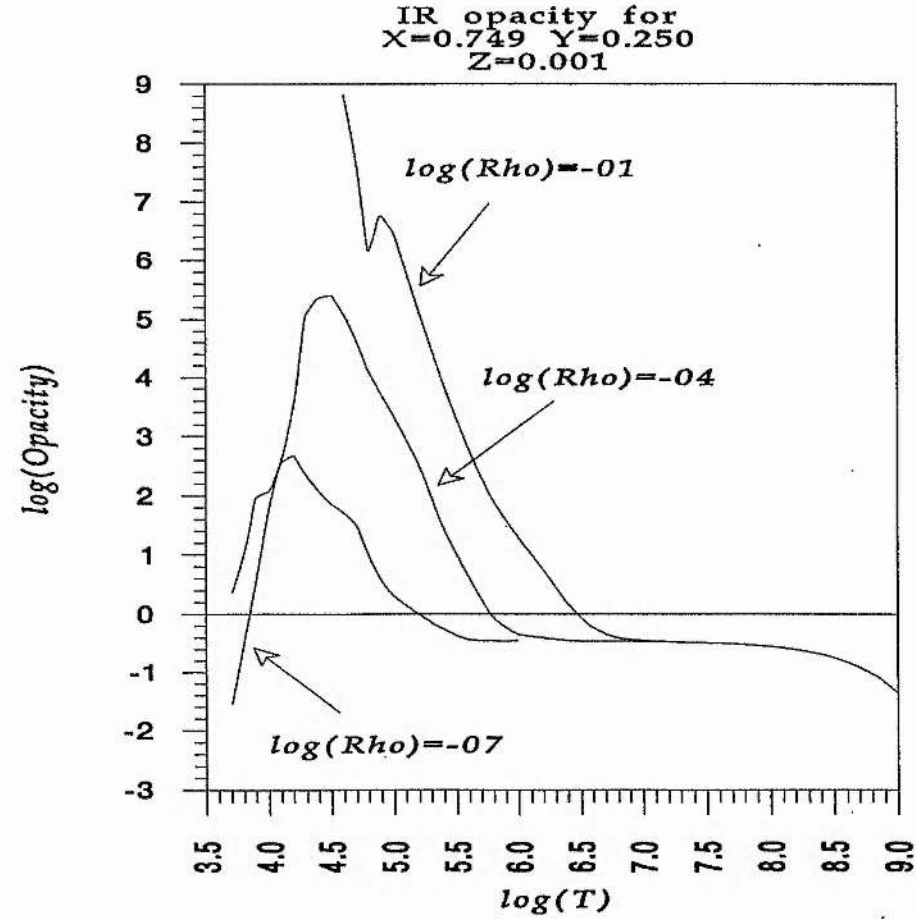
IR opacity for
X=0.749 Y=0.250
Z=0.001
log(Rho)=-01
log(Rho)=-04
log(Rho)=-07
log(Opacity)
log(T)
9
8
7
6
5
4
3
2
1
0
-1
-2
-3
3.5
4.0
4.5
5.0
5.5
6.0
6.5
7.0
7.5
8.0
8.5
9.0

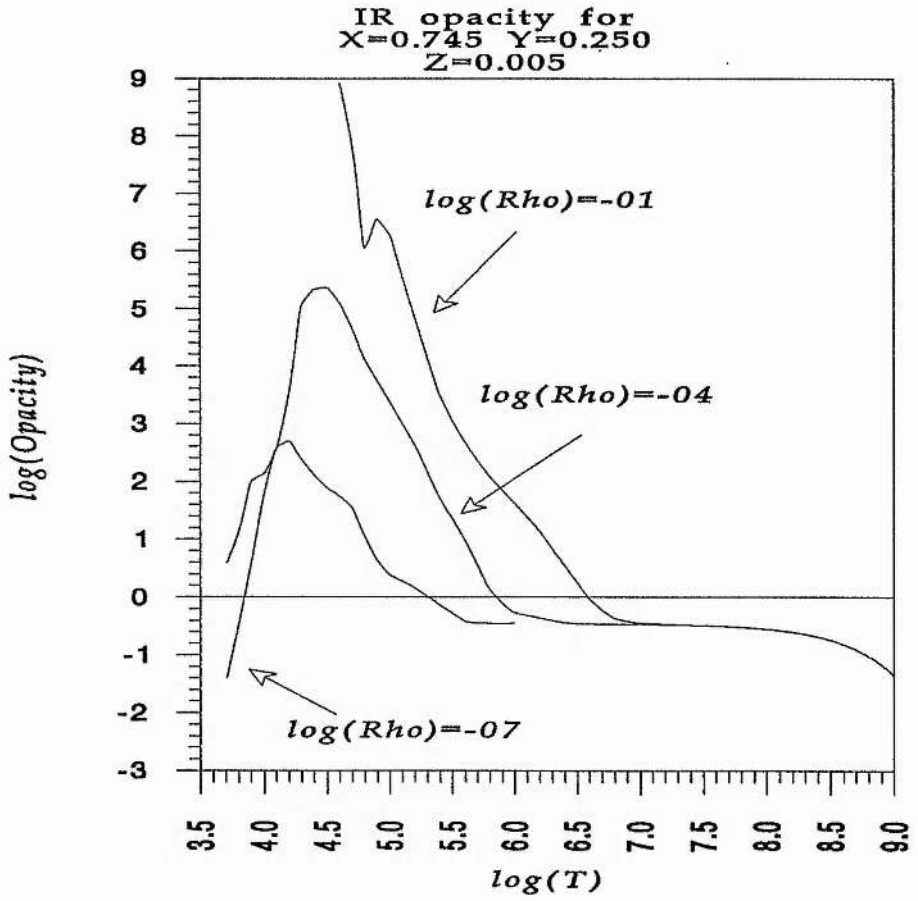
IR opacity for
X=0.745 Y=0.250
Z=0.005
log(Rho)=-01
log(Rho)=-04
log(Rho)=-07
log(Opacity)
log(T)
9
8
7
6
5
4
3
2
1
0
-1
-2
-3
3.5
4.0
4.5
5.0
5.5
6.0
6.5
7.0
7.5
8.0
8.5
9.0

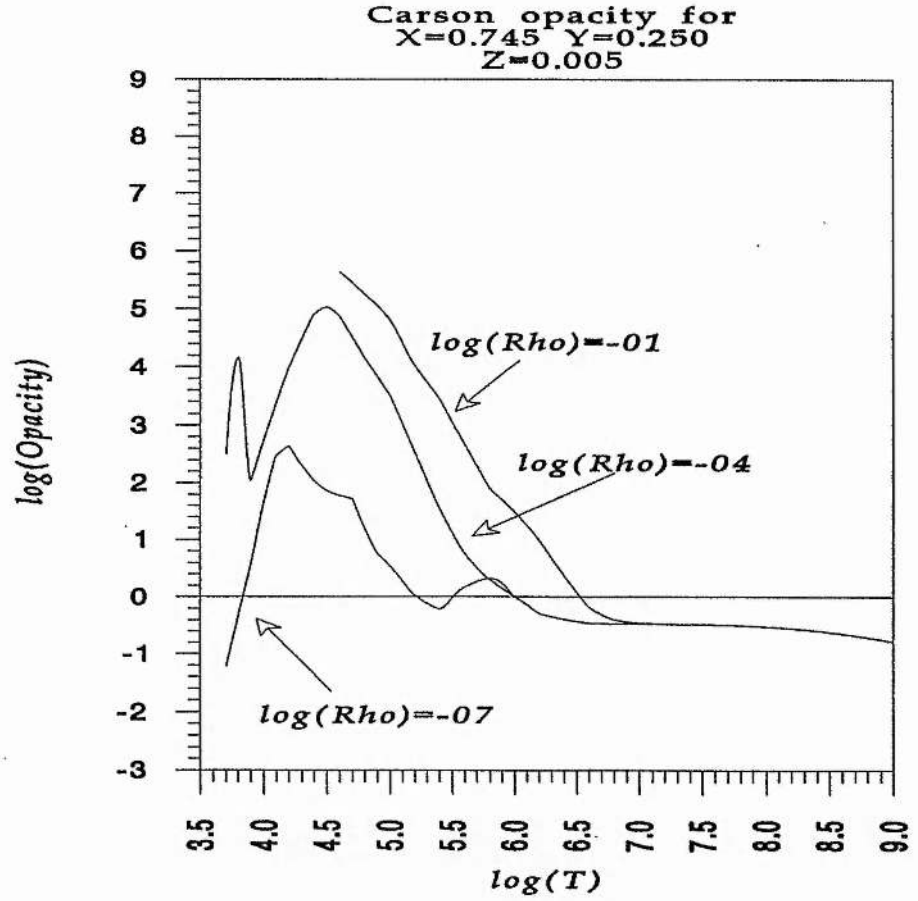
Carson opacity for
X=0.745 Y=0.250
Z=0.005
log(Rho)=-01
log(Rho)=-04
log(Rho)=-07
log(Opacity)
log(T)
9
8
7
6
5
4
3
2
1
0
-1
-2
-3
3.5
4.0
4.5
5.0
5.5
6.0
6.5
7.0
7.5
8.0
8.5
9.0

Following we represent a comparison between the IR and Carson opacities for each value of $\log(\rho)$, see text for more detail.

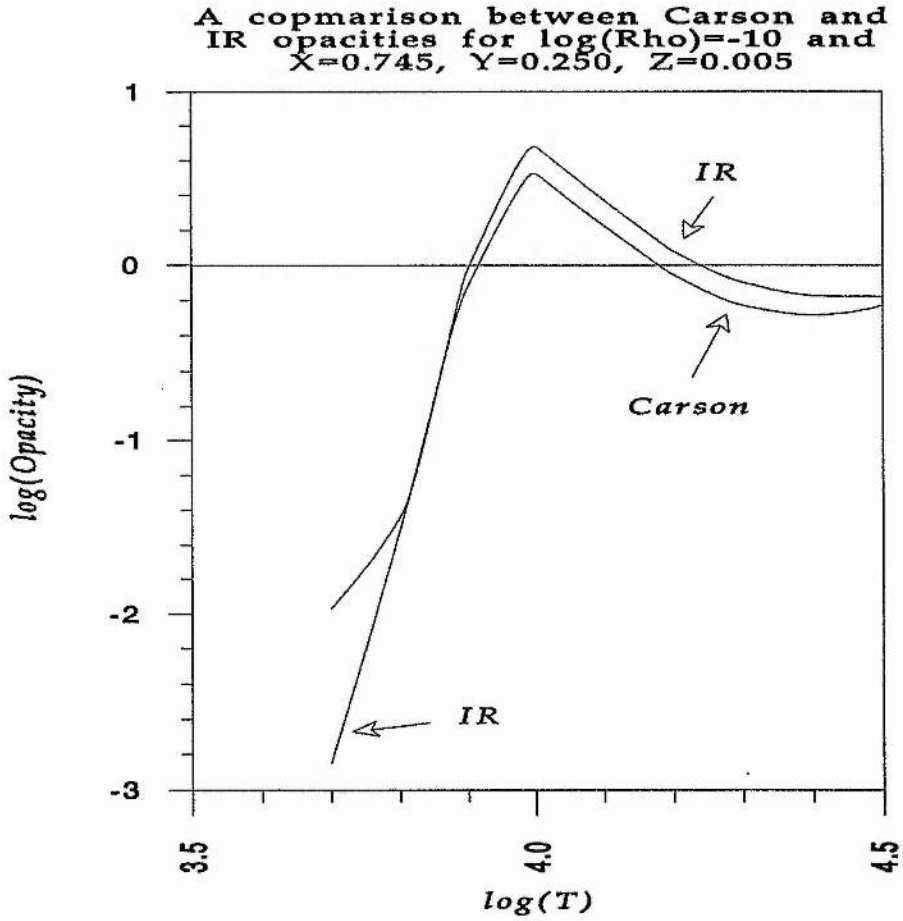
A copmarison between Carson and
IR opacities for log(Rho)=-10 and
X=0.745, Y=0.250, Z=0.005
1
0
-1
-2
-3
log(Opacity)
IR
Carson
IR
3.5
4.0
4.5
log(T)

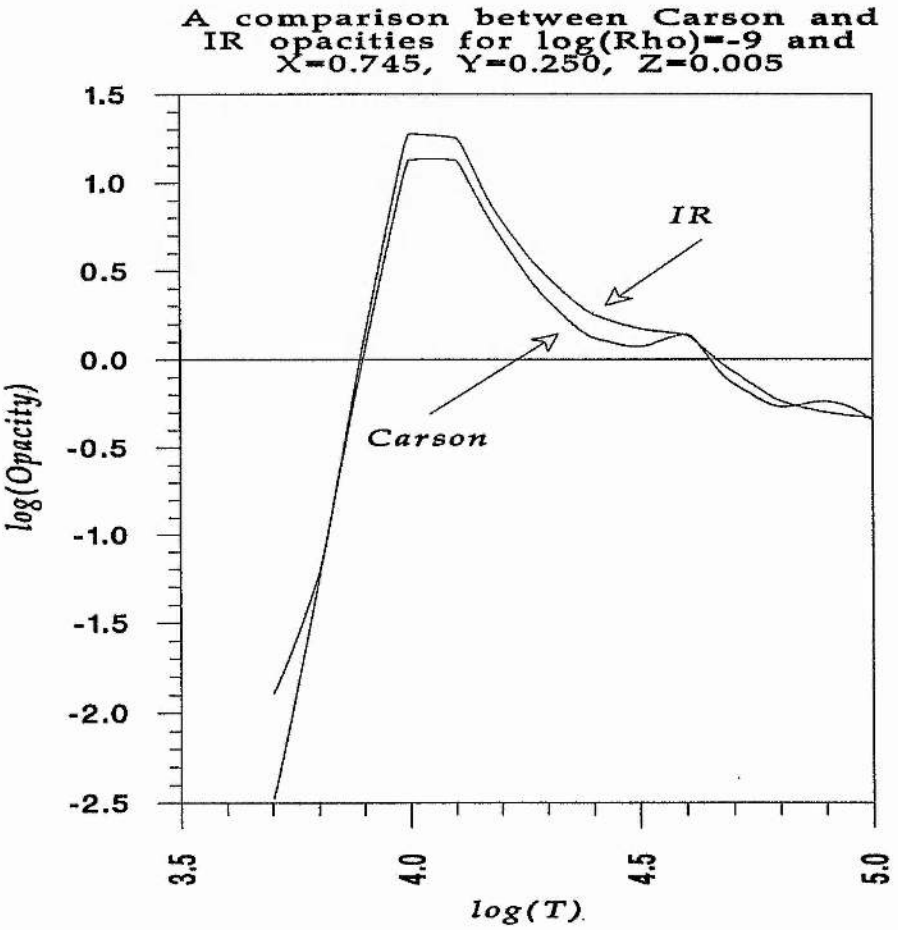
A comparison between Carson and
IR opacities for log(Rho)=-9 and
X=0.745, Y=0.250, Z=0.005
1.5
1.0
0.5
0.0
-0.5
-1.0
-1.5
-2.0
-2.5
log(Opacity)
IR
Carson
3.5
4.0
4.5
5.0
log(T)

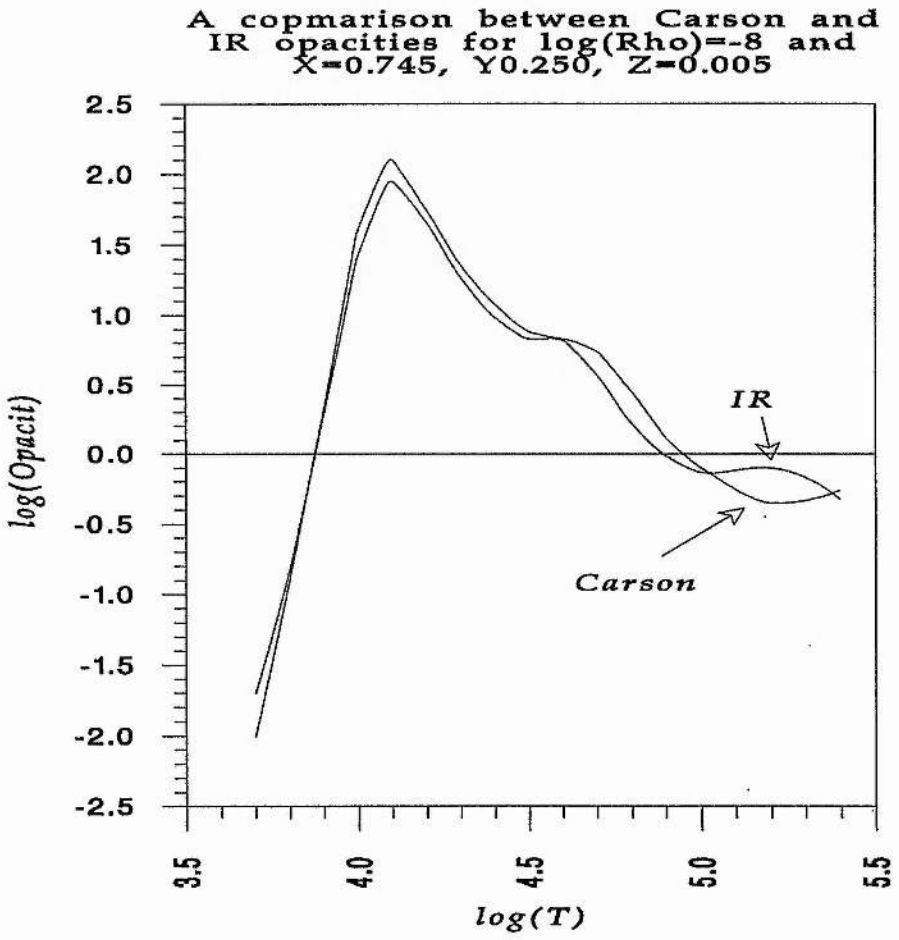
A copmarison between Carson and
IR opacities for log(Rho)=-8 and
X=0.745, Y0.250, Z=0.005
2.5
2.0
1.5
1.0
0.5
0.0
-0.5
-1.0
-1.5
-2.0
-2.5
log(Opacit)
IR
Carson
3.5
4.0
4.5
5.0
5.5
log(T)

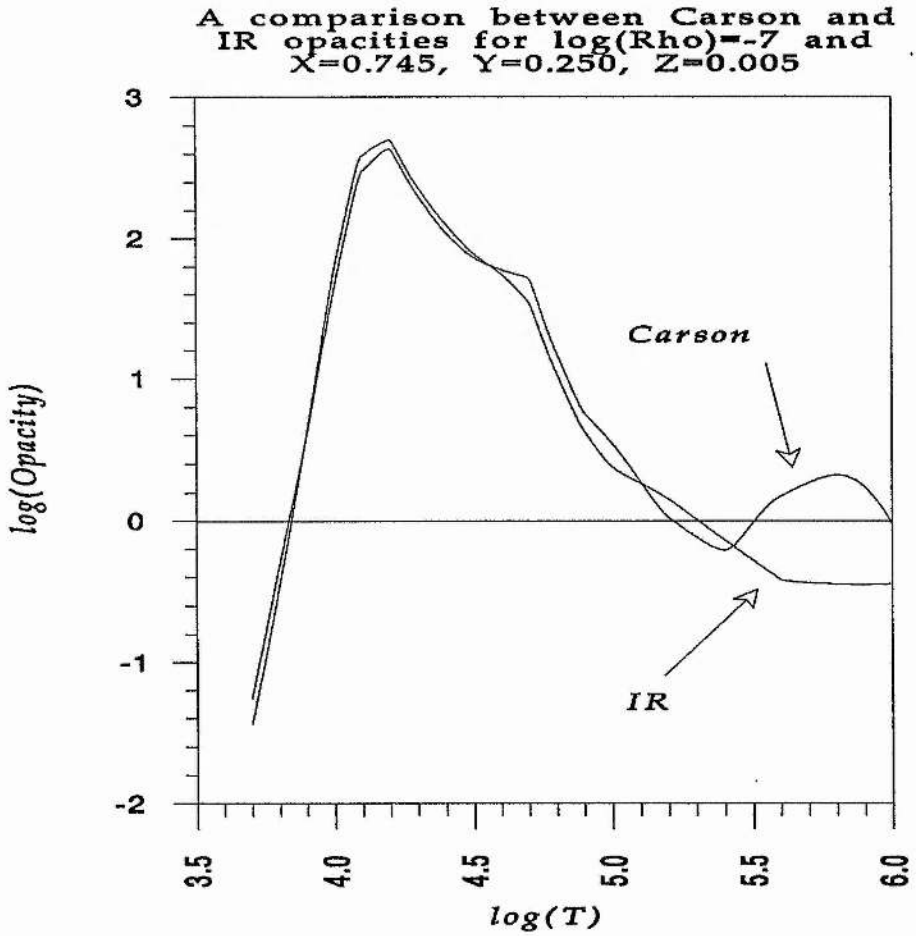
A comparison between Carson and
IR opacities for log(Rho)=-7 and
X=0.745, Y=0.250, Z=0.005
log(Opacity)
3
2
1
0
-1
-2
3.5
4.0
4.5
5.0
5.5
6.0
log(T)
Carson
IR

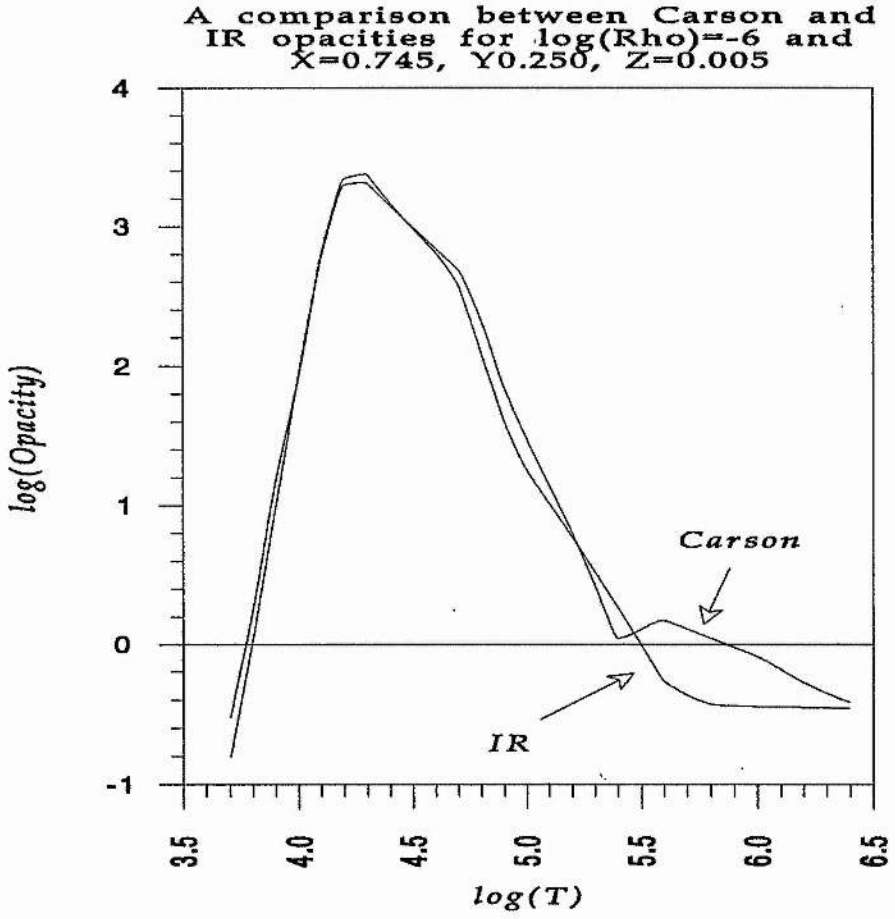
A comparison between Carson and IR opacities for log(Rho)=-6 and X=0.745, Y0.250, Z=0.005
log(Opacity)
4
3
2
1
0
-1
3.5
4.0
4.5
5.0
5.5
6.0
6.5
log(T)
Carson
IR

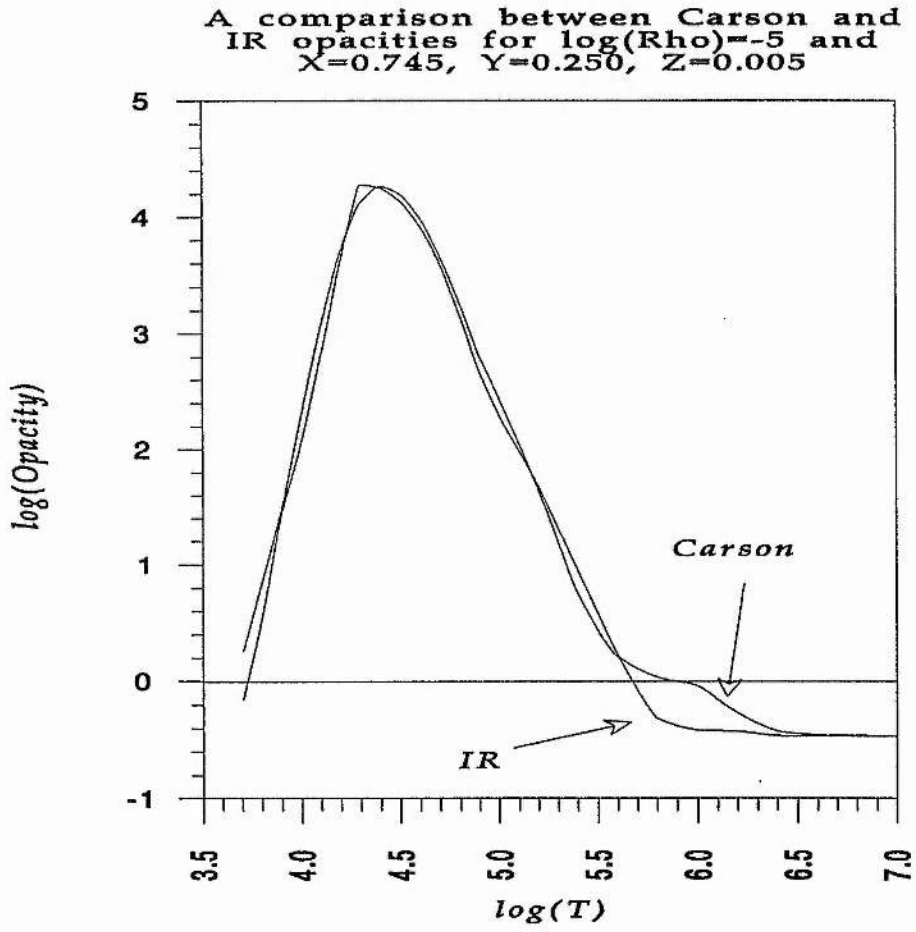
A comparison between Carson and IR opacities for log(Rho)=-5 and X=0.745, Y=0.250, Z=0.005
log(Opacity)
5
4
3
2
1
0
-1
3.5
4.0
4.5
5.0
5.5
6.0
6.5
7.0
log(T)
Carson
IR

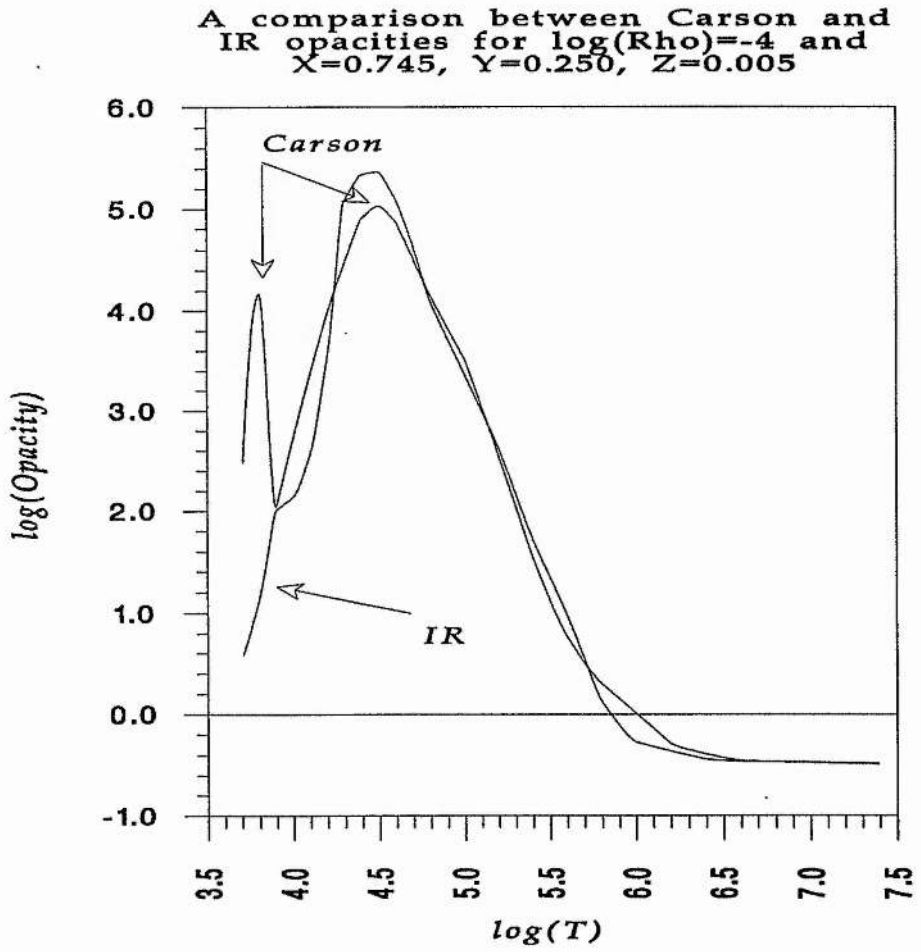
A comparison between Carson and
IR opacities for log(Rho)=-4 and
X=0.745, Y=0.250, Z=0.005
Carson
IR
log(Opacity)
log(T)
6.0
5.0
4.0
3.0
2.0
1.0
0.0
-1.0
3.5
4.0
4.5
5.0
5.5
6.0
6.5
7.0
7.5

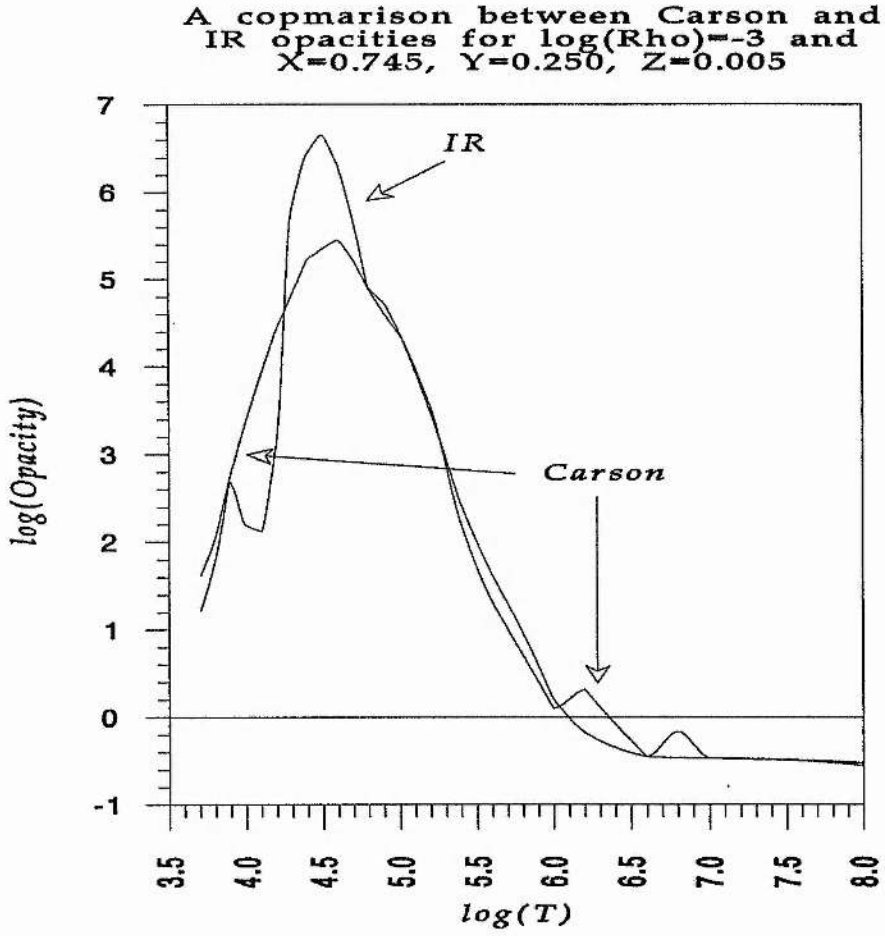
A copmarison between Carson and
IR opacities for log(Rho)=-3 and
X=0.745, Y=0.250, Z=0.005
IR
Carson
log(Opacity)
log(T)
7
6
5
4
3
2
1
0
-1
3.5
4.0
4.5
5.0
5.5
6.0
6.5
7.0
7.5
8.0

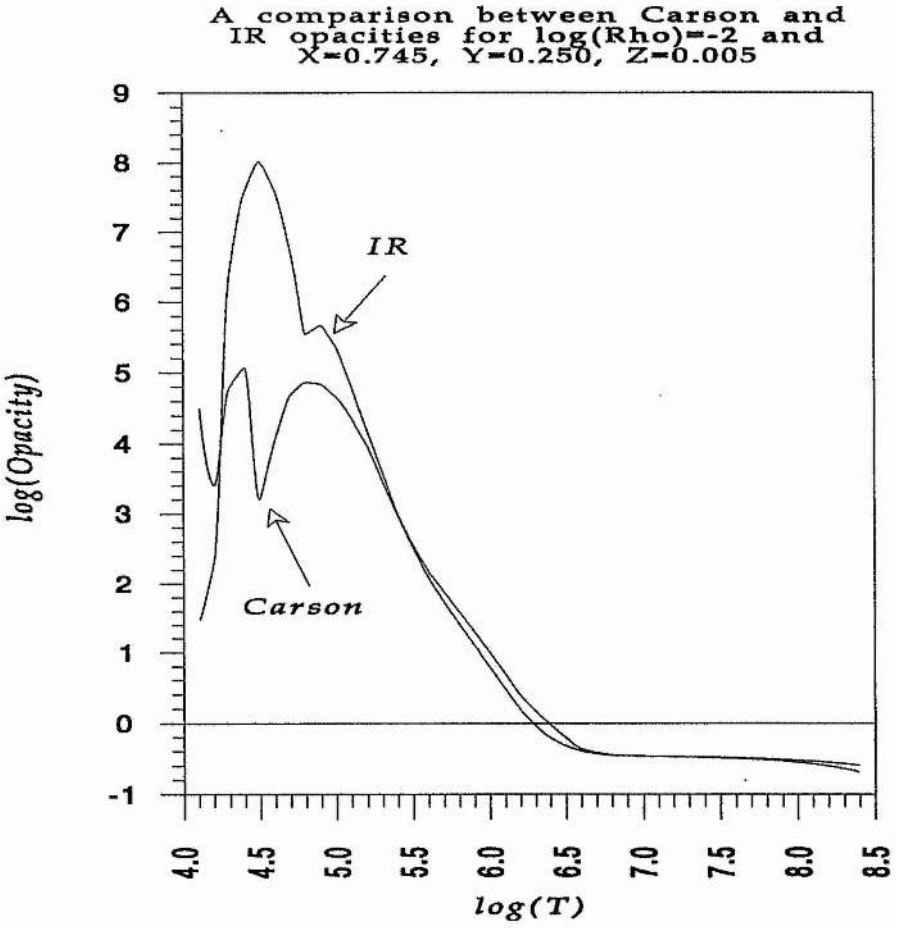
A comparison between Carson and
IR opacities for log(Rho)=-2 and
X=0.745, Y=0.250, Z=0.005
IR
Carson
log(Opacity)
log(T)
9
8
7
6
5
4
3
2
1
0
-1
4.0
4.5
5.0
5.5
6.0
6.5
7.0
7.5
8.0
8.5

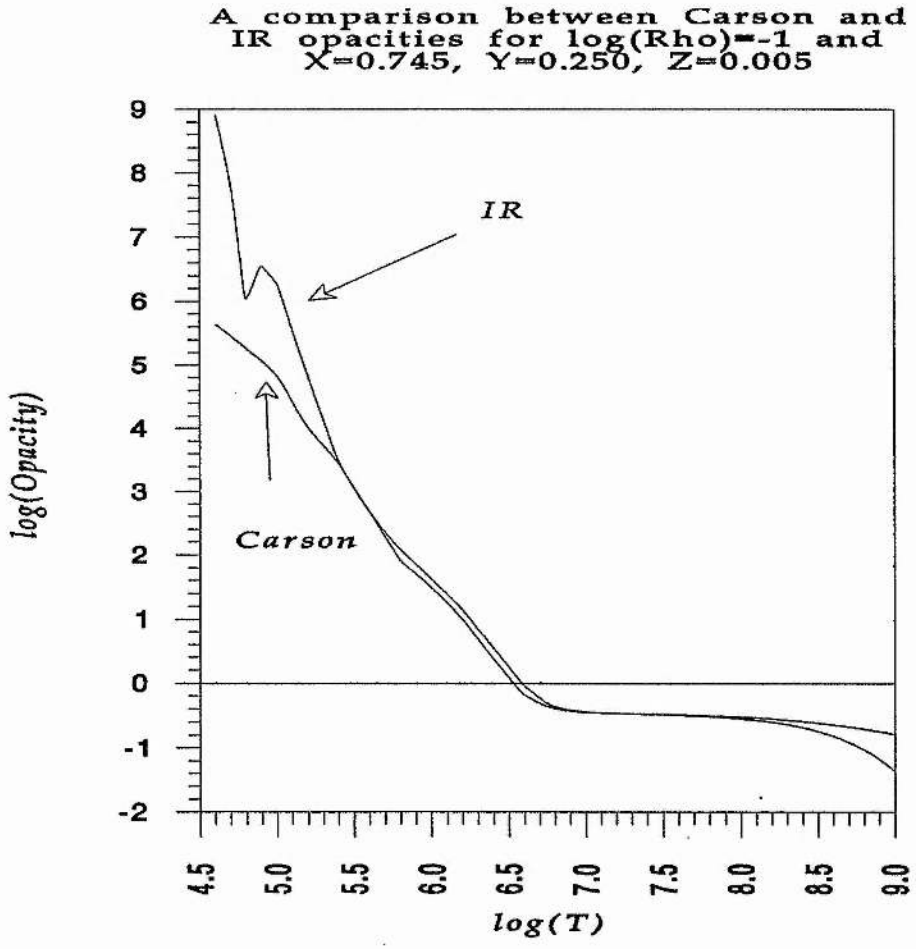
A comparison between Carson and
IR opacities for log(Rho)=-1 and
X=0.745, Y=0.250, Z=0.005
log(Opacity)
9
8
7
6
5
4
3
2
1
0
-1
-2
IR
Carson
4.5
5.0
5.5
6.0
6.5
7.0
7.5
8.0
8.5
9.0
log(T)

APPENDIX *D*

D-1. THE LINEAR THEORY:-

In the linear theory of stellar pulsation , the mathematics are linearized and the physics are approximated, i.e. the will known mathematical procedures after the linearization can be applied to obtain the solution.

The adiabatic theory, assumes purely adiabatic heat changes, and is useful for obtaining pulsation period alone, on the other hand the non-adiabatic theory allows us to determine whether the model is stable against pulsation or not and also to find the pulsation properties near the surface.

Following we are going to present the equations that we need for solving the problem of linear radial pulsation for a stellar model divided into a finite number of mass zones (the method of solution is out of the scope of this work and can be found in Castor (1971) and Milligan (1989)). The stars that we are going to discus are always spherically symmetric, the energy transports by radiation and in which we neglect the magnetic field and viscosity. Also we have to assume that the stellar material is chemically homogenous.

D-2. THE EQUATIONS:-

The model will be divided into N spherical shells, in which the mass is fixed. Zones (shells) are numbers from 1 to N, where 1 being the innermost and N being the

outermost (adjacent to the surface). The spheres bounding these shells we are going to call them interfaces and numbered from 1 to N+1, where interface 1 being the stationary bottom boundary and interface N+1 being the surface.

The radius and the luminosity defined on interfaces, where the other thermodynamic variables such as pressure, temperature, density,...etc. defined within shells (zones).

The difference equations of linear non-adiabatic theory can be written as follows:

$$\frac{d^2 r_i}{dt^2} = -\frac{GM_i}{r_i^2} - 4\pi r_i^2 \frac{P_i - P_{i-1}}{DM2_i} \qquad \textbf{(D-1)}$$

$$L_i = -\frac{4\sigma}{3}(4\pi r^2)^2 \frac{T_i^4 - T_{i-1}^4}{\frac{1}{2}(\kappa_i DM1_i + \kappa_{i-1} DM1_{i-1})} \qquad \textbf{(D-2)}$$

$$T_i \frac{dS_i}{dt} = -\frac{L_{i+1} - L_i}{DM1_i} \qquad \textbf{(D-3)}$$

$$V_i = \frac{4\pi}{3} \frac{r_{i+1}^3 - r_i^3}{DM1_i} \qquad \textbf{(D-4)}$$

where the mass of shell i is

$$DM1_i = M_{i+1} - M_i \qquad \textbf{(D-5)}$$

and the mass within the interface i is

$$DM2_i = \frac{1}{2}(DM1_{i+1} - DM1_{i-1}) \qquad \textbf{(D-6)}$$

According to the difference equations (D-1) - (D-4) with time derivative set to zero, we assume that we are dealing with a model that is in equilibrium. Following the prefix δ will indicate the infinitesimal deviation on any variable from its value in the model. The structure variable without this prefix will refer to the equilibrium model. Equations (D-1) -(D-4) will be linearized by expanding all the functions appearing in them in Taylor series about the equilibrium model, retaining only terms of zero or first order in perturbation. The zero order terms vanish by assumption. All the perturbation will be eliminated except those of r and S using equations (D-2) and (D-4) and the equation of state, hence we define

$$X_i = \sqrt{DM2_i}\ \delta r_i \qquad \textbf{(D-7)}$$

$$Y_i = T_i\ \delta S_i \qquad \textbf{(D-8)}$$

The linearization of equation (D-4) for specific volume Vi

$$-\delta\rho_i = \frac{4\pi\rho_i^2}{DM1_i}\left(r_{i+1}^2\delta r_{i+1} - r_i^2\delta r_i\right) \qquad \textbf{(D-9)}$$

$$\frac{\delta\rho_i}{\rho_i} = \frac{\rho_i}{DM1_i}\left(\frac{4\pi r_i^2}{\sqrt{DM2_i}}X_i - \frac{4\pi r_{i+1}^2}{\sqrt{DM2_{i+1}}}X_{i+1}\right) \qquad \textbf{(D-10)}$$

$$\frac{\delta\rho_i}{\rho_i} = DR1_i X_i + DR2_i X_{i+1} \qquad \textbf{(D-11)}$$

$$DR1_i = \frac{4\pi r_i^2\ \rho_i}{DM1_i\ \sqrt{DM2_i}} \qquad \textbf{(D-12)}$$

$$DR2_i = \frac{-4\pi r_{i+1}^2\ \rho_{i+1}}{DM1_i\ \sqrt{DM2_{i+1}}} \qquad \textbf{(D-13)}$$

A very useful forms of the non-linear equations for P and T are as follows,

$$\frac{d\ln P}{dt}=\Gamma_1\frac{d\ln\rho}{dt}+\frac{\rho\,(\Gamma_3-1)}{P}\frac{dQ}{dt}$$
$$\left(=\Gamma_1\frac{d\ln\rho}{dt}+\frac{\chi_T}{c_v T}\frac{dQ}{dt}\right) \qquad \textbf{(D-14)}$$

$$\frac{d\ln T}{dt}=(\Gamma_3-1)\,\frac{d\ln\rho}{dt}+\frac{1}{c_v T}\frac{dQ}{dt} \qquad \textbf{(D-15)}$$

where c_v denotes the specific heat per unit constant volume, and

$$\chi_T\equiv\left(\frac{\partial\ln P}{\partial\ln T}\right)_\rho \qquad \textbf{(D-16)}$$

and the gammas are the adiabatic exponents:

$$\Gamma_1\equiv\left(\frac{\partial\ln P}{\partial\ln\rho}\right)_{ad} \qquad \textbf{(D-17)}$$

$$\Gamma_3-1\equiv\left(\frac{\partial\ln T}{\partial\ln\rho}\right)_{ad} \qquad \textbf{(D-18)}$$

$$\frac{\Gamma_2-1}{\Gamma_2}\equiv\left(\frac{\partial\ln T}{\partial\ln P}\right)_{ad}\equiv\frac{\Gamma_3-1}{\Gamma_1} \qquad \textbf{(D-19)}$$

therefore equation (D-14) becomes

$$\frac{d}{dt}\left(\frac{\delta P_i}{P_i}\right)=\delta\,(\Gamma_1)_i\ \frac{d\rho_i}{dt}+(\Gamma_1)_i\ \frac{d}{dt}\left(\frac{\delta\ \rho_i}{\rho_i}\right)+\frac{(\Gamma_3-1)_i\,\rho_i}{P_i}\ \frac{d(\delta\ Q)}{dt}$$

$$+\left[\frac{\delta\ (\Gamma_3)_i}{(\Gamma_3-1)_i}+\frac{\delta\ \rho_i}{\rho_i}-\frac{\delta\ P_i}{P_i}\right]*\frac{(\Gamma_3-1)_i\ \rho_i}{P_i}\ \frac{dQ_i}{dt}$$

(D-20)

if the system, in its unperturbed state, is static and in thermal equilibrium so that

$$\frac{d\,\rho_i}{dt}=o \qquad \textit{and} \qquad \frac{d\,Q_i}{dt}=o$$

$$\frac{d}{dt}\left(\frac{\delta P_i}{P_i}\right)=(\Gamma_1)_i\ \frac{d}{dt}\left(\frac{\delta\,\rho_i}{\rho_i}\right)+\frac{(\Gamma_3-1)_i\rho_i}{P_i}\ \frac{d(\delta\ Q)}{dt} \qquad \textbf{(D-21)}$$

The corresponding equation for the temperature variation is

$$\frac{d}{dt}\left(\frac{\delta\,T_i}{T_i}\right)=(\Gamma_3-1)_i\ \frac{d}{dt}\left(\frac{\delta\,\rho_i}{\rho_i}\right)+\frac{1}{c_{v,i}\,T_i}\ \frac{d(\delta\ Q)}{dt} \qquad \textbf{(D-22)}$$

Therefore we can write equations (D-21) and (D-22) as follows

$$\frac{\delta\ P_i}{P_i}=(\Gamma_1)_i\ \frac{\delta\,\rho_i}{\rho_i}+\frac{(\Gamma_3-1)_i\,\rho_i}{P_i}\ T_i\delta\ S_i \qquad \textbf{(D-23)}$$

and

$$\frac{\delta\ T_i}{T_i}=(\Gamma_3-1)_i\ \frac{\delta\,\rho_i}{\rho_i}+\frac{1}{c_{v,i}}\ \delta\ S_i \qquad \textbf{(D-24)}$$

Dropping equations (D-8) and (D-11) into (D-23) and (D-24) we get;

$$\frac{\delta P_i}{P_i}=\frac{(\Gamma_3-1)_i\rho_i}{P_i}\ Y_i+(\Gamma_1)_i\ (DR1_i X_i+DR2_i X_{i+1}) \qquad \textbf{(D-25)}$$

$$\frac{\delta T_i}{T_i}=\frac{Y_i}{c_{v,i}T_i}+(\Gamma_3-1)_i\ (DR1_i X_i+DR2_i X_{i+1}) \qquad \textbf{(D-26)}$$

The linearization of equation (D-2) gives ;

$$\frac{\delta L_i}{L_i}=4\frac{\delta R_i}{R_i}+\left[4\frac{T_{i-1}^4}{T_{i-1}^4-T_i^4}-\frac{\kappa_{i-1}DM1_{i-1}\kappa_{T\,(i-1)}}{\kappa_{i-1}DM1_{i-1}+\kappa_i DM1_i}\right]\frac{\delta T_{i-1}}{T_{i-1}}$$

$$+\left[4\frac{-T_i^4}{T_{i-1}^4-T_i^4}-\frac{\kappa_i DM1_i\kappa_{T\,(i)}}{\kappa_{i-1}DM1_{i-1}+\kappa_i DM1_i}\right]\frac{\delta T_i}{T_i}$$

$$-\frac{\kappa_{i-1}DM1_{i-1}\kappa_{\rho\,(i-1)}}{\kappa_{i-1}DM1_{i-1}+\kappa_i DM1_i}\frac{\delta\rho_{i-1}}{\rho_{i-1}}$$

$$-\frac{\kappa_i DM1_i\kappa_{\rho\,(i)}}{\kappa_{i-1}DM1_{i-1}+\kappa_i DM1_i}\frac{\delta\rho_i}{\rho_i}$$

(D-27)

We are looking for the normal modes of radial pulsation by assuming that the time dependence is exponential. therefore we have to remove a factor ***exp(ιωt)*** from all the perturbation and replace ***d/dt*** by ***ιω***, then we get

$$-\omega^2\ \delta R_i=4\frac{GM_i}{R_i^3}\ \delta R_i-\frac{4\pi R_i^2}{DM2_i}(\delta P_i-\delta P_{i-1}) \qquad \textbf{(D-28)}$$

$$\iota\omega\ T_i\delta S_i=\frac{\delta L_i-\delta L_{i-1}}{DM1_{i-1}} \qquad \textbf{(D-29)}$$

Castor (1971) after some algebra he found

$$\omega^2 X_i = G11_i X_{i-1} + G12_i X_i + G13_i X_{i+1} + G21_i Y_{i-1} + G22_i Y_i$$

(where $i = 2, N$) **(D-30)**

$$\iota\,\omega\, Y_i = K11_i X_{i-1} + K12_i X_i + K13_i X_{i+1} + K14_i X_{i+2} + K21_i Y_{i-1} + K22_i Y_i + K23_i Y_{i+1}$$

(where $i = 2, N\text{-}1$) **(D-31)**

where ***G***'s and ***K***'s are elements of matrices **G1** , **G2** , **K1** and **K2** , Milligan (1989). In matrix form, these equations becomes

$$\omega^2 X = \underline{G1}\, X + \underline{G2}\, Y \cdot \quad \textbf{(D-32)}$$

$$\iota\omega Y = \underline{K1}\, X + \underline{K2}\, Y \quad \textbf{(D-33)}$$

In equations (D-32) and (D-33) we have been used the following vectors $X = X_i, (i = 2, N+1)$ and $Y = Y_i, (i = 1, N)$.

If $\boldsymbol{Y}$ in (D-31) is equal to zero, then the adiabatic eigenfrequencies and eigenvectors obtained,

$$\omega^2 X = \underline{G1}\, X. \quad \textbf{(D-34)}$$

G1 is real, symmetric tridiagonal matrix because of the way that we defined X.

The linear, adiabatic wave equation (D-1) becomes in finite difference form as:

$$-\omega^2 \delta R_i = \frac{2GM_i}{R_i^3}\,\delta R_i - \frac{4\pi}{DM2_i}\left[2R_i\,\delta R_i (P_i - P_{i-1}) + R_i^2(\delta P_i - \delta P_{i-1})\right]$$

(D-35)

where

$$\delta P_i = \left[\Gamma_1 P \frac{\delta \rho}{\rho}\right]_i \qquad \textbf{(D-36)}$$

then using equation (D-11) we get

$$\delta P_i = (\Gamma_1 P)_i \left(DR1_i X_i + DR2_i X_{i+1}\right) \qquad \textbf{(D-37)}$$

$$\delta P_{i-1} = (\Gamma_1 P)_{i-1} \left(DR1_{i-1} X_{i-1} + DR2_{i-1} X_i\right) \qquad \textbf{(D-38)}$$

An alternative expression for $(P_i - P_{i-1})$ can be found if the acceleration in equation (D-1) be zero then:

$$\frac{GM_i}{R_i^2} = -4\pi R_i^2 \frac{P_i - P_{i-1}}{DM2_i} \qquad \textbf{(D-39a)}$$

Then we get:

$$\frac{2GM_i}{R_i^3} \delta R_i = -8\pi R_i \frac{(P_i - P_{i-1})}{DM2_i} \delta R_i \qquad \textbf{(D-39)}$$

using equations (D-7) and (D-39), equation (D-35) becomes as follows:

$$\omega^2 X_i = -\frac{4GM_i}{R_i^3} X_i + \frac{4\pi R_i^2}{\sqrt{DM2_i}} \left\{-(\Gamma_1 P)_{i-1} DR1_{i-1} X_{i-1} + \left[(\Gamma_1 P)_i DR1_i - (\Gamma_1 P)_{i-1} DR2_{i-1}\right] X_i + (\Gamma_1 P)_i DR2_i X_{i+1}\right\} \qquad \textbf{(D-40)}$$

Now the matrix equation (D-34) can be written as follows:

$$\omega^2 X_i = G11_i X_{i-1} + G12_i X_i + G13_i X_{i+1} \quad \textbf{(D-41)}$$

Hence, we can get the values of G's by comparing (D-40) and (D-41)

$$G11_i = \frac{-4\pi R_i^2}{\sqrt{DM2_i}} (\Gamma_1 P)_{i-1} DR1_{i-1} \quad \textbf{(D-42)}$$

$$G12_i = \frac{-4GM_i}{R_i^3} + \frac{4\pi R_i^2}{\sqrt{DM2_i}} \left[(\Gamma_1 P)_i \, DR1_i - (\Gamma_1 P)_{i-1} DR2_{i-1} \right] \quad \textbf{(D-43)}$$

$$G13_i = \frac{4\pi R_i^2}{\sqrt{DM2_i}} (\Gamma_1 P)_i \, DR2_i \quad \textbf{(D-44)}$$

G1 is symmetric matrix, that means $G11_{i+1} = G13_i$, which can be shown by using (D-12) and (D-13)

$$G11_{i+1} = \frac{-4\pi R_{i+1}^2}{\sqrt{DM2_{i+1}}} (\Gamma_1 P)_i \, DR1_i$$

$$= \frac{-4^2 \pi^2 R_i^2 R_{i+1}^2 \rho_i}{DM1_i \sqrt{DM2_i} \sqrt{DM2_{i+1}}} (\Gamma_1 P)_i \quad \textbf{(D-45)}$$

$$G13_i = \frac{4\pi R_i^2}{\sqrt{DM2_i}} (\Gamma_1 P)_i \, DR2_i$$

$$= \frac{-4^2 \pi^2 R_i^2 R_{i+1}^2 \rho_i}{DM1_i \sqrt{DM2_i} \sqrt{DM2_{i+1}}} (\Gamma_1 P)_i \quad \textbf{(D-46)}$$

Up to this point its possible to calculate most of the elements of the matrix **G1**.

Some of the references that are useful here are, Castor (1971), Cox (1980), Bridger (1983), Worrell (1985) and Milligan (1989).

REFERENCES

Becker, S. A. ,1986, " The evolution of variable stars" pp16-26 in 'Stellar Pulsation' Cox, A. N. ; Sparks, W. M. & Starrfield, S. G.(edt.) Los Alamos USA 1986.

Becker, S. A., 1985, Cepheid Evolution, in Madore, B. F.(edit.) Cepheids : Theory and observations ,Cambridge University press 1985 pp104-125.

Bohm-Vitense, E. , 1989 (1), Introduction to Stellar Astrophysics, Volume 1, basic stellar observation and data, Cambridge University press.

Bohm-Vitense, E. ; Szkody, P. ;Wallerstein, G. & Iben, I. Jr. , 1974, APJ, 194 , 125-135.

Bowers, R. L & Deeming, T. ,1984, Astrophysics I stars, Jones and Bartlett Publishers, INC, Boston.

Bridger, A., 1983, Ph.D. Thesis University of St. Andrews.

Bridger, A., 1984, Theoretical Models of W Virginis Variables, in Madore, B.F. (edit.), Cepheids : Theory and observations, Cambridge University press, 1985, 246-249.

Buchler, J.R. ,1990,The modeling of non-linear stellar pulsations , in "The Numerical Modelling of Non-linear Stellar Pulsation", Buchler, J. R.(edt.) Kluwer Academic Puplishers, 1990 ,1-26.

Buchler, J.R. & Moskalik, P , 1992, APJ, 391 , 736-749.

Carson, T. R & Stothers, R.,(**CS82**), 1982 , APJ, 259 ,740-748.

Carson, T. R ; Stothers, R. & Vemury, S. K.,(**CSV81**),1981, APJ, 244 ,230-241.

Carson, T. R. & Sharp ,1991, Rev. Mexicana Astron. Astrof., 23 ,217-221.

Carson, T. R. ,1994, Private Communication.

Castor, J. I., 1971, APJ, 166 109-129.

Chiosi, C. ; Wood, P. & Bertelli, G., 1992 , APJ, 387 ,320-328.

Christy, R. F., 1966 , APJ, 144 ,108-179.

Christy, R. F., 1967, Computational Methods in Stellar Pulsation, in "Methods in computational Physics" Alder, B.(edt.) New York Academic Press, 7 ,191-218.

Clayton, D. D., 1968, " Principles of Stellar Evolution and Nucleosynthesis" Mc Grraw Hill.

Clement, C. M. ; Sawyer Hogg, H. & Yee, A., 1988, AJ, 96 ,1642- 1648.

Clement, C.; Sawyer Hogg, H. & Lake, K., 1985, The Two Pop II Cepheids In The Globular cluster Messier 10, in Mdore, B. F.(edit.) Cepheids : Theory and observations ,Cambridge University press 1985 pp260-261.

Clement, C. C. & Sawyer Hogg, H. , 1978, AJ, 83, 167-171.

Copeland, H. ; Jensen, O. & Jorgensen, H.E.,1970, AA, 5, 12-34.

Cox, A. N., 1991, APJ, 38 , L71-L74.

Cox, A. N. & Kidman, R. B.,1985, A new possible resonance for Population II Cepheids, in " Cepheids : Theory and observations" , Madore, B. F. (edit.) Cambridge University press, 1985, pp 250-253.

Cox, J. P. & Giuli, R. T. 1968 " Principles Of Stellar Structure" volume 1. Gordon and Breach, Scince Publishers

Cox, J. P., 1974, Rep. Prog. Phys., 37 ,563-698.

Cox, J. P., 1980, "Theory of stellar pulsation" Princeton University Press, New Jersey.

Cox, J. P.,1985, Theory of Cepheid Pulsation Excitation Mechanisms, in "Cepheids : Theory and observations", Madore, B. F.(edit.), Cambridge University press 1985 pp126-146.

Cox, A. N. ; Hodson, S. W. & Clancy, S. P. , 1983, APJ, 266 ,94-104.

Davis, C. G., 1972 , APJ, 172 , 419-421.

Davis, C. G., 1974 , APJ, 187 ,175-177.

Dean, J. F. ; Cousins, A. W. J. ; Bywater, R. A. & Warren, P. R. ,1977, Mem. R. Astr. Soc. ,83 ,69-93.

Demers, S. & Harris,W. E., 1974, APJ, 79 ,627-630.

Deupree, R. G., 1977**a** , APJ, 211 ,509-526.

Deupree, R. G., 1977**b**, APJ, 214 ,502-509.

Deupree, R. G.,1976, A Treatment of Time Dependent Convection in Non-linear stellar Pulsation Calculation, in " Proceeding of the Solar and Stellar Pulsation Conference", (edit) Cox, A. N. & Deupree, R. G., pp 222-228.

Diethelm, R. , 1983, AA, 124 ,108-115.

Fadeyev, Yu. A. ,1993 , MNRAS, 262 , 119-127.

Fokin, A. ,1990, Astrophy.Space.Science., 164 ,95-106.

Gingold, R. A. , 1976, APJ, 204 ,116- 130.

Hubickyj, E. O. ,1983, Ph.DThesis, The City University of New York.

Iben, I. Jr. ,1971, Publ. Astron. Soc. Japan , 83, 697-740.

Igalesias, C. A. & Rogers, F., 1991, APJ, 371 , L73-L75.

Keeley, D. A., 1970 , APJ, 161 ,657-667.

Kippenhahn, R.& Weigert, A. ,1990, Stellar Structure and Evolution, Springer-Verlag, A&A library.

Kovacs, G. & Buchler, J. R., 1988, APJ, 334 ,971-994

Kovacs, G., 1990, Numerical Sensitivity of Non-linear Stellar Pulsation, in "The Numerical Modelling of Non-linear Stellar Pulsation", Buchler, J. R.(edt.) Kluwer Academic Puplishers, 1990 pp73-88.

Kovacs, G. ; Buchler, J. R. & Marom, A.,1991, AA , 252 ,L27-L30.

Kraft, R. P., 1972, Observational Aspects of RR Lyrae and W Viriginis stars: Some Conundrums of stellar Population and Galactic distribution, in "The evolution of population II star" ,Philip,A.G. D Report no.4 Dudley Observatory, New York 1972 p 69-96

Kwee, K. K. & Diethelm, R. , 1984, AA Suppl., 55,77-86.

Kwee, K. K.& Braun, L. D. , 1967, Bull. Astr. Inst. Netherlands Suppl. , 2,77-96.

Kwee, K. K., 1967, Bull. Astr. Inst. Netherlands Suppl. , 19 ,260-274.

Kwee, K. K. , 1968, Bull. Astr. Inst. Netherlands Suppl. , 19 ,374-390.

Lawrence, S. P. A. ,1985, M.Sc. Thesis, St Anderws University.

Lebre, A. & Gillet, D., 1992 , AA, 255 ,221-232.

Lee, S. W. , 1974, Observatory, 94, 74-79.

Lloyd Evans, T. ; Wisse, P. N. J. & Wisse, M. ,1972, MNRAS, 159 ,67-78.

Lub, J. ,1987, field RR Lyrae Stars, in " Lecture Notes in Physics, Stellar Pulsation" (edts.) Cox, A. N. ; Sparks, W. M. & Starrfield, S. G., Springer-Verlag, p218-229.

Michalowska-Smak, A. & Smak, J. ,1965, Acta Astr. ,15 ,33-341.

Milligan, H., 1989, Ph.D. Thesis, University of St. Andrews.

Mitchell, R. I. ; Steinmetz, D. & Johnson, H. L. ,1964, Boletin DE Los Observatorios TONANTZINTLA y TACUBAYA, 3 ,No.24,153.

Moskalik, P. ; Buchler, J.R. & Marom, A. , 1992, APJ, 385 ,685-693.

Novotny, E., 1973, "Introduction to stellar Atmospheres and Interiors" Oxford University press.

Payne-Gaposchkin, C. ,1956, Vistas Astr. ,2 ,1142-9.

Pel, J. W. ,1985, Fundamental Parameters of Cepheids, in "Cepheids : Theory and observations" , Madore, B. F. (edt.) Cambridge University press, 1985, pp1-16.

Pijpers, F. P., 1993 , AA, 267 ,471-489.

Schmidt, E. G. ; Loomis, C. G. ; Groebner, A. T. & Potter, C. T. , 1990, APJ, 360 , 604-611.

Schwarzschild, M. & Harm, R., 1970, AP, 160 ,341-344.

Smith, H. A. ; Jacques, J. ; Lugger, P. M. ; Deming, D. & Butler, D. ,1978, Pup. A. S. P. ,90 ,422-428.

Stellingwerf, R. F., 1975, APJ, 195 ,441-466.

Stothers, R. B. & Chin, C. -w. , 1991, APJ, 381 ,L67-L70.

Strohmeier, W. ,1972 , in "Variable Stars", Pergamon Press.

Unno, W.,1965 , Pulbl. Astron. Soc. Japan, 17 ,205

Van Albada, T. S. & Baker, N. ,1971, APJ, 169 ,311-326.

Wallerstein, G. & Cox, A. N.,1984 , Pup.Astron.Soci.Pasfic, 96 ,677- 691.

Wallerstein, G., 1970, APJ, 160 ,345

Zessevich, V. ,1966, Sky & Telescope, 32 ,199-202.

الحمد لله رب العالمين

Praise be to Allah The Cherisher and Sustainer of the Worlds